MODELING THE IMPACT OF ROAD GRADE ON VEHICLE OPERATION, VEHICLE ENERGY CONSUMPTION, AND EMISSIONS

A Dissertation
Presented to
The Academic Faculty

by

Haobing Liu

In Partial Fulfillment
of the Requirements for the Degree
Doctor of Philosophy in the
School of Civil & Environmental Engineering

Georgia Institute of Technology
August, 2018

MODELING THE IMPACT OF ROAD GRADE ON VEHICLE OPERATION, VEHICLE ENERGY CONSUMPTION, AND EMISSIONS

Approved by:

Dr. Randall Guensler, Advisor
School of Civil and Environmental Engineering
Georgia Institute of Technology

Dr. Michael Hunter
School of Civil and Environmental Engineering
Georgia Institute of Technology

Dr. Michael O. Rodgers
School of Civil and Environmental Engineering
Georgia Institute of Technology

Dr. Yao Xie
School and Industrial and System Engineering
Georgia Institute of Technology

Dr. Jorge Laval
School of Civil and Environmental Engineering
Georgia Institute of Technology

Date Approved: July 27, 2018

To my father Gengye Liu, and my mother Kunxiang Liu

献给我的 父亲 刘耕野 和 母亲 刘坤香

In memory of my grandfather: Haitao Liu

纪念我的爷爷：刘海涛

ACKNOWLEDGEMENTS

I would like to express my deepest gratitude to my advisors, Dr. Randall Guensler and Dr. Michael Rodgers, for their continuous guidance, encouragement, support and understanding. I am also the most grateful for the advice and comments from the other members of my dissertation committee: Dr. Jorge Laval, Dr. Michael Hunter, and Dr. Yao Xie. Their patience and flexibility have given me the opportunity to grow and succeed, and prepare me for life after graduation.

My gratitude also goes to the friends I have made while at Georgia Tech: Ann & Cody, Xiaodan, Fangru, Jinqi & Wenwen, Honghan, Yingping, Yipu, Tu, Daejin, Hongyu, Ross, and Alice, to name a few. Their friendship and company have filled my doctoral experience with joy. I also wish to thank the staff of transportation program: Dr. Yanzhi Xu, Marjorie Jorgenson, Winston Yang, and Michael Anderson for their invariably timely help. This work was sponsored by the USDOT's UTC program via the National Center for Sustainable Transportation. I would also like to thank Dr. Mehmet Belgin and Dr. Fang Liu in GT PACE Center for distributed computing technical support.

I am profoundly thankful to my wife Fei Tang, who has been my pillar of support. Her love and patience are the sources of my strength, the very reason that I kept on going. Finally, my gratitude towards my parents and parents-in-law are beyond words: 感谢父母含辛茹苦以及对我无私的爱。无论在哪，父母都是我永远的精神支撑，期盼早日回国和父母团聚。特别感谢岳父母在我读博最后半年赴美帮助我们一起照顾刚出生的女儿小冰糖，这对我能顺利完成论文至关重要。

TABLE OF CONTENTS

ACKNOWLEDGEMENTS iv

LIST OF TABLES viii

LIST OF FIGURES ix

LIST OF SYMBOLS AND ABBREVIATIONS xii

SUMMARY xiii

CHAPTER 1. Introduction 1
1.1 Research Objectives and Tasks 4
1.2 Develop Streamlined Method to Generate Large-scale Road Grade Data 5
1.3 Append Derived Grade Data onto "Big Data" of Vehicle Trajectories 6
1.4 Build MOVES-Matrix for Energy Consumption and Emissions Modeling 7
1.5 Identify Grade Impact on Freeway Operations 8
1.6 Identify Grade Impact on Acceleration Mode at Arterials 9
1.7 Examine Potential Improvement on Energy Consumption, Emissions, and Near-road Air Quality Modeling 10
1.8 Dissertation Outline 11

CHAPTER 2. literature Review 13
2.1 Road Grade 13
2.2 Data and Method for Grade Generation 15
2.2.1 Vehicle On-board Equipment 15
2.2.2 Design Drawings 17
2.2.3 Light Detection and Ranging (LiDAR) 18
2.2.4 Open Source Elevation Data 19
2.3 Impact of Road Grade on Vehicle Operation 21
2.4 Impact of Road Grade on Vehicle Energy Consumption and Emissions 24
2.5 Impact of Vehicle Operation on Energy Consumption and Emissions 27
2.6 Energy Consumption/Emissions Modeling and MOVES Model 28
2.7 Summary of Literature Review 34

CHAPTER 3. Grade Generation USING THE USGS DEM 36
3.1 DEM Data 36
3.2 Methodology 39
3.2.1 Elevation Extraction 41
3.2.2 Elevation Data Cleaning and Infill 44
3.2.3 Cubic Smoothing Spline 46
3.3 Verification and Discussion 52
3.3.1 Real-World Road Grade Collection 52
3.3.2 Road Grade Verification 54
3.4 Discussion of λ Selection 58

3.5 Summary 60

CHAPTER 4. Data Processing Methodology 64
4.1 Data Support 64
4.1.1 Vehicle GPS Data 64
4.1.2 EPA Certification Database 67
4.1.3 Road Information and Surrounding Environment 69
4.2 Appending Grade on GPS Data 71
4.3 Energy Consumption and Emissions Modeling based on MOVES-Matrix 73
4.3.1 MOVES-Matrix Concept Design 73
4.3.2 Input 75
4.3.3 Modeling Algorithm 76
4.4 Data Sample and Summary 79

CHAPTER 5. Freeway Operations 83
5.1 Trace Segmentation 83
5.2 Operations Modeling in Uncongested Condition 88
5.2.1 Model Setup 88
5.2.2 Parameter Estimation 94
5.2.3 Model Results 103
5.3 Impact on Shape of SAJD 115
5.3.1 Extreme and Mean Accelerations at Each Speed Level 116
5.3.2 Width of SAJD: Extreme Acceleration and Deceleration Separation 122
5.3.3 Skewness 125
5.4 Summary 127

CHAPTER 6. Energy and Emissions On Freeways 129
6.1 Emission Modeling Scenarios 129
6.2 Near-Road PM2.5 Dispersion Impact - A Case Study 139
6.3 Summary 152

CHAPTER 7. Acceleration Behavior on ArterialS 153
7.1 Trace Segmentation in Arterials 153
7.2 Acceleration Data 155
7.3 Target Speed Model 158
7.3.1 Regression Model 158
7.3.2 Model Results 159
7.3.3 Impact on Extreme Target Speeds and Distributions 161
7.4 Speed-Acceleration Path Model 163
7.4.1 Preliminary Analysis 164
7.4.2 Model Setup 166
7.4.3 Model Result 173
7.5 Shape of SAJD Formed by Accelerations 182
7.6 Acceleration Distance and Duration 185
7.7 Summary 186

CHAPTER 8. Energy and Emissions on Arterials 189
8.1 Impact on Energy Consumption 190
8.2 Spatial Distribution of $PM_{2.5}$ Emissions 193
8.3 Near-Road Air Quality Modeling 199
8.4 Summary 208

CHAPTER 9. Conclusion and Future Research 209
9.1 Conclusion of Road Grade Generation 209
9.2 Implications of Modeling Grade Impact on Operations 210
9.3 Implications for Energy Consumption and Emissions Modeling 211
9.4 Limitations and Future Research 213
9.5 Contributions 220

APPENDIX A. Conditional Distribution of $\boldsymbol{\gamma_{i,j}}$ 222

APPENDIX B. Conditional Distribution of $\boldsymbol{\varphi_i}$ and $\boldsymbol{\Sigma_i}$ 224

APPENDIX C. Conditional Distribution of $\boldsymbol{\sigma_{vi,j2}}$ 227

APPENDIX D. Coefficients of Acceleration Model 229

REFERENCES 235

VITA 242

LIST OF TABLES

Table 1 – MOVES VSP/STP Operating Mode Bins 30
Table 2 – Data Collection Summary 53
Table 3 – Description of Vehicle Lookup Table Based on EPA Certification Data 68
Table 4 – Content of Input File for MOVES-Matrix 75
Table 5 – Summary of Comprehensive Dataset 80
Table 6 – Sample Size (in Seconds) of Passenger Car Operations by Trace Average Speed Bin and Grade 86
Table 7 – Sample Size (in Seconds) of Passenger Truck Operations by Trace Average Speed Bin and Grade 86
Table 8 – Sample Size (in Seconds) of Passenger Truck Operations by Trace Average Speed Bin and Grade 87
Table 9 – Variable Descriptions for Bayesian Hierarchical Model 104
Table 10 – Speed and Acceleration Model Result: Fleet-Level Effect 109
Table 11 – Criteria for segmenting traces 154
Table 12 – Number of Acceleration Traces by Vehicle Type and Target Speed Group 158
Table 13 – Speed (mph) Model Result: Population-Level Effect 160
Table 14 – Intercept (Speed-Accelerations with Grade = 0%) 175
Table 15 – Negative Grade Impact on Accelerations 177
Table 16 – Positive Grade Impact on Accelerations 178

LIST OF FIGURES

Figure 1 – Gravity Acting on Vehicle 14
Figure 2 – Sample Models. (a): Accelerometer, (b): Barometer, (c): Differential GPS 15
Figure 3 – Road Longitudinal Profile with Road Grades (GDOT, 2018) 18
Figure 4 – Profile of Elevation Contour from LiDAR 19
Figure 5 – USGS DEM Cloud Point in Pittsburgh 20
Figure 6 – Truck Acceleration/Deceleration Curves in Response of Road Grade (TRB, 2010) 22
Figure 7 – Desired Acceleration Processes (Laval et al., 2014) 23
Figure 8 – Sensitivity of Trip Percent Energy Increase to Average Grade and RMSE Grade for Conventional Vehicle (CV) and Hybrid Electric Vehicle (HEV) (Wood et al., 2014a) 25
Figure 9 – Change in Operating Mode Distributions With and Without Grade (Sentoff et al., 2015) 27
Figure 10 – Emission Modeling Framework 29
Figure 11 – CO_2 Emission Rates by OpMode Bin for Passenger Trucks (MY2016 in Calendar Year 2016) 31
Figure 12 – MOVES Data Processing in Project-Level 32
Figure 13 – The United States Elevation Map Produced using the USGS DEM 38
Figure 14 – Google® Satellite Layer, Google® Street, and USGS Elevation Map (3×3 Meter Resolution) of I-75 and I-85 Interchange in Atlanta, Georgia, USA 39
Figure 15 – Data Flowchart of Road Grade Generation 40
Figure 16 – Pre-sample Method 42
Figure 17 – Post-sampling Method 43
Figure 18 – Elevation Data Cleaning and Infill 46
Figure 19 – Real-World Elevation/Grade Collection Tool: (a) Leica® P40 LiDAR Scanner, (b) Leica® Scan-station 2, (c) 48-Inch SmartTool® Digital Level 52
Figure 20 – Road Segment Layout 53
Figure 21 – RMSE in Response of λ by Road 55
Figure 22 – Measurement-Estimate Grade Comparison by Road Types and DEM Resolutions 57
Figure 23 – Distance-Grade Profile for North Highland Avenue 58
Figure 24 – Optimum λ in Response of $|S''x|$ 60
Figure 25 – Atlanta Road Network with Grade Available 63
Figure 26 – Grade Distribution of Freeways and Arterials in Atlanta 63
Figure 27 – Model Year Distribution of Light-duty Vehicles from ARC Survey 65
Figure 28 – Number of Vehicles by Body Style 66
Figure 29 – GRTA Express Bus (Left) and MARTA Urban Transit Bus (Right) 67
Figure 30 – Engine Displacement and Gross Vehicle Weight Ratio (GVWR) by Vehicle Regulatory Class 69
Figure 31 – Road Horizontal Curve 70
Figure 32 – a) Road Network; b) GPS Trajectories; c) Estimated Routes 72
Figure 33 – MOVES-Matrix Work Concept 74

Figure 34 – Energy Rate of MARTA Bus by Operating Mode Bin 77
Figure 35 – Energy Rate of MARTA Bus at Grade of (a) -3%; (b) 0%; (c) +3% 78
Figure 36 – From (a) MARTA Bus Speed Trajectory to (b) Speed-Acceleration Joint Distribution (SAJD) 79
Figure 37 – Sample Trajectory of A Passenger Car. A) Second-By-Second Speed and Acceleration; B) Road Grade; C) Calculated VSP With Actual and 0 Grade; D) Operating Mode Bin With Actual and 0 Grade; E) Estimated Energy Rate With Actual and 0 Grade 82
Figure 38 – Example of Segmented Freeway Speed Traces 84
Figure 39 – Speed-Acceleration Joint Distribution of Traces in Average Speed of (a): 70 mph, and (b): 40 mph 88
Figure 40 – Hierarchical Structure of Vehicle Traces 89
Figure 41 – A Graphical Representation of the Hierarchical Regression Model 91
Figure 42 – Combined Gibbs Sampler and Metropolis Algorithm with MCMC Simulation 96
Figure 43 – The Normalized Residual Density and Standard Normal Density (a): LDV Speed Model; (b): LDV Acceleration Model 106
Figure 44 – ACF Plot of Normalized Residuals in LDV Speed Model. (a): Without Correlation Structure (ρ=0); (b): With First-order Autoregressive Structure 107
Figure 45 – Coefficients of Passenger Car Speed Model 113
Figure 46 – Coefficients of Passenger Truck Model 114
Figure 47 – The 2.5th (Extreme Deceleration), Mean, and 97.5th (Extreme Acceleration) Percentile of Accelerations by Grade – Passenger Car 118
Figure 48 – The 2.5th (Extreme Deceleration), Mean, and 97.5th (Extreme Acceleration) Percentile of Accelerations by Grade – Passenger Truck 118
Figure 49 – The 2.5th (Extreme Deceleration), Mean, and 97.5th (Extreme Acceleration) Percentile of Accelerations by Grade – Express Bus 119
Figure 50 – Envelope of SAJD at Uncongested Condition 119
Figure 51 – Mean and Confidence Interval of Grade Impact Slope θ_{v1} on 97.5-Percentile Accelerations (Extreme Accelerations) 121
Figure 52 – Mean and Confidence Interval of Grade Impact Slope θ_{v1} on Average Accelerations 121
Figure 53 – Mean and Confidence Interval of Grade Impact Slope θ_{v1} on 2.5-Percentile Accelerations (Extreme Decelerations) 122
Figure 54 – Acceleration Distribution and Width between Extreme Accelerations and Decelerations on Average Speed 65 mph 123
Figure 55 – Mean and Confidence Interval of Grade Impact on Width β_{v1} 124
Figure 56 – Symmetric Level and Skewness Value 126
Figure 57 – Mean and Confidence Interval of Grade Impact on Skewness 127
Figure 58 – Passenger Car VSP Distribution from 3 Scenarios at Avg Speed 65 mph 132
Figure 59 – Passenger Car Energy Rate (KJ/hr) and PM2.5 Rate (grams/hr) 136
Figure 60 – Passenger Truck Energy Rate (KJ/hr) and PM2.5 Rate (grams/hr) 137
Figure 61 – Express Bus Energy Rate (KJ/hr) and PM2.5 Rate (grams/hr) 138
Figure 62 – Speed Distribution of I-85 Case 141

Figure 63 – I-85 Line Source Dispersion Modeling Case Study. (a) Wind Rose Diagram for Atlanta in 2016. (b) Case Study Map. (c) Grade Distribution. (d) Line Source and Receptors Setup 142
Figure 64 - Road Segmentation by Grade for Real-world Trace Assignment 144
Figure 65 – Annual Average $PM_{2.5}$ Concentration from AERMOD 145
Figure 66 – Absolute Difference of Concentration between Baseline (Observed Real-World Operations with Actual Grade Applied in Each Segment) and Candidate Scenarios 148
Figure 67 – RMSEs of Candidate Scenarios 149
Figure 68 – Actual Difference of Concentrations between Baseline and Candidate Scenarios (Candidate Scenario – Baseline Scenario) 150
Figure 69 – Concentration Differences between S1 (Baseline) and (a) S2: grade = 0%, and (b) S3: Grade and SAJD Independent 151
Figure 70 – Decomposed time-speed traces by modal types 155
Figure 71 – Passenger car time-speed and speed-acceleration (1 trace and 20 traces) 156
Figure 72 – Transit bus time-speed and speed-acceleration (1 trace and 20 traces) 157
Figure 73 – Grade Impact in Population-Level and Vehicle-Level 161
Figure 74 – Grade Impact on Distribution and 97.5-percentile of Target Speed 163
Figure 75 – Mean of Accelerations by Grade 165
Figure 76 – Graphic expression of speed-acceleration model for vehicle i with Target Speed V_{target} = 40 mph (Acceleration Traces from 0 to 40 mph) 167
Figure 77 – Structure of Hierarchical Regression Acceleration Model 168
Figure 78 – MCMC Simulation Process 173
Figure 79 – Simulated σj of Acceleration Trace Model (0-40 mph) by Speed Piece 175
Figure 80 – Observed v.s. Estimated 0-40 mph Speed-Acceleration by Grade 181
Figure 81 – 2.5-Percentile (Extreme Deceleration) and 97.5-Percentile (Extreme Acceleration) of SAJD by Grade 183
Figure 82 – Acceleration Distribution by Speed and Grade in 0-40 mph Traces 184
Figure 83 – Acceleration mean distance (meter) and 95%-CI range 185
Figure 84 – Acceleration mean duration (second) and 95%-CI range 186
Figure 85 – Energy Consumption of Acceleration Traces 192
Figure 86 – $PM_{2.5}$ Emissions Rate in Acceleration Distances: Passenger Car 195
Figure 87 – $PM_{2.5}$ Emissions Rate in Acceleration Distances: Passenger Truck 196
Figure 88 – $PM_{2.5}$ Emissions Rate in Acceleration Distances: Transit Bus 197
Figure 89 – Emission Rate Differences (Scenario 3 – Scenario 1) by Distance 199
Figure 90 – Novel Acceleration Segment and Receptors Setup 201
Figure 91 – Concentrations (0.4 ug/m^3) Based on Accelerations and Paired Grades 203
Figure 92 – LDVs: Concentration Differences (0.4 ug/m^3) Compared to Scenario 1 206
Figure 93 – Bus: Concentration Differences (0.4 ug/m^3) Compared to Scenario 1 207
Figure 94 – Trajectories of LDVs and Buses Near Intersection 215
Figure 95 – LDV Trajectories, Grade, Duration, and PM2.5 Rates Near Intersection 217
Figure 96 – Bus Trajectories, Grade, Duration, and PM2.5 Rates near Intersection 218

LIST OF SYMBOLS AND ABBREVIATIONS

ARC	Atlanta Regional Commission
DEM	Digital Elevation Model
GHG	Greenhouse Gas
GPS	Global Positioning System
GRTA	Georgia Regional Transportation Authority
LiDAR	Light Detection and Ranging
MARTA	Metropolitan Atlanta Rapid Transit Authority
MOVES	MOtor Vehicle Emission Simulator
NAAQS	National Ambient Air Quality Standards
NHTSA	National Highway Traffic Safety Administration
OBD	On-Board Diagnostics
PACE	Partnership for an Advanced Computing Environment (PACE)
PEMS	Portable Emissions Measurement System
RMSE	Root Mean-Squared Error
SAJD	Speed-Acceleration Joint Distribution
SAGJD	Speed-Acceleration-Grade Joint Distribution
STP	Scaled Tractive Power (STP)
USEPA	U.S. Environmental Protection Agency
USGS	U.S. Geographic Survey
VSP	Vehicle Specific Power

SUMMARY

Road grade affects the vehicle engine operations. When the vehicle is moving uphill, the gravitational load acting against the vehicle increase engine load. In contrast, on a downhill road, the gravity assists vehicle motion and decreases engine load. Previous studies have reported that drivers are likely to, actively or passively, adjust their driving behavior as road grade changes, due to the limitation of engine capacity, sight distance, as well as driver's behavior and psychological status. Although grade is one of the key inputs in modeling vehicle energy consumption and emissions, in practice, grade has essentially been ignored in regional energy and emissions analyses due to the lack of available road grade data, and limited knowledge about the potential bias introduced by ignoring grade's impact on operations, energy consumption and emissions. Generating large-scale road grade data, appending grade information to vehicle operations, and understanding how road grade impacts vehicle operations are essential components of modeling vehicle power, energy consumption, and emissions.

The U.S. Geographic Survey (USGS) Digital Elevation Model (DEM) is used to generate grade data for the Atlanta freeways and arterial network. The dissertation develops a streamlined method to extract roadway elevation profile from DEM database, including elevation extraction, erroneous elevation detection and refill, and cubic smoothing spline to generate road grades at high-resolution. By comparing generated grade with field measurement, the method is able to develop highly-accurate road grade, with root mean-square error (RMSE) of estimated road grades at 0.2-0.23% for freeways and 0.5-0.6% for arterials. Considering that the DEM is open source and widely available

through the United States, there is great potential value in using the DEM to generate road grade in any region across the country.

With grade data available, the dissertation explores the impacts of road grade on vehicle speed and acceleration, and how the impacts interact with, and vary across: road classifications, traffic conditions, vehicle classes, and individual monitored vehicles. Multiple sources of second-by-second vehicle trajectories collected with Global Positioning System (GPS) devices are available to support the study, covering operations of light-duty vehicles, urban transit buses (operated mainly on arterials and local roads), and express buses (operated mainly on freeways). The generated road grades are appended to second-by-second GPS vehicle trajectories for analysis. Roadway geometry, vehicle configuration, and environmental information are also used as control variables.

Bayesian Hierarchical linear modeling is used to assess the overall grade impact on freeway speeds and accelerations, and heterogeneity of such impacts across vehicles (or drivers). Results of the analyses indicate that under uncongested conditions (average speed $\geq$ 55 mph), the majority of drivers tend to drive more gently with lower speeds and accelerations on segments with higher grades (towards uphill) than on segments with lower grades (towards downhill). Significant diversity is also observed in vehicle-level parameters across vehicles, where some drivers behave more sensitively to grade than others, with very few drivers behaving more aggressively on higher grades. For energy consumption and emissions modeling purposes, the speed and acceleration joint distribution (SAJD) is selected as the representative parameter for vehicle operating characteristics, as SAJD can be used as the direct input for energy consumption and emissions modeling. Analysis of the shape of SAJD indicates a drop of extreme

accelerations with increase of road grade; the impact is observed to be much more significant for express buses than light-duty vehicles. Such phenomena, however, are not as obvious under congested conditions on freeways, and a larger sample size may be required to confirm this relationship.

This dissertation also explores the impact of grade on vehicle operations on arterials. Acceleration traces starting from low speed (≤ 5 mph) is the focus in arterial analysis. In this study, acceleration traces are decomposed from trajectories, and grouped by target speed (or end speed) and grade level. Bayesian Hierarchical modeling is used again to estimate operating behavior of light-duty vehicles and transit buses across different groups of acceleration traces. Piecewise linear regression is built in to model grade impact on multiple speed pieces from the beginning to the end of acceleration traces. Model results indicate a large diversity of response across vehicles, but also shows a general decrease of average acceleration (or more gentle driving behavior) on higher grades. Also, grade impact is more significant on acceleration traces with a higher target speed, and in the middle range acceleration traces. In addition, due to the limited crawling capacity of heavy-duty vehicles, and perhaps bus driver behavior (for example, bus drivers may tend to drive more carefully when vehicle is crawling, especially when passengers standing in the corridor, or with disabled persons on the bus), traces of transit buses are much more sensitive to grade changes than light-duty vehicles.

The dissertation uses MOVES-Matrix for energy consumption and emissions modeling. Given a clear description of grade-operation relationship, comparative analysis is conducted to show the potential improvement of integrating grade and grade-operation correlation on the emissions result. Ignoring grade causes a significant under-estimation

of engine power, energy consumption, and emissions on uphill segments, and over-estimation on downhill segments. Additionally, because vehicle speed and acceleration distribution shows a less aggressive trend on higher grades, ignoring such negative correlation between operation and grade can cause over-estimate energy consumption and emissions on uphill segments, and under-estimate on downhill segments. The bias is larger for heavy-duty buses, given the stronger correlation between grade and operation observed.

The dissertation also applies EPA recommended dispersion model AERMOD to show the importance of modeling engine load by integrating grade and grade-operation correlation on near-road air quality modeling (or project-level hot-spot analysis). For dispersion modeling, integrating grade impact requires a more detailed strategy of road segmentation to classify links based on grade levels. Grade also impacts acceleration duration, distance, and emission distributions along acceleration distances. Hence, grade could be employed as a parameter in setting the length of acceleration segments in dispersion modeling near intersections.

From a technical perspective, results from this dissertation are expected to enhance the accuracy in energy consumption and emissions modeling from microscale to macroscale, with grade information available, and lead to a better understanding of grade interaction with vehicle operations. It also provides analytical results to potentially improve microscopic simulation models in modeling vehicle operations on regions with uneven terrain. Results also provide policy implications to potentially improve conformity and hot spot analyses, and lead to enhanced agency guidance on improved emissions modeling.

CHAPTER 1. INTRODUCTION

Motor vehicle emissions are a primary concern in cities as their potential contribution to local air pollution and effect on global atmospheric conditions. On-road vehicles, including cars, light trucks, and heavy-duty vehicles, also account for the majority of petroleum consumption in the United States.

To reduce Greenhouse Gas (GHG) emissions and improve fuel economy, The US Environmental Protection Agency (USEPA) and Department of Transportation's National Highway Traffic Safety Administration (NHTSA) issued final rules extending the National Program for vehicles model years 2017 through 2025 light-duty vehicles. The USEPA established national GHG emissions standards under the Clean Air Act (USEPA, 2012), and NHTSA established Corporate Average Fuel Economy (CAFE) standards under the Energy Policy and Conservation Act, as amended by the Energy Independence and Security Act (NHTSA, 2012). On the other hand, to reduce the air pollution of vehicle source, transportation conformity is required by the Clean Air Act section 176(c) (42 U.S.C. 7506(c)), to ensure that federal funding and approval are given to highway and transit projects that are consistent with ("conform to") the air quality goals established by a state air quality implementation plan (SIP) (USEPA, 2016a). Conformity, to the purpose of the SIP, means that transportation activities will not cause new air quality violations, worsen existing violations, or the delay attainment of the national ambient air quality standards (NAAQS) (USEPA, 2016b).

Quantifying energy consumption and emissions is the key step in identifying the major sources of air pollution, evaluating whether transportation activities are consistent

with air quality goals, and providing decision makers with a reference for implementation of new policies that maintain a sustainable development. A wide range of measurements is usually not feasible from both technical and cost perspective, due to the large amount and diversity of vehicle fleet compositions, complicated roadway networks, and dynamics of transportation operations.

Mathematical models are commonly used to estimate or predict vehicle energy and emissions. In an effort to improve the fidelity of energy and emission estimates, EPA released MOVES (MOtor Vehicle Emission Simulator), the approved regulatory model for estimating emissions from the vehicle fleet in the United States (USEPA, 2015). MOVES is required for use in all regulatory analyses for regional emissions inventory generation, including EPA greenhouse gas inventory sources and regulatory support. MOVES has also been used for local area emissions inventory generation, such as SIP, conformity analysis, and microscale emissions modeling, i.e., project-level environmental assessments and hot-spot analysis for conformity. The release of MOVES can help maintain consistency in energy consumption and emissions modeling processes for meaningful comparison between strategies and with standards.

Vehicle energy consumption and emissions are a function of vehicle characteristics, engine performance, environmental conditions, and operating conditions that influence engine load. Vehicle-specific power (VSP) for light-duty vehicles or scaled tractive power (STP) for heavy-duty vehicles are widely used in evaluation of engine load, and it is represented as a function of vehicle mass, vehicle dynamic parameters (rolling/drag coefficient), driving behavior (speed and acceleration), and road conditions (gravitational acceleration and road grade). In the MOVES model, speed and VSP (or

STP) levels directly relate to vehicle energy consumption and emission rates, due to their high statistical correlations in model development. The VSP/STP equation is shown below.

$$VSP_t\ (STP_t) = \left(\frac{A}{M}\right) v_t + \left(\frac{B}{M}\right) {v_t}^2 + \left(\frac{C}{M}\right) {v_t}^3 + \left(\frac{m}{M}\right)(a_t + g * \sin\theta_t)v_t \quad (1)$$

Where:

v_t = velocity at time t (m/sec)

a_t = acceleration at time t (m/sec^2)

θ_t = road grade

g = graviational acceleration ($9.81\ m/sec^2$)

m = vehicle mass (tonnes)

M = fixed mass factor for the source type (tonnes)

A = rolling resistance ($kW - sec/m$)

B = rotating resistance ($kW - sec^2/m^2$)

C = aeodynamic drag ($kW - sec^3/m^3$)

M in VSP = fixed mass factor (tonnes), used for light duty vehicles

M in STP = scaling factor from payload (tonnes), used for heavy duty vehicles.

Vehicle mass and dynamic parameters relate to vehicle configurations. Second-by-second speed and acceleration activity, VSP distributions, or detailed speed-acceleration joint distributions that reflect real-world operations are required for estimating engine power, and modeling vehicle energy consumption and emissions. Road grade is another critical variable that affects engine load, as vehicles must provide additional work against gravity when going uphill, and reduces required work from gravity when going downhill.

Real-world vehicle speeds and accelerations can be easily collected through Global Positioning System (GPS) devices and On-Board Diagnostics (OBD) devices. However, there is very limited attention that has been paid to the impact of real-world road grade on energy consumption and emission studies, regardless of the significant

effects on vehicle engine load, especially at hilly regions. In MOVES model, the effect of the road grade is ignored in national-level and regional-level (or county-level) modeling. Unless the second-by-second road grade is provided along with speed traces, grade is usually assumed as 0% even in project-level (or micro level), due to the lack of grade information, or the unawareness of significant impact. Additionally, road grade is expected to impact vehicle operations due to drivers' response of uphill and downhill driving, or vehicle performance. However, it remains unclear that how the vehicle operation varies across different road grade levels, and how the interaction of operation and road grade affect engine power, energy consumption, emission, and near-road air quality modeling (or hot-spot analysis). This dissertation aims at filling these research gaps through a series of studies.

The remainder of the chapter will introduce the objective and research tasks of this study, and outline the remaining chapters of the dissertation.

1.1 Research Objectives and Tasks

The dissertation aims at accomplishing the following four objectives:

1. Develop streamlined and straightforward method of generating large-scale road grade data based on open-source dataset, so that researchers can easily obtain the open-source data and implement in other regions
2. Explore road grade impact on vehicle operations, including speed and accelerations at freeways
3. Explore road grade impacts on vehicle accelerations at arterials

4. Explore the impact of integrating grade and complex grade-operation interactions on modeling of energy consumption and emissions.

The dissertation has identified six tasks to accomplish the objectives of this study. Details of each task is discussed its own section.

1. Develop a streamlined method to generate large-scale road grade data based on U.S. Geological Survey (USGS) Digital Elevation Model (DEM)
2. Append derived grade data onto monitored vehicle trajectories ("big data")
3. Build MOVES-Matrix for vehicle energy consumption and emissions modeling
4. Develop statistical model to explore road grade impact on vehicle operations at freeways
5. Identify grade impact on acceleration behavior at arterials
6. Examine the potential improvement of integrating grade, and grade-operation correlations, on predictions of energy consumption, emissions, and near-road air quality modeling for freeways and arterials

1.2 Develop Streamlined Method to Generate Large-scale Road Grade Data

The first goal of this research is to propose a method to obtain high-accuracy roadway grade data from the Digital Elevation Model (DEM), a nation-wide open source of digital cartographic/geographic dataset of elevations maintained by U.S. Geological Survey (USGS, 2016). Considering that the DEM is widely available across the United States and free of access, it is of great potential value in developing a streamlined grade generation method that researchers can easily follow. Large-scale grade data are valuable

for a variety of transportation and vehicle performance analyses, energy consumption and emissions modeling, and roadway design applications.

Although the USGS DEM data cover most of the nation, data resolution and the presence of roadway cut and fill sections affects spatial grade accuracy and requires a solid strategy to remove or infill these segments. Cubic smoothing spline is applied to minimize the impact of noisy data, and improve grade estimation accuracy. The selection of the key parameter λ in the spline method is also discussed to balance between smoothing out noisy elevation data, and retaining vertical fluctuations along the road. Using real-world measurements as ground truth, the relationship between optimum λ that minimizes root-mean-square error (RMSE) and road fluctuation is also explored to develop recommendations on λ selection. The results will demonstrate the validity and applicability of DEM in generating high-accuracy roadway grade data. The research integrates the method in the Georgia Tech Partnership for an Advanced Computing Environment (PACE) parallel computing cluster, and generate the elevation profile for the entire Atlanta network to support the following research tasks.

1.3 Append Derived Grade Data onto "Big Data" of Vehicle Trajectories

Second-by-second operations from a massive number of vehicles in Atlanta are available to be statistically representative for describing operating conditions. In this study, the operation data came from multiple sources, including:

1. 2011 Atlanta Household and Activity Travel Survey in a 20 County Region of Atlanta conducted by Atlanta Regional Commission (ARC), in which one week of

second-by-second trip traces for 1,653 light-duty vehicles in 911 households were recorded using in-vehicle GPS devices.

2. The cooperation with Metropolitan Atlanta Rapid Transit Authority (MARTA) in 2006 that collected 13 heavy-duty transit buses data by GPS devices mainly on non-freeways.
3. The cooperation with express bus agency - Georgia Regional Transportation Authority (GRTA) in 2014 that collected GPS data from 13 heavy-duty intercity express buses operating mainly on freeways.

Most of the GPS data listed above were collected within our Atlanta research area. A total of 344,181 vehicle-miles of operations were recorded. With large-scale of grade data and the Atlanta GIS road network shapefile available, this research develops an automatic procedure to extract trip route based on the matchup between GPS data and the GIS file, and append grade data from the route onto vehicle GPS trajectories. Georgia Tech PACE computing cluster is used again to finish this computationally intensive procedure. More details will be introduced in the corresponding section of Chapter 4. After this step, vehicle operations with paired grade data are available for statistical analysis and emissions modeling.

1.4 Build MOVES-Matrix for Energy Consumption and Emissions Modeling

This study employs MOVES-Matrix in vehicle energy consumption and emissions modeling. MOVES-Matrix is essentially a multi-dimensional array containing emission rate outputs from a huge number of MOVES model runs (Guensler, et al., 2016). The basic process is to run the MOVES model across all variables that affect

output emission rates: all vehicle source types, all model years, all on-road operating condition, a wide range of calendar year, other applicable regional regulatory parameters (fuel properties, inspection and maintenance program characteristics), and a wide range of temperature and humidity conditions. MOVES2014a was the latest version of MOVES model at the time this research was conducted. After conducting the MOVES runs, the resulting MOVES energy and emission rate matrix (MOVES-Matrix) can be queried to obtain the exact same energy and emission rates that are obtained from any individual MOVES model run.

In MOVES, energy rates and emission rates are modal in nature, representing emissions as a function of power surrogates, which depend on speed, acceleration, and road grade. MOVES models energy consumption and emission rates based on speed and VSP (STP) values. This mechanism allows MOVES to take second-by-second speed, acceleration, and grade data as activity input. MOVES-Matrix enables users to link emission rates to big data of operations, and evaluate changes in energy consumption and emissions due to the change of vehicle operation, grade setup, and other input of interests. Modeling with MOVES-Matrix is 200-times faster than using the MOVES graphic user interface in the same computer environment and predicts exactly the same emissions result (Guensler, et al., 2016).

1.5 Identify Grade Impact on Freeway Operations

One of the main objectives of this research is to understand how grade impacts vehicle operations on freeways, and how the impact varies across vehicles, vehicle types (light-duty vehicles versus heavy-duty buses), and traffic conditions (uncongested versus

congested). Vehicle trajectories from freeways are classified by average speed, indicating the traffic conditions in which the vehicle is involved in each trace. For each vehicle type, Bayesian Hierarchical regression is built to identify grade impact on speed, accelerations, and the impact heterogeneity across vehicles. Additionally, the study describes the shape speed-acceleration joint distribution in response to grades using extreme acceleration profile and skewness of acceleration distribution by speed bins. Results from this study can be used to better model energy consumption and emissions, by improving vehicle activity input at freeways segments with various grades. It also provides a reference to microscopic speed and acceleration choices model on hilly freeway.

1.6 Identify Grade Impact on Acceleration Mode at Arterials

Another objective of the research is to explore the grade impact on arterial operations. The study will mainly focus on the acceleration mode starting from low speed (≤5 mph), as higher engine load and hence higher energy consumption and emissions are involved in accelerations compared with other modes (cruising, deceleration, and idling). Acceleration traces are extracted from arterial trajectories and then grouped based on the target speed (final speed) of each trace. Statistical relationship between grade and speed-acceleration path are studied for light-duty vehicles and transit buses, including average acceleration at each speed bin, and the extreme acceleration values. With clear description of the correlation between grade and operations, we will be able to better estimate energy consumption and emissions especially in the intersections, where accelerations are frequently observed. Results of this study can also be used to improve microscopic acceleration models for arterial segments with grade integrated.

1.7 Examine Potential Improvement on Energy Consumption, Emissions, and Near-road Air Quality Modeling

From the literature, it is clear that grade is likely to impact onroad vehicle operations on freeways and arterials. For light-duty vehicles and heavy-duty buses, the study explores impact of integrating grade, as well as integrating grade-operation correlation on the modeling of energy consumption and emissions. Energy consumption and emissions will be estimated based on several scenarios for comparison purpose:

- Scenario 1: Observed vehicle activity and paired grade data are assessed as the baseline scenario (i.e., activity is based on speed-acceleration-grade joint distribution directly observed in vehicle trajectories);
- Scenario 2: Observed vehicle activity is assessed assuming that the grade on which the vehicles operated was zero (grade = 0%);
- Scenario 3: Observed vehicle operations and observed grade are assumed to be independent, i.e., a speed-acceleration-grade joint distribution is obtained for all operations and applied to grade distribution;

The comparison between Scenario 1 and Scenario 2 reflects impact of ignoring road grade on energy consumption and emission modeling. Comparison between Scenario 1 and Scenario 3 shows impact of not considering the correlation between grade and vehicle operation.

A freeway corridor in Atlanta is selected as a case study to explore the impact on near-road air quality modeling. Using AERMOD, emission rates of the above four scenarios are applied in the selected corridor, plus emission rates of using MOVES

default driving cycles, which is also a strategy commonly used by agencies (Kall, 2013). From these studies, we will obtain better knowledge on the how integrating grade as well as grade interaction with vehicle operations under different road types and traffic conditions will help improve energy and emission modeling by better describing vehicle activity. For accelerations on arterials, the study aligns acceleration traces by distance, explores spatial distribution of $PM_{2.5}$ concentrations along acceleration direction, and examines how grade impacts such distributions. The study can contribute in transportation conformity and hot-plot analysis from improving vehicle activity input.

1.8 Dissertation Outline

A review of relevant literature is outlined in Chapter 2. Including methods and data source that can be used to generate road grade. Chapter 2 summarizes studies of road grade impact on vehicle operation, road grade impact on energy consumption and emissions, and relationship between vehicle operation and energy consumption and emissions. Chapter 2 also introduces modal-based framework of energy and emission modeling, especially MOVES model. A summary follows in each section, in which research gaps are identified.

Chapter 3 describes in detail the methodology of generating road grade based on USGS DEM data, including the characteristics of DEM data. Data processing includes elevation extraction, data clean/infill, spline smoothing of elevation profiles, and grade derivation. Chapter 4 introduces data source used in the research, procedures for appending grade on GPS data, and MOVES-Matrix energy/emissions modeling techniques.

Studies of grade impact on freeway operations are introduced in Chapter 5, and studies of arterial acceleration impact are introduced in Chapter 7. The operation study results and discussions lend further insight on energy and emissions modeling. Following the operation impact studies, the impact of considering the grade-operation correlation in vehicle energy and emissions modeling on freeways and arterials intersections are shown respectively in Chapter 6 and Chapter 8. Summary of the study are stated at the end of each chapter. Chapter 9 concludes the entire dissertation research. It also outlines limitations of the current research, techniques for improving data quality, and directions for future research are presented.

CHAPTER 2. LITERATURE REVIEW

Chapter 2 provides a comprehensive literature review and introduces the definition of road grade. Several methods and data source that can be used to generate road grade have been identified. This chapter summarizes studies on road grade impact on vehicle operation, road grade impact on energy consumption and emissions, and impact of operation on energy consumption and emissions. It also reviews energy and emission modeling method embedded in MOVES model, which MOVES-Matrix that are used for emissions modeling in this dissertation. A summary is presented at the end of this chapter.

2.1 Road Grade

Road grade is quantified as the ratio of vertical rise (Δh) and horizontal run distance (d), and the ratio is expressed as positive for upgrade, and negative for downgrade. Figure 1 shows the gravitational force acting on the vehicle when driving on the slope. The force of gravity can be decomposed into the force perpendicular to the ground ($mg \cos\Theta$), and force parallel to the ground along the driving direction ($mg \sin\Theta$). When vehicle is driving uphill (Figure 1(a)), the component force of gravity is in opposite direction of the driving direction, and the engine must produce more work against gravity. In contrast, when vehicle is driving downhill (Figure 1(b)), as the decomposed gravity force is in the same direction of the driving direction, the engine can produce less work due to the contribution from gravity.

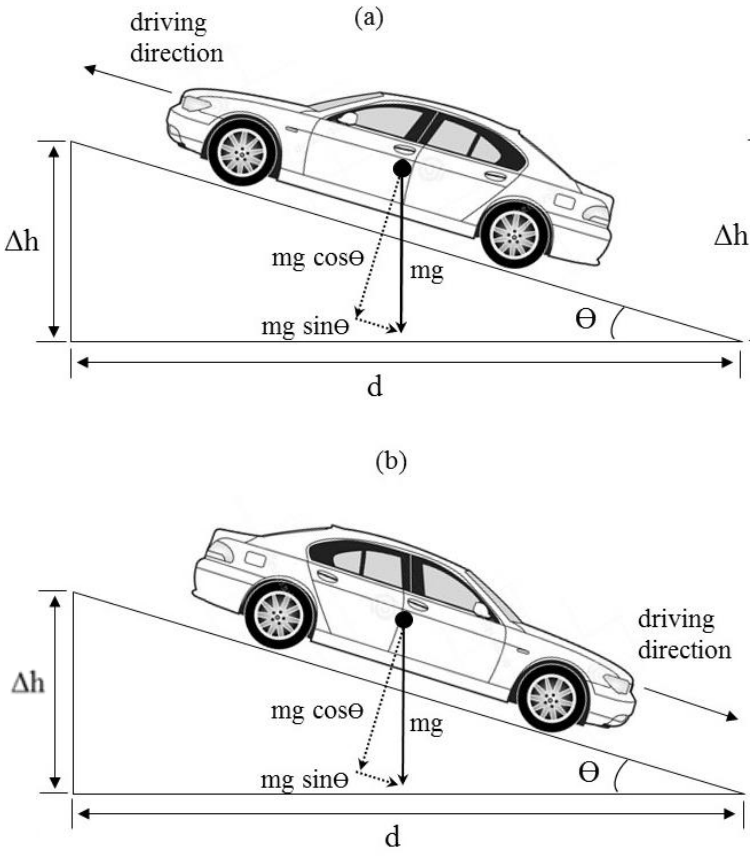

Figure 1 – Gravity Acting on Vehicle

Roadway grade is a valuable data source for a variety of transportation and vehicle performance analyses, and roadway design applications. The Highway Capacity Manual (TRB, 2010) provides truck speed performance in response to different road grade values, to reflect that the operating performance of heavy-duty vehicles is significantly reduced by steep grade and grade length. In addition, road grade significantly influences vehicle energy use and emissions, at both regional (Barth and Boriboonsomsin, 2009; Levin, et al., 2014; Wood et al., 2014a; Sentoff, et al., 2015; Zhu et al., 2016) and individual vehicle levels (Barth and Boriboonsomsin, 2009; Franzese and Davidson, 2011; Wyatt, et al., 2014; Wood et al., 2014a; Zhang et al., 2015).

Previous studies also show that crash rates on steep grade sections are significantly higher than for level sections (Glennon, 1987; Yu and Abdel-Aty, 2014). The research from Hamdar, et al., (2016) indicated that driver behavior is less influenced by weather conditions than roadway challenges, including vertical and horizontal changes.

2.2 Data and Method for Grade Generation

Road grade information can be obtained from measurements of vehicle on-board equipment, collection from road design drawings, or derivation from Light Detection and Ranging (LIDAR). Nowadays, there are elevation open data sources that can be used to generate grade.

2.2.1 Vehicle On-board Equipment

Road grade information can be measured using vehicle on-board equipment, including accelerometers (Ikwut-Ukwa, 2001; Bonnedahl, 2010), vehicle sensors (Sahlholm, et al., 2007), barometric altimeters (Parviainen, et al., 2009), and GPS (Awuah-Baffour et al., 1997; Bae, et al., 2001; Ogaja, 2011, Boroujeni, et al., 2013; Boroujeni and Frey, 2014). Figure 2 shows sample models of the equipment.

(a) (b) (c)

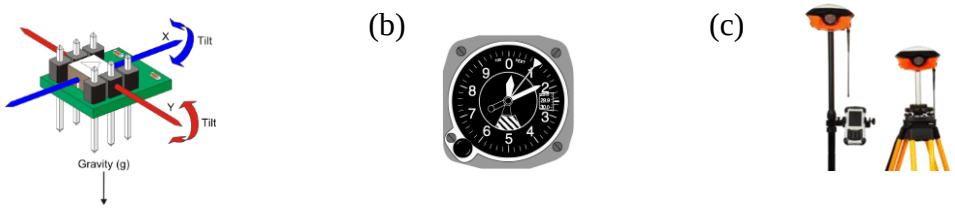

Figure 2 – Sample Models. (a): Accelerometer, (b): Barometer, (c): Differential GPS

Accelerometers installed in a vehicle can provide road slope data, but the measurement is noisy because vehicle acceleration and vibration associated with vehicle movement (unrelated to road grade) interfere with the readings (Rogers and Trayford, 1984). The barometric altimeter technique uses the relationship between atmospheric pressure and altitude to calculate elevation changes, and the road grade can be derived from the elevation profile (Xia et al., 2015), but the accuracy is questionable because the pressure values do not solely depend on the elevation (ambient temperature and pressure vary with meteorology in space and time).

GPS data loggers can also be used to measure location and elevation data (Boroujeni and Frey, 2014) although the resolution is relatively low. Vertical elevation errors from GPS are much larger than horizontal errors and can be negatively impacted by signal reflection from nearby buildings, trees, or bridges, (Awuah-Baffour et al., 1997; Wing, et al., 2005), or when satellite constellation changes (number and angle of satellites, which affect position calculation accuracy). Road grade is so sensitive to elevation changes that regular GPS loggers alone cannot meet the resolution requirement. Systems built for collecting road grade data usually combine GPS loggers with other equipment (i.e., sensors, barometric altimeter, or accelerometer), because GPS is more robust when recording horizontal positions (longitude and latitude) than the vertical position (altitude). For example, if sample size is large enough to ensure the precision, a GPS logger with barometric altimeter can effectively measure road grades (Boroujeni, Frey, and Sandhu, 2013). Other examples include the GPS-vehicle sensor systems (Sahlholm and Johansson, 2010), and the GPS-accelerometer system (Cheng, Wang and Tao, 2012). Although differential GPS (DGPS) can reduce common errors related to

satellite signals when using lower cost GPS loggers (Ogaja, 2011), the accuracy can still be affected by structures and tree canopy (Holden, et al., 2001) and DGPS is much more expensive than conventional GPS equipment. Despite the technical concerns, the main limitation of using on-board equipment for collecting road grade data is spatial coverage, given the cost and effort to collect such data for the large networks used in regional and national vehicle energy consumption and emission analysis.

2.2.2 Design Drawings

Road grades can be directly extracted from roadway design drawings. An example of road elevation profile with road grade is shown in Figure 3. However, design drawings are not easily obtained, and may only be available only for large road projects such as freeways, bridges, arterials, and interchanges. In addition, during roadway construction, grades may deviate from original design specifications in the pre-construction drawings due to the modifications or other possible implementation issues (Zhang and Frey, 2006). Sometimes, "as-built" drawings are prepared to reflect the final construction design, but these specifications also may not be precise.

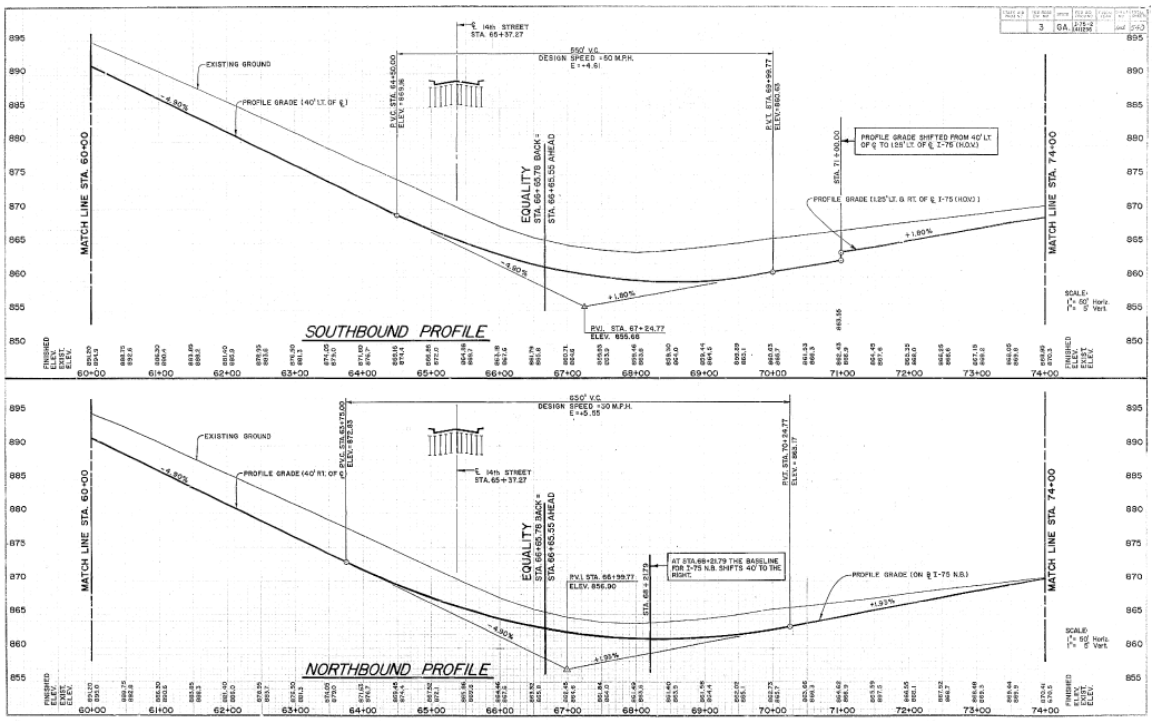

Figure 3 – Road Longitudinal Profile with Road Grades (GDOT, 2018)

2.2.3 Light Detection and Ranging (LiDAR)

Road grade data can also be collected through light detection and ranging (LiDAR) systems, using aircraft-mounted or on-road vehicle-mounted lasers to measure topographic data (Heywood, Cornelius and Carver, 2006). An example of elevation contour profile derived from high-resolution LiDAR is presented in Figure 4.

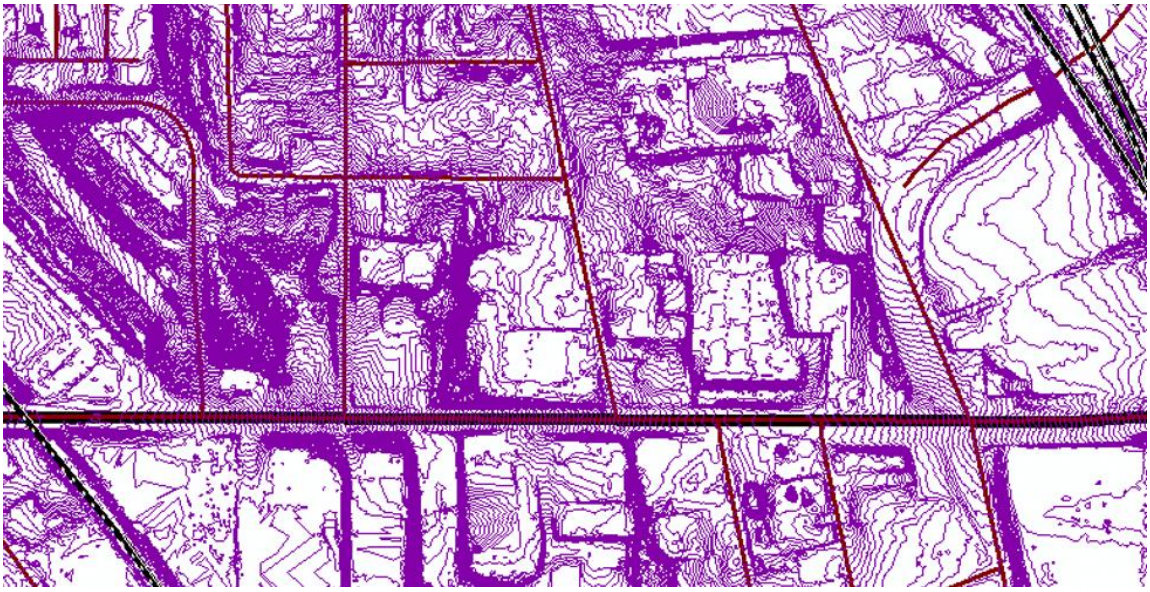

Figure 4 – Profile of Elevation Contour from LiDAR

LiDAR can provide accurate terrain profiles for estimating roadway grades on highways and arterials (Zhang and Frey, 2006). However, the cost is relatively high (Hummel et al, 2011), and the accuracy on local roads can be affected when trees block the signal, or when roads fly over railroad crossings rivers, and canyons (Wood et al., 2014a).

2.2.4 Open Source Elevation Data

Compared with the data collection methods listed above, several open-source elevation data sets are available at little, if any, cost. Many of these data sources have a wide-scale of spatial coverage, including Google® Elevation Data and the USGS DEM. For example, Zhu, et al., (2016) extracted elevation dataset through the Google Earth Application Platform Interface, and estimated the impact of grades on fuel consumption for the Interstate highway system in the United States. Li and Smith (2014) estimated road grades based on highway elevation data from Google® Earth, and modeled the impact of

road grades and curvature on truck driving. The USGS DEM is an elevation database constructed from their 3-Dimensional Elevation Program (3DEP) derived from LiDAR and interferometric synthetic aperture radar data (USGS, 2016).

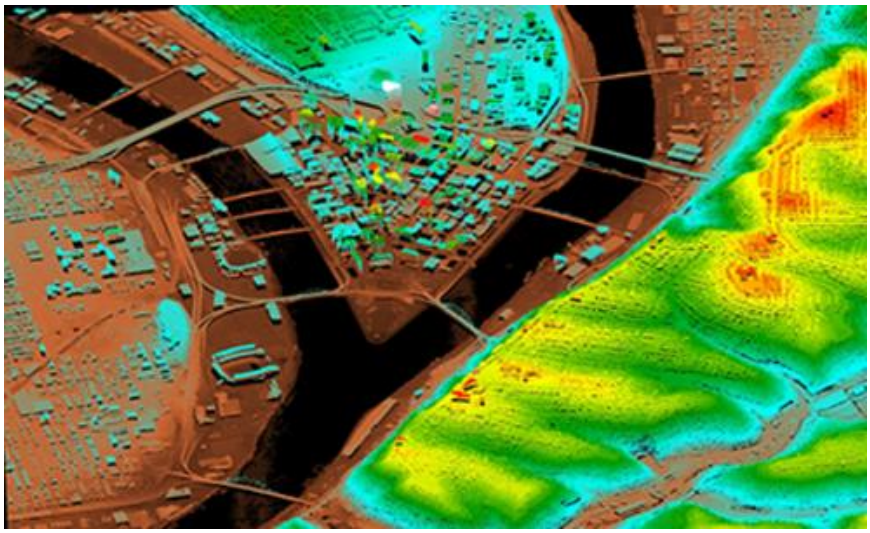

Figure 5 – USGS DEM Cloud Point in Pittsburgh

Several previous studies (Wood et al., 2014a; Sentoff, Aultman-Hall, and Holmen, 2015) joined DEM elevation data to GPS speed traces for energy and emission modeling. The research by Wood et al. (2014b) showed that the accuracy of roadway grades derived from the DEM is promising. Wood et al. (2015) compared DEM data with the TomTom® Advanced Driving Attributes (ADA) road grade data layer, collected using a combination of aggregated mobile terrestrial sensing data and advanced mobile terrestrial sensing data (TomTom International, 2013), and the Southwest Research Institute (SwRI) Mobile Autonomous Robotics Technology Initiative (MARTI) measurements, based on three-axis inertial measurement unit with multiple accelerometers and gyroscopes (Southwest Research Institute, 2014).

The DEM is likely to be one of the most attractive sources to estimate road grades because it is convenient to access, free of charge, and covers the entire United States (USGS, 2016). The dissertation will utilize DEM to generate road grade. However, until now, few studies have thoroughly discussed the detailed methodology of generating high-resolution roadway grade information from DEM that researchers can easily follow. Chapter 3 of the dissertation attempts to fill the gap, where more details on DEM data will also be introduced.

2.3 Impact of Road Grade on Vehicle Operation

Studies have shown that road grade significantly influences vehicle speeds, depending on vehicle and roadway characteristics. In the Geometric Design of Highway and Streets Guide published by AASHTO (AASHTO, 2001), although road grades affect passenger car drivers' practice, it is generally accepted that most of passenger cars can easily negotiate road grades as steep as 5% without a significant loss in speed. For heavy-duty vehicles, which include heavy-duty trucks and heavy-duty buses, the published speed effect of road grade is much more pronounced than for passenger cars. The truck speed performance in response to different road grades was provided in Highway Capacity Manual (TRB, 2010) as shown in Figure 6, indicating that the speed of heavy-duty vehicles depends on the magnitude of grade and grade length.

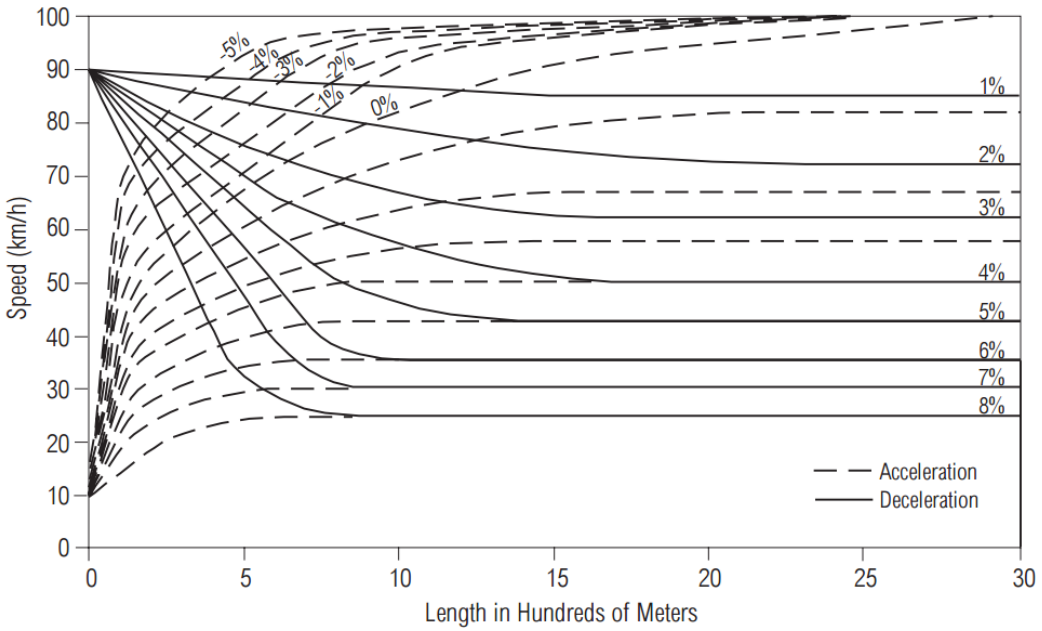

Figure 6 – Truck Acceleration/Deceleration Curves in Response of Road Grade (TRB, 2010)

Several studies have focused on modeling the impacts of road grade on truck operations. Li and Smith (2014) proposed a truck driver model for vehicle simulation to imitate actual driving behavior in negotiating road grade and curvature. The research selected Gipps model (Gipps, 1981) as the baseline driving model for this study, assuming the drivers will travel as close to their desired speed as possible and considering the dynamics limitations. In considering road grade and curvature simultaneously, an empirical adjustment factor for the desired speed is introduced as:

$$f_{road} = \left(1 - p_g \sin \varphi\right) \cos \omega \qquad (2)$$

Where p_g is driver-dependent parameter for the effect of road grade, φ is road grade, and ω is partial deflection angle. The proposed model performed well in predicting speed choices of one truck in negotiation of grade and curves. The study also suggested there is limited research in estimating acceleration behavior under impact of road grades. Since

vehicle the modeling of energy consumption and emission is sensitive to speed-acceleration profile, further studies on modeling the combined speed-acceleration behavior have become crucial.

Laval, et al., (2014) introduced a vehicle kinematics model, in which the authors justified a linear relationship between speed and acceleration in the desired acceleration model. The data in Figure 7 were collected during the acceleration process at signalized intersections, where vehicles were located as the leader of the platoon.

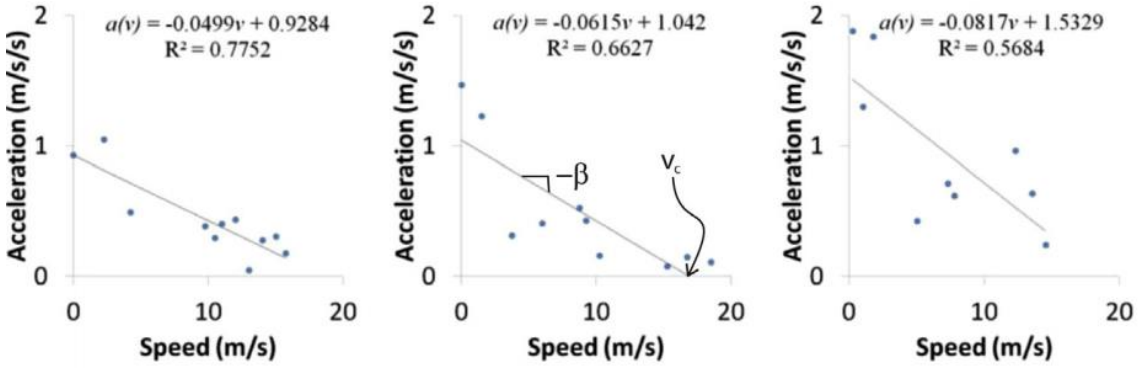

Figure 7 – Desired Acceleration Processes (Laval et al., 2014)

The crawling speed is then given by:

$$v(x) = u - gG(x)/\beta \quad (3)$$

Where u is the desired speed on a flat roadway, g = 9.81 m/s^2 is the acceleration of gravity. G(x) is the grade at location x. This relationship is appropriate given the assumption that drivers step on the gas pedal in the same extend on different grades. However, the assumption has not been validated yet; drivers may adjust the way they accelerate in negotiating grades.

Liu and Frey (2015) proposed the effective acceleration, or acceleration envelop of light-duty vehicles road grade. The relationship is given by:

$$\mathrm{acc}_e = \mathrm{acc} + 0.3566 \times \mathrm{G} \quad (4)$$

Where acc_e is the effective acceleration in km/h, acc is acceleration at 0 grade, and G is the grade. In Chapter 5 of the dissertation, larger sample size will be used to assess this proposed relationship, and explore whether the relationship varies across vehicle types (i.e., light-duty and heavy-duty vehicles) and speed levels.

2.4 Impact of Road Grade on Vehicle Energy Consumption and Emissions

Several studies have shown the significant impact of road grade on vehicle energy consumption and vehicle emissions for both microscale (Franzese and Davidson, 2011; Wyatt, et al., 2014; Wood, et al, 2014b) and macroscale levels (Levin, et al., 2014; Wood, et al., 2014b; Sentoff, et al., 2015; Zhu, 2016).

Researchers have documented grade impacts on energy and emissions at the microscale level. Wyatt, et al., (2014) generated road grade profiles based on LIDAR and Geographic Information System (GIS), and measured CO_2 emissions of a passenger car by Portable Emission Measurement System (PEMS). The results showed that in modeling microscale vehicle emissions, failing to consider road grade could result in highly inaccurate estimates of real-world emissions, even it is a relatively modest terrain. Wood et al., (2014a) estimated that at the trip level, the grade energy consumption penalty shows a roughly linear relationship with average road grade. Even for trips with zero average elevation change, energy use can be significantly impacted (-5% to 23%) by road grade distributions, as shown in Figure 8.

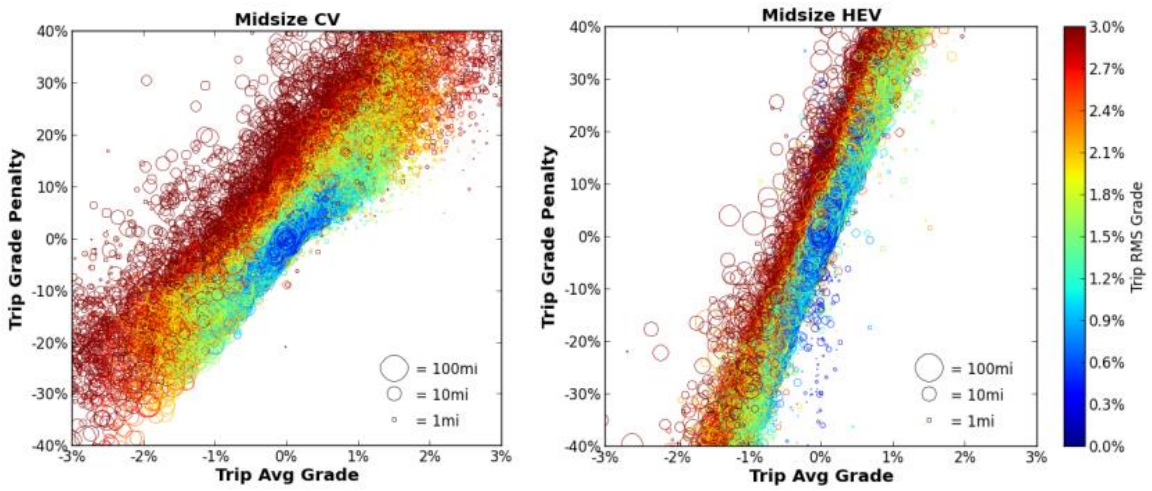

Figure 8 – Sensitivity of Trip Percent Energy Increase to Average Grade and RMSE Grade for Conventional Vehicle (CV) and Hybrid Electric Vehicle (HEV) (Wood et al., 2014a)

At the macroscale level, it is incorrect to assume that the increase in energy use and emissions on uphill sections is completely offset by the decrease in energy use and emissions on paired downhill sections. Levin et al., (2014) estimated the citywide road grade impact of energy consumption by incorporating a mathematical model of energy consumption within a dynamic traffic assignment (DTA) model. They found that ignoring grade under-predicts energy consumption by 10.5% in Austin and 3.6% in Nicosia. Wood et al., (2014b) selected a large dataset of real-world vehicle drive cycles collected via GPS in 10 cities, appended road grade values to cycle data via a filtered DEM, and simulated the dataset over the vehicle models to examine the incremental impacts of road grade on energy consumption. The results indicated that, in city-wide, light-duty vehicles experienced approximately 1% to 3% average energy consumption penalty as a result of including road grade in the simulation. Also, the conventional vehicles experienced larger grade penalties (25% to 73% greater) than their hybrid and electric vehicle counterparts, which is assumed to result from the benefits of the

regenerative braking systems, especially when decelerating on a downhill grade and recapturing energy that would otherwise be lost as heat during conventional braking for conventional vehicles. Sentoff, et al., (2015) collected 2.5 million 1 Hz records of real-world vehicle operating data from 82 Volunteer drivers with OBD and GPS loggers equipped in passenger cars and passenger trucks, an appended with road elevation data based the Vermont road elevation database from DEM. They demonstrated that omission of the road grade in the VSP calculation resulted in overestimating the amount of operating time in the mid-range MOVES operating mode bins and underestimating time in both the operating modes that are related with high or low emissions, which ended up with a large amount of misallocation of VSP bin assignment. This misallocation translated to emission error of 10-48%. Zhu, et al., (2016) estimated the impact of road grade on fuel consumption for national interstate highway system using the Comprehensive Modal Emissions Model (CMEM). From their aggregated statistical analysis, at the interstate level, high energy consumption and energy loss correspond to regions with large terrain variations. The braking energy loss and idling energy loss represented less than 5% of the total energy consumption.

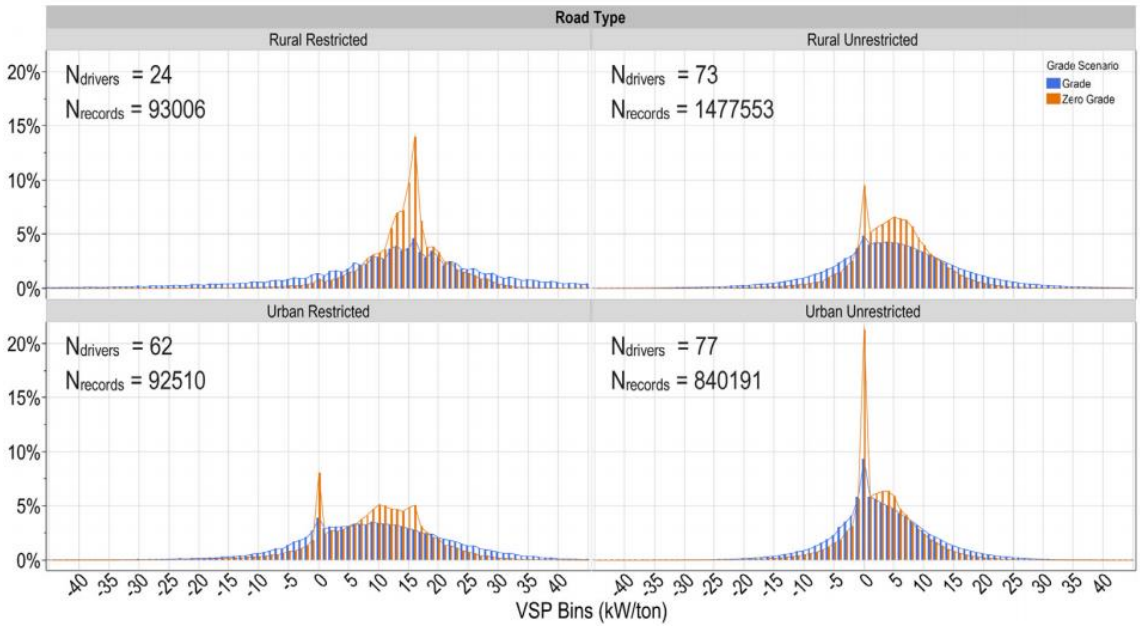

Figure 9 – Change in Operating Mode Distributions With and Without Grade (Sentoff et al., 2015)

Despite all of the relevant research described above, modelers continue to ignore road grade in emissions modeling, mainly due to the lack of grade data, and perhaps because they remain unaware of the significant bias that ignoring grade may cause in their specific research. In the MOVES model, the national-level and regional-level analysis do not provide grade input as an option, and grade is assumed to be zero, which causes non-negligible errors in hilly regions such as Atlanta or San Francisco.

2.5 Impact of Vehicle Operation on Energy Consumption and Emissions

Numerous studies indicate that driving behavior is an important factor affecting vehicle energy consumption and emissions, and this is especially true for acceleration behavior, considering its high proportion of the total operation time (Barlow et al., 2009) and associated high fuel rate in urban area (Ying, 2012). Sivak et al., (2011) investigated

the potential effect of driving decisions and behaviors on fuel economy of light-duty vehicles, and they found that avoiding aggressive driving could reach an increase of fuel economy by as much as 25%, which is consistent with the results from Thitipatanapong and Luangnarutai (2014). Gonder et al. (2012) compared fuel differences of driving trials with different driving style, and the driving differences could result in 30% of fuel consumption differences in urban driving cycles, and 20% in highway cycles.

Considering the potential benefit from the change of driving behavior, eco-driving training becomes a cost-effective way to reduce fuel consumption and emissions. Numerous studies have evaluated the benefits of driving behavior improvement through real-world implementation, through simulated vehicle activity data, or a combination of implementation and simulation. In real-world demonstrations, observed eco-driving fuel savings range from 2% to 14% (Barth and Boriboonsomsin, 2009; Beusen, et al., 2009; Dib, et al., 2014; Ho, et al., 2015; Rutty, et al., 2013; Strömberg and Karlsson, 2013; Wåhlberg, 2007; Zarkadoula, et al., 2007).

2.6 Energy Consumption/Emissions Modeling and MOVES Model

The modeling of vehicle energy and emissions are composed of three modules: vehicle population, vehicle activity, and emission rates associated with vehicle and activity. Vehicle population includes the number of vehicles by each vehicle type and model year. Vehicle activity describes the miles or hours of vehicle operation at each traffic level (usually speed level) and facility type, including grades. Emission rates are emissions per unit distance or time for each vehicle type, model year, and under each operation condition. Figure 10 presents the framework for on-road vehicle energy and

emission modeling. Almost all state-of-art models commonly used, including MOVES (U.S. EPA, 2015), EMFAC (CARB, 2016), and COPERT (EMISIA, 2016) follow this basic structure. The differences across the models are mainly reflected in the design within each module, the way that the modules connect, and the emission rates they employ.

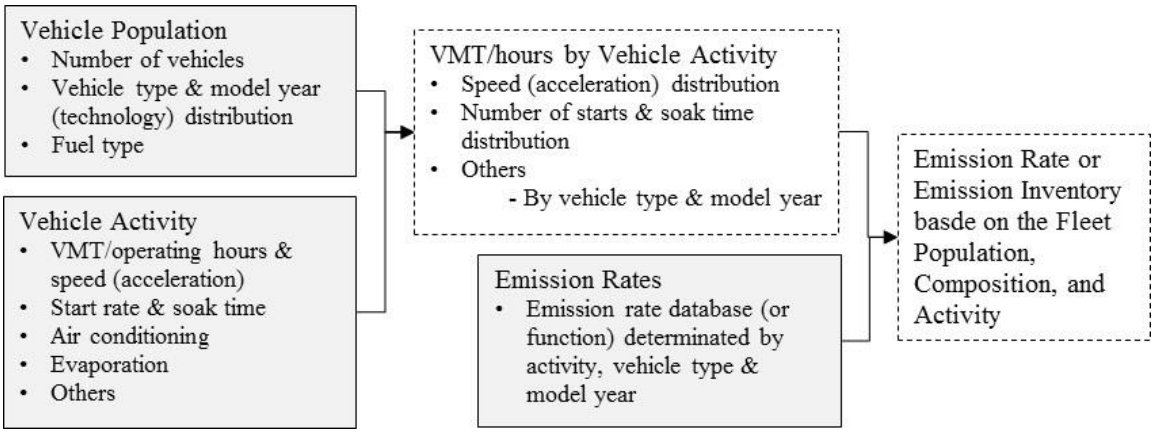

Figure 10 – Emission Modeling Framework

EMFAC and COPERT define emissions as a function of average speed, irrespective of acceleration. In the MOVES model, emissions are defined as a function of speed and vehicle-specific power (VSP) for light-duty vehicles, and scaled tractive power (STP) for heavy-duty vehicles, which better reflects acceleration and impacts on engine load. As mentioned previously, VSP and STP are a function of vehicle mass, dynamic parameters, speed, acceleration, and grade. Instantaneous VSP and STP are calculated as presented earlier in equation (1). In general, higher speed, higher acceleration, and higher grade corresponds to higher VSP or STP values.

MOVES employs a binning approach to emissions modeling, such that higher VSP and STP values within specific operating speed bins are linked to higher energy

consumption, greenhouse gas emissions, and criteria pollutant emissions. Operating mode bins are established by operation (braking, idle, and cruise-acceleration), by average speed group for cruise-acceleration, and then by VSP or STP range for cruise-acceleration within each average speed group. Table 1 listed the description and definition of each operating mode bin in MOVES.

Table 1 – MOVES VSP/STP Operating Mode Bins

Operating Mode ID	Operating Mode Description	VSP/STP (VSP_t, kW/tonne)	Speed (v_t, mph)	Acceleration (a, mph/sec)
0	Deceleration/Braking			$a_t \leq -2.0$ or ($a_t < -1$ & $a_{t-1} < -1$ & $a_{t-2} < -1$)
1	Idle		$-1 \leq v_t < 1$	Any
11	Coast	$VSP_t < 0$	$0 \leq v_t < 25$	Any
12	Cruise/Acceleration	$0 \leq VSP_t < 3$	$0 \leq v_t < 25$	Any
13	Cruise/Acceleration	$3 \leq VSP_t < 6$	$0 \leq v_t < 25$	Any
14	Cruise/Acceleration	$6 \leq VSP_t < 9$	$0 \leq v_t < 25$	Any
15	Cruise/Acceleration	$9 \leq VSP_t < 12$	$0 \leq v_t < 25$	Any
16	Cruise/Acceleration	$12 \leq VSP_t$	$0 \leq v_t < 25$	Any
21	Coast	$VSP_t < 0$	$25 \leq v_t < 50$	Any
22	Cruise/Acceleration	$0 \leq VSP_t < 3$	$25 \leq v_t < 50$	Any
23	Cruise/Acceleration	$3 \leq VSP_t < 6$	$25 \leq v_t < 50$	Any
24	Cruise/Acceleration	$6 \leq VSP_t < 9$	$25 \leq v_t < 50$	Any
25	Cruise/Acceleration	$9 \leq VSP_t < 12$	$25 \leq v_t < 50$	Any
27	Cruise/Acceleration	$12 \leq VSP_t < 18$	$25 \leq v_t < 50$	Any
28	Cruise/Acceleration	$18 \leq VSP_t < 24$	$25 \leq v_t < 50$	Any
29	Cruise/Acceleration	$24 \leq VSP_t < 30$	$25 \leq v_t < 50$	Any
30	Cruise/Acceleration	$30 \leq VSP_t$	$25 \leq v_t < 50$	Any
33	Cruise/Acceleration	$VSP_t < 6$	$50 \leq v_t$	Any
35	Cruise/Acceleration	$6 \leq VSP_t < 12$	$50 \leq v_t$	Any
37	Cruise/Acceleration	$12 \leq VSP_t < 18$	$50 \leq v_t$	Any
38	Cruise/Acceleration	$18 \leq VSP_t < 24$	$50 \leq v_t$	Any
39	Cruise/Acceleration	$24 \leq VSP_t < 30$	$50 \leq v_t$	Any
40	Cruise/Acceleration	$30 \leq VSP_t$	$50 \leq v_t$	Any

Figure 11 below presents an example of CO_2 emission rate for model year (MY) 2016 passenger truck of each operating mode bin (defined by speed and VSP ranges) extracted from MOVES. High speeds, moderate accelerations at high speed, and hard accelerations at moderate or high speed will push on-road activity into higher VSP bins, which are associated with higher fuel consumption and emission rates.

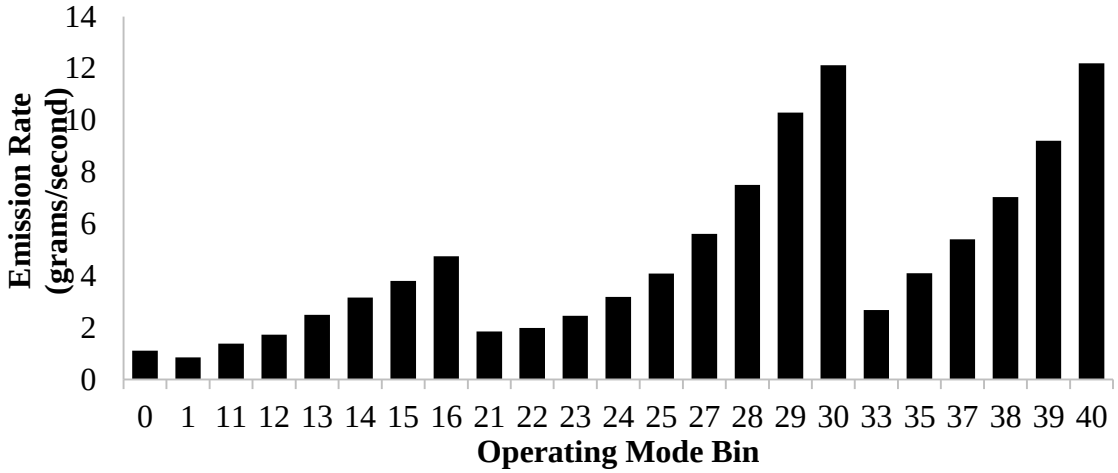

Figure 11 – CO_2 Emission Rates by OpMode Bin for Passenger Trucks (MY2016 in Calendar Year 2016)

In MOVES, driving cycles (speed-acceleration) and paired road grade are used to calculate VSP, allowing driving cycles to be decomposed into operating mode bins and modeled as a function of time spent operating in each bin. MOVES includes an energy and emission database with base emission rates for each pollutant under each operating mode bin, for each vehicle regulatory class, model year from 1960 and project to 2050, and at each model year. Hence, emission rates and vehicle activity are connected through these operating mode bins. Figure 12 summarizes MOVES data processing. Through internal calculations, emission rates are weighted by operating mode distribution, and adjusted for air conditioning, fuel specification, inspection/maintenance (I/M), and

meteorology factors, and then aggregated by using vehicle type composition and vehicle mileage data to obtain comprehensive fleet emission rate and emission inventory. This innovative design enables MOVES to provide common emission rates for all modeling scales (macroscale, mesoscale, and microscale). MOVES model is capable of using self-defined driving cycle and allows users to incorporate local vehicle operation by importing local driving cycles and operating mode distributions directly.

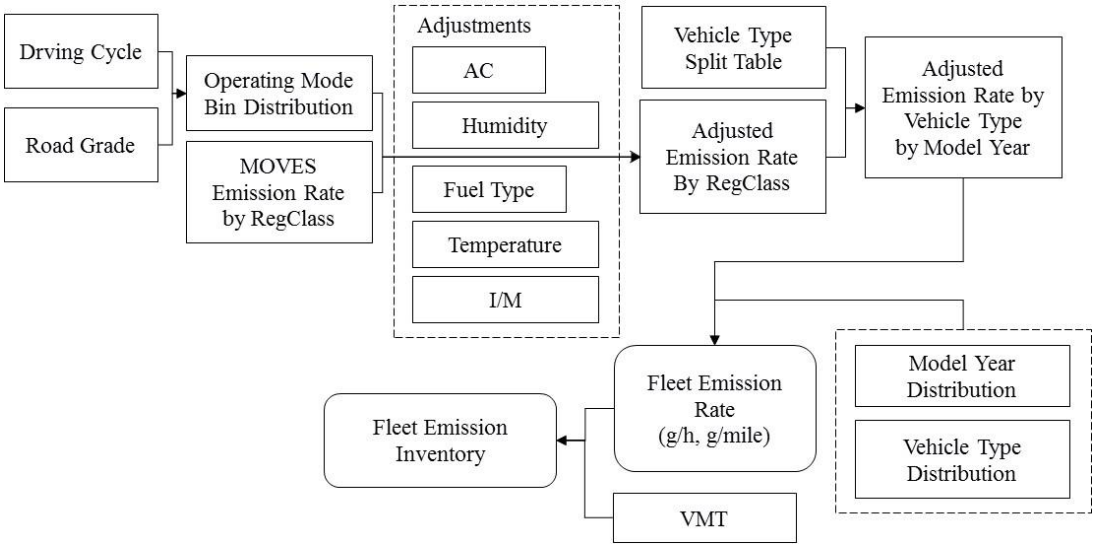

Figure 12 – MOVES Data Processing in Project-Level

The latest MOVES model was developed from laboratory and field data collected via a number of advanced methods. Portable emissions monitoring systems (PEMS) collect instantaneous exhaust emission rate data for HC, CO, NOx, PM, toxics, and greenhouse gases, and global positioning system (GPS) data, that allow analysts to link on-road emission measurements with the location and speed of the vehicle. On-Board Diagnostics systems (OBD) also provide concurrent engine and vehicle operation information. Grade is another critical variable required for estimating vehicle specific power in emissions modeling. However, road grade information has always been a

challenge to obtain, especially at a large spatial scale, due to the lack of consistent data sources and methods to process these data. Thus, road grade is typically omitted from most analyses. For example, in MOVES model, road grade is assumed to equal zero when analyses are conducted at the national and regional-level. This is because road grade data were either not collected or were not paired with real-world vehicle second-by-second driving data (Sentoff, Aultman-Hall, and Holmen, 2015).

In the most regions of United States, regulations require that the latest approved regulatory model (i.e., MOVES 2014a) be used in all transportation and air quality planning and assessment work (U.S. EPA, 2015). However, the MOVES interface makes it difficult to assess complicated transportation networks and to undertake analyses of "big data" of vehicle operations. To improve modeling efficiency, but at the same time ensure that regulatory requirements for use of MOVES are met, the Georgia Tech team developed MOVES-Matrix (Guensler et al., 2016). The MOVES model was run hundreds of thousands of times to generate an emission rate matrix for all combinations of MOVES input variables. The MOVES-Matrix emission rates described in this paper can be queried for any analytical purpose that can be conducted by MOVES, without ever having to launch MOVES or transfer MOVES modeling output files into the analyses.

The Georgia Tech team has successfully implemented MOVES-Matrix into various emission modeling research, including emission impact of HOV-HOT conversion (Xu, et al., 2014), transit eco-driving (Xu et al., 2016a), emission benefit of transit deadheading reduction (Li, et al., 2016), MOVES sensitivity analysis (Liu et al., 2015), and connection applications with travel demand model (Xu, et al., 2018; Xu, et al. 2016b) and Vissim® model (Xu et al., 2016c). From those applications, the results from

MOVES-Matrix were consistent with using MOVES model. MOVES-Matrix will be used through the dissertation for energy consumption and emissions modeling. More details on MOVES-Matrix modeling method will be presented in Chapter 4.

2.7 Summary of Literature Review

Aside from a few studies that rely on grade data collected using on-board equipment, road design drawings, and local LiDAR data, little research has incorporated grade into energy and emissions modeling, mainly because of the challenges from data availability and a lack of easy-to-implement grade generation methods. It is difficult to obtain grade data for large-scale road network, not to mention maintain computing support for large-scale energy consumption modeling and emissions analysis.

Most of the research conducted to date has separately analyzed road grade effects on vehicle energy and emissions, road grade effects on vehicle speed, or vehicle operation effects on vehicle energy and emissions. Despite the fact that research has found that grade significantly influences energy and emissions (i.e., uphill and downhill grade effects do not cancel each other out) modelers continue to ignore road grade in regional and project-level emissions modeling. This is perhaps because grade data are not widely available, grade data are difficult to integrate into modeling efforts, and there is some concern that interaction effects between grade, operations, and energy/emissions require more exploration. Most studies have assessed the impacts of grade on operations, or have assessed the impacts of grade on driving cycle apportionment into VSP bins for emissions modeling, but studies have not conducted both assessment efforts together to see how fleet operations differ on grades and how these operations affect energy use and

emissions. Additionally, no studies have explored how grade-operation correlation varies across road types, traffic conditions, and vehicle types. Without large scale data support, including operation data and paired grade data, it is difficult to conclude with any certainty that how large these impacts will be.

CHAPTER 3. GRADE GENERATION USING THE USGS DEM

This chapter explores the use of the U.S. Geological Survey (USGS) Digital Elevation Model (DEM), a publicly-available, open-source elevation database that covers the entire United States (USGS, 2016), to estimate road grade. Because of its wide coverage, the DEM has the potential to generate road grade estimates at various scales, and be used to append the grade information onto vehicle GPS trajectories to analyze the influence of grade on vehicle activity, vehicle crashes, energy use, and emissions from macroscale to microscale analysis.

This section provides an introduction to USGS DEM data. Later, the methodology for generating road grades using DEM data is presented. The procedures include elevation extraction from DEM, cleaning and infilling to replace erroneous elevation data, smoothing noisy data with the cubic spline method, and using distance-elevation derivation to generate road grade. The performance of the method is assessed by comparing results to field-collected road grade measurements. The selection of a key parameter λ in the cubic spline method used for data smoothing is also discussed to properly balance the smoothing of noisy elevation data versus maintaining the accuracy of vertical fluctuations along the road.

3.1 DEM Data

The USGS Digital Elevation Model (DEM) is a digital cartographic/geographic dataset of LiDAR elevation readings. The terrain elevations for ground positions are sampled at regularly-spaced horizontal intervals. The DEM contains data at multiple

resolutions, providing single-point elevation values assigned to the center of each cell in a grid. Grid sizes range from 100×100 feet (30×30 meter, 1 arc-second, the lowest resolution), 30×30 feet (10×10 meter, 1/3 arc-second), 10×10 feet (3×3 meter, 1/9 arc-second), to 3×3 feet (1×1 meter, 1/27 arc-second, the highest resolution). Elevations are pixel-centered in raster datasets, representing the value at the center of each cell (Gesch, et al., 2014). Figure 13 represents the layout of USGS DEM coverage in the United States with the highest available resolution. Currently, DEM data at the 10×10 meter resolution level is the most refined dataset that covers almost the entire United States (except Alaska). The 1×1 meter resolution data are available for less than 5% of the country, and 3×3 meter resolution data are available for about 25% of the country. Part of Alaska currently has DEM data at the 30×30 meter resolution level, but 5×5 meter will eventually become the highest-resolution elevation dataset across Alaska (USGS, 2016). The USGS is continuously expanding the coverage of elevation data at 1×1 meter resolution, and a dataset with national coverage at this high resolution will be ultimately be supported (Sugarbaker et al., 2014; Wood et al., 2015).

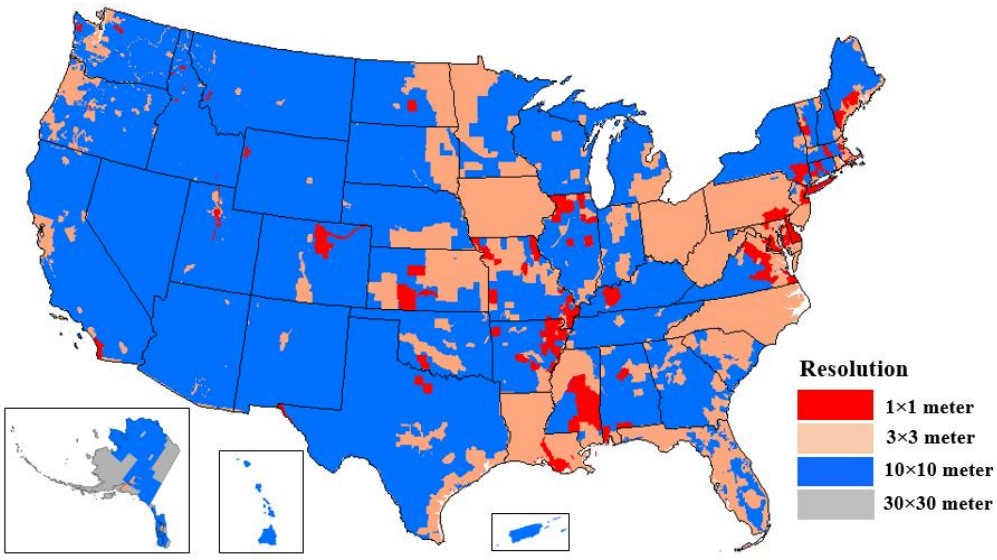

Figure 13 – The United States Elevation Map Produced using the USGS DEM

Figure 14 gives an example of the I-75 and I-85 interchange in Atlanta, Georgia, shown in Google® Satellite, Google® StreetView, and the USGS elevation map at 10×10 meter resolution. In the elevation map, the freeway profile can be recognized based on the color scheme, reflecting elevation changes between the freeway surface and its surroundings. According to Gesch, et al. (2014), overall absolute vertical accuracy of 10×10 meter USGS DEM data is approximately 1.55 meters root-mean-square error (RMSE). The vertical accuracy of 3×3 meter and 1×1 meter data has not been reported in the literature, but it is reasonable to assume they achieve a higher accuracy than 10×10 meter data. Even with an average elevation error of 1.55 meters, these data are still be useful for road grade estimation, because it is the accuracy of the change in elevation (or relative error) that matters. In this study, DEM datasets at 1×1 meter, 3×3 meter, and 10×10 meter resolution are assessed for use in road grade generation. As shown earlier in Figure 13, the combination of the three datasets covers most of the regions in the United States.

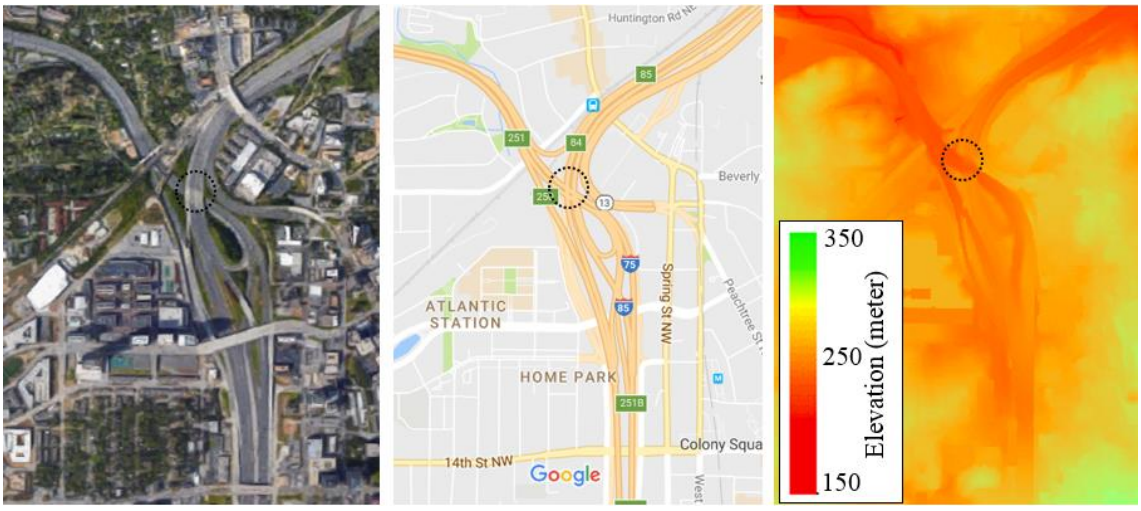

Figure 14 – Google® Satellite Layer, Google® Street, and USGS Elevation Map (3×3 Meter Resolution) of I-75 and I-85 Interchange in Atlanta, Georgia, USA

Elevation data need to be extracted from the DEM along the direction of each roadway. In doing so, it is important to identify the specific roadway locations where elevation data will need to be extracted from the DEM. The nationwide GIS roadway data across the United States are publicly available from the Topologically Integrated Geographic Encoding and Reference (TIGER) system (US Census, 2017). The GIS network contains roadway characteristics such as geographic locations, road type (i.e., freeway and local), distance, etc. The GIS roadway network centerline file for Atlanta was obtained from the Atlanta Region Commission (ARC).

3.2 Methodology

This section describes the process for extracting and processing elevation values from DEM. The methodology includes: 1) the generation of a point layer along GIS road centerlines, to which DEM elevations are appended to each point; 2) data cleaning, to remove erroneous elevation data and to infill data for roadway bridges that span the unrealistic elevation drops caused by the presence of canyons, rivers, underpasses, etc.; 3) the application of cubic spline smoothing, to reduce noisy elevation data (given that road surfaces are actually smooth by design); and 4) the calculation of grade as the derivative of elevation data over the roadway distance. A process flow diagram is illustrated in Figure 3, and each step is described in more detail later in this section.

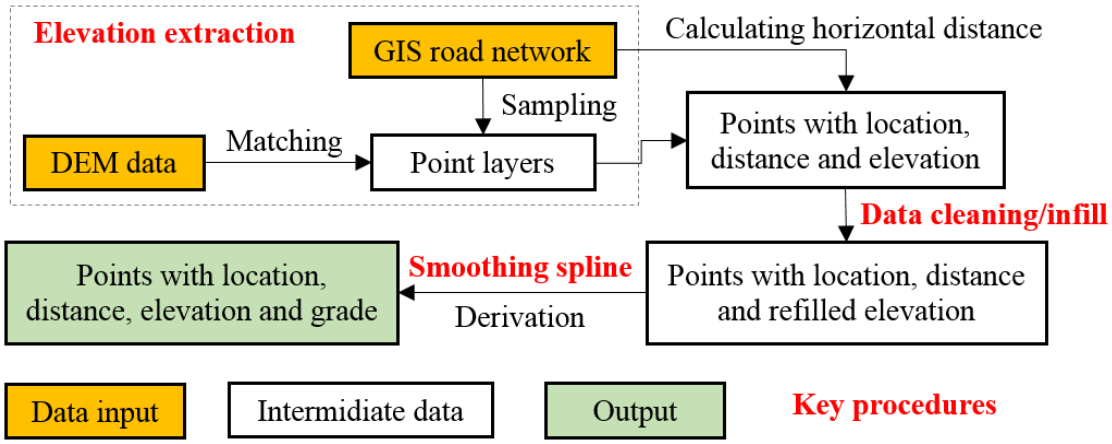

Figure 15 – Data Flowchart of Road Grade Generation

In general, at least four factors can cause bias or errors of road grade estimation:

1. The absolute elevation deviation from DEM due to LiDAR measurement error.
2. Similar to other LiDAR sources, since USGS DEM is a "bare-earth" dataset and returns the lowest elevation at a given point; hence, the DEM elevation has the same accuracy issue as other LiDAR data, and may not reflect the true road elevation when tree canopies block signals, or when bridges pass over railroad crossings, rivers, and canyons.
3. Roadway link and node positions in the roadway network may be inaccurate, resulting in alignment error, or nodes may be of insufficient density in the GIS roadway centerline shapefile and inaccurately represent roadway centerlines (Hong, et al., 2013), especially for curved roads.
4. The elevation value in the DEM raster data reflects the elevation at the center point of a DEM raster grid; however, the center point may not fall on the roadway centerline.

The influence of the first two factors (LiDAR measurement error and bare-earth issues) can be eliminated by setting proper criteria for elevation data cleaning, and applying a spline smoothing technique as will be discussed in the following sections. Errors resulting from the use of inaccurate roadway centerline data (the third factor above) can be minimized by using GIS data that best represent the horizontal alignment of the real-world roadways and by assigning a proper projection coordination system. It is important to mention that some GIS network files used for travel demand modeling are too simplified to reflect correct geometry alignment. Errors associated with raster resolution (the fourth factor above) can be very large in low resolution DEM data (i.e., larger raster cell), and this is discussed in more detail in the next section.

3.2.1 Elevation Extraction

Roadway elevation is represented by its sampling points' elevation, extracted from the elevation values of its corresponding DEM raster grids. Two methods are proposed to create roadway sampling points, i.e. pre-sampling and post-sampling.

3.2.1.1 Pre-sampling Method

The pre-sampling method for extracting DEM elevation data and assigning elevation values to roadway segments generates initial elevation sampling points at a fixed frequency along roadways, as shown in Figure 16a. For each sample point, the method assigns the elevation value of the DEM grid into which that sample point falls, as shown in Figure 16b and 4c. The interval of generating sampling points ($\mathbf{d_f}$) needs to be properly determined. If the interval is too short, consecutive sampling points may fall into the same cell, yielding duplicate elevation data at adjacent data points, creating a

noisy elevation profile, and increasing computational efforts (proportional to sample size). To avoid this issue, the interval should be wider than the length of the DEM grid, shown as $\mathbf{d_r}$ in Figure 16. However, if the interval is too long, it may fail to catch necessary details of the road elevation profile. After conducting a series of sensitivity analysis, a 10-meter sampling interval along the roadway length was found to perform well when using DEM data at 1×1 meter or 3×3 meter resolution levels, and thus $\mathbf{d_f}$ is set to 10 meters in this study. In this pre-sampling method, if the DEM cell is small, the elevation at the center of the DEM raster cell can be used as an approximate value along the centerline of the road. However, when using 10×10 meter DEM data, the pre-sampling method causes significant errors because the center points of DEM grids can be far from the roadway centerline. To deal with this potential issue, a Post-sampling method is discussed in the next section.

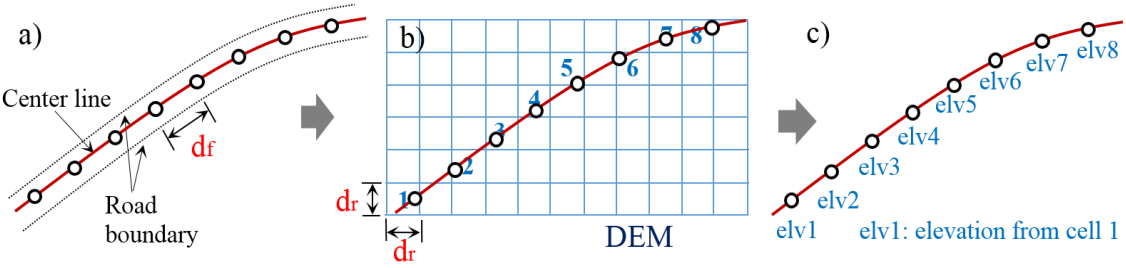

Figure 16 – Pre-sample Method

3.2.1.2 Post-sampling Method

The post-sampling method uses center points of DEM grids to segment roadway centerlines and then generates sampling points based on segment vertices. The two main steps are:

1. Create a buffer along the road centerline with width $\mathbf{d_b}$, and identify the DEM grids whose center points fall into the buffer shown in Figure 17a). Ideally, $\mathbf{d_b}$ is set as road pavement width so that it can cover as many representative DEM grids as possible. In this study, $\mathbf{d_b}$ is set 5 meters since the road width is unknown.
2. Project center points of selected DEM grids to the roadway centerline to generate roadway sampling points, with each sampling point carrying the elevation value of its corresponding center point as shown in Figure 17b and 5c.

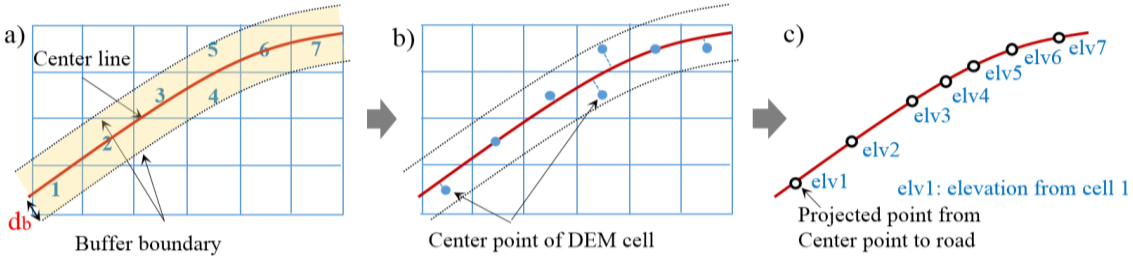

Figure 17 – Post-sampling Method

Roads are crowned at the center, cross slopes are provided for drainage, and super-elevation is provided for high-speed turns. However, the elevation differences associated with changes in cross section are small relative to elevation fluctuation along the road centerline and can be effectively ignored in calculating linear road grade. This assumption ensures that elevation from DEM cell can represent elevation of the point on the road centerline to which the DEM cell is projected.

3.2.1.3 Pre-sampling vs. Post-sampling

The pre-sampling method is preferred when using DEM data at 1×1 meter or 3×3 meter resolution levels because it is more computational efficient, and only requires

matching each sample point to a DEM raster. The post-sampling method is preferred when using DEM data at 10×10 meter resolution, to reduce the error due to the location mismatch of DEM grids and roadway centerline (elevation value represent the center DEM cell). However, the post-sampling method is more computational intensive than pre-sampling method, due to the additional step of projecting the center of DEM cell to the road GIS polyline.

3.2.2 Elevation Data Cleaning and Infill

In locations where elevated roadways and bridges are present, USGS DEM usually returns the lowest surface elevation values, representing the elevation of the ravine, river, rail, underpass road, etc., over which the bridge spans (labeled as dashed circle in Figure 14) instead of the target roadway (Wood, et al., 2014b). This will cause unrealistic elevation drop and incorrect roadway grades, requiring additional data processing. In this study, the elevation value of a point is identified as erroneous if the elevation changing rate (shown in Equation (5) exceeds certain thresholds, i.e. 15% on local roads and 8% on freeways (excluding ramps) as road grade does not exceed 15% and 8% for local roads and freeways (TxDOT, 2014).

$$\left|\frac{\Delta Elv_t}{\Delta Dist_t}\right| > \bar{a} \qquad 5)$$

Where:

$\Delta Elv_t = Elv_t - \Delta Elv_{t-1}$: elevation difference between Point t and its previous Point t-1;

$\Delta Dist_t$: the linear distance between Point t and t-1, calculated based on their geographic coordinates;
$\bar{a}$: threshold value.

An automatic processing script was used to identify erroneous elevation points via two nested loops (forward and backward), and then to clean and infill data to replace the erroneous values (Figure 18). The forward loop starts point-by-point along the roadway link direction. When an erroneous elevation point is detected, a bracket in length of L is created starting from the erroneous point (labeled as Point A), and the following points within the bracket are selected. The backward loop is then triggered to loop from the last point in the bracket, and it stops when the first erroneous point is detected (labeled as Point B). All of the data points between A and B are identified as an erroneous region and all of these data points are removed. Then, the forward loop jumps to a point after the end of the bracket and restart the process. In this study, three rounds of nested loops were conducted with bracket length (L) values of 30 meters, 100 meters, and 150 meters in sequence, which were used to filter out various elevation gap lengths, such as a bridge crossing railway or creek spanning much shorter gaps than a bridge or interchange crossing a river. In this study, the automated process was able to identify 70% of the erroneous elevation points in this study; the remaining 30% were identified through a manual check. Additional efforts to improve screening tools for the application of USGS DEM data for road grade estimation purposes are warranted.

After cleaning erroneous elevation points, new elevation data are re-generated using ordinary least squares (OLS)-based cubic regression by inputting 6 “good” elevation values (3 points before and 3 after the erroneous region).

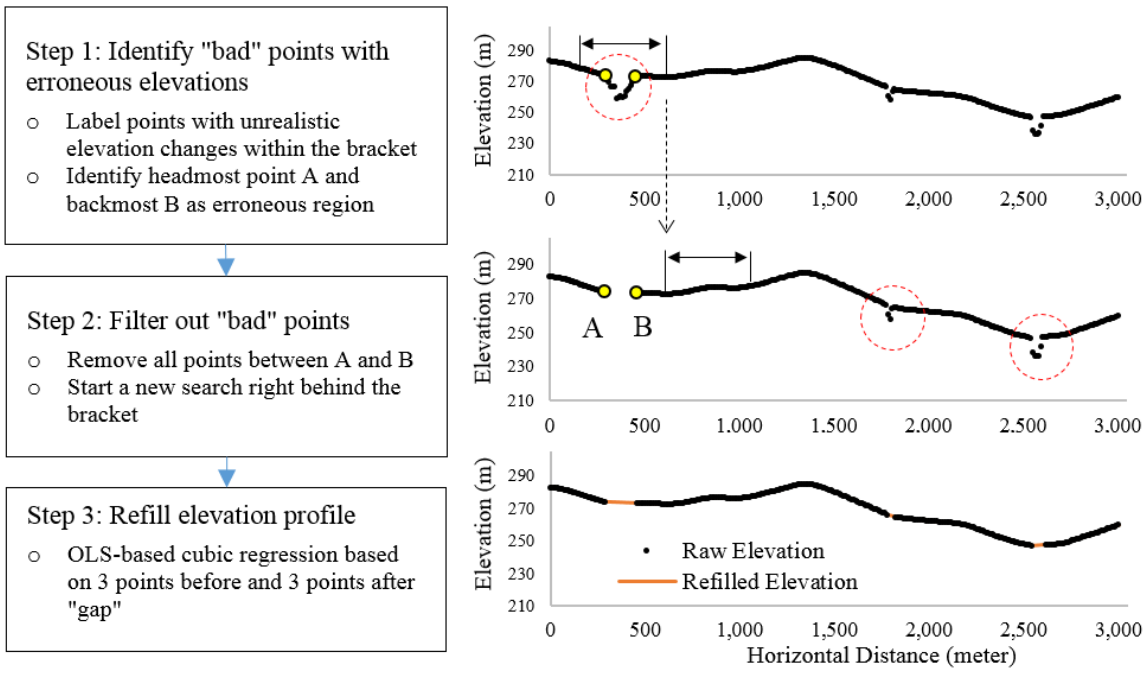

Figure 18 – Elevation Data Cleaning and Infill

3.2.3 Cubic Smoothing Spline

Smoothing with a cubic spline provides a flexible way of estimating the underlying relationship when noisy data are present (Green and Silverman, 1993). In transportation research, studies have applied cubic smoothing splines in characterizing regimes in daily cycles of urban traffic (Kamarianakis, et al., 2010), and geometric modeling of freeways (Castro, et al., 2006). Although it can be defined with higher orders, a cubic (3rd order) spline was used because of its capability of approximating linear, quadratic, and cubic relationships. It is also the lowest degree of the polynomial function that supports an inflection to estimate elevation changes between the top and bottom of roadways.

The distance-elevation point is denoted as (x_i, y_i), with x_i as linear distance and y_i as elevation, and i = 0,1,2,…, n. A spline function $\mathrm{s}(x)$ is constructed in Equation (6) to minimize the value of:

$$L = \alpha \underbrace{\sum_{i=0}^{n} w_i \left[y_i - \mathrm{s}(x_i)\right]^2}_{Sum\ of\ Square\ Error} + (1-\alpha) \underbrace{\int_{x_0}^{x_n} [\mathrm{s}''(x)]^2 dx}_{Regularization\ Term} \tag{6}$$

where:

$\mathrm{s}(x_i)$: smoothed elevation value of spline function at x_i;
w_i: weight of each point, set as equal for all points, i.e., $w_0 = w_1 = \cdots = w_n = 1$;
α: weight factor, $\alpha \in [0,1]$

The sum of squared errors is used for evaluating goodness of fit (Green and Silverman, 1993). The regularization term evaluates smoothness; that is, the term is large $\mathrm{s}''(x)$ is "wiggly". L trades off goodness-of-fit with smoothness (Wasserman, 2006). For notational convenience, we use f_i to denote $\mathrm{s}(x_i)$. Therefore, (x_i, f_i) i = 0,1,2,…,n, are the nodes to be determined. Next, we want to prove that:

$$\int_{x_0}^{x_n} [s''(x)]^2 dx = \boldsymbol{\sigma}^T \boldsymbol{M} \boldsymbol{\sigma} \tag{7}$$

Where $\boldsymbol{\sigma}$ is a vector with second order derivative $\sigma_i = \mathrm{s}''(x_i)$, i = 0,1,2,…,n, and:

$$\boldsymbol{\sigma} = \boldsymbol{M}^{-1} \boldsymbol{Q} \boldsymbol{f} = [\sigma_1, \quad \cdots, \quad \sigma_{n-1}]^T \in \boldsymbol{R}^{(n-1)\times 1}$$

Where $\boldsymbol{M}$, $\boldsymbol{Q}$, and $\boldsymbol{f}$ are:

$$\boldsymbol{M} = \begin{bmatrix} \frac{1}{3}(h_0+h_1) & \frac{h_1}{6} & 0 & \dots & 0 & 0 \\ \frac{h_1}{6} & \frac{1}{3}(h_1+h_2) & \frac{h_2}{6} & \dots & 0 & 0 \\ 0 & \frac{h_2}{6} & \frac{1}{3}(h_2+h_3) & \dots & 0 & 0 \\ \vdots & \vdots & \vdots & \ddots & \vdots & \vdots \\ 0 & 0 & 0 & \dots & \frac{1}{3}(h_{n-3}+h_{n-2}) & \frac{h_{n-2}}{6} \\ 0 & 0 & 0 & \dots & \frac{h_{n-2}}{6} & \frac{1}{3}(h_{n-2}+h_{n-1}) \end{bmatrix}$$

$$\in \boldsymbol{R}^{(n-1)\times(n-1)}$$

$$\boldsymbol{Q} = \begin{bmatrix} \frac{1}{h_0} & \left(-\frac{1}{h_0}-\frac{1}{h_1}\right) & \frac{1}{h_1} & 0 & \dots & 0 \\ 0 & \frac{1}{h_1} & \left(-\frac{1}{h_1}-\frac{1}{h_2}\right) & \frac{1}{h_2} & \dots & 0 \\ \vdots & \vdots & \ddots & \ddots & \ddots & \vdots \\ 0 & 0 & 0 & \frac{1}{h_{n-2}} & \left(-\frac{1}{h_{n-2}}-\frac{1}{h_{n-1}}\right) & \frac{1}{h_{n-1}} \end{bmatrix}$$

$$\in \boldsymbol{R}^{(n-1)\times(n+1)}$$

$$\boldsymbol{f} = [f_0, \quad f_1, \quad \dots, \quad f_n]^T \in R^{(n+1)\times 1}$$

Where, h_i is inter-point linear distance $h_i = x_{i+1} - x_i$.

The left side of Equation (7) can be written as sum of decomposed parts, with each as integral of the square of second derivative $s_0''(x)$

$$\int_{x_0}^{x_n} [s''(x)]^2 dx = \int_{x_0}^{x_1} [s_0''(x)]^2 dx + \int_{x_1}^{x_2} [s_0''(x)]^2 dx + \cdots + \int_{x_{n-1}}^{x_n} [s_{n-1}''(x)]^2 dx = \sum_{j=0}^{n-1} \int_{x_j}^{x_{j+1}} \left[s_j''(x)\right]^2 dx \quad (8)$$

We can show that:

$$s_j''(x) = \sigma_j \frac{(x_{j+1} - x)}{h_j} + \sigma_{j+1} \frac{(x - x_j)}{h_j}, \quad j = 0, \dots, n-1 \tag{9}$$

Incorporating Equation (9) into each individual part in Equation (8), we can get that:

$$\begin{aligned} \int_{x_j}^{x_{j+1}} \left[s_j''(x)\right]^2 dx &= \int_{x_j}^{x_{j+1}} \left[\sigma_j \frac{(x_{j+1} - x)}{h_j} + \sigma_{j+1} \frac{(x - x_j)}{h_j}\right]^2 dx \\ &= \frac{1}{{h_j}^2} \int_{x_j}^{x_{j+1}} \left[{\sigma_j}^2 (x_{j+1} - x)^2 + 2\sigma_j \sigma_{j+1} (x_{j+1} - x)(x - x_j)\right. \\ &\quad \left. + {\sigma_{j+1}}^2 (x - x_j)^2\right] dx \end{aligned} \tag{10}$$

Also, for the first part of Equation (10):

$$\begin{aligned} \int_{x_j}^{x_{j+1}} {\sigma_j}^2 (x_{j+1} - x)^2 dx &= -{\sigma_j}^2 \frac{1}{3} (x_{j+1} - x)^3 \Big|_{x=x_j}^{x=x_{j+1}} = \frac{1}{3} {\sigma_j}^2 (x_{j+1} - x_j)^3 \\ &= \frac{1}{3} {\sigma_j}^2 {h_j}^3 \end{aligned} \tag{11}$$

Similarly, for the third part of Equation (10):

$$\int_{x_j}^{x_{j+1}} {\sigma_{j+1}}^2 (x - x_j)^2 dx = \frac{1}{3} {\sigma_{j+1}}^2 {h_j}^3 \tag{12}$$

And, for the second part of Equation (10):

$$\begin{aligned} \int_{x_j}^{x_{j+1}} 2\sigma_j \sigma_{j+1} (x_{j+1} - x)(x - x_j) dx &= 2\sigma_j \sigma_{j+1} h_j \int_0^1 (1 - z) z dz \\ &= \frac{1}{3} \sigma_j \sigma_{j+1} h_j \end{aligned} \tag{13}$$

Incorporating Equation (11), (12), and (13) into Equation (10) and simplifying we obtain:

$$\int_{x_j}^{x_{j+1}} \left[s_j''(x)\right]^2 dx = \frac{h_j}{3} ({\sigma_j}^2 + \sigma_j \sigma_{j+1} + {\sigma_{j+1}}^2) \tag{14}$$

So Equation (7) get proved by:

$$\int_{x_0}^{x_n}[s''(x)]^2dx = \sum_{j=0}^{n-1}\int_{x_j}^{x_{j+1}}\left[s_j''(x)\right]^2dx$$
$$= \frac{1}{3}\sum_{j=0}^{n-1}h_j({\sigma_j}^2 + \sigma_j\sigma_{j+1} + {\sigma_{j+1}}^2) \quad (15)$$
$$= \frac{1}{6}\sum_{j=1}^{n}[h_j\sigma_{j-1}\sigma_j + 2{\sigma_j}^2(h_{j-1} + h_j) + h_j\sigma_j\sigma_{j+1}] = \boldsymbol{\sigma}^T\boldsymbol{M}\boldsymbol{\sigma}$$

By integrating Equation (7) into Equation (6) and re-writing L as a matrix function, we get:

$$L = \alpha(\boldsymbol{y} - \boldsymbol{f})^T\boldsymbol{W}(\boldsymbol{y} - \boldsymbol{f}) + (1-\alpha)\boldsymbol{f}^T\boldsymbol{Q}^T\boldsymbol{M}^{-1}\boldsymbol{Q}\boldsymbol{f} \quad (16)$$

where:

$$\boldsymbol{y} = [y_0, \quad y_1, \quad \dots, \quad y_n]^T \in R^{(n+1)\times 1}, \quad \boldsymbol{W} = \begin{bmatrix} 1 & 0 & \cdots & 0 \\ 0 & 1 & \cdots & 0 \\ \vdots & \vdots & \ddots & \vdots \\ 0 & 0 & \cdots & 1 \end{bmatrix} = I_{(n+1)\times(n+1)}$$

The derivative of $\boldsymbol{f}$ is set as zero, and we get the solution of $\boldsymbol{f}$ as $\hat{\boldsymbol{f}}$ that minimize L are:

$$\hat{\boldsymbol{f}} = [\alpha\boldsymbol{W} + (1-\alpha)\boldsymbol{Q}^T\boldsymbol{M}^{-1}\boldsymbol{Q}]^{-1}\alpha\boldsymbol{W}\boldsymbol{y} = [\hat{f}_0, \quad \hat{f}_1, \quad \dots, \quad \hat{f}_n]^T \in R^{(n+1)\times 1} \quad (17)$$

From this end, the position of each node is obtained $(x_i, \hat{f}_i)$, i = 0,1,2,…,n, that determine spline functions $\mathrm{s}(x)$. By definition, the cubic interpolating spline $\mathrm{s}(x)$ is a function on the interval $[x_0, x_n]$ satisfying:

1. $\mathrm{s}(x)$ is the cubic polynomial for each node-to-node interval $[x_\mathrm{i}, x_{i+1}]$
2. $\mathrm{s}(x_i) = \hat{f}_i$ at each node x_i
3. $\mathrm{s}''(x)$ is continuous throughout the entire interval $[x_0, x_n]$
4. at the terminal nodes, $\mathrm{s}''(x_0) = \mathrm{s}''(x_n) = 0$

The equations denote $s(x)$ within interval $[x_i, x_{i+1}]$ as $s_i(x)$, i = 0,1,…,n-1. Based on the criteria that need to be satisfied above, $s_i(x)$ can be written as:

$$s_i(x) = \frac{\sigma_i}{6h_i}(x_{i+1} - x)^3 + \frac{\sigma_{i+1}}{6h_i}(x - x_i)^3 + c_1(x - x_i) + c_2(x_{i+1} - x) \quad (18)$$

Where, σ_i can be calculated with $\hat{\boldsymbol{f}}$ substituted, and c_1, c_2 can be determined from 0th order continuity requirement:

$$s(x_{i+1}) = \hat{f}_{i+1} = \frac{\sigma_{i+1}}{6}{h_i}^2 + c_1 h_i \quad \rightarrow \quad c_1 = \frac{\hat{f}_{i+1}}{h_i} - \frac{\sigma_{i+1}}{6}h_i \quad (19)$$

$$s(x_i) = \hat{f}_i = \frac{\sigma_i}{6}{h_i}^2 + c_2 h_i \quad \rightarrow \quad c_2 = \frac{\hat{f}_i}{h_i} - \frac{\sigma_i}{6}h_i \quad (20)$$

Given the position x_i, the estimated road grade $\hat{G}(x_i)$ is generated by taking derivative of $s(x)$, the ratio of vertical height and linear distance:

$$\hat{G}(x_i) = \frac{\partial\, s(x)}{\partial\, x}|_{x=x_i} \quad (21)$$

For notational convenience, $\lambda = (1 - \alpha)/\alpha$ is a weight factor, where $\lambda \in [0, \infty)$. A larger λ value means putting more weight on maintaining the smoothness of the distance-elevation profile rather than goodness-of-fit. Intuitively, freeway or roadways in flat terrain should apply a larger λ for smoothing than would be applied on local or hilly roads. This is because sharp elevation fluctuations are expected to be reflected in smoothing spline. Selection of λ will be discussed in the next section.

3.3 Verification and Discussion

3.3.1 Real-World Road Grade Collection

Freeway grade data were derived from Georgia Department of Transportation (GDOT) elevation survey data, collected by using LiDAR scanners that which achieve position accuracy of 4 millimeters; Leica® Scan-station 2 and Leica® P40 LiDAR Scanner (see Figure 19a and 7b. Road surface elevations were measured by GDOT contractors every 1×1 meter grid. In this study, freeway road grades are calculated by taking the ratio of elevation difference to linear distance difference, and data are obtained in interval of every 30 meters along the road. Grades for local roads were manually measured using a 48-inch SmartTool® digital level with an accuracy of 0.1 degree (i.e., the ratio of vertical height and linear distance is 0.17%). Local road measurements were taken every 5-15 meters along the center line of the road (see Figure 19c). Each sample point was measured three times and the average value was used for verification.

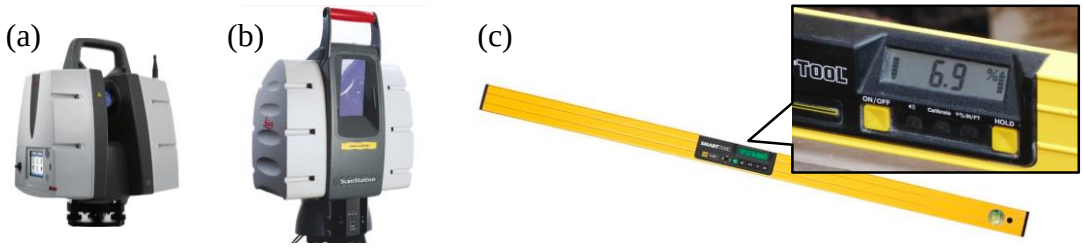

Figure 19 – Real-World Elevation/Grade Collection Tool: (a) Leica® P40 LiDAR Scanner, (b) Leica® Scan-station 2, (c) 48-Inch SmartTool® Digital Level

Road grade data used for verification consisted of five freeway and two local road segments in Atlanta, shown in Figure 20. All seven segments have DEM data at all three

resolution levels, except I-20 at Candler Road, which does not have 1×1 meter resolution. Data details are summarized in Table 1.

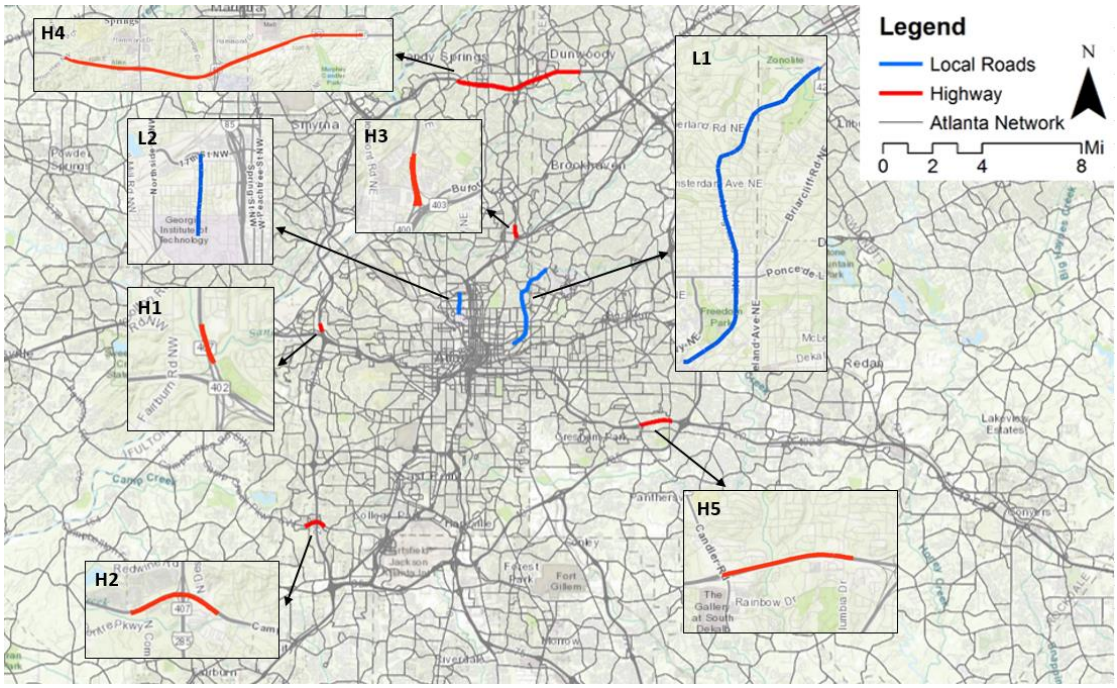

Figure 20 – Road Segment Layout

Table 2 – Data Collection Summary

Road Type	ID	Description	Length (meter)	Measurement Tool	Number of Measurement	DEM Availability		
						1x1 m	3x3 m	10x10 m
Freeway	H1	I-285 at Camp Creek Pkwy.	1,436	Leica® Scan-station 2 / Leica® P40 LiDAR Scanner	138	✓	✓	✓
	H2	I-285 at Collier Access Road	561		52	✓	✓	✓
	H3	SR400 at I-85	1,372		87	✓	✓	✓
	H4	I-285 at 400	10,289		79	✓	✓	✓
	H5	I-20 at Candler Rd.	2,082		198	na	✓	✓
	Freeway Total		15,740		554			
Local	L1	Highland Avenue	6,067	Digital Level	346	✓	✓	✓
	L2	State Street	1,429		150	✓	✓	✓
	Local Road Total		7,497		496			
Total (Freeway + Local)			23,236		1,050			

3.3.2 Road Grade Verification

The root-mean-square error (RMSE) between estimated and measured grades is defined in Equation (22). RMSE represents the average error of grade estimation, and it is used to evaluate the effectiveness of the proposed grade estimation method.

$$RMSE = \sqrt{\frac{1}{n}\sum_{i=1}^{n}(G(x_i) - \hat{G}(x_i))^2} \tag{22}$$

Where x_i is position of the measured point i; $G(x_i)$ is measured grade of point i by digital level or LiDAR scanner; $\hat{G}(x_i)$ is the estimated grade from Equation (21).

RMSE by road are calculated with λ (defined as $\lambda = (1-\alpha)/\alpha$) ranging from 10 to 100,000, and the results are shown in Figure 21. In general, for local roads, RMSE is small when λ is within 300-1000, and RMSE reaches the minimum when λ = 500. However, the λ required to minimize RMSE is higher for freeways than for local roads. For the freeways, RMSE is small when λ is within 1,000-10,000. Intuitively, freeways are flat and smooth, and thus require a larger weight on smoothness (the second part of Equation (6)) rather than goodness-of-fit. Also, road grade is estimated with lower RMSE for freeways (< 0.2%) than for local roads (> 0.5%). This relates to the fact that local roads are often hilly and it is more challenging to estimate the vertical profile grade for local roads than it is for freeways. A comparison of RMSE across the red and green areas in Figure 9 indicates a significant improvement when smoothing is applied to the raw data. However, if the λ value is set too high, over-smoothing will increase error, especially on local roads (yellow area in Figure 21).

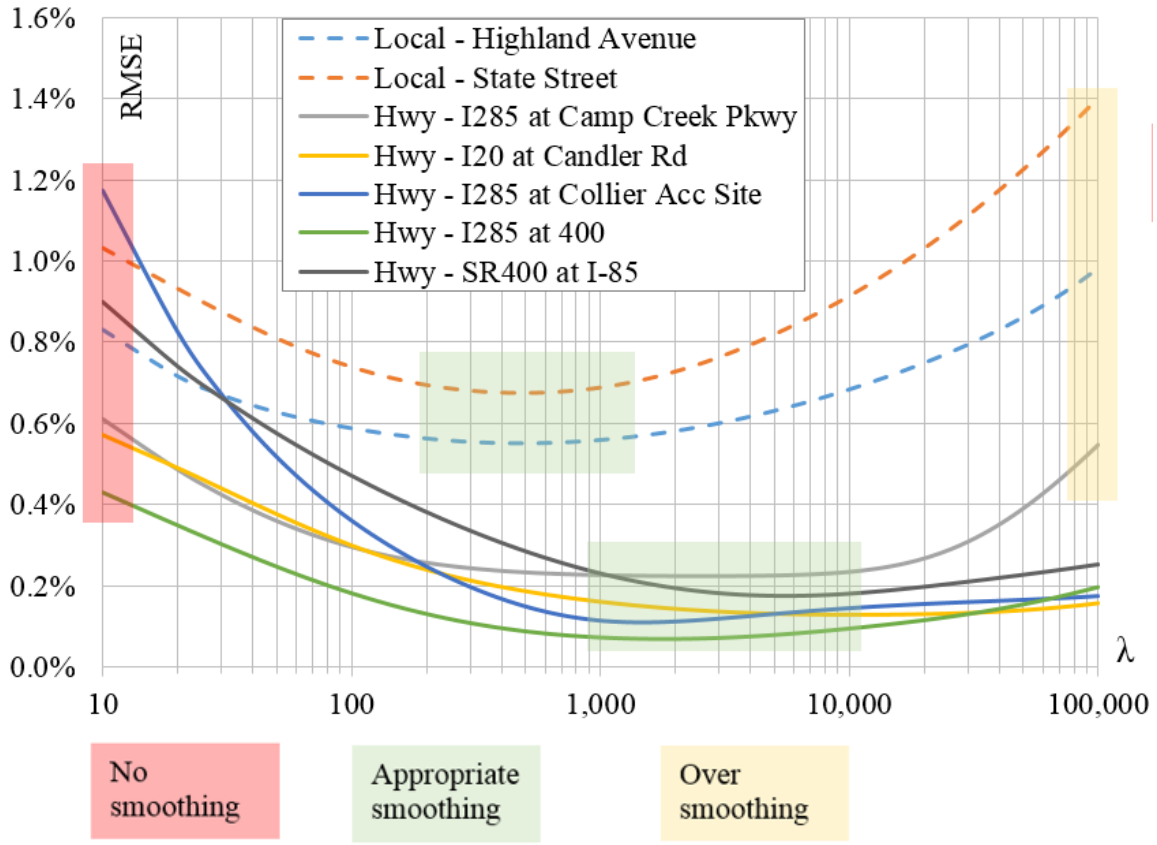

Figure 21 – RMSE in Response of λ by Road

The grade comparison of DEM-derived grade vs. measured grade is shown in Figure 22 by road type and DEM resolution. The λ value is set to 500 for arterials and local roads and 3000 for freeways. From this comparison, several findings are summarized here:

1. Depending on the DEM resolution used, the average estimation error is 0.5-0.58% on local roads, and 0.21%-0.23% on freeways, without obvious bias across grade levels.
2. The proposed method generates good grade estimation results at all three DEM resolutions, with better accuracy at the finest DEM resolution. Still, the

nationally available 10×10 DEM data can generate reasonable results, with RMSE that is only 0.081% higher on local roads, and only 0.025% higher on freeways than using the 1×1 meter DEM data (Figure 22).

3. The estimated grade points from infilled segments (labeled as red triangle) have good accuracy, with most RMSE within 1% (see RMSE_r as RMSE from infilled segment in Figure 22).

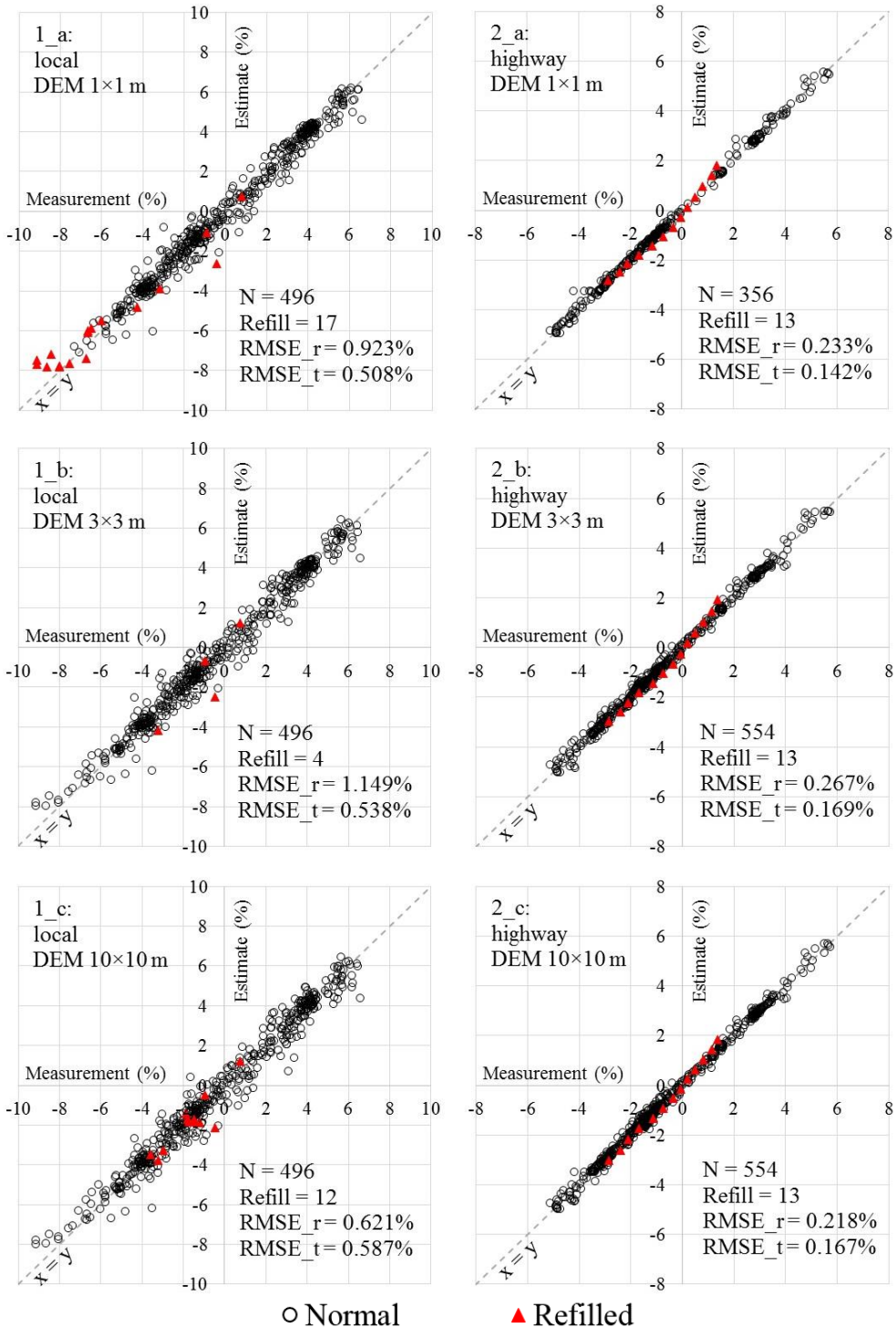

Figure 22 – Measurement-Estimate Grade Comparison by Road Types and DEM Resolutions

An example of a distance-grade profile for North Highland Avenue in Atlanta, GA, based on 10×10 meter DEM data, is shown in Figure 23. The overall estimated grade profile fit well with manual measurements.

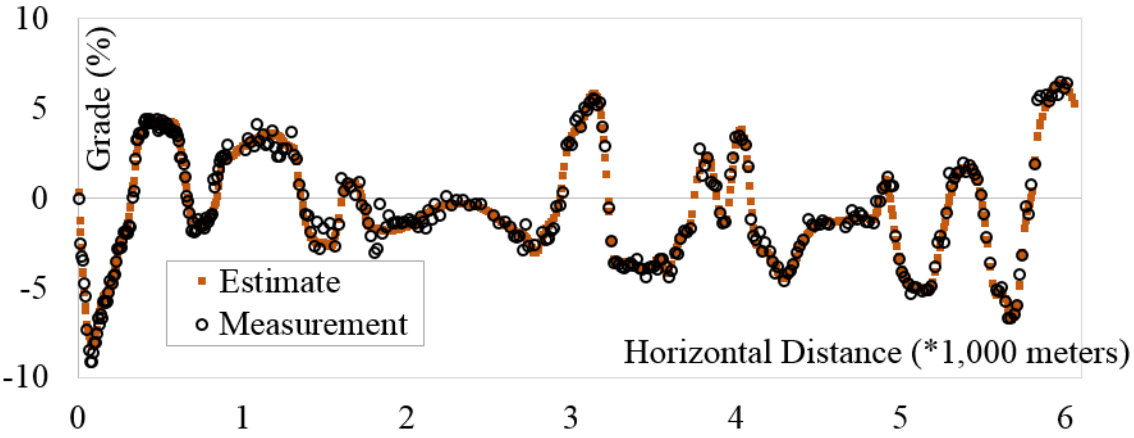

Figure 23 – Distance-Grade Profile for North Highland Avenue

3.4 Discussion of λ Selection

It is important to assign a proper value to the parameter λ in the cubic spline process, with the aim to achieve small fitting errors without losing smoothness of the roadway elevation profile. As briefly mentioned before, selecting λ is affected by terrain fluctuations, and thus a series of sensitivity analysis is conducted to examine how fitting errors change in response to different λ values. Terrain fluctuation is reflected by $S''(x)$, used as part of the regularization term in Equation (6), representing the rate of road grade changes. The procedures for quantifying the effect of $S''(x)$ on λ selection for minimizing estimation error are listed below:

Step 1: For each road, equally partition into sub-segments with each in length of 500-700 meters containing 70-100 measurements. The total number of sub-segments is 20.

Step 2: Apply cubic spline smoothing for each sub-segment with λ. By default, λ = 1000 because the spline $S_{\lambda=1000}(x)$ can generally describe the elevation profile.

Step 3: Per point $x_{i\ i=1,2,\ldots,n}$ in each sub-segment, calculate $s''(x_i)$, and average the absolute value $\overline{|S''(x)|}$. Larger $\overline{|S''(x)|}$ indicates more fluctuation in sub-segment vertical curve. The formula of $\overline{|S''(x)|}$ is:

$$\overline{|S''(x)|} = \left|\frac{1}{n}\sum_{i=1}^{n} \frac{\partial^2 S(x)}{\partial x^2}|_{x=x_i}\right| \tag{23}$$

Step 4: Per sub-segment, apply cubic smoothing spline with λ_i set from 10 to 1E+07 in 50 point intervals, and calculate RMSE for each λ_i.

Step 5: Obtain optimum λ (λ_{opt}) that minimize RMSE (λ_{opt} = argmin RMSE) for each sub-segment, and its optimum range RMSE ≤ min RMSE + 0.05% and RMSE ≤ min RMSE + 0.1%.

The λ_{opt} in response of $\overline{|S''(x)|}$ are plotted in Figure 24. Clearly, smaller λ is needed to minimize RMSE as $\overline{|S''(x)|}$ becomes larger. Based on the limited samples (10 sub-segments), the ordinary least squares (OLS) regression function is proposed to select λ_{opt}:

$$\lambda_{opt} = 10^{\left(-2.0961\times|\overline{S''(x)}| + 4.616\right)} \tag{24}$$

To assess the validity, Highland Avenue was re-partitioned into 9 sub-segments with each having a length of 670 meters, and λ_{opt} in each sub-segment is determined by applying Equation (24). The overall RMSE is 0.5216%, and this is better than applying a fixed λ across the whole road, which can only achieve RMSE 0.5509%, as shown in Figure 21. However, more data are needed to better model the relationship between λ_{opt} and $\overline{|S''(x)|}$.

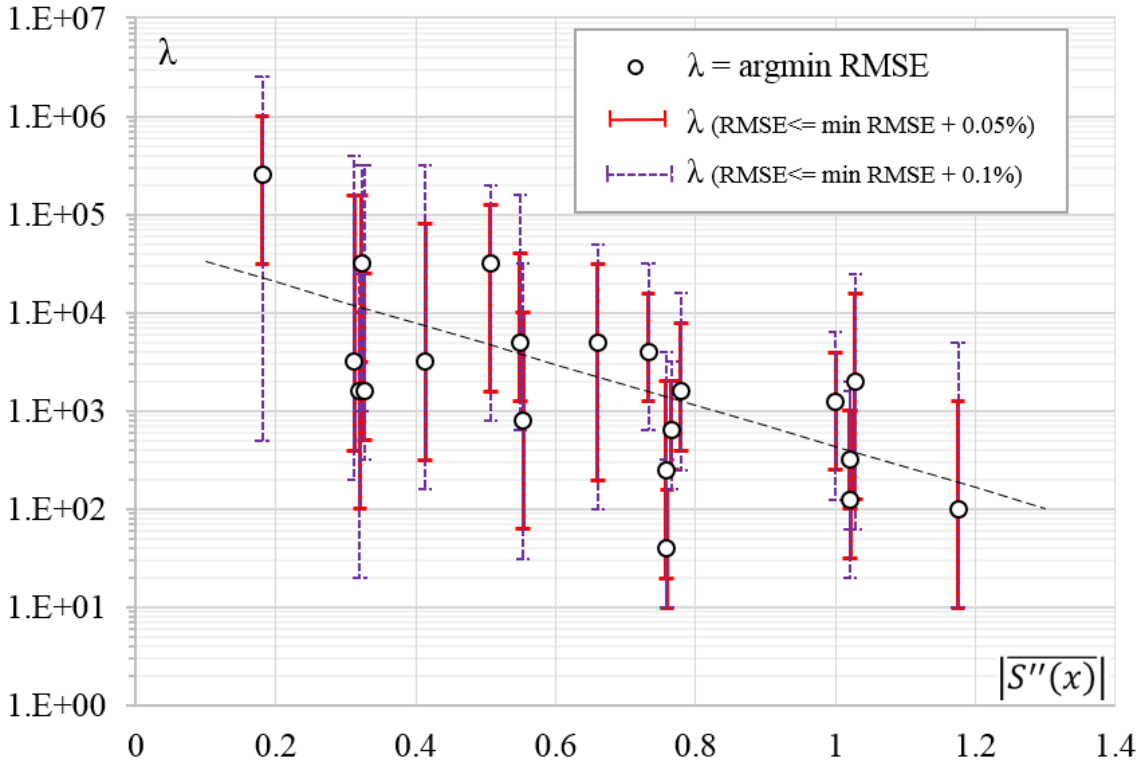

Figure 24 – Optimum λ in Response of $\overline{|S''(x)|}$

3.5 Summary

This chapter proposes a strategy for generating high-accuracy roadway grade based on USGS DEM database that is publicly available and covers most of the nation in the United States. The strategy includes elevation extraction, erroneous elevation

cleaning and infill, and applying a cubic smoothing spline. The cubic smoothing spline was applied in this study to minimize the impact of noisy data, and to improve grade estimation accuracy. The selection of a key parameter λ in spline method was also discussed to balance between goodness-of-fit and regularization of elevation fluctuation. Different λ values are recommended for arterials and local roads (500) and freeways (3000) because these roads exhibit different terrain fluctuations. The result demonstrated the validity of DEM in generating high-resolution road grade. Even by using the DEM 10×10 data that is the lowest resolution used in the study, the road grade is generated in promising accuracy, with the average RMSE is 0.58% for local roads, and 0.23% for freeways. Although the study focused on the application of USGS DEM, for grade generation purpose, it is reasonable to infer that the proposed strategy can be applied with other source of LiDAR data or survey data that include position and elevation information. The following conclusions can be drawn from results of this chapter:

1. The USGS DEM is a valuable resource, and the elevation data from USGS DEM along the road are sufficiently accurate for generating road grade. While the higher resolution DEM is recommended when available, the verification results indicate good accuracy at all three resolutions (1×1 meter, 3×3 meter, and 10×10 meters);
2. The data cleaning and infill strategy can effectively interpolate elevation, and predict road grade where erroneous elevation data were provided by the DEM (e.g., in river/bridge, and freeway/overpass intersections). This is because roads are generally flat, and sharp elevation fluctuations associated with bridges are relatively easy to detect;

3. In applying cubic smoothing spline method, the key parameter λ needs to be selected carefully to tradeoff least squares error (goodness of fit) with smoothness. It is recommended that λ be selected by segment, based on the elevation fluctuation of the road, which is represented by the absolute rate of grade change $\overline{|S''(x)|}$ in this study.

The 10×10 meter resolution DEM is available in the entire Atlanta region. The 3×3 meter resolution is available in Fulton County, Chamblee County, and DeKalb County. Fulton County is the only county in Atlanta where 1×1 meter resolution is available. The grade generation method was programmed in Python for execution on the Georgia Tech PACE parallel computing cluster, and the system has generated road grade for the entire Metro Atlanta Area, including 1,435 miles of freeways, 7,493 miles major arterials, and 11,935 miles minor arterials or local roads. Figure 25 shows a map of Atlanta road network with generated grade available for this dissertation. Elevations from the highest 1x1 meter DEM resolution was implemented where available. When extracting elevations, ground positions were sampled at 5 to 15 meters spaced horizontal intervals along the roads, and road grade data is further interpolated in 3 meters interval. In this manner, a road grade point layer in intervals of 3 meters was created for the entire Atlanta network. Grade distribution of freeways and arterials are shown in Figure 26. It shows that constrained by the road design rules, most of grades estimated on freeways range from -5% to +5%, and most of grades on arterials range from -10% to +10%. The grade data will be matched with second-by-second vehicle GPS data for energy and emission calculation in the next chapters.

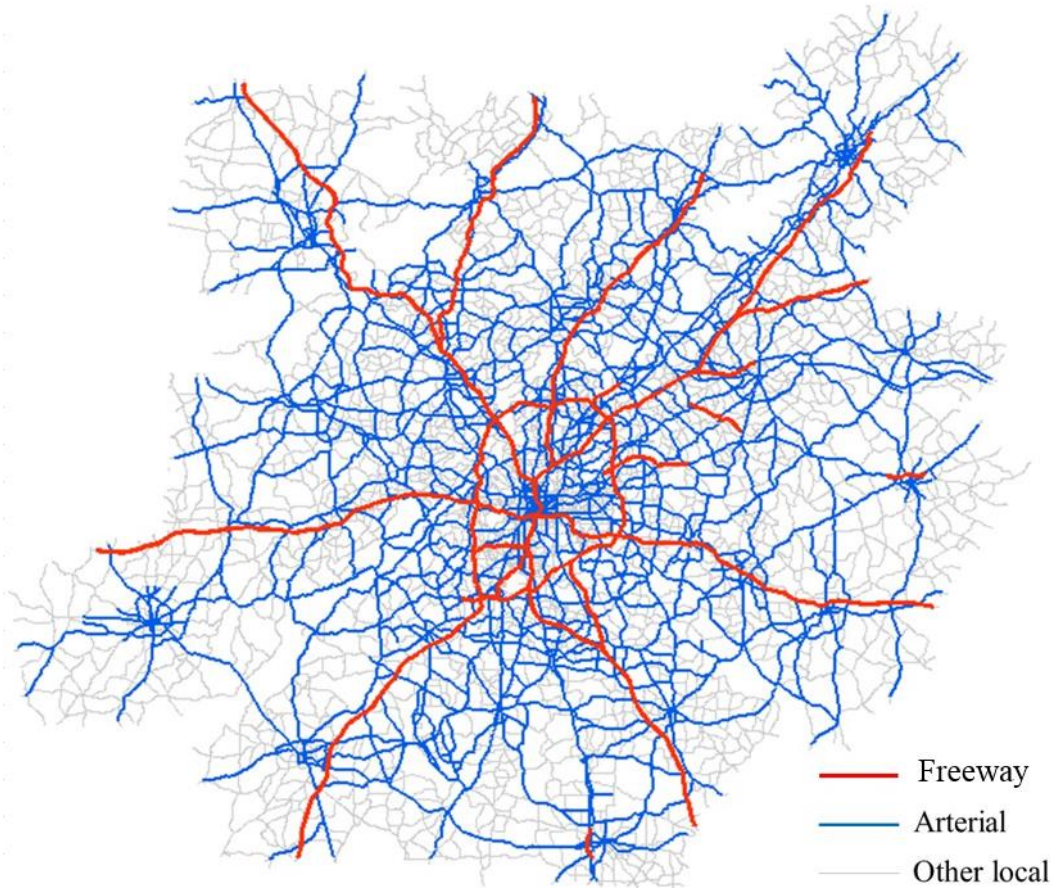

Figure 25 – Atlanta Road Network with Grade Available

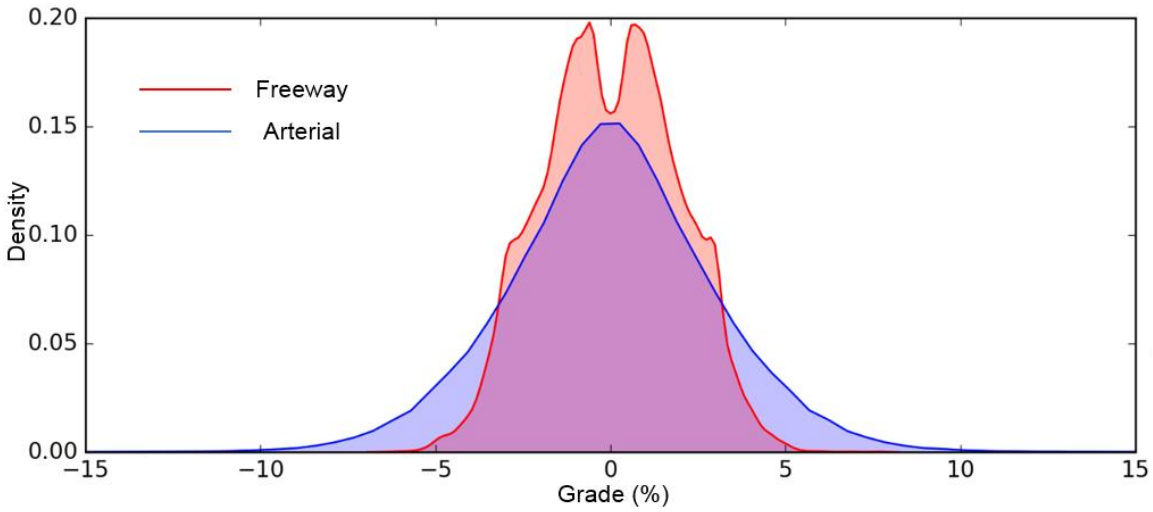

Figure 26 – Grade Distribution of Freeways and Arterials in Atlanta

CHAPTER 4. DATA PROCESSING METHODOLOGY

The purpose of Chapter 4 is to generate the base data that can be easily aggregated for further analysis of operations, energy consumption, and emissions in Chapter 5 to Chapter 8. Data support for the dissertation research includes GPS data, road information, surrounding environment information, and the EPA certification database. After data introduction, a streamlined procedure to append derived grade data on vehicle GPS trajectories is presented. Because MOVES-Matrix will be used as the platform to model energy consumption and emissions through the dissertation, the chapter will introduce in details the procedure of energy consumption and emissions modeling in MOVES-Matrix (inputs, modeling algorithms, and outputs).

4.1 Data Support

Source and general statistics of vehicles information, and GPS information will be introduced in this section. Road information from Atlanta Regional Commission (ARC)'s GIS road network file, and vehicle parameters from EPA Certification database are also incorporated as potential control variables for statistical modeling of vehicle speed and acceleration in the next chapters

4.1.1 Vehicle GPS Data

Second-by-second GPS trajectories from a massive number of vehicles are available for describing operating conditions. The data came from multiple sources, covering light-duty vehicles, express transit buses, and urban transit buses.

4.1.1.1 Light-duty Vehicle Data

In 2011, the Atlanta Regional Commission (ARC) conducted the Atlanta Household and Activity Travel Survey in the 20-county region of Atlanta. Household travel diaries were collected from more than 10,000 households and served as the basis for ARC travel demand model development. In addition, one week of second-by-second trip trajectories for 1,653 light-duty vehicles in 911 households were recorded using in-vehicle GPS devices. Second-by-second data were collected for more than 40,000 trips totaling 279,297 miles. Vehicle make, model, and model year are also available. The 1,653 vehicles cover a wide range of model years and vehicle body styles, as shown in Figure 27 and Figure 28.

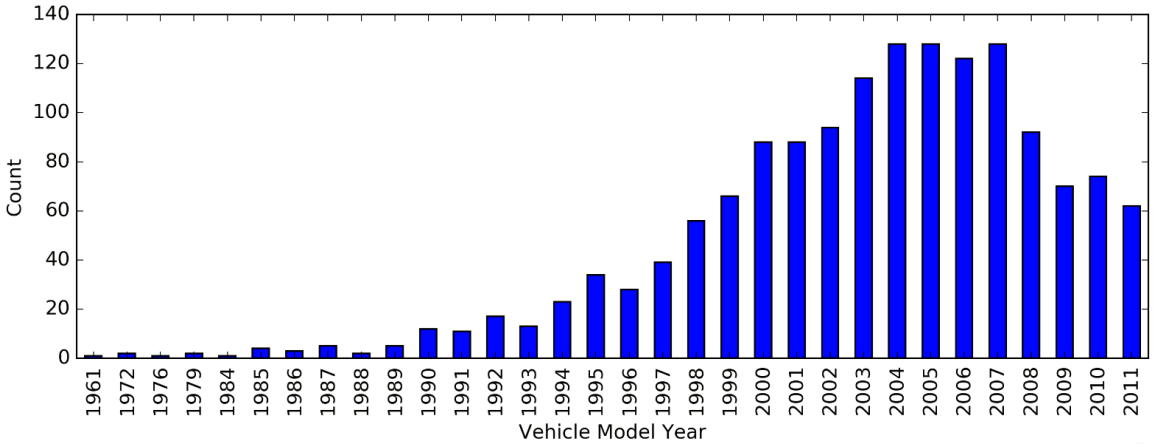

Figure 27 – Model Year Distribution of Light-duty Vehicles from ARC Survey

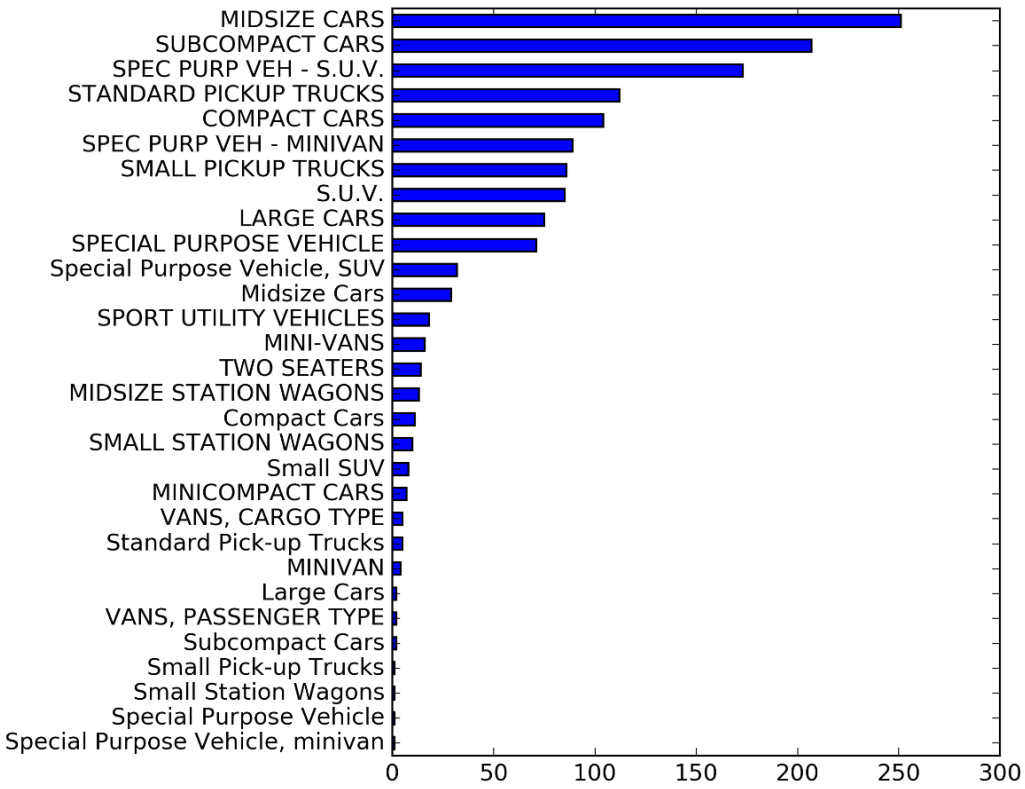

Figure 28 – Number of Vehicles by Body Style

4.1.1.2 Heavy-duty Bus Data

Operations of two transit bus fleet are available in the study: express transit fleet and urban transit fleet. For express transit buses, data were collected via spot sampling (typically two to three day deployments between August 6, 2013 and March 3, 2014). Qstarz BT-Q1000eX GPS data loggers were temporarily installed on 13 Georgia Regional Transportation Authority (GRTA) 48-seat express buses in this sampling effort. There are 3,637 miles of second-by-second data collected. Because Express buses are mainly serving inter-county trips, most of the operations collected on highways. For urban transit bus operations, Metropolitan Atlanta Rapid Transit Authority (MARTA) operations data were collected on 13 buses for 381 days (June 28, 2004 to Oct 24, 2005)

using the Georgia Tech Trip Data Collector (Ogle, et al., 2005), totaling 61,247 miles of operation data mostly on non-highways. Figure 29 shows pictures of a GRTA Express bus and a MARTA Urban transit bus.

Source: http://www.xpressga.com/ Source: http://www.itsmarta.com/

Figure 29 – GRTA Express Bus (Left) and MARTA Urban Transit Bus (Right)

Ideally, heavy-duty truck should also be included for a complete analysis, as operations of trucks, especially loaded freight trucks were expected to be more sensitive to grades. Unfortunately, operations of heavy-duty trucks were not available for this study. This will be one of the future research needs.

4.1.2 EPA Certification Database

The USEPA vehicle certification and compliance testing database (USEPA, 2017) is used in this dissertation to extract more detailed light-duty vehicle information based on vehicle make, model, and model year from ARC survey data. The EPA certification database contains almost all light-duty vehicles models that are and sale in the United States. These models were tested by National Vehicle and Fuel Emissions Laboratory for compliance with the USEPA's exhaust emissions standards. EPA provides annual certification test results data for every year since 1979, however, only the data from 1997 and later years are machine-readable. Thus, information of vehicles for 1997 and later

model years can be mined from the database. The Georgia Tech research team created a vehicle lookup database with vehicle make, model and model year as the key columns for use in a variety of research efforts. The vehicle database contains a total of 9,068 unique vehicles. To link with energy consumption and emissions rates from MOVES model, light-duty vehicles are further classified to passenger car and passenger truck following the process described in Liu, et al., (2015). It is not a strict condition, but in general, vehicles with body style of 2-door and 4-door sedan, station wagon, compact-SUVs, and mini vans are classified as passenger cars, body style of median- to large-SUVs, pick-up trucks, vans, and limousines are classified as passenger trucks. A description of vehicle lookup table is summarized in Table 3.

Table 3 – Description of Vehicle Lookup Table Based on EPA Certification Data

Variables	Description of variables
vehicleModelID	Unique ID for make, model, and model year
vehicleMake	Vehicle maker in epa certification test results
vehicleModel	Vehicle model in epa certification test results
vehicleModelYear	Vehicle model year in epa certification test results
vehicleFuelType	Vehicle fuel type
standardLevel	Standard tier code
displacement	Vehicle engine displacement (liter)
vehicleTransType	Vehicle transmission type
vehicleGearNumber	Number of gears
vehicleHybridCheck	Y: Hybrid, N is otherwise
ratedHorsepower	Vehicle rated horsepower 2)
vehicleWheelType	Vehicle wheel type
vehicleGrossWeight	Vehicle gross weight (lbs.)
vehicleCurbWeight	Vehicle curb weight (lbs.) 3)
epaVehicleClass	EPA's vehicle classification
movesVehicleClass	MOVES's vehicle classification
movesSourceTypeId	MOVES's source type

By pairing vehicle make, model, and model year from ARC survey with the USEPA's certification database, we are able to append vehicle-specific information including regulatory class, gross vehicle weight rating (GVWR), vehicle wheel type, engine displacement, vehicle rated horsepower, etc., which can potentially be used as vehicle-specific control variables in operations analysis. Figure 30 presents engine displacement and gross weight distribution by vehicle regulatory classes from participated vehicles. Participating vehicles in ARC survey represent a wide range of vehicle engine power and vehicle weight.

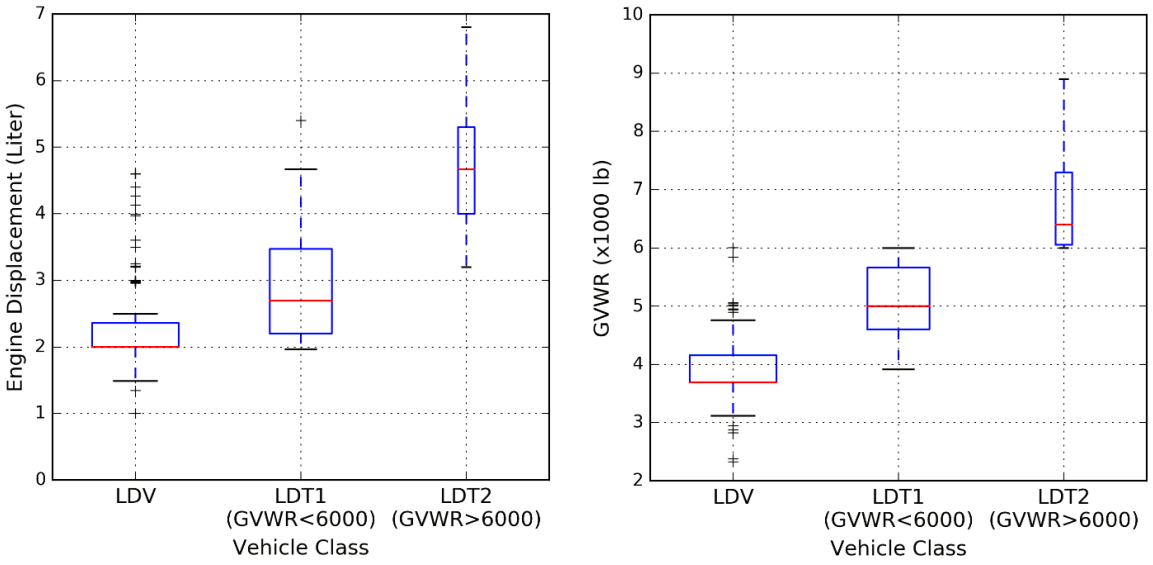

Figure 30 – Engine Displacement and Gross Vehicle Weight Ratio (GVWR) by Vehicle Regulatory Class

4.1.3 Road Information and Surrounding Environment

The GIS roadway centerline network file for Atlanta was obtained from the ARC. The GIS network contains roadway characteristics such as geographic locations, road type (freeways, arterial, local, and ramp), length, number of lanes, speed limit, location of

traffic signal, etc. Road horizontal curve is represented as inside-corner radius, and is approximated by smoothing horizontal alignment and taking the reciprocal of angle change rate. Based on the geometric relationship shown in Figure 31, radius of the road segments can be derived from the following equation:

$$R = \frac{L}{\theta} \tag{25}$$

where R is the radius of the segment. θ is the angle change from point A to point B. L is the road length from A to B, which is determined by sampling interval.

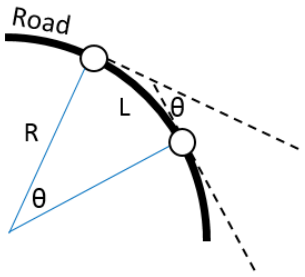

Figure 31 – Road Horizontal Curve

As mentioned in Chapter 3, this study generated point layers along GIS-based road network, obtained elevation information for each point, and calculated grade between points using the vertical DEM change and horizontal distance between points. The GIS-based road network was used to identify road coordinates where road grade information was generated. Hence, it is important that any GIS road polyline used in this process accurately represent the horizontal alignment of the real world roadways. Nationwide GIS roadway data for the United States is also publicly available from the

Topologically Integrated Geographic Encoding and Reference (TIGER) system (US Census, 2017).

Additionally, given the local time that GPS devices recorded data, a dummy variable of day (1) / night (0) is also generated for each GPS second, by using sunrise and sunset time of the collection date.

4.2 Appending Grade on GPS Data

With GPS data available, an automatic process to append grade along with other road information becomes one of the critical procedures not only for this dissertation, but for any research that wishes to integrate grade into operational analysis, energy consumption modeling, and emissions modeling. A method with four steps is proposed as follows for each GPS trajectory:

Step 1: Set a 300-meter buffer of GPS points, and narrow down road network search range by filtering out roads that are do not intersect with the buffer

Step 2: Set a 100-meter buffer (with flat end) for each link of the filtered small network, calculate weight of the link using the equation below:

$$w_i = \begin{cases} \frac{L_i}{n_i \bar{v}_i} & if\ n_i > 0 \\ 10{,}000 & if\ n_i = 0 \end{cases} \quad (26)$$

Where w_i is weight of the link i, L_i is length of the link I in meter, n_i is number of non-idled GPS points (speed > 0 mph) involved in 100-meter buffer, and $\bar{v}_i$ is average speed in m/s of non-idled GPS points involved. The idea of the equation is simple: weight is the average distance interval (or reciprocal of GPS

points density) adjusted by average speed. A smaller ratio L_i/n_i indicates more GPS points involved in unit length of link i, and the weight is thus increased. Also, $\bar{v}_i$ is an adjusting factor since the intervals between consecutive GPS points becomes larger when vehicle is operating at high speed, and thus more likely to be missed from second-by-second density. On the other hand, if no GPS points are involved, weight is simply set an arbitrarily large number (100,000) for the link i.

Step 3: Identify the route (or sequence of links) that GPS trajectory traverses, by implementing Dijkstra's shortest path algorithm with target function as minimizing sum of weights. An example of GPS trajectories and estimated route based on this method is shown in Figure 32. The algorithm is proved to be very stable through author's QA/QC tests

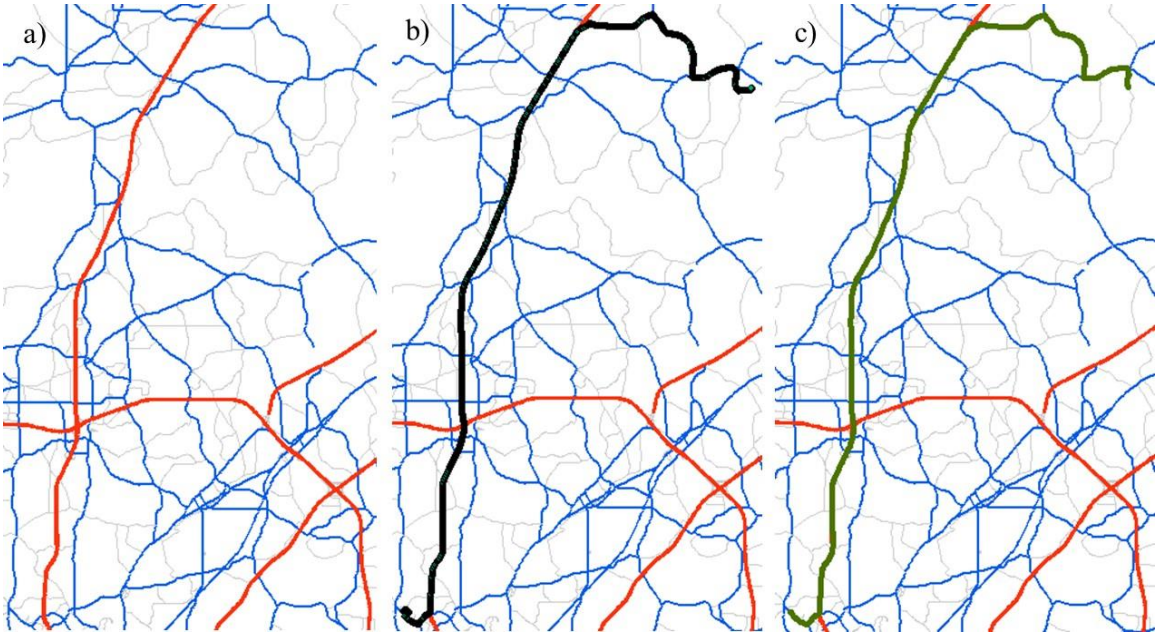

Figure 32 – a) Road Network; b) GPS Trajectories; c) Estimated Routes

Step 4: Map road grade point layer of the estimated route generated in Chapter 3 with GPS points based on shortest distance principle, and append grade information from matched grade point to GPS point.

Other road information can also be matched to GPS data with this process. It is important to notice that extracting the route through Step 1 to Step 3 helps eliminate interference from adjacent roads.

4.3 Energy Consumption and Emissions Modeling based on MOVES-Matrix

4.3.1 MOVES-Matrix Concept Design

MOVES-Matrix (Guensler, et al., 2016) compiles the results from a huge number of MOVES runs. MOVES is iterated across all variables that affect output emission rates, and each iteration yields emission rates for all kinds of air pollutant for a uniform source type, uniform model year (age group), for a specific vehicle fuel type (gasoline, diesel, CNG, etc), specific onroad operating characteristics (average speed and road type, or on-road VSP/STP operating mode bin, or speed-acceleration-grade joint distribution) with a given calendar year and for applicable regional regulatory parameters (fuels properties, I/M), under specific temperature and humidity conditions. Run outputs are compiled into a large multi-dimensional emission rate array. Once in place, a user is able to use Python scripts from within other modeling operations to call for MOVES-Matrix emission rates and obtains exactly the same emission predictions as using the MOVES model directly, without ever having to launch MOVES or transfer MOVES outputs into the analyses.

Figure 33 provides an overview of MOVES-Matrix work concept. Basically, a user can determine the subset of Matrix from calendar year, fuel month and meteorology information, and then for the MOVES-Matrix it can grab each cell of applicable emission rate and weight by on-road activity (per cell) to assemble a fleet emission rate.

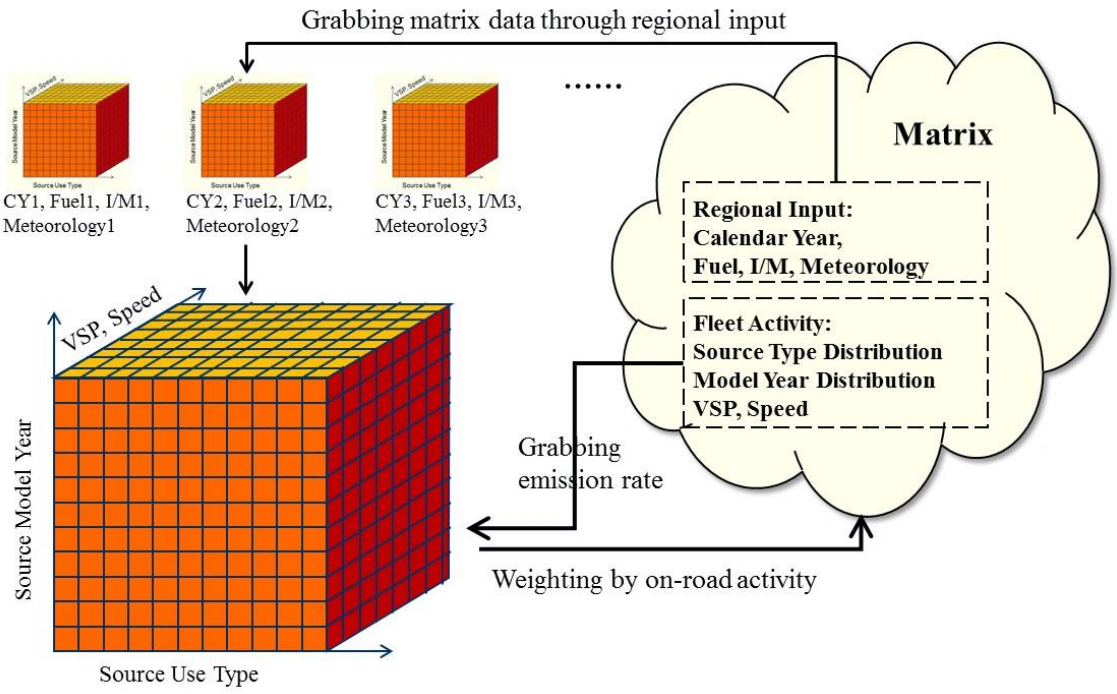

Figure 33 – MOVES-Matrix Work Concept

Developing the MOVES-Matrix energy and emissions rate database for the metro Atlanta region required a total of 146,853 MOVES runs (calendar year 2010-2025, 2030, 2035, 2040, 2045, 2050; fuel: winter fuel, summer fuel, and transition fuel, temperature: 10-110 F in interval of 1F, humidity: 0-100% in interval of 5%; i.e., 21 years×3 local fuels for each year×111 temperatures×21 humidity). Running MOVES 146,853 times is a huge task. The Georgia Tech team has configured MOVES into PACE system to implement the model runs, compile the results, and prepare the matrices. The energy

consumption and emission rate model runs are parallel-processed on available PACE cores.

4.3.2 Input

The description of input data to run MOVES-Matrix is summarized in Table 4. Users can identify the subset of the MOVES-Matrix they need, by specifying calendar year, region, month, and meteorology data. Then, the user can access each cell that contains an energy rate and emission rate for a specific vehicle type and model year from MOVES-Matrix, and weight each emission rate by on-road activity to reassemble to obtain the comprehensive emission result.

Table 4 – Content of Input File for MOVES-Matrix

Input	Description
Calendar year and month	Modeling year and month
Region	Used for identifying emission sub-matrix for Atlanta. Default fuel specification and I/M strategies have been applied
Meteorology	Used for identifying emission sub-matrix at specific meteorology. - Temperature choose from 0-110º F with 1º F-bin interval - Humidity choose from: 0%-100% with 5%-bin interval
Source type	Vehicle source types, including light-duty vehicles, buses, and heavy-duty trucks
Model year	Vehicle model year (vehicle age 0-30)
Speed-acceleration-grade joint distribution	Distribution representing operation characteristics for each source type; used to calculate operating mode distribution

The key input to describe vehicle operations is the Speed-Acceleration-Grade Joint Distribution (SAGJD). It is a frequency distribution of speed, acceleration, and grade joint bins from on-road driving cycles or vehicle trajectories describing

characteristics of operation. The distribution can be easily aggregated from results in section 4.2. In MOVES-Matrix, users can input speed-acceleration-grade joint distribution as operation information. Given a vehicle type, VSP/STP values for each speed-acceleration-grade bin is calculated from equation 1, since VSP is a function of speed, acceleration and grade.

4.3.3 Modeling Algorithm

The MOVES-Matrix application consists of three modules: 1) input, 2) emission database, and 3) output. To support typical applications in each region, the MOVES-Matrix emission database was grouped into 146,853 sub-matrices, with each sub-matrix storing emission rates for all source types, all source model years, all on-road operations (operating mode bins), for one specific calendar year, one fuel month, one temperature, one relative humidity, one fuel supply (by year, month), and one I/M strategy (by year). This way, a small subset of emission rates can be extracted from the matrix based on the user's year, month, region, and meteorology inputs. This structure helps support emission control strategy analysis, given that activity impact on emissions is the focus in the dissertation.

After the sub-matrix of emission rates is identified and accessed, emission rate processing is the same as in MOVES project-level modeling. The emission rates in the sub-matrix are connected to vehicle activity data through MOVES-Matrix algorithms. VSP or STP is calculated for each second of a vehicle trajectory paired with grade, and then assigned its proper operating mode bin. Energy and emission rate of that specific

source type and model year vehicle at specific second is then extracted from sub-matrix based on the assigned operating mode bin.

Figure 34 shows energy rate of a model year 2011 transit bus by operating mode bin (speed and VSP/STP bins). These rates are assigned to speed-acceleration joint bins through bin definition at grade of -3% (downhill), 0% (flat) and +3% (uphill) as shown in Figure 35. It is obvious to see: 1) high speeds and hard accelerations push on-road activity into higher power bins, which then corresponds to higher energy consumption and emission rates; 2) the increase of engine load due to grade change is reflected in the binning method, with more speed-acceleration bins falling into high VSP or STP range and high energy consumption range.

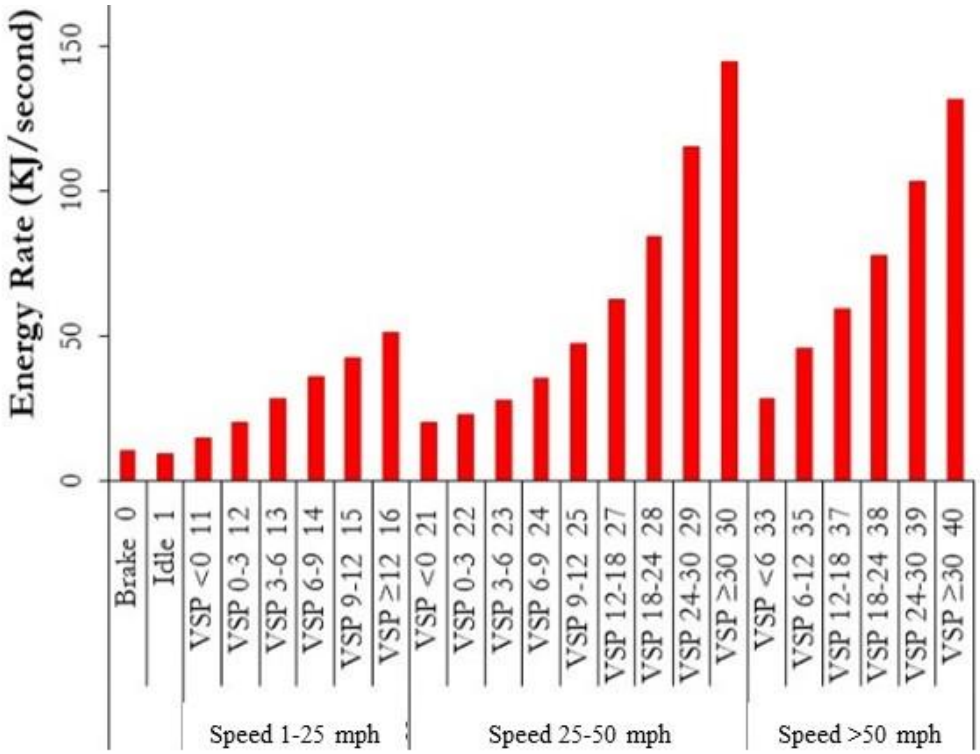

Figure 34 – Energy Rate of MARTA Bus by Operating Mode Bin

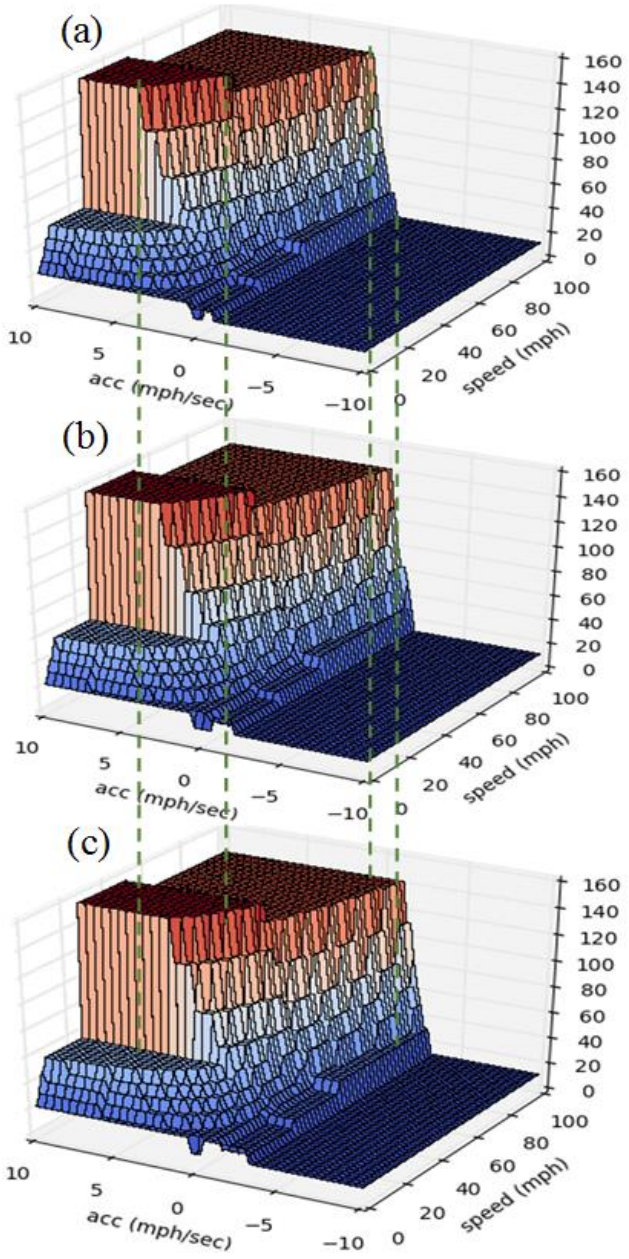

Figure 35 – Energy Rate of MARTA Bus at Grade of (a) -3%; (b) 0%; (c) +3%

MOVES-Matrix also provides algorithms to aggregate energy consumption and emissions outputs for a trip, road segment, or corridor. To calculate energy consumption of a MARTA bus operating with the speed trace in Figure 36 (a) on 3% grade, we can convert the trajectories to Speed-Acceleration Joint Distribution (Figure 36 (b)), and

weight energy rate for grade = 3% (Figure 35 (c)) by the speed-acceleration bins. By summing weighted energy rate, we obtain the energy rate per unit time, which can be multiplied by operating time to obtain total energy consumption for the bus in a complete operation (e.g., a complete trace). Similarly, for a route or route segment with certain grade, appropriate energy rates map are applied. The calculation procedure is coded in MOVES-Matrix.

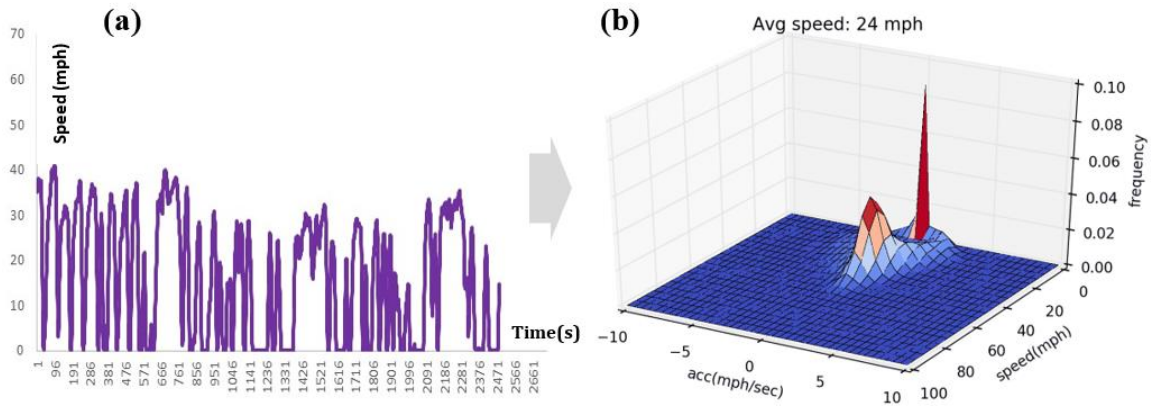

Figure 36 – From (a) MARTA Bus Speed Trajectory to (b) Speed-Acceleration Joint Distribution (SAJD)

4.4 Data Sample and Summary

Through all these data processing steps, we have obtained GPS trajectories paired with vehicle information (e.g., vehicle type, model year, rated horsepower, gross weight), road information (e.g., road grade, horizontal curve, number of lanes, location of traffic signal), surrounding environment (day or night), and calculated energy rate and emissions rate for each second with actual or zero grade. A description of comprehensive dataset is summarized in Table 5.

Table 5 – Summary of Comprehensive Dataset

Operation data	**Description**	**Format (or unit)**
Date	Date of GPS collection	yyyy-mm-dd
Time	Time of day	hh:mm:ss
Latitude	Latitude	XX.XXXXXX
Longitude	Longitude	XX.XXXXXX
Speed	Vehicle speed	mph
Acceleration	Derivative of speed in time	mph/second
Vehicle information		
Light-duty vehicle	**Description**	**Range (or count)**
MOVES source type	MOVES source type classification	passenger car (ID = 21); passenger truck (ID = 31)
Vehicle ID	Unique identification of vehicle	1,653 vehicles in 911 households
Make & model	Vehicle make and model	401 make & models
Model year	Model year of the vehicle	1961-2011
Engine displacement	Engine displacement of the vehicle	1.5 to 6.8 liters
GVWR	Gross vehicle weight rating	2,325 to 10,000 lbs
Regulatory class	EPA classification for emission standards	LDV, LDT1(GVWR<6,000 lbs), LDT2(GVWR 6,000-10,000 lbs)
Rated horsepower	Rated horsepower of vehicle	90 to 380
Gear number	Number of gears	4 to 8
Heavy-duty vehicle	**Description**	**Range (or count)**
Express transit bus	48-seats GRTA diesel bus	13 buses
Urban transit bus	56-seat MARTA diesel bus	13 buses
Road & environment	**Description**	**Range (or count)**
Grade	Ratio of vertical elevation change and horizontal movement	-15% to +15%
Horizontal curve	Changing rate of centerline angle per unit horizontal distance (degree/100 feet)	0 to 16
Number of lanes	Number of lanes in segment	2 to 7
Traffic signal	Traffic light at the segment (1/0)	-
Day/night	Day: from sunrise to sunset	day-1; night-0
Power, energy and emission rate (actual grade and 0 grade)	**Description**	**Unit**

VSP/STP	VSP/STP per second	KW/tonne
opModeBin	Assigned operating mode bin	-
Energy rate	Energy consumption per second	KJ/second
Emission rate	Emission (including CO, NO_X, CO_2, $PM_{2.5}$) per second	Grams/second

A data sample showcase from a processed vehicle trajectory ends the chapter, including second-by-second speed, acceleration, grade profile, VSP, operating mode bin, and energy rate, with actual grade and zero grade implemented respectively, as shown in Figure 37. Looking at VSPs and energy rates for the 1st to 50th second, and around the 200th second, where significant upgrade (grade>0%) or downgrade (grade<0%) exist, the difference of VSPs and energy results between actual grade and zero grade scenario indicate a significant impact on energy consumption and emissions modeling. A series of analyses from Chapter 5 to Chapter 8 aims at exploring these problems.

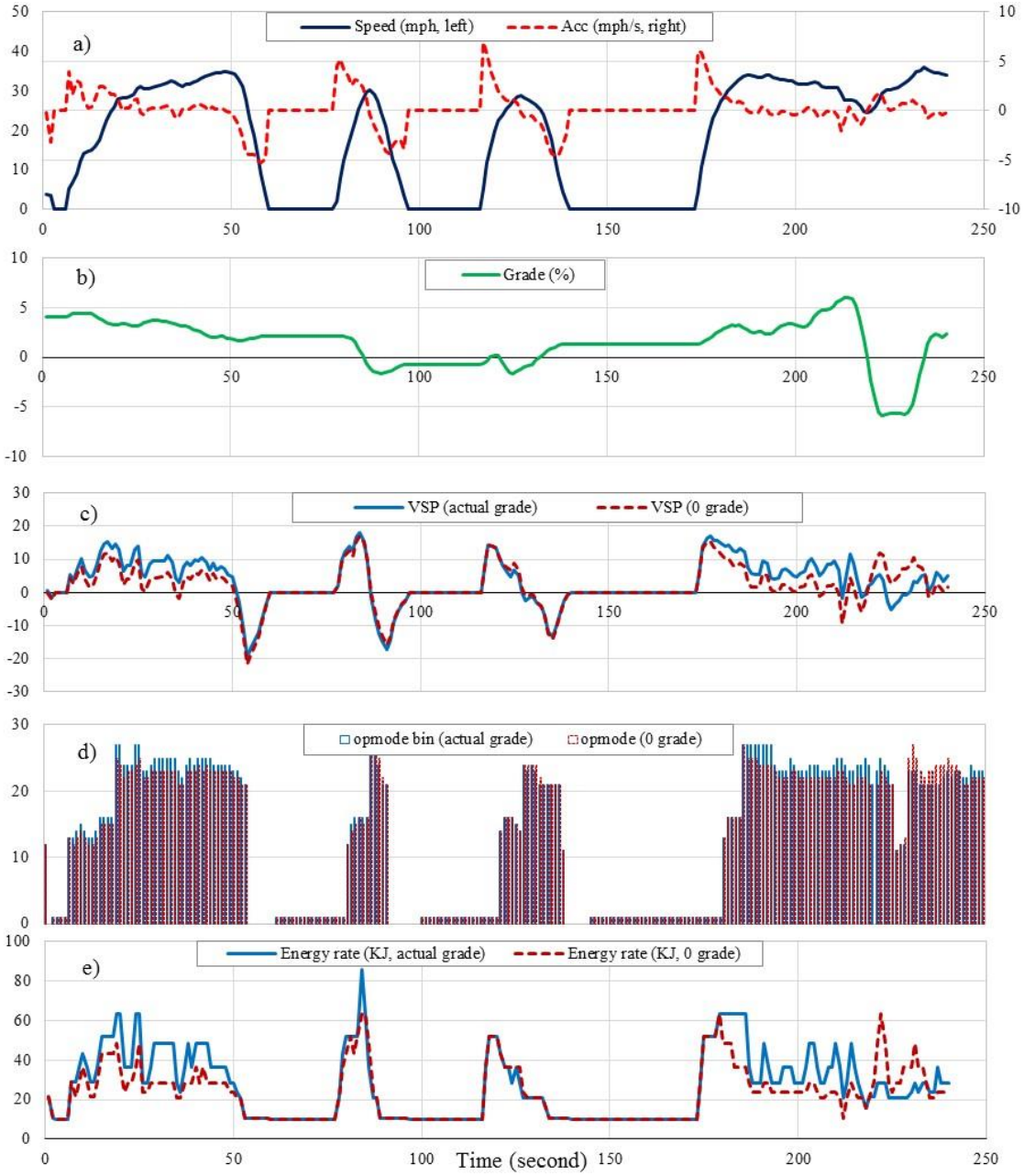

Figure 37 – Sample Trajectory of A Passenger Car. A) Second-By-Second Speed and Acceleration; B) Road Grade; C) Calculated VSP With Actual and 0 Grade; D) Operating Mode Bin With Actual and 0 Grade; E) Estimated Energy Rate With Actual and 0 Grade

CHAPTER 5. FREEWAY OPERATIONS

This chapter focuses on freeway operations, and aims to assess how road grade impacts vehicles speeds and accelerations on freeways, and how the impacts vary across vehicles, vehicle types, and traffic conditions. The study will build foundational knowledge reasoning of grade impact on freeway energy consumption, emissions in Chapter 6.

Bayesian Hierarchical linear regression is utilized to explore grade impact and impact heterogeneity across vehicles on operation at uncongested conditions (with average speed of traces larger than 55 mph), including speeds and accelerations. The shape of speed-acceleration joint distribution (SAJD) in response to grade is also described in detail using extreme accelerations, width of SAJD, and skewness. Results analyses and discussions are followed after each method.

5.1 Trace Segmentation

The average speed of a trace is a reflection of on-road traffic conditions, driver's speed choice behavior, and possibly vehicle performance. To explore the possible heterogeneity of grade impact on operations under different traffic conditions, freeway traces need to be further segmented into smaller traces, with each trace having a relatively stable average speed (or in relatively stable operating condition). A standard regression tree method is applied with second-by-second time-step and speed to minimize speed variance within segmented traces. Minimum length of trace is set as 300 seconds to ensure that each trace last at a certain speed level as a stable process for at least 5

minutes. An example of segmented freeway speed traces is presented in Figure 38. One of the main benefits of such trace segmentation, is to eliminate confounding issue of grade impact on operations with impact of on-road traffic flow condition or driver's behavior. That is the average speed of the smaller traces should mainly be determined by traffic flow conditions and driver's speed choices, and grade impact will be used to explain speed variation under these traffic conditions.

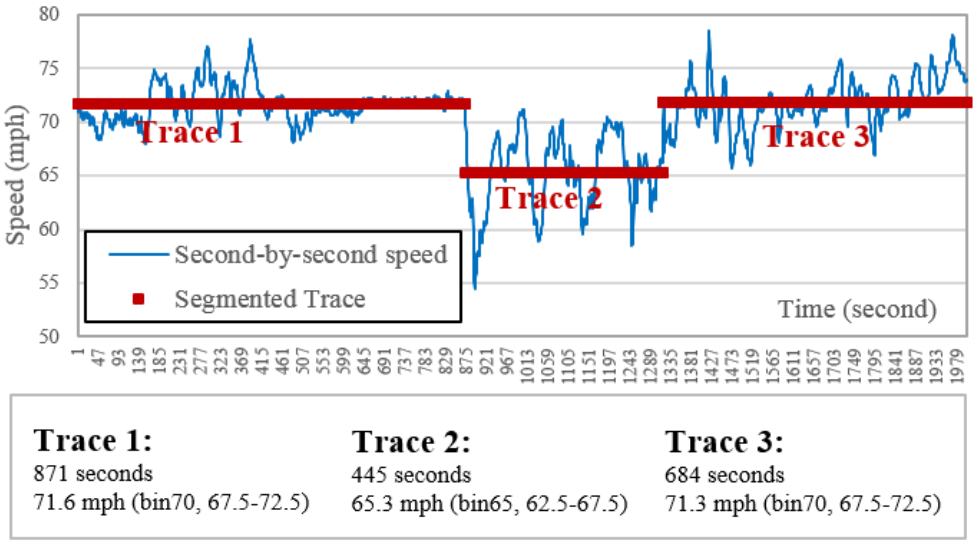

Figure 38 – Example of Segmented Freeway Speed Traces

Segmented traces are classified into 17 average speed bins from 0 mph to 80 mph in 5-mph intervals, with each bin defined as average speed range of (v - 2.5 mph, v + 2.5 mph), which is consistent with the definition in MOVES (USEPA, 2016). For example, all data in traces with average speed 62.5 to 67.5 mph are labeled as trace with average speed bin 65. Table 6 to Table 8 summarizes sample size (in seconds) of GPS data of passenger cars, passenger trucks and express buses by grade level and average speed bins. In general, most of GPS data are collected in grade of -3% to +3%. Most of the operations data collected on freeways are at speed levels ≥ 55 mph. It indicates a more

robust result for analysis at uncongested traffic conditions compared with congested conditions from this study.

Table 6 – Sample Size (in Seconds) of Passenger Car Operations by Trace Average Speed Bin and Grade

	Trace Average Speed (mph)																
Grade (%)	**0**	**5**	**10**	**15**	**20**	**25**	**30**	**35**	**40**	**45**	**50**	**55**	**60**	**65**	**70**	**75**	**80**
-5	4	146	307	229	215	160	178	207	124	163	305	822	2,001	3,220	2,651	1,444	259
-4	49	679	793	850	1,057	772	865	712	694	777	1,398	3,745	8,794	15,152	12,363	5,573	1,230
-3	190	4,388	3,532	4,261	3,331	2,945	2,982	2,673	2,962	2,820	5,708	12,268	33,170	56,329	56,954	26,397	6,070
-2	1,158	5,257	5,357	5,992	4,808	4,533	4,746	4,186	4,477	3,978	7,906	18,955	47,067	81,656	82,819	40,326	9,018
-1	3,765	8,214	9,021	9,394	8,661	7,762	6,570	6,332	7,065	6,609	11,634	28,179	73,439	127,914	129,180	59,879	12,751
0	675	5,178	7,084	6,235	5,852	5,458	5,736	5,611	5,542	5,296	9,386	22,363	58,208	101,637	107,567	52,844	11,870
1	687	9,160	8,540	8,874	7,788	7,456	6,779	7,549	7,350	7,705	11,796	28,351	74,689	127,683	125,359	58,439	12,791
2	1,145	6,531	5,182	5,011	5,362	4,812	4,529	5,005	5,362	5,600	8,837	20,269	50,061	84,733	82,832	38,243	8,664
3	129	3,458	4,504	3,739	3,272	3,433	3,747	3,631	3,625	4,012	6,464	15,229	35,034	58,706	54,761	23,960	5,185
4		520	900	971	1,118	996	1,099	958	1,125	957	1,645	4,733	10,036	16,711	13,445	5,178	950
5		150	297	177	155	245	87	200	207	181	437	1,060	2,309	3,144	2,539	1,127	202

Table 7 – Sample Size (in Seconds) of Passenger Truck Operations by Trace Average Speed Bin and Grade

Grade (%)	**0**	**5**	**10**	**15**	**20**	**25**	**30**	**35**	**40**	**45**	**50**	**55**	**60**	**65**	**70**	**75**	**80**
-5		113	270	198	151	145	87	107	51	76	213	523	1,273	1,608	1,428	811	204
-4		472	965	613	744	382	450	360	188	427	676	2,140	4,999	8,011	6,904	3,742	1,047
-3	638	1,763	2,104	2,036	1,888	1,288	1,521	1,530	1,357	1,310	2,496	7,998	19,095	31,711	30,547	16,877	3,848
-2	704	2,568	3,181	2,785	2,607	2,248	2,601	2,682	2,260	2,115	3,925	13,056	29,285	45,106	46,482	26,585	5,786
-1	1,824	3,226	4,787	4,522	4,590	4,393	4,237	3,664	3,021	3,993	6,629	19,834	43,814	70,712	72,650	39,272	7,972
0	909	2,139	4,017	3,533	2,858	3,261	3,204	3,692	2,817	3,399	5,844	16,560	36,089	60,517	62,890	36,498	7,759
1	366	3,141	4,216	4,027	3,155	3,355	3,517	3,985	3,327	3,949	6,374	19,851	43,661	73,512	72,660	38,769	8,050
2	108	2,225	2,868	3,212	2,532	2,743	2,747	2,580	2,539	2,985	4,791	13,192	29,741	46,830	47,025	25,542	5,104
3	659	2,244	2,588	1,938	1,500	1,605	1,810	1,655	1,682	2,122	3,914	10,040	20,999	31,640	31,191	15,921	3,443
4		194	805	617	773	668	561	645	369	610	1,262	2,676	6,098	8,282	7,050	3,313	885
5		51	135	102	112	149	109	142	72	128	304	756	1,285	1,496	1,302	648	187

Table 8 – Sample Size (in Seconds) of Passenger Truck Operations by Trace Average Speed Bin and Grade

	Trace Average Speed (mph)												
Grade (%)	**10**	**15**	**20**	**25**	**30**	**35**	**40**	**45**	**50**	**55**	**60**	**65**	**70**
-5	0	0	0	79	15	27	3	11	57	56	69	126	46
-4	46	20	22	47	70	58	36	28	85	202	131	432	423
-3	248	30	156	156	223	202	236	346	366	715	513	2,357	2,292
-2	383	367	402	463	429	566	459	624	923	1,509	1,423	5,507	5,723
-1	1,062	497	571	520	613	1,047	751	896	1,526	2,020	2,230	7,939	8,391
0	1,099	645	595	501	470	737	714	678	1,336	1,902	1,976	7,086	8,251
1	1,026	442	616	551	588	884	818	1,002	1,326	2,251	2,292	7,794	8,325
2	348	244	481	316	501	634	522	573	886	1,389	1,642	5,420	5,810
3	196	200	303	165	316	480	288	461	497	686	856	2,829	3,041
4	71	71	156	123	32	157	77	72	55	144	182	484	417
5	98	21	91	72	18	40	20	11	27	41	71	161	93

Sample size (in seconds):

< 500 ≥ 500 ≥ 1,000 ≥ 1,000

5.2 Operations Modeling in Uncongested Condition

An example of speed-acceleration joint distribution (SAJD) from traces with average speed of 70 mph and 40 mph is shown in Figure 39. For uncongested operations (average speed of cycles > 55 mph), traces perform like stationary random process, with the speed and acceleration approximately normally distributed, so the linear model is appropriate. This model, however, does not apply for traces under congested condition.

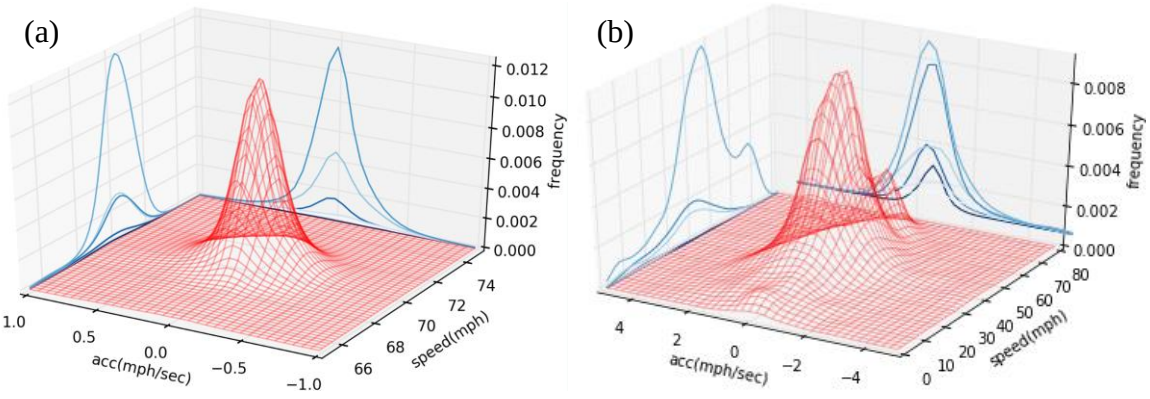

Figure 39 – Speed-Acceleration Joint Distribution of Traces in Average Speed of (a): 70 mph, and (b): 40 mph

5.2.1 Model Setup

The GPS data are, in essence, hierarchically structured, with second-by-second speed and acceleration data that belongs to one trace, and a higher level consisting of all traces collected from a single vehicle. The variance of operations across vehicles may be caused by differences in vehicle performance characteristics and heterogeneity of driver behavior. The operational variance across traces within the same vehicle are most likely caused by the external operating environment at different locations, traffic conditions, and weather. Data from light-duty vehicles were collected for each vehicle paired via a

specific GPS device; hence, data can be pre-processed in to a hierarchical structure, as shown in Figure 40. However, during the express bus data collection, GPS devices were used in multiple vehicles across multiple routes (buses do not necessarily operate on the same routes on different days), so the analyses were not able to organize the bus data into the same vehicle/trace hierarchical structure as the light-duty vehicles. Instead, the bus data were organized into trace groups, and the variance resulting from vehicle, driver, and operating conditions are confounded. However, this should not be a major problem because express bus drivers are expected to operate their vehicles safely and consistently and the performance capabilities of buses in the fleet are not nearly as diverse as those of privately owned and operated light-duty vehicles. Nevertheless, this issue remains a limitation associated with the use of these express bus data.

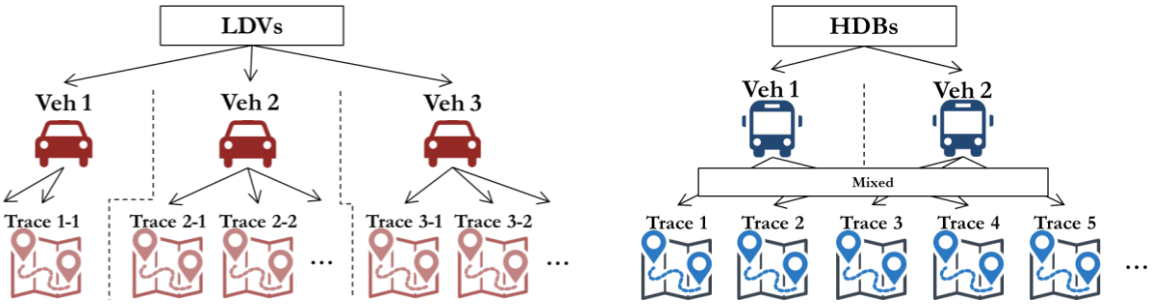

Figure 40 – Hierarchical Structure of Vehicle Traces

A simple way of estimating grade impacts is by multiple linear regression, with a response variable as speed or acceleration, and the independent variable as grade and other control variables with fixed parameters. By using multiple regression, an analysis essentially disaggregates grouped data at the individual level and all predictors are tied to an individual unit of analysis. This leads to at least two potential problems (Luke, 2004). First, by ignoring the vehicle-trace group structure, the model assumes that the regression

coefficients apply equally to all vehicles and traces groups, thus propagating the notion that processes work the same way in different contexts. This is likely not a good assumption, as vehicles performance and driving behavior are diverse in nature. The second problem is that, all of the variance due to un-modeled contextual errors are pooled into the single error term of the multiple regression model. This is problematic, as individuals belonging to the same group will presumably have correlated errors, which violates a basic assumption in multiple regression.

Another approach is to fit separate models for each individual vehicle. However, may lead to overfitting with limited individual vehicle data, which is true in this study (for some vehicles only hundreds of GPS points on a narrow range of grade levels were captured, while thousands of data points are available from other vehicles on grades ranging from -5% to +5%).

Hierarchical models are a natural choice for describing the heterogeneity across several groups (Pinheiro and Bates, 2000) while sharing all data information in one model to ensure a stable estimation without creating an overfitting problem (Gelman and Hill, 2007; Luke, 2004). In the hierarchical model, some variables can be expressed as *fixed-effects* (or in this case fleet-effects), where the parameters present the impact associated with an entire sample that do not vary across groups. On the other hand, some variables can be expressed to have different effects across experimental groups (i.e., vehicles and traces). Because these variables can be treated as random draw from the whole sample set, they constitute *random effects*. In this study, the random-effects include the impacts associated with the vehicles and the traces within each vehicle. It is intuitive to think that vehicle traces are randomly sampled among all possible operations,

and that these traces are collected by vehicles from a very large number of onroad vehicles that include the wide variety of vehicles and drivers. Given that the sample does not reflect the entire onroad population, this does remain a limitation of the modeling work. Considering these relationships, a model with three-level variables is structured: fleet-level, vehicle-level, and trace-level. A graphical representation of the hierarchical model appears in Figure 41.

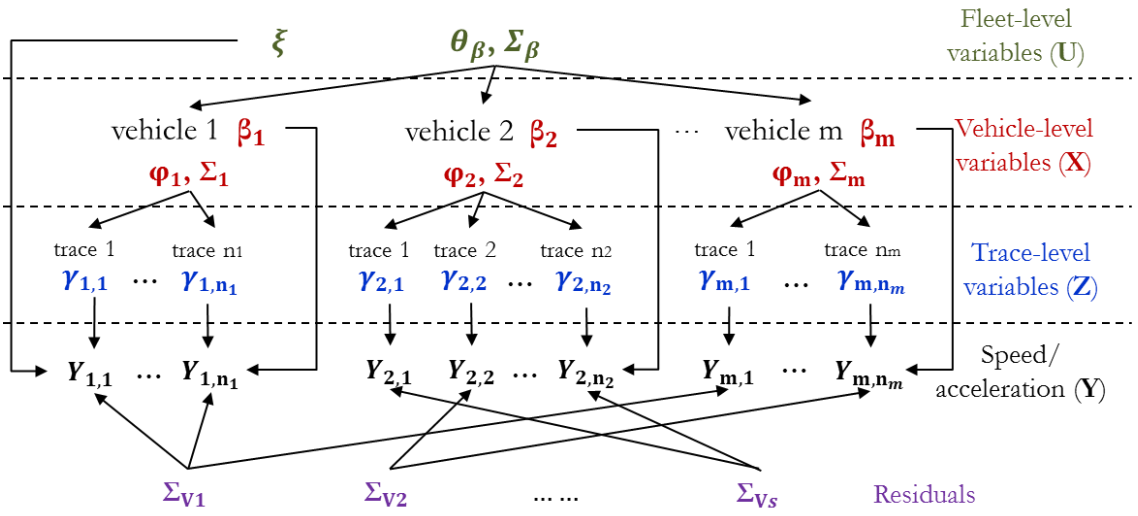

Figure 41 – A Graphical Representation of the Hierarchical Regression Model

As mentioned above, for uncongested operations (average speed of cycles > 55 mph), traces perform much like stationary random processes, with the speed and acceleration normally distributed. Hence, hierarchical linear models are applied. Expressed symbolically, the within-group sampling model is:

$$y_{i,j,k} = \underbrace{u_{i,j,k}\xi}_{fleet} + \underbrace{x_{i,j,k}\beta_i}_{vehicle} + \underbrace{z_{i,j,k}\gamma_{i,j}}_{trace} + \underbrace{\varepsilon_{i,j,k}}_{error} \quad (27)$$

Where $y_{i,j,k}$ is observed speed or acceleration at the k-th second of trace j within vehicle i. Speed and acceleration data in each trace can be written as vector $\boldsymbol{y}_{i,j}$ =

$[y_{i,j,1}, y_{i,j,2}, \ldots, y_{i,j,n_{ij}}]^T$, i = 1, …, m (number of vehicles), j = 1,…,n_i (number of traces from vehicle i), referring to vector of observed speed (or acceleration) of trace j that collected from vehicle i, with trace length n_{ij}.

The fleet-level effects model matrices are $\boldsymbol{u}_{i,j,k}$, of size $1 \times p_{pop}$, where p_{pop} is the number of fleet-level variables, and $\boldsymbol{\xi}$ is vector of fixed-effects parameters to be estimated. Variables that do not vary across vehicles are treated as the fleet-level effects. Vehicle characteristics are included as fleet-level variables, as each vehicle only owns one property. In addition, the number of lanes is assigned to the fleet-level, because it does not vary significantly within vehicle-level operation given trace size. The vehicle-level parameters $\boldsymbol{\beta_i}$ represent heterogeneity across vehicles, and the vector is assumed to be independent across vehicles. This is an appropriate assumption, because each vehicle has its own performance characteristics and each vehicle's associated driver is assumed fixed. Assuming diversity exists in drivers' and/or vehicles' response to road grade, horizontal curves, interaction of grade and operational speed, and day/night, these variables are treated as vehicle-level effects. The results will verify the validity of this assumption. The intercept is treated as a trace-level parameter, representing average speed (or acceleration) of each trip. Setting the trace-level intercept can avoid confounding the impacts of grade, on-road traffic flow, and driver behavior, because average trip speed should be mainly determined by traffic flow and driver speed choices, where grade impact is used to explain speed variation within each trace. A grade-speed interaction term can also be used to identify differences in impacts across speed levels, if any. The trace-level parameter of random effects $\boldsymbol{\gamma_{i,j}}$ are assumed to be independent for different vehicle i or trace j, and to be independent of vehicle-level random effects. This

assumption comes from the data collection situation: data are collected across multiple days, time-periods, and roads, and there are very few data could be collected at the same time and the same location, so it becomes very unlikely that traffic flow interactions exist between any two sampled vehicles used in the dataset.

The terms $\boldsymbol{x_{i,j,k}}$ and $\boldsymbol{z_{i,j,k}}$ are corresponding random effects at the vehicle-level and trace-level, respectively, for vehicle i, and for trace j within vehicle i. $\boldsymbol{\beta_i}$ and $\boldsymbol{\gamma_{i,j}}$ can be expressed as random draws from distribution that represent the whole sample set and vehicle i, respectively. Symbolically, it is written as:

$$\boldsymbol{\beta_i} \sim \boldsymbol{N}(\boldsymbol{\theta_\beta}, \boldsymbol{\Sigma_\beta}), \qquad \boldsymbol{\gamma_{i,j}} \sim \boldsymbol{N}(\boldsymbol{\varphi_i}, \boldsymbol{\Sigma_i})$$

The term $\boldsymbol{\theta_\beta}$ has an important interpretation: it is fleet-level effect from the aggregation of vehicle-level variable. For example, if $\boldsymbol{\beta_i}$ represents the grade impact on operations of vehicle i, $\boldsymbol{\theta_\beta}$ can then be explained as overall impact of grade on the sampled vehicles fleet. A large variance value of $\boldsymbol{\beta_i}$ within $\boldsymbol{\Sigma_\beta}$ indicate diversity of such variable in vehicle-level. $\boldsymbol{\varphi_i}$ can be interpreted as the average speed level of sampled traces from vehicle i.

The error term of the model is denoted as $\boldsymbol{\varepsilon_{i,j}} = [\boldsymbol{\varepsilon_{i,j,1}}, \boldsymbol{\varepsilon_{i,j,2}}, \dots, \boldsymbol{\varepsilon_{i,j,n_{i,j}}}]^{\boldsymbol{T}}$ and can be expressed as:

$$\varepsilon_{i,j} \sim MVN(\mathbf{0}, \boldsymbol{\Sigma_{v_{i,j}}})$$

Heteroscedasticity possibly exists across traces with different speed levels. This study will take this into account by introducing a unique error term for each average speed level from 55 mph to 80 mph, in 5 mph-intervals, i.e., $\sigma^2_{\boldsymbol{v_{i,j}}}$ where $\boldsymbol{v_{i,j}}$ is average

speed bin of trace j from vehicle i, and are set from values of 55, 60, 65, 70, 75, and 80 mph. Additionally, by looking at speed and acceleration traces, it is easy to see that speed and acceleration are highly auto-correlated. This means we must choose the covariance matrix $\boldsymbol{\Sigma}$ that can represent positive correlation between sequential observations. One simple, popular class of covariance matrices for temporally-correlated data is the first-order autoregressive structure (Hamilton, 1994). Under this covariance matrix the variance of $\mathbf{Y_{i,j}}$ is $\sigma^2_{v_{i,j}}$ but the correlation between y_i and y_{i+t} is ρ^t, which decreases to zero as the time difference t becomes larger.

$$\boldsymbol{\Sigma}_{\boldsymbol{v_{i,j}}} = \sigma^2_{v_{i,j}} C_\rho = \sigma^2_{v_{i,j}} \begin{bmatrix} 1 & \rho & \rho^2 & \cdots & \rho^{n_{ij}-1} \\ \rho & 1 & \rho & \cdots & \rho^{n_{ij}-2} \\ \rho^2 & \rho & 1 & \cdots & \rho^{n_{ij}-3} \\ \vdots & \vdots & \vdots & \ddots & \vdots \\ \rho^{n_{ij}-1} & \rho^{n_{ij}-2} & \rho^{n_{ij}-3} & \cdots & 1 \end{bmatrix}_{n_{ij} \times n_{ij}} \tag{28}$$

5.2.2 Parameter Estimation

5.2.2.1 MCMC Simulation

Maximum Likelihood Estimation (MLE) can be implemented to estimate parameters for this model, but it is a challenging option for solving such model with hierarchical structured parameters, as the likelihood function can be complicated, and sometimes cumbersome to conduct derivation. In this study, the Bayesian method is applied to estimate posterior distribution of parameters. The idea of estimating posterior joint distribution of parameters based on Bayesian method is expressed below:

$$\begin{aligned} \boldsymbol{P}(\boldsymbol{\psi}|\boldsymbol{u},\boldsymbol{x},\boldsymbol{z},\boldsymbol{y}) &= \frac{\boldsymbol{P}(\boldsymbol{y},\boldsymbol{\psi}|\boldsymbol{u},\boldsymbol{x},\boldsymbol{z})}{\boldsymbol{P}(\boldsymbol{y}|\boldsymbol{u},\boldsymbol{x},\boldsymbol{z})} = \frac{\boldsymbol{P}(\boldsymbol{y}|\boldsymbol{\psi},\boldsymbol{u},\boldsymbol{x},\boldsymbol{z})\boldsymbol{P}(\boldsymbol{\psi}|\boldsymbol{u},\boldsymbol{x},\boldsymbol{z})}{\boldsymbol{P}(\boldsymbol{y}|\boldsymbol{u},\boldsymbol{x},\boldsymbol{z})} \\ &\propto \boldsymbol{P}(\boldsymbol{y}|\boldsymbol{\psi},\boldsymbol{u},\boldsymbol{x},\boldsymbol{z})\boldsymbol{P}(\boldsymbol{\psi}) \end{aligned} \tag{29}$$

Where $\boldsymbol{\psi}$ is a vector of parameters need to be estimated, and in this study refers to:

$$\left[\xi,\ \boldsymbol{\theta_\beta},\ \boldsymbol{\Sigma_\beta},\ \boldsymbol{\beta_1}, \dots, \boldsymbol{\beta_m},\ \boldsymbol{\varphi_1}, \dots, \boldsymbol{\varphi_m}, \boldsymbol{\Sigma_1}, \dots, \boldsymbol{\Sigma_m},\ \boldsymbol{\gamma_{1,1}}, \boldsymbol{\gamma_{1,2}} \dots, \boldsymbol{\gamma_{m,n_m}},\ \boldsymbol{\sigma^2_{v_1}}, \dots, \boldsymbol{\sigma^2_{v_s}}, \boldsymbol{\rho}\right]$$

The term $\boldsymbol{P}(\boldsymbol{\psi})$ is the prior distribution of $\boldsymbol{\psi}$, and $\boldsymbol{P}(\boldsymbol{\psi}|\boldsymbol{u}, \boldsymbol{x}, \boldsymbol{z}, \boldsymbol{y})$ is the posterior distribution of the given observations. With the joint posterior parameter distribution available, Markov Chain Monte Carlo (MCMC) techniques can be used to simulate (or sample) the posterior distribution of parameters (Robert and Casella, 2013). For most of the parameters, the full conditional distribution can be written in closed form with an appropriate assumption of the prior distribution (conjugate prior, see Gelman, 2014). In that case, a posterior approximation can be made via a Gibbs sampler, an iterative algorithm that constructs a dependent sequence of parameter values whose distribution converges to the target joint posterior distribution.

However, the posterior distribution of the correlation parameter $\boldsymbol{\rho}$ cannot be presented in standard form, so the Metropolis algorithm was implemented. The MCMC simulation strategy is presented in Figure 42, with posterior density functions for sampling presented in the following subsections. Based on the bottom-up simulation strategy (Holf, 2009), for each iteration, the trace-level parameters are updated first, followed by vehicle-level parameters (with trace-level updated), and then the fleet-level parameters (with trace-level and vehicle-level updated). Finally, the error term and correlation parameters are updated, conditional on updated parameters across all three levels.

For *s* in 1 to N:
{ **For *i* in vehicles:**
{ **For *j* in traces in vehicle *i:***
{
Compute $[\boldsymbol{\gamma_{i,j}}^{(s)}|{\sigma_{vij}}^{2(s)}, \rho^{(s)}, \boldsymbol{\varphi_i}^{(s)}, \boldsymbol{\Sigma_i}^{(s)}, \boldsymbol{\beta_i}^{(s)}, \boldsymbol{\xi}^{(s)}]$. Sample $\boldsymbol{\gamma_{i,j}}^{(s+1)}$
}
Compute $[\boldsymbol{\varphi_i}^{(s)}|\boldsymbol{\gamma_{i,j}}^{(s+1)}, \boldsymbol{\Sigma_i}^{(s)}]$. Sample $\boldsymbol{\varphi_i}^{(s+1)}$
Compute $\left[\boldsymbol{\Sigma_i}^{(s)}\middle|\boldsymbol{\gamma_{i,j}}^{(s+1)}, \boldsymbol{\varphi_i}^{(s+1)}\right]$.Sample $\boldsymbol{\Sigma_i}^{(s+1)}$
Compute $[\boldsymbol{\beta_i}^{(s)}|{\sigma_{vij}}^{2(s)}, \rho^{(s)}, \boldsymbol{\gamma_i}^{(s+1)}, \boldsymbol{\theta_\beta}^{(s)}, \boldsymbol{\Sigma_\beta}^{(s)}, \boldsymbol{\xi}^{(s)}]$. Sample $\boldsymbol{\beta_i}^{(s+1)}$
}
Compute $[\boldsymbol{\theta_\beta}^{(s)}|\boldsymbol{\beta}^{(s+1)}, \boldsymbol{\Sigma_\beta}^{(s)}]$. Sample $\boldsymbol{\theta_\beta}^{(s+1)}$
Compute $\left[\boldsymbol{\Sigma_\beta}^{(s)}\middle|\boldsymbol{\beta}^{(s+1)}, \boldsymbol{\theta_\beta}^{(s+1)}\right]$. Sample $\boldsymbol{\Sigma_\beta}^{(s+1)}$
Compute $[\boldsymbol{\xi}^{(s)}|{\sigma_{vij}}^{2(s)}, \rho^{(s)}, \boldsymbol{\gamma}^{(s+1)}, \boldsymbol{\beta}^{(s+1)}]$. Sample $\boldsymbol{\xi}^{(s+1)}$
Compute $\left[{\sigma_{vij}}^{2(s)}\middle|\rho^{(s)}, \boldsymbol{\gamma}^{(s+1)}, \boldsymbol{\beta}^{(s+1)}, \boldsymbol{\xi}^{(s+1)}\right]$. Sample ${\sigma_{vij}}^{2(s+1)}$
Metropolis method to sample $\rho^{(s+1)}$
}

Figure 42 – Combined Gibbs Sampler and Metropolis Algorithm with MCMC Simulation

Since no prior information was acquired, all prior information is set as non-informative by setting the variance to a large value (10,000). Four chains are run with different starting points, with each chain containing a 1,000-iteration loop, using parameter values from the 201st to 1000th iterations. Values from first 200th iterations were removed, as they are draw from the "burn-in" period (Holf, 2009), in which the Markov chain moves from its initial value to a region of the parameter space that has a high posterior probability.

5.2.2.2 Trace-Level Parameters $\boldsymbol{\gamma_{1,1}, \ldots, \gamma_{m,n_m}}$

At the trace-level, the hierarchical model shares information across traces within one vehicle via the parameter $\boldsymbol{\varphi_i}$, $\boldsymbol{\Sigma_i}$, $\boldsymbol{\beta_i}$, $\boldsymbol{\xi}$ and σ^2. Referring to Figure 41, from the perspective of a given $\boldsymbol{\gamma_{i,j}}$ the model looks like an ordinary least squares regression where

the prior mean and variance for $\boldsymbol{\gamma_{i,j}}$ are $\boldsymbol{\varphi_i}$ and $\boldsymbol{\Sigma_i}$. The joint probability density of observed data $y_{i,j,1}, y_{i,j,2}, \ldots, y_{i,j,n_{ij}}$conditional upon $\boldsymbol{u_{i,j}}$, $\boldsymbol{x_{i,j}}$, $\boldsymbol{z_{i,j}}$, $\boldsymbol{\xi}$, $\boldsymbol{\beta_i}$, $\boldsymbol{\gamma_{i,j}}$ and σ^2 can be written as a multivariate normal distribution:

$$\boldsymbol{P}\left(\boldsymbol{y_{i,j}}\middle|\boldsymbol{u_{i,j,k}}, \boldsymbol{x_{i,j,k}}, \boldsymbol{z_{i,j,k}}, \boldsymbol{\psi}\right) \sim MVN\left(\boldsymbol{u_{i,j}\xi} + \boldsymbol{x_{i,j}\beta_i} + \boldsymbol{z_{i,j}\gamma_{i,j}}, \sigma^2_{v_{i,j}} C_\rho\right) \tag{30}$$

Based on to appendix A, the posterior distribution $\boldsymbol{\gamma_{i,j}}$ is a multivariate normal distribution with:

$$Var(\boldsymbol{\gamma_{i,j}}|\boldsymbol{y_{i,j}}, \boldsymbol{u_{i,j}}, \boldsymbol{x_{i,j}}, \boldsymbol{z_{i,j}}, \sigma^2_{v_{i,j}}, \boldsymbol{\psi}) = (\boldsymbol{\Sigma_i}^{-1} + \boldsymbol{z_{i,j}}^T {C_\rho}^{-1} \boldsymbol{z_{i,j}} / \sigma^2_{v_{i,j}})^{-1} \tag{31}$$

$$\begin{aligned} E\left(\boldsymbol{\gamma_{i,j}}\middle|\boldsymbol{y_{i,j}}, \boldsymbol{u_{i,j}}, \boldsymbol{x_{i,j}}, \boldsymbol{z_{i,j}}, \sigma^2_{v_{i,j}}, \boldsymbol{\psi}\right) & \\ = \left(\boldsymbol{\Sigma_i}^{-1} + \boldsymbol{z_{i,j}}^T {C_\rho}^{-1} \boldsymbol{z_{i,j}} / \sigma^2_{v_{i,j}}\right)^{-1} & \left(\boldsymbol{\Sigma_i}^{-1} \boldsymbol{\varphi_i}\right. \\ - \boldsymbol{z_{i,j}}^T {C_\rho}^{-1} \boldsymbol{u_{i,j}\xi} / \sigma^2_{v_{i,j}} - \boldsymbol{z_{i,j}}^T {C_\rho}^{-1} & \boldsymbol{x_{i,j}\beta_i} / \sigma^2_{v_{i,j}} \\ \left. + \boldsymbol{z_{i,j}}^T {C_\rho}^{-1} \boldsymbol{y_{i,j}} / \sigma^2_{v_{i,j}}\right) & \end{aligned} \tag{32}$$

5.2.2.3 Conditional Distribution of $\boldsymbol{\varphi_i}$ and $\boldsymbol{\Sigma_i}$

The sampling model for the $\boldsymbol{\gamma_{i,j}}$'s is that the trace level effects $\boldsymbol{\gamma_{i,j}}$ in vehicle i are i.i.d. samples from a vehicle i-specific multivariate normal distribution with mean $\boldsymbol{\varphi_i}$ and variance $\boldsymbol{\Sigma_i}$. For example, if $\boldsymbol{\gamma_{i,j}}$ refers to average speed of a trace, $\boldsymbol{\varphi_i}$ represents the average speed of traces collected from vehicle i, with a variance-covariance matrix of average speed $\boldsymbol{\Sigma_i}$. Therefore, the full distribution of mean $\boldsymbol{\varphi_i}$ is multivariate normal with an expectation value equal to a combination of prior expectation and the sample mean $\boldsymbol{\gamma_{i,j}}$, and a precision equal to the sum of the prior and data precisions. In the context of the hierarchical regression model, given $\boldsymbol{\Sigma_i}$ and samples of regression coefficients

$\boldsymbol{\gamma_{i,1}, \gamma_{i,2}, \ldots, \gamma_{i,n_i}}$, a convenient prior distribution for the multivariate mean $\boldsymbol{\varphi_i}$ is a multivariate normal distribution, parameterized as:

$$\boldsymbol{\varphi_i} \sim MVN(\boldsymbol{\varphi_{i,0}}, \boldsymbol{\Sigma_{i,0}})$$

Based on the proof in Appendix B, the full conditional distribution $\boldsymbol{[\varphi_i | \gamma_{i,1}, \gamma_{i,2}, \ldots, \gamma_{i,n_i}, \Sigma_i]}$ is a multivariate normal distribution with:

$$Var(\boldsymbol{\varphi_i} | \boldsymbol{\gamma_{i,1}, \gamma_{i,2}, \ldots, \gamma_{i,n_i}, \Sigma_i}) = (\boldsymbol{\Sigma_{i,0}}^{-1} + \boldsymbol{n_i \Sigma_i}^{-1})^{-1} \tag{33}$$

$$E(\boldsymbol{\varphi_i} | \boldsymbol{\gamma_{i,1}, \gamma_{i,2}, \ldots, \gamma_{i,n_i}, \Sigma_i}) = (\boldsymbol{\Sigma_{i,0}}^{-1} + \boldsymbol{n_i \Sigma_i}^{-1})^{-1} (\boldsymbol{\Sigma_{i,0}}^{-1} \boldsymbol{\varphi_{i,0}} + \boldsymbol{n_i \Sigma_i}^{-1} \boldsymbol{\bar{\gamma}_i}) \tag{34}$$

Where n_i is number of traces collected from vehicle i, $\boldsymbol{\bar{\gamma}_i}$ is the vector average $\frac{1}{\boldsymbol{n_i}} \sum_j \boldsymbol{\gamma_{i,j}}$. $\boldsymbol{\varphi_{i,0}}$ and $\boldsymbol{\Sigma_{i,0}}$ are prior mean and variance-covariance matrix of $\boldsymbol{\varphi_i}$. The posterior distribution of $\boldsymbol{\Sigma_i}$:

$$\boldsymbol{[\Sigma_i | \gamma_{i,1}, \gamma_{i,2}, \ldots, \gamma_{i,n_i}, \varphi_i]} \sim \text{inverse} - \text{Wishart}\left(\eta_{i,0} + n_i, \left[S_{i,0} + \sum_{j=1}^{n_i} (\boldsymbol{\gamma_{i,2}} - \boldsymbol{\varphi_i})(\boldsymbol{\gamma_{i,2}} - \boldsymbol{\varphi_i})^T \right]^{-1} \right) \tag{35}$$

Where $\eta_{i,0}$ and $S_{i,0}$ are parameters of the prior distribution $\boldsymbol{\Sigma_i}$.

5.2.2.4 Vehicle-Level Parameters $\boldsymbol{\beta_1, \ldots, \beta_m}$

At the vehicle level, $\boldsymbol{\beta_i}$ represents heterogeneity of impacts across vehicles. The model shares information across vehicles via the parameters $\boldsymbol{\theta_\beta}, \boldsymbol{\Sigma_\beta}$, $\boldsymbol{\gamma_i}$, $\boldsymbol{\xi}$ and $\boldsymbol{\sigma^2}$. Referring to Figure 41, from the perspective of a given $\boldsymbol{\beta_i}$, the model looks like an ordinary least squares regression where the prior mean and variance for $\boldsymbol{\beta_i}$ are $\boldsymbol{\theta_\beta}$ and $\boldsymbol{\Sigma_\beta}$. Following the similar procedure presented in deriving $[\boldsymbol{\gamma_{i,j}}|\boldsymbol{y_{i,j}}, \boldsymbol{u_{i,j}}, \boldsymbol{x_{i,j}}, \boldsymbol{z_{i,j}}, \boldsymbol{\psi}]$, we concluded that $\{\boldsymbol{\beta_i}|\boldsymbol{y_i}, \boldsymbol{u_i}, \boldsymbol{x_i}, \boldsymbol{z_i}, \boldsymbol{\psi}\}$ has a multivariate normal distribution with:

$$Var(\boldsymbol{\beta_i}|\boldsymbol{y_i}, \boldsymbol{u_i}, \boldsymbol{x_i}, \boldsymbol{z_i}, \boldsymbol{\psi}) = \left(\boldsymbol{\Sigma_\beta}^{-1} + \boldsymbol{x_i}^T {C_\rho}^{-1} \boldsymbol{x_i} / \sigma^2_{v_{i,j}}\right)^{-1} \tag{36}$$

$$\begin{aligned} E(\boldsymbol{\beta_i}|\boldsymbol{y_i}, \boldsymbol{u_i}, \boldsymbol{x_i}, \boldsymbol{z_i}, \boldsymbol{\psi}) \\ = \left(\boldsymbol{\Sigma_\beta}^{-1} + \boldsymbol{x_i}^T {C_\rho}^{-1} \boldsymbol{x_i} / \sigma^2_{v_{i,j}}\right)^{-1} \left(\boldsymbol{\Sigma_\beta}^{-1} \boldsymbol{\theta_\beta}\right. \\ - \boldsymbol{x_i}^T {C_\rho}^{-1} \boldsymbol{u_i} \boldsymbol{\xi} / \sigma^2_{v_{i,j}} - \boldsymbol{x_i}^T {C_\rho}^{-1} \boldsymbol{z_i} \boldsymbol{\gamma_i} / \sigma^2_{v_{i,j}} \\ \left. + \boldsymbol{x_i}^T {C_\rho}^{-1} \boldsymbol{y_i} / \sigma^2_{v_{i,j}}\right) \end{aligned} \tag{37}$$

Where $\boldsymbol{y_i}$ refers to observations of all traces in vehicle i, $\boldsymbol{y_i} = \left[\boldsymbol{y_{i,1}}, \boldsymbol{y_{i,2}}, \dots, \boldsymbol{y_{i,n_i}}\right]^T$. Similarly, $\boldsymbol{u_i}, \boldsymbol{x_i}, \boldsymbol{z_i}$ and $\boldsymbol{\gamma_i}$ are aggregated from the trace-level to vehicle-level.

5.2.2.5 Conditional Distribution of $\boldsymbol{\theta_\beta}$ and $\boldsymbol{\Sigma_\beta}$

The sampling model for the $\boldsymbol{\beta_i}$'s is that the vehicle-level effects $\boldsymbol{\beta_i}$ are i.i.d. samples from a multivariate normal distribution with mean $\theta_{\boldsymbol{\beta}}$ and variance $\Sigma_{\boldsymbol{\beta}}$. Therefore, the full distribution of mean $\theta_{\boldsymbol{\beta}}$ is multivariate normal with an expectation value equal to a combination of the prior expectation and the sample mean $\boldsymbol{\beta_i}$, and precision equal to the sum of the prior and data precisions. This is essentially an aggregating process effect to reflect the fleet-level effect of vehicle-level variables. In the context of the hierarchical regression model, given $\Sigma_{\boldsymbol{\beta}}$ and samples of regression

coefficients $\boldsymbol{\beta_1, \beta_2, \dots, \beta_m}$. following similar procedures in deriving $\boldsymbol{[\varphi_i | \gamma_{i,1}, \gamma_{i,2}, \dots, \gamma_{i,n_i}, \Sigma_i]}$, the full conditional distribution of $\theta_{\boldsymbol{\beta}}$ is a multivariate normal distribution is:

$$Var(\theta_{\boldsymbol{\beta}} | \boldsymbol{\beta_1, \beta_2, \dots, \beta_m}, \Sigma_{\boldsymbol{\beta}}) = (\boldsymbol{\Sigma_{\beta,0}}^{-1} + m\Sigma_{\boldsymbol{\beta}}^{-1})^{-1} \tag{38}$$

$$\begin{aligned} E(\theta_{\boldsymbol{\beta}} | \boldsymbol{\beta_1, \beta_2, \dots, \beta_m}, \Sigma_{\boldsymbol{\beta}}) \\ = (\boldsymbol{\Sigma_{\beta}}^{-1} + m\Sigma_{\boldsymbol{\beta,0}}^{-1})^{-1} (\boldsymbol{\Sigma_{\beta,0}}^{-1} \theta_{\boldsymbol{\beta,0}} \\ + m\Sigma_{\boldsymbol{\beta}}^{-1} \overline{\boldsymbol{\beta}}) \end{aligned} \tag{39}$$

Where m is number of vehicles that operation data is collected, $\overline{\boldsymbol{\beta}}$ is the vector average $\frac{1}{\boldsymbol{m}} \sum_j \boldsymbol{\beta_i}$. $\theta_{\boldsymbol{\beta,0}}$ and $\boldsymbol{\Sigma_{\beta,0}}$ are prior mean and variance-covariance matrix of $\theta_{\boldsymbol{\beta}}$, respectively. As mentioned earlier, a convenient prior distribution for the variance-covariance matrix $\Sigma_{\boldsymbol{\beta}}$ is an inverse-Wishart distribution (Leonard and Hsu, 1992). Following the similar procedures in deriving $\left[\boldsymbol{\Sigma_i} \middle| \boldsymbol{\gamma_{i,1}, \gamma_{i,2}, \dots, \gamma_{i,n_i}, \varphi_i}\right]$, the full conditional distribution of $\Sigma_{\boldsymbol{\beta}}$ is:

$$\begin{aligned} \left[\Sigma_{\boldsymbol{\beta}} \middle| \boldsymbol{\beta_1, \beta_2, \dots, \beta_m}, \theta_{\boldsymbol{\beta}}\right] \sim \text{inverse} - \text{Wishart}(\eta_0 \\ + m, [\mathrm{S}_0 + \sum_{i=1}^{m} (\boldsymbol{\beta_i} - \theta_{\boldsymbol{\beta}})(\boldsymbol{\beta_i} - \theta_{\boldsymbol{\beta}})^T]^{-1}) \end{aligned} \tag{40}$$

Where η_0 and S_0 are parameters of the prior distribution $\Sigma_{\boldsymbol{\beta}}$.

5.2.2.6 Fleet-Level Fixed-Effects $\boldsymbol{\xi}$

If effects remain that do not vary across traces and vehicles and traces (i.e., overall effects associated with the whole sample set), they can classify be classified as fleet-level fixed-effects $\boldsymbol{\xi}$, assuming homogeneity impact across all vehicles and traces.

Following the similar procedure presented in deriving $[\boldsymbol{\gamma}_{i,j}|\boldsymbol{y}_{i,j}, \boldsymbol{u}_{i,j}, \boldsymbol{x}_{i,j}, \boldsymbol{z}_{i,j}, \boldsymbol{\psi}]$, we concluded that $[\boldsymbol{\xi}|\boldsymbol{y}, \boldsymbol{u}, \boldsymbol{x}, \boldsymbol{z}, \boldsymbol{\psi}]$ has a multivariate normal distribution with:

$$Var(\boldsymbol{\xi}|\boldsymbol{y}, \boldsymbol{u}, \boldsymbol{x}, \boldsymbol{z}, \boldsymbol{\psi}) = \left(\boldsymbol{\Sigma_{\xi,0}}^{-1} + \boldsymbol{u}^T {C_\rho}^{-1} \boldsymbol{u}/\sigma^2_{v_{i,j}}\right)^{-1} \tag{41}$$

$$\begin{aligned} E(\boldsymbol{\xi}|\boldsymbol{y}, \boldsymbol{u}, \boldsymbol{x}, \boldsymbol{z}, \boldsymbol{\psi}) \\ = \left(\boldsymbol{\Sigma_{\xi,0}}^{-1} + \boldsymbol{u}^T {C_\rho}^{-1} \boldsymbol{u}/\sigma^2\right)^{-1} \left(\boldsymbol{\Sigma_{\xi,0}}^{-1} \boldsymbol{\theta_{\xi,0}}\right. \\ - \boldsymbol{u}^T {C_\rho}^{-1} \boldsymbol{x\beta}/\sigma^2_{v_{i,j}} - \boldsymbol{u}^T {C_\rho}^{-1} \boldsymbol{z\gamma}/\sigma^2_{v_{i,j}} \\ \left. + \boldsymbol{u}^T {C_\rho}^{-1} \boldsymbol{y}/\sigma^2_{v_{i,j}}\right) \end{aligned} \tag{42}$$

Where $\boldsymbol{\theta_{\xi,0}}$ and $\boldsymbol{\Sigma_{\xi,0}}$ refers to the mean and variance-covariance matrix of the prior distribution $\boldsymbol{\xi}$. $\boldsymbol{y}$ refers to observations of all vehicles and all traces, $\boldsymbol{y} = [\boldsymbol{y_1}, \boldsymbol{y_2}, \dots, \boldsymbol{y_m}]^T$. Similarly, $\boldsymbol{u}, \boldsymbol{x}, \boldsymbol{z}$ and $\boldsymbol{\gamma}$ are aggregated from trace-level and vehicle-level to the fleet-level.

5.2.2.7 Conditional Distribution of $\sigma^2_{v_{i,j}}$

The parameter $\sigma^2_{v_{i,j}}$ represents the error variance, which varies across average speed of traces. As in most normal sampling problems, the semi-conjugate prior distribution for $\sigma^2_{v_{i,j}}$ is an inverse-gamma distribution. Letting $\lambda = 1/\sigma^2_{v_{i,j}}$ be the measurement precision, and $\lambda \sim \text{gamma}(\nu_0/2, \nu_0 {\sigma^2}_0/2)$. The prior distribution is:

$$\mathrm{P}(\lambda) = \frac{\lambda^{\frac{\nu_0}{2}-1} \exp(-\lambda \nu_0 {\sigma^2}_0/2)}{\Gamma(\frac{\nu_0}{2})} \propto [\lambda^{\frac{\nu_0}{2}-1} \exp(-\lambda \nu_0 {\sigma^2}_0/2)] \tag{43}$$

Based on the proof in Appendix C, the posterior distribution of σ^2 is an inverse-gamma distribution:

$$\left[\sigma^2_{v_{i,j}} \middle| \boldsymbol{y}, \boldsymbol{u}, \boldsymbol{x}, \boldsymbol{z}, \boldsymbol{\gamma}, \boldsymbol{\beta}, \boldsymbol{\xi}\right] \sim \text{inverse} - \text{gamma}(\left[\nu_0 + \boldsymbol{n}_{v_{i,j}}\right]/2, \\ [\nu_0 {\sigma^2}_0 + \\ \sum_{i=1}^{m}\sum_{j=1}^{n_i}\sum_{k=1}^{n_{i,j}} \left(\boldsymbol{y_{i,j,k}} - \boldsymbol{z_{i,j,k}}\boldsymbol{\gamma}_{i,j} - \boldsymbol{x_{i,j,k}}\boldsymbol{\beta_i} - \boldsymbol{u_{i,j,k}}\boldsymbol{\xi}\right)^T {C_\rho}^{-1} \left(\boldsymbol{y_{i,j,k}} - \boldsymbol{z_{i,j,k}}\boldsymbol{\gamma}_{i,j} - \boldsymbol{x_{i,j,k}}\boldsymbol{\beta_i} - \boldsymbol{u_{i,j,k}}\boldsymbol{\xi}\right)]/2) \quad (44)$$

Where ν_0 and ${\sigma^2}_0$ are prior parameters of $\sigma^2_{v_{i,j}}$. $n_{v_{i,j}}$ refers to the sample size (in seconds) from all traces with an average speed $v_{i,j}$.

5.2.2.8 Sampling ρ based on Metropolis Algorithm

The full conditional distribution for ρ will be nonstandard for most prior distributions, suggesting that the Gibbs sampler is not applicable. Thus, the Metropolis-Hastings algorithm is applied instead (Holf, 2009). To apply this algorithm, we first propose ρ* from a uniform distribution (0,1), and compute the acceptance ratio:

$$r = \frac{P\left(\boldsymbol{y}\middle|\boldsymbol{u}, \boldsymbol{x}, \boldsymbol{z}, \sigma^2_{v_{i,j}}, \rho^*, \boldsymbol{\gamma}, \boldsymbol{\beta}, \boldsymbol{\xi}\right) P(\rho^*)}{P\left(\boldsymbol{y}\middle|\boldsymbol{u}, \boldsymbol{x}, \boldsymbol{z}, \sigma^2_{v_{i,j}}, \rho^{(s)}, \boldsymbol{\gamma}, \boldsymbol{\beta}, \boldsymbol{\xi}\right) P(\rho^{(s)})} \quad (45)$$

And sample u ~ uniform(0,1). If u < r set $\rho^{(s+1)} = \rho^*$, otherwise $\rho^{(s+1)} = \rho^{(s)}$.

The Bayesian model results include MCMC draws from the posterior distribution of the parameters. Via post-processing of these MCMC draws, 95% credible intervals can be easily obtained for the probability of an operation impact. The highest probability density interval is then reflected from the draws. Credible intervals have an advantage over confidence interval obtained from classical MLE method of which the interpretation are more intuitive. The classical MLE treats the parameters around which the confidence interval is built as fixed, in that case, 95% confidence interval means over repeated sampled confidence intervals, 95% of them includes will contain the fixed parameters. In

contrast, the Bayesian approach treats parameters as random, and 95% indicates that the parameters have 5% of chance failing to fall within the 95% credible interval (Gelman, et al., 2014).

5.2.3 Model Results

Light-duty vehicles were further decomposed into two classes, based on EPA regulatory classes: LDV (mostly sedan, station wagon, compact SUV, and minivan) and LDT (mostly middle- to large-size SUV, limo, van, and pick-up trucks), because there are significant differences between these two classes in terms of vehicle weight, engine displacement, and vehicle performance. Hence, there are three vehicle types are employed: LDV, LDT, and express bus, with statistical models developed respectively.

The descriptions of variables from fleet-level, vehicle-level, and trace-levels of the BHM is shown in Table 9. The vehicle model year is converted to a dummy variable as post-2002 (1) and 2002 and earlier (0), implying the potential effect of engine improvement on vehicle crawling capability due to the phase in of the Tier 1 emissions standard. The grade variable is decomposed to negative (<0%) and positive (≥0%) to capture the possible impact difference between downgrade and upgrade. The interaction of road grade and average speed of traces are included as vehicle-level effects to identify any differences of grade impacts across traffic conditions. Similarly, the interaction of road grade and day/night are included as vehicle-level effects to identify any differences of grade impact between daylight and night. To consider antedating response to upgrade/downgrade drivers sight distance, the study also generated variables “Grade (FlatToUp)” and “Grade (FlatToDown)”, which are quantified as grade differences

between a flat segment that vehicles are in, and uphill or downhill segments that the flat segment is connected to within the next 100 feet (around 35 meters). Given the methods used to collect the express bus data, we are not able to organize express bus data in the same vehicle/trace hierarchical structure as the light-duty vehicles. Hence, bus data were organized in a fleet-trace group. For express buses, all variables at vehicle-level shown in Table 9 are moved to the fleet-level.

Table 9 – Variable Descriptions for Bayesian Hierarchical Model

Variables	Description	Value Range
Fleet-level		
#Lanes	Number of lanes along the direction of the road	2-7
Model year	The year vehicle is manufactured	After 2002: 1 2002 and before: 0
Engine displacement	Engine displacement of the vehicle (liters)	1.5 to 6.8
GVWR	Gross vehicle weight rating (1,000 lbs)	2.325 to 10
Vehicle-level (can be aggregated to reflect fleet-level effect)		
Grade (<0%)	Downhill grade (always negative, %)	-6.0 to 0.0
Grade (≥0%)	Uphill grade (always positive, %)	0.0 to +6.0
Grade (<0%) ×avgspeed	Interaction of downhill grade (%) by average speed (mph). Average speed scaled to median as 70, i.e., avgspeed-70	-
Grade (≥0%) ×avgspeed	Interaction of uphill grade (%) by average speed (mph). Average speed scaled to median as 70, i.e., avgspeed-70	-
100/Radius	Curve changing rate per 100 meters movement, calculated as 100 divided by radius (meters) of horizontal curve	0 to 16
Day	Daylight or night, based on sunrise and sunset time, an indicator of visibility	Day: 1, night: 0
Grade (<0%)×Day	Interaction of downhill grade by day/night	-
Grade (≥0%)×Day	Interaction of uphill grade by day/night	-
Grade (FlatToUp)	Grade difference (always positive, %) when vehicle is on flat roads ($-1\%<G_{flat}<1\%$) but an uphill grade 30 meter ahead of driver's vision ($G_{ahead50} > 1\%$), calculated as $G_{ahead100}-G_{flat}$	0.0 to +6.0
Grade (FlatToDown)	Grade difference (always negative, %) when vehicle is on flat roads ($-1\%<G_{flat}<1\%$) but an downhill grade 30 meter ahead	-6.0 to 0.0

	of driver's vision ($G_{ahead50}$ <-1%), calculated as $G_{ahead100}$-G_{flat}	
Trace-level		
Intercept	Constant indicating average speed or acceleration of each trace	52.5 to 81 mph

5.2.3.1 Model Examination

Before making inferences, it is necessary to check whether the underlying distributional assumptions appear valid for the residuals. There are two basic distributional assumptions for the BHM considered in this study: The first assumption is, the errors are normally distributed, with mean zero and variance as $\sigma^{2}_{v_{i,j}}$, which depend on the average speed level $v_{i,j}$ of trace j from vehicle i. The second assumption is that errors within a trace are temporally correlated, and that the correlation can be appropriately represented by the first order autocorrelation structure.

In assessing the adequacy of the assumptions, it is useful to consider diagnostic plots of normalized residuals, in this model defined as:

$$\boldsymbol{v_{i,j}} = \hat{\sigma}^{-1}_{v_{i,j}} \left(\widehat{C_{\rho}}^{-\frac{1}{2}} \right)^{T} (\boldsymbol{y_{i,j}} - \boldsymbol{\hat{y}_{i,j}}) \qquad (46)$$

Where $\hat{\sigma}^{2}_{v_{i,j}} \widehat{C_{\rho}}$ denotes the estimated variance-covariance matrix for the within-group error of trace j from vehicle i. The *normalized residuals* should be approximately distributed as independent standard normal random vector, i.e., $\boldsymbol{v_{i,j}} \sim \boldsymbol{N}(\boldsymbol{0}, \boldsymbol{I})$ (Cox and Snell, 1968; Pinheiro and Bates, 2000). Figure 43 shows the distribution of the normalized residuals from the LDV speed model and acceleration model. In general, the density indicate that normalized residuals are approximately standard normal distributed

with a symmetric shape, mode at zero, and most probabilities are concentrated in the range (-1.96, 1.96), which is 95% confidence interval of standard normal distribution.

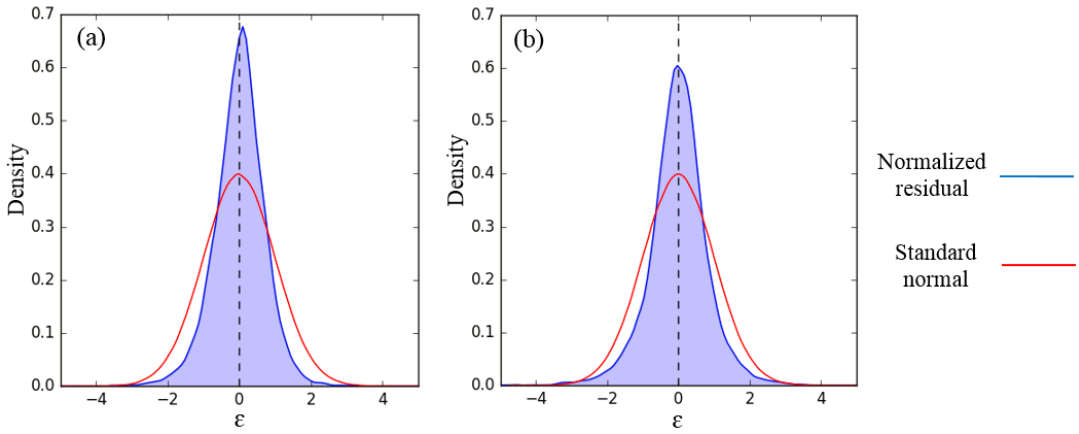

Figure 43 – The Normalized Residual Density and Standard Normal Density (a): LDV Speed Model; (b): LDV Acceleration Model

The empirical autocorrelation function (ACF) of normalized residuals is used to examine whether the autocorrelation characteristics are captured by the first-order autoregressive structure proposed in the model. By definition, the empirical ACF at lag l is defined as (Hamilton, 2014):

$$\hat{\rho}(l) = \frac{\sum_{i=1}^{m}\sum_{j=1}^{n_i}\sum_{k=1}^{n_{i,j}} v_{i,j,k} v_{i,j,(k+l)} \,/N(l)}{\sum_{i=1}^{m}\sum_{j=1}^{n_i}\sum_{k=1}^{n_{i,j}} v_{i,j,k}^2 \,/N(0)} \tag{47}$$

Where $N(l)$ is the number of residual pairs used in the summation at lag l.

Figure 44 shows the empirical ACF values in lag from 0 to 50 seconds, with and without the correlation matrix embedded. These results indicate that when autocorrelation is not considered (see Figure 44 (a), by setting ρ=0 from equation (2), there exist

significant autocorrelations in the normalized residuals. When the correlation matrix is applied, although weak correlations still exist across the normalized residuals, the ACF values Figure 44 (b) shrinks from 0.8 to under 0.45 for lag 1, and under 0.2 for lag 3 or higher. It indicates the first-order autoregressive matrix is capable of capturing most of the correlation patterns. There is also only one parameter in first-order autoregressive structure, makes it quite convenient to estimate. The plots for other models are quite similar to Figure 43 and Figure 44.

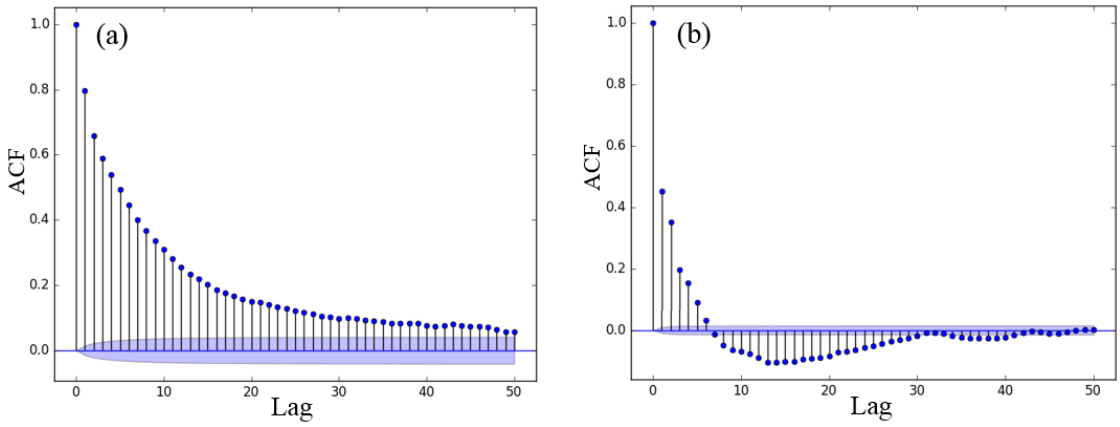

Figure 44 – ACF Plot of Normalized Residuals in LDV Speed Model. (a): Without Correlation Structure (ρ=0); (b): With First-order Autoregressive Structure

5.2.3.2 Fleet-Level Effect

Coefficients of fleet-level effects to speed and acceleration models for three vehicle types are presented in Table 10, reflecting overall impact on operations of the sampled fleet. For LDVs, vehicle speed dropped by 0.227 mph for 1% of grade increase (changing from more downgrade to more flat) at downhill operations. For uphill operations, vehicle speed dropped by 0.191 for 1% of grade increase (changing from more flat to more extreme upgrade). Grade impact significance is >99.9% for all vehicle

types. For LDTs, the parameters are -0.151 and -0.256 respectively, indicating that compared to LDVs, LDTs fleet speeds are more sensitive to uphill segments than downhill segments. Compared to the light-duty vehicle models, the grade parameters from bus speed model are significantly more negative (-0.271 and -0.277), showing that speed of heavy-duty buses dropped more than light-duty vehicles to negotiate grades on freeways.

Additionally, coefficients of flat to uphill and flat to downhill segments all have a positive impact on vehicle speed. Hence, when an "average" driver driving on flat segment observes an uphill segment ahead, he/she tends to increase the vehicle speed prior to the uphill crawl. In contrast, if a downhill is ahead, he/she tends to decrease the vehicle speed to let the vehicle slide down with the help of gravity. The extent of such speed adjustments depends on the steepness of the leading segment. This result is consistent with a drivers' psychological stats and behavior, as we tend to prepare ahead based on what we have seen or expect within the sight distance (Layton, 2012). In terms of interactions between grade and other variables, for the LDV and LDT models, the coefficients associated with interaction of grade and average trace speed are insignificant, inferring that grade impacts do not vary across traffic conditions for average speed > 55 mph. However, for express buses, grade impact becomes more sensitive for traffic conditions with higher average speeds, which make sense because higher speed likely implies less interruption from traffic flow, as well as high power demand that makes it more challenging for vehicles to overcome upgrades while maintaining high operating speed. Small coefficients of interaction to day/night indicate the invariance of grade impact during the day compared to at night.

The horizontal curve coefficient is shown to have significant impact on vehicle speed, with speed decrease of 0.211 and 0.259 mph for each increase of unit of angle changing rate per 100 meters for LDVs and LDTs. This increases to 0.319 for express buses, implying more speed sensitivity to horizontal curves for express buses. This is intuitive because heavy-duty vehicles usually experience a much larger centripetal force when driving along curves. Speed is also estimated to be a little higher during the day compared to night, and this difference is smaller for express buses, perhaps because bus drivers are more skilled and more familiar with routes. For light-duty vehicles, none of the vehicle parameters (GVWR, engine displacement, and model year) were significant, implying that vehicles do not appear to behave differently across regulatory groups within a vehicle class. The correlation coefficients of 0.87 to 0.88, represent highly positive autocorrelation between sequential speeds that cannot be ignored. The differences of σ^2 across speed validate the heteroscedasticity across average speed levels.

Table 10 – Speed and Acceleration Model Result: Fleet-Level Effect

	Speed Model (mph)			Acceleration Model (mph/s)		
	LDV	LDT	Bus	LDV	LDT	Bus
Variables	**Coef.**	**Coef.**	**Coef.**	**Coef.**	**Coef.**	**Coef.**
Model year	0.045	0.012	-	0.004	-0.002	-
Engine displacement	0.018	-0.000	-	0.020	-0.000	-
GVWR	-0.003	-0.002	-	-0.000	0.007	-
Grade (<0%)	-0.227***	-0.151***	-0.271***	-0.025***	-0.013***	-0.03***
Grade (≥0%)	-0.191***	-0.256***	-0.277***	-0.026***	-0.037***	-0.042***
Grade (<0%) ×avgSpeed	-0.007	0.014	-0.021***	0.000	0.000	0.004
Grade (≥0%) ×avgSpeed	0.009^	0.003	-0.018***	0.000	0.000	0.001
100/Radius	-0.211***	-0.259***	-0.319***	0.007	0.016	-0.095***
Day (1-Day, 0-Night)	0.762***	0.133^	0.096	-0.006	0.002	-0.004
Grade (<0%)×Day	0.029^	0.013	-0.035*	-0.0007	-0.015	0.001
Grade (≥0%)×Day	-0.015	0.028*	-0.083***	-0.0004	0.003	0.001
#Lanes	-0.030***	-0.045***	0.06***	0.000	0.000	0.006***
Grade (FlatToUp)	0.305***	0.239***	0.219***	-0.081***	-0.086***	-0.192***
Grade (FlatToDown)	0.302***	0.247***	0.262***	-0.079***	-0.079***	-0.165***

		Speed Model (mph)			Acceleration Model (mph/s)		
		LDV	**LDT**	**Bus**	**LDV**	**LDT**	**Bus**
Variables		**Coef.**	**Coef.**	**Coef.**	**Coef.**	**Coef.**	**Coef.**
ρ		0.87	0.87	0.88	0.43	0.42	0.44
Sigma^2 ($\boldsymbol{\sigma}^2$) by trace avg speed (mph)	55	2.86	2.74	4.65	0.13	0.128	0.299
	60	2.04	3.02	3.91	0.13	0.12	0.275
	65	2.50	1.38	1.48	0.11	0.098	0.138
	70	1.28	1.59	0.98	0.11	0.10	0.096
	75	1.61	1.06	-	0.11	0.10	-
	80	1.07	0.85	-	0.10	0.08	-
N		2,181,191	1,454,128	105,247	2,181,191	1,454,128	105,247
-2 log(Likelihood)		697,486	508,800	150,426	1,265,922	923,609	272,476

*****99.9%, **99%, *95%, ^90%**

From the parameters in the acceleration models, vehicle acceleration dropped by 0.025 mph/s for LDVs and 0.013 mph/s for LDTs for 1% of grade increase at downhill operations, while this number is much larger (0.03) for express bus. For uphill operations, acceleration of light-duty vehicle dropped by 0.026 (0.037 mph/s for LDTs) for 1% of grade increase; this number is 0.042 for express bus. This implies that grade has much greater impact on express bus acceleration behavior compared to light-duty vehicles, and this change is especially significant on downhill grades. Additionally, coefficients of flat to uphill and flat to downhill segments all have negative impact on vehicle acceleration. The parameter estimation for horizontal curve rate does not show a significant impact on accelerations of light-duty vehicles, but the significant coefficient in the express bus model implies a much more sensitive impact of horizontal curve on acceleration behavior of heavy-duty buses. The reason is possibly the same for speed impact given that heavy-duty vehicles usually suffer much larger centrifugal force when rounding curves. Coefficients for the day/night variable do not show a significant impact across any

vehicle types. The small coefficients of interactions between grade and other variables indicate that there are no significant interactions affecting vehicle acceleration.

5.2.3.3 Vehicle-Specific Effect

Figure 45 and Figure 46 show the posterior distribution of population-level coefficients and vehicle-level coefficients from the speed model and acceleration model of passenger car and light-duty truck, respectively. Taking the parameter of grade (<0%) in the LDV speed model as an example, the fact that the coefficients are extremely unlikely to be positive only indicates that the pooled average of vehicle-level slopes is negative. Alternatively, on average, the speed of LDV fleet dropped by 0.22 mph with every 1% increase of road grade. In contrast, the posterior predictive distribution of vehicle-level parameters, plotted as blue curves in Figure 45 and Figure 46, is much more spread out than the posterior distribution of fleet-level parameters, reflecting the heterogeneity of grade impact across vehicles in the LDV fleet (and same for the LDT fleet).

Although overall grade has a negative impact on vehicle speed and acceleration, several vehicles/drivers appear to be more sensitive to grade changes than other vehicles/drivers. For example, using the Monte Carlo approximation, the proportion of vehicles of which speed dropped by 0.4 mph or more with every unit increase of grade, increase of grade, i.e., $P(\beta < -0.4|\boldsymbol{y}, \boldsymbol{x}, \boldsymbol{\psi}) = 27\%$. The proportion of vehicles that are less sensitive to grade changes, for example, with speed dropped less than 0.1 mph per unit grade change, i.e., $P(-0.2 < \beta < 0|\boldsymbol{y}, \boldsymbol{x}, \boldsymbol{\psi}) = 16\%$. There are a few vehicles that tend to operate even more aggressive with the rise of grade: we have simulated the

proportion of vehicles of which the grade coefficient is larger than 0, i.e., $P(\beta > 0|\boldsymbol{y}, \boldsymbol{x}, \boldsymbol{\psi}) = 8\%$, indicating that 8% of vehicles captured were operating more aggressively with the increase of grade. This proportion is small, but not negligible, and further supports the assertion that hierarchical models should be applied to estimate the impacts.

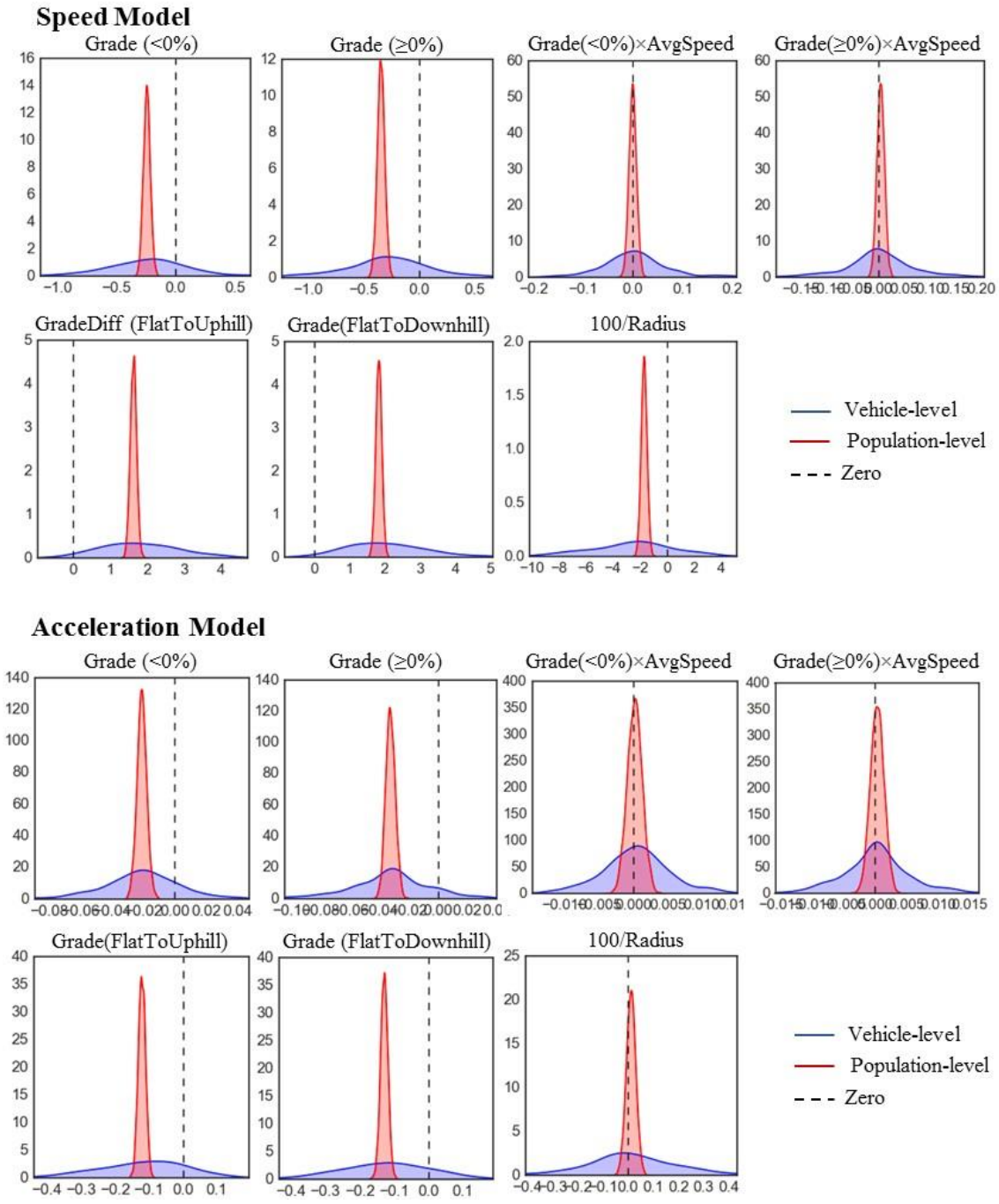

Figure 45 – Coefficients of Passenger Car Speed Model

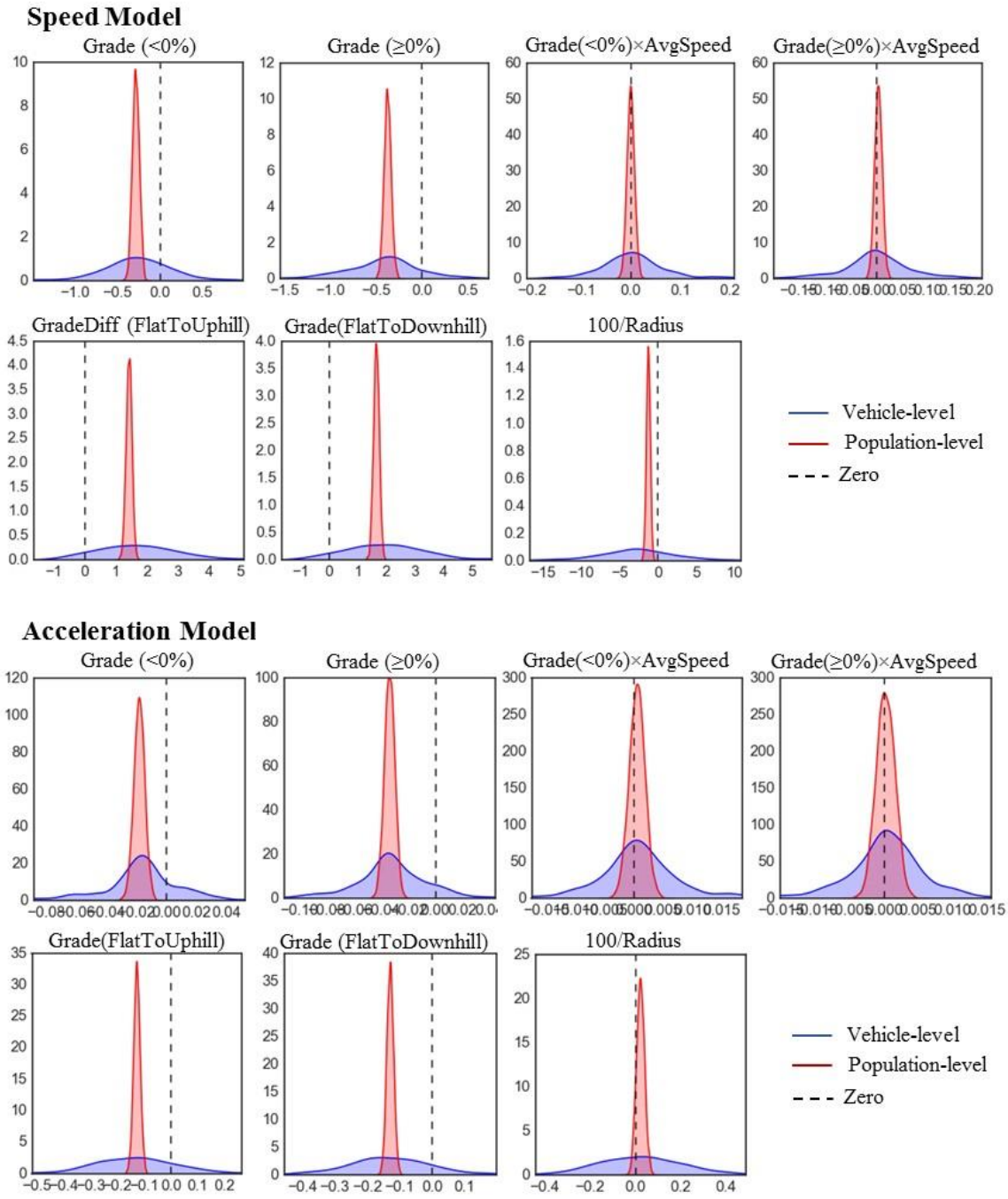

Figure 46 – Coefficients of Passenger Truck Model

The Bayesian Hierarchical model identifies grade impacts under uncongested conditions (average speed ≥ 55 mph). For congested conditions, speed or acceleration traces are more like non-Gaussian and non-stationary process (as shown in Figure 39), which do not fit with assumptions of linear model. Another barrier is the small sample size captured in congested condition as shown from Table 6 to Table 8. This will lead to unstable result compared to uncongested part, especially, if data are processed in a hierarchical structure, where not enough samples are assigned within several groups. Considering the restrictions above, the dissertation will use a different approach in which data are combined and the shape of SAJD is analyzed in the following section. In that way, only characteristics from population level will be reflected.

5.3 Impact on Shape of SAJD

Detailed and accurate driving cycles or speed-acceleration joint distributions (SAJDs) that reflect real-world vehicle activity are required as input for calculating VSP or STP, and modeling vehicle energy consumption and emissions. SAJDs are usually classified by road type, vehicle type, and traffic condition, for vehicle energy consumption and emissions modeling (NCHRP, 2005; Wang, et al., 2008; USEPA, 2009). The SAJD is also treated as a critical index in assessing whether driving cycles represent rea-world driving conditions (Dai, et al., 2008; Lin and Niemeier, 2002). The Bayesian Hierarchical model used in the last section to explore grade impact on average speed and acceleration. However, rather than comparing averages, the SAJD distributions that are used for VSP or STP calculation, energy consumption and emissions modeling are compared. To illustrate the distribution, we group all speed and acceleration points by grade level. Four factors are then extracted to represent shape SAJD characteristics:

1. Extreme accelerations at each speed level
2. Mean accelerations at each speed level
3. Width, or separation distance, between extreme acceleration and decelerations
4. Skewness of acceleration distributions at each speed level

5.3.1 Extreme and Mean Accelerations at Each Speed Level

The 2.5 percentile acceleration (representing extreme deceleration or braking), mean acceleration (representing average acceleration at both congested and uncongested conditions), and 97.5 percentile acceleration (representing extreme acceleration) are extracted in 1 mph speed intervals from 5 mph to 80 mph, and across grade range of -3% to +3% in 1% interval, as shown in Figure 47, Figure 48, and Figure 49, representing passenger cars, passenger trucks, and express buses. Because too few samples are available on grades of ±4% and ±5%, they are not presented in these figures.

Under uncongested conditions, a clear trend in curve of extreme accelerations and average accelerations moving from larger down to smaller values can be observed for all vehicle types as grade increases from -3% to +3%. As for extreme decelerations, a similar trend is observed at passenger cars and passenger trucks, in which the extreme deceleration curve further moves down to more negative acceleration values as grade increases from -3% to +3%, while this is not clear in express bus data (Figure 50 shows a zoomed view).

This clear trend, however, is not observed under congested condition. Assuming these data are sufficient and reflect real relationships, this may be because traffic flow and car following become the dominant factors affecting vehicle operations,

overwhelming any effects from grade. More data under congested conditions will be required to make more robust conclusions.

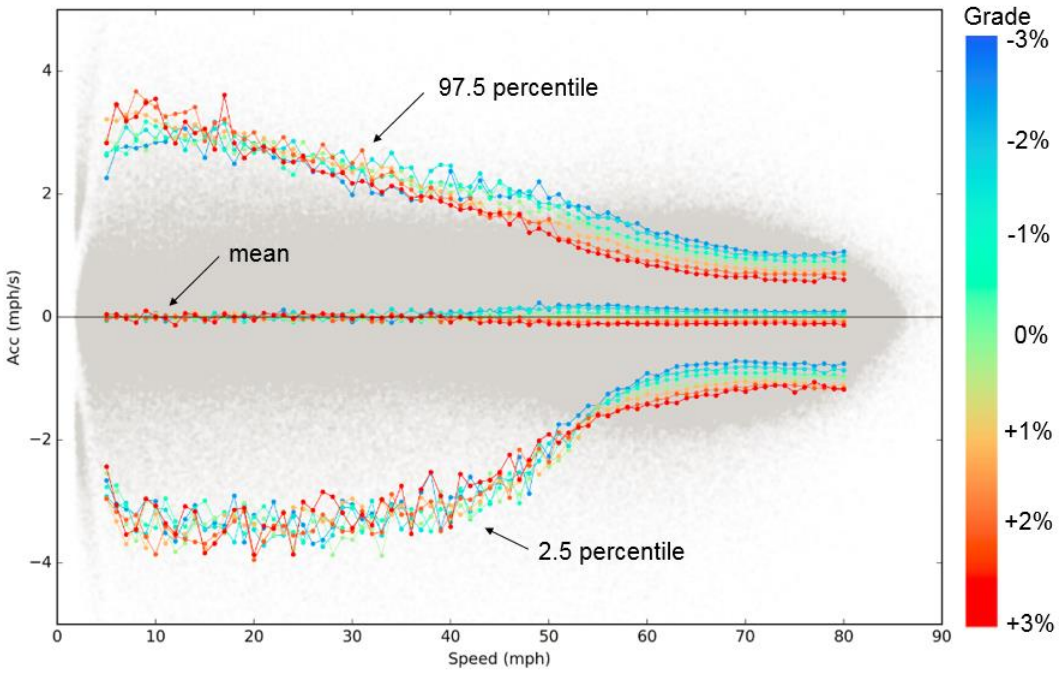

Figure 47 – The 2.5th (Extreme Deceleration), Mean, and 97.5th (Extreme Acceleration) Percentile of Accelerations by Grade – Passenger Car

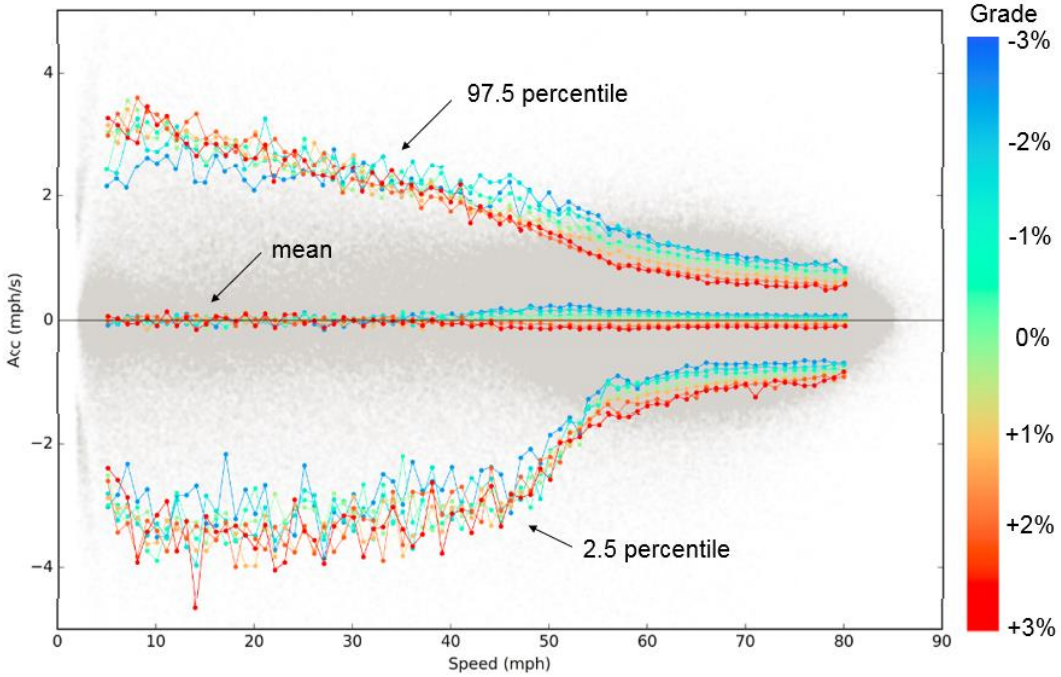

Figure 48 – The 2.5th (Extreme Deceleration), Mean, and 97.5th (Extreme Acceleration) Percentile of Accelerations by Grade – Passenger Truck

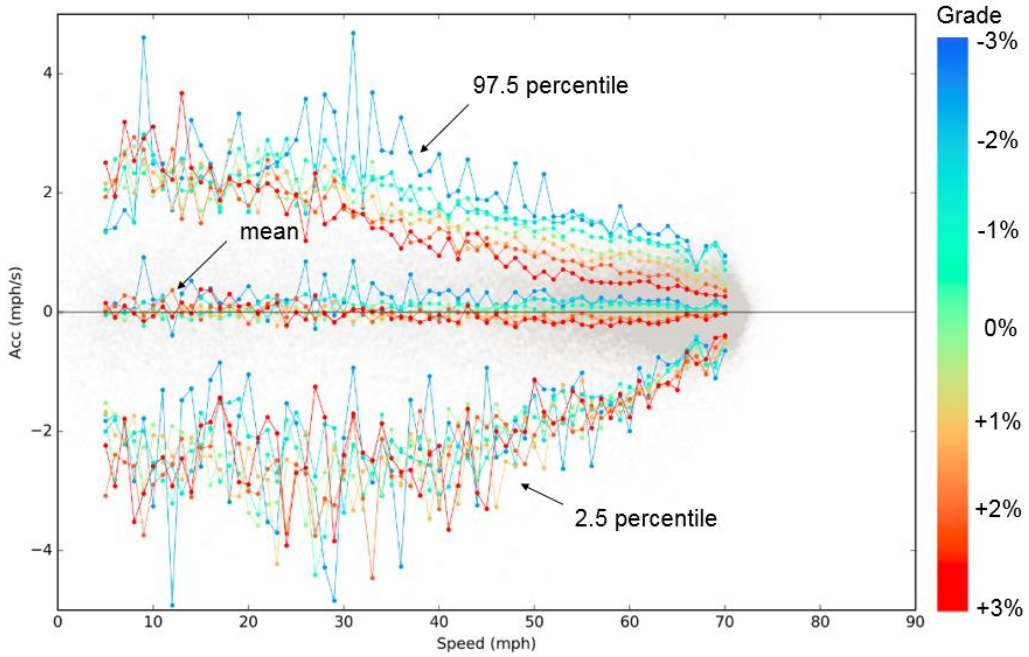

Figure 49 – The 2.5th (Extreme Deceleration), Mean, and 97.5th (Extreme Acceleration) Percentile of Accelerations by Grade – Express Bus

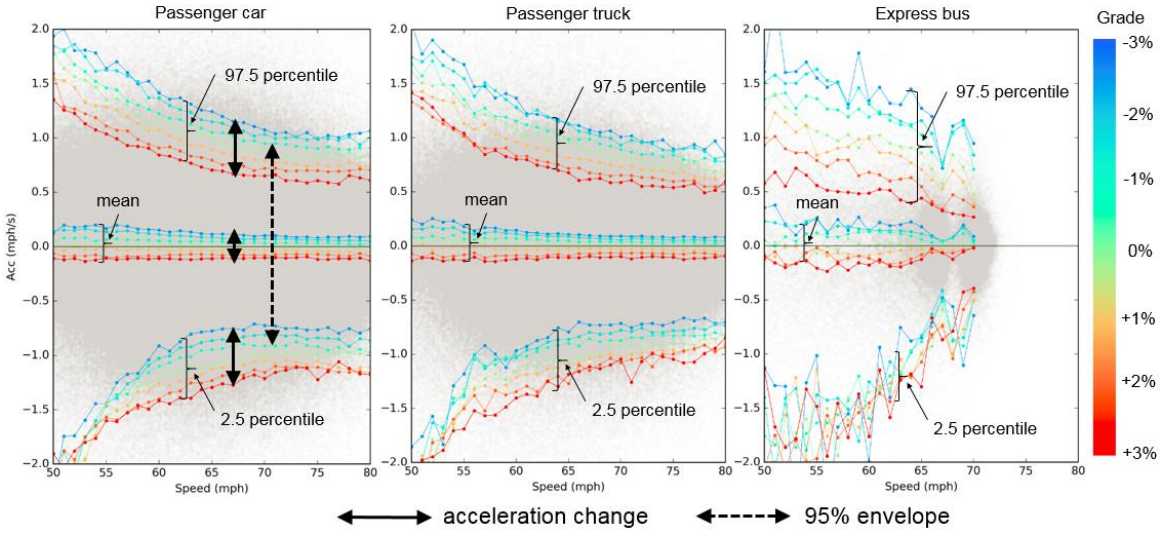

Figure 50 – Envelope of SAJD at Uncongested Condition

To better quantify the grade impact on extreme acceleration/deceleration rates, and average accelerations across each speed bin, ordinary least square (OLS) was applied

to fit the linear relationships between grade (from -3% to +3%) and acceleration for the speed levels of 5-80 mph (i.e., $Acc_v = \theta_{0v} + \theta_{1v}Grade + \varepsilon_v$, where Acc_v refers to extreme/mean accelerations in speed bin v given the grade level. θ_{0v} is the intercept, or acceleration when grade = 0% and θ_{1v} is the linear slope of acceleration in response to grade). Figure 51, Figure 52 and Figure 53 show mean and 95% confidence interval (CI) of θ_{v1}'s across speed levels for extreme acceleration, mean acceleration, and extreme deceleration respectively. The right side of dashed lines labeled in Figure 51 to Figure 53 represent speed bins in which grade has negative impact on accelerations.

As indicated in Figure 51, for passenger cars and passenger trucks, increasing grade significantly reduces extreme accelerations and average accelerations (with θ_{v1}s< 0 and CI > 95%) in speed bins 40 mph or higher, and θ_{1v} ranging from -0.05 to -0.10 indicate the average acceleration drop in mph/second with 1% increase of road grade, which is fairly consistent with the findings from Liu and Frey (2015). This impact is more obvious in the operations of express buses, as θ_{v1} from express buses is about twice as large as (-0.10 to -0.20), covering wider range of speed bins from 30 mph and higher. This is reasonable, as grade is known to have a greater impact on acceleration behavior of heavy-duty buses, considering their payloads and diesel-engines. As seen in Figure 52, increasing grade significantly pulls down average accelerations for all three vehicle types for speed bins 40 mph or higher, and the value dropped by -0.05 to -0.075 mph/second for each 1% increase of grade. From Figure 53, for light-duty vehicles, increasing grade also significantly pulls down extreme decelerations to "even more extreme" values, while no clear impact is observed on extreme decelerations of express buses (with most of 95% CI of θ_{v1}'s include 0).

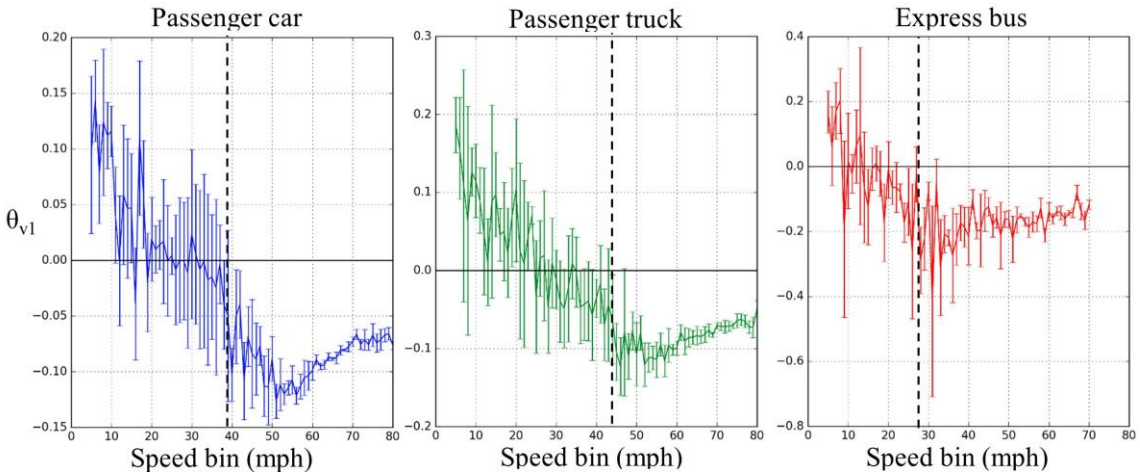

Figure 51 – Mean and Confidence Interval of Grade Impact Slope θ_{v1} on 97.5-Percentile Accelerations (Extreme Accelerations)

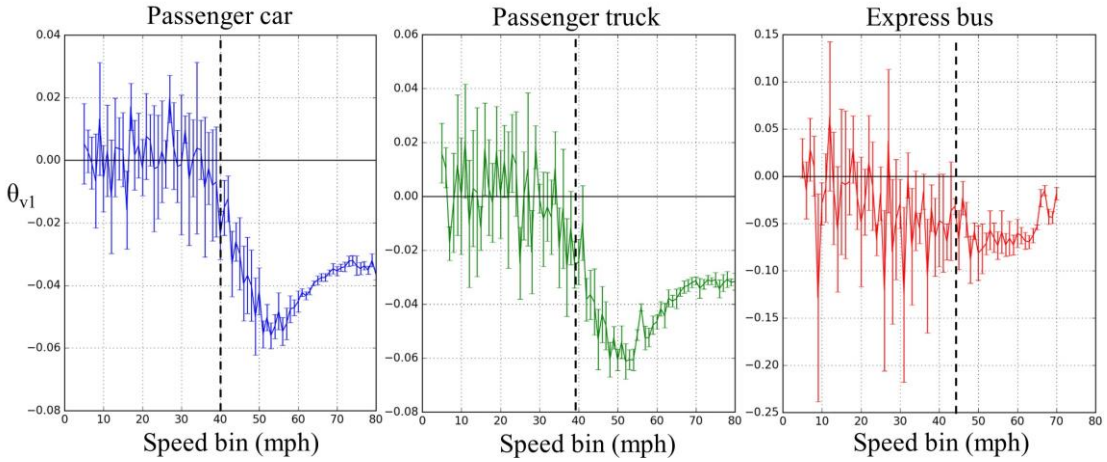

Figure 52 – Mean and Confidence Interval of Grade Impact Slope θ_{v1} on Average Accelerations

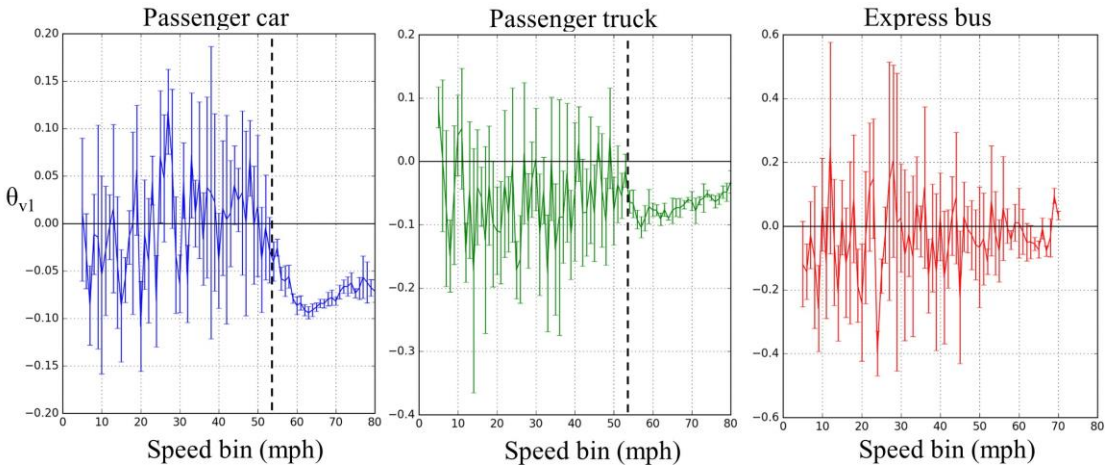

Figure 53 – Mean and Confidence Interval of Grade Impact Slope θ_{v1} on 2.5-Percentile Accelerations (Extreme Decelerations)

The analytical result indicate that increasing grade significantly pulls down extreme accelerations and average accelerations (with θ_{v1}s< 0 and CI > 95%) for all three vehicle types across uncongested conditions (> 50 mph), with more sensitive impact on express buses than light-duty vehicles (θ_{v1} for express buses is about twice as large as for light-duty vehicles). This is reasonable as grade is supposed to have greater impact on acceleration behavior of heavy-duty buses than of light-duty vehicles. Similarly, for light-duty vehicles, increasing grade also significantly pulls down extreme decelerations to "more extreme" values, while no clear impact is observed on extreme decelerations of express buses (with most of 95% CI of θ_{v1}s include 0). On the other hand, under congested conditions (< 50 mph), most of confidence interval for θ_{v1}'s contain 0, indicating no significant grade impact observed under congested conditions.

5.3.2 Width of SAJD: Extreme Acceleration and Deceleration Separation

The width between extreme acceleration and decelerations is also explored to identify the effective value range of SAJD. An intuitive expression of width between

accelerations and decelerations is presented in Figure 54, showing acceleration distribution and the width at grade +3% (red arrow) and -3% level (green arrow) under speed 65 mph. The widths from +3% and -3% do not show obvious difference for light-duty vehicles, While for express buses, the significant drop of extreme acceleration with the increase of road grade push the acceleration into a narrower shape.

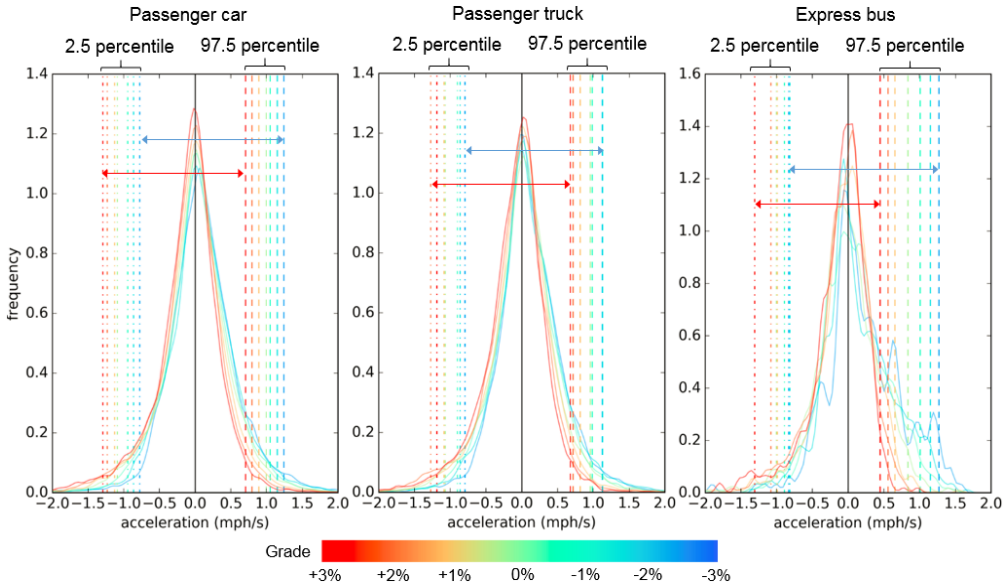

Figure 54 – Acceleration Distribution and Width between Extreme Accelerations and Decelerations on Average Speed 65 mph

The OLS method is applied again here, to quantify the linear relationships between grade (from -3% to +3%) and the width between extreme accelerations and decelerations in speed levels of 5-80 mph (i.e., $Width_v = \beta_{0v} + \beta_{1v}Grade + \varepsilon_v$,), where notation v refers to speed level from 5 to 80 mph. $width_v$ refers to width between extreme acceleration and deceleration in speed level v given the grade level. β_{0v} is intercept, or width when grade = 0%. β_{1v} is linear slope of width in response of grade. Figure 55 shows mean and 95% confidence interval of β_{v1} across different speed levels.

Under uncongested conditions, we learned that increasing grade does not change and width significantly for light-duty vehicles and in most of speed levels, while for express buses, increasing grade narrows down the width on most of speed levels (with $\theta_{v1} < 0$ and CI > 95%). While for congested condition, change of grade does not impact the width significantly for all vehicles and in most of speed levels.

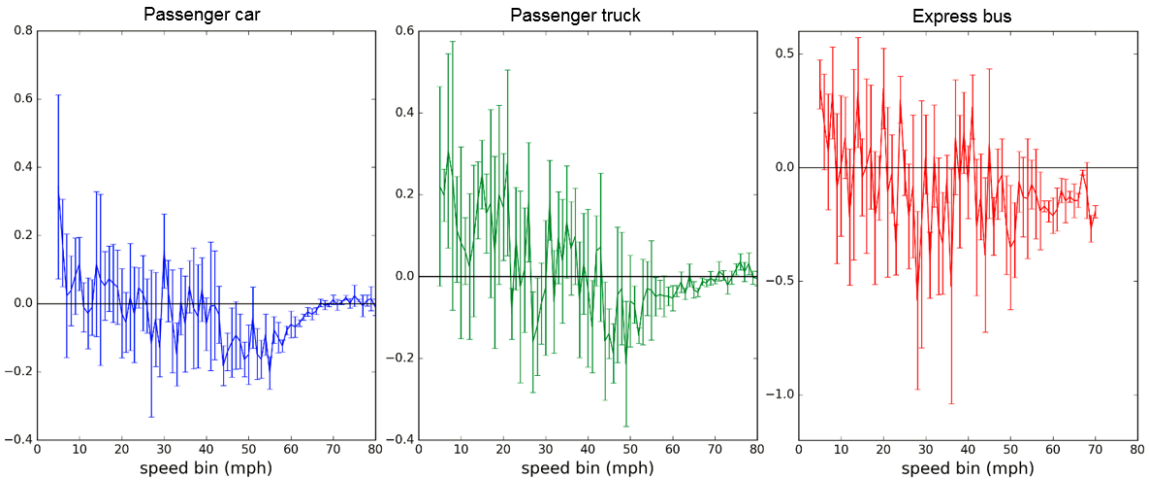

Figure 55 – Mean and Confidence Interval of Grade Impact on Width β_{v1}

The results indicate that under uncongested conditions, or free-flow traffic condition, where vehicle interaction is not taking place very often, the SAJD for light-duty vehicles shifts from higher accelerations to lower accelerations as grade increases, with the separation width of extreme values in the distribution remaining relatively fixed. For express bus, the extreme acceleration curve decreases significantly (twice as fast compared to light-duty vehicles), and the SAJD envelop also becomes more and more narrow because the curve of extreme deceleration does not change as significantly as extreme acceleration. Under congested conditions, traffic flow and car following are

more likely to constrain and dominate vehicle operations, covering up effects from other factors.

5.3.3 Skewness

Further characterization of the SAJD includes a fundamental assessment of skewness. Skewness is a measure of symmetry, or more precisely, the lack of symmetry. A distribution is symmetric if it looks the same to the left and right of the center point. The equation of skewness is ratio of the third moment and standard deviation cubed, as follows:

$$S = \frac{1}{n}\frac{\sum_{i=1}^{n}(x_i - \bar{x})^3}{\sigma^3} \tag{48}$$

Figure 56 shows skewness values of distributions with symmetric levels, and normal distribution (dashed curve). If the bulk of the data is to the left (to the negative side) and the right tail (more positive side) is longer, we say that the distribution is skewed right (positively skewed), and skewness is larger than zero. In contrast, if the bulk of the data to the right (to the positive side) and the left tail (more negative side) is longer, we say that the distribution is skewed left or negatively skewed, and skewness is smaller than zero. For data with symmetric shape, like a normal distribution, the skewness is equal to zero.

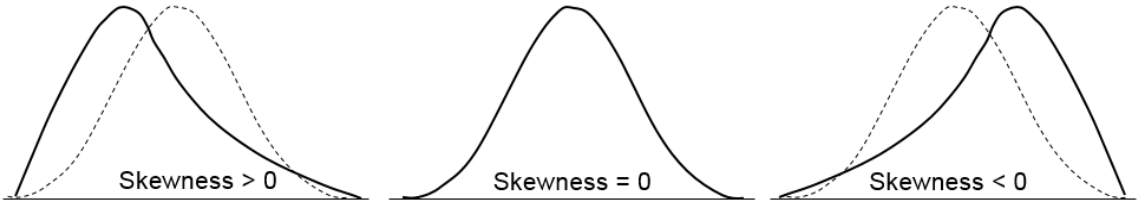

Figure 56 – Symmetric Level and Skewness Value

For each speed bin, skewness of acceleration distribution by grade category is calculated. Smaller (or more negative) skewness for acceleration distribution can be interpreted that there is a "hinder" preventing vehicle from accelerating, or from reaching larger acceleration values. The OLS method is applied here again to quantify the linear relationships between grade (from -3% to +3%) and skewness of accelerations in speed levels of 5-80 mph. Figure 57 shows mean and 95% confidence interval of slope of grade impact on skewness across different speed levels and vehicle types. It shows that under uncongested conditions, skewness of accelerations vehicles decreased with increase of grade level, implying that more uphill grade prevents vehicles from reaching extreme accelerations.

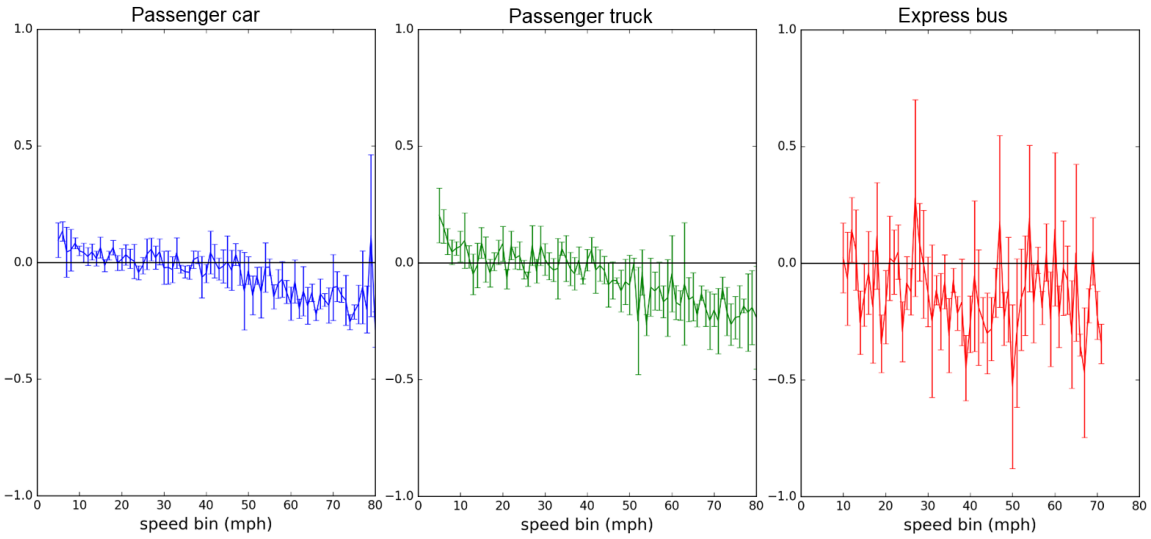

Figure 57 – Mean and Confidence Interval of Grade Impact on Skewness

5.4 Summary

This study explored road grade impact on vehicle operations at freeways, including average speed and acceleration, and the shape of SAJD. Result from the Bayesian Hierarchical linear regression indicates significant grade impact on vehicle speed and accelerations: vehicles tend to operate more "gently", i.e., speed and acceleration decreases with the rise of grade. It also shows that accelerations of express buses are more sensitive to grade changes than light-duty vehicles. The predicted distribution of vehicle-level parameters also demonstrated heterogeneity across vehicles, including impact from grade, horizontal curve, and other road variables.

The "shape" of SAJD in respond to grade is also described in detail using extreme accelerations/deceleration, width of SAJD, and skewness. Results of this analysis shows a significant grade impact on extreme accelerations, or SAJD envelope. This impact is especially significant on extreme accelerations of express buses. However, such impacts

were not observed under congested conditions, where traffic flow might constrain and dominate vehicle operations. More data is required to support this conclusion.

In general, under uncongested conditions, there exists clear grade impact on vehicle operations, and ignoring the correlation may end up with biased estimate of engine load distribution at freeways, and is expected to influence accuracy of energy consumption and emissions modeling. More details on such impacts will be introduced in the Chapter 6.

CHAPTER 6. ENERGY AND EMISSIONS ON FREEWAYS

As discussed in Chapter 5, correlation between grade and SAJDs is observed in the higher speed ranges. This chapter applies this information to vehicle energy and emissions modeling, and explores how engine load and emissions results are impacted by ignoring road grade, as well as ignoring grade-SAJD correlation. Several scenarios are proposed to prepare speed-acceleration-grade joint distribution (SAGJD), to show the potential result impact on energy and emission estimation if grade is ignored, or, if correlation between grade and operation is ignored. The first scenario (Scenario 1) uses the actual speed-acceleration-grade joint distribution from direct collection of real-world data. The second scenario (Scenario 2) ignores grade (assumes grade is zero) and uses the monitored vehicle speed and acceleration profiles on each link with an assumed zero grade. The third scenario (Scenario 3) assumes independence between onroad operations (SAJD) and grades, such that the overall SAJD for the trace (i.e., the average vehicle activity for the trace) applies to each transportation link with the actual grade on that link.

A freeway case study presents the impacts of ignoring grade and grade-operation correlation on near-road air quality modeling. In addition to the three scenarios mentioned above. “MOVES default cycle” and “MOVES default cycle with zero grade” scenarios are also added to estimate the potential bias caused by using MOVES default driving cycle as agencies usually do (Kall, 2013).

6.1 Emission Modeling Scenarios

As shown in Equation 1, second-by-second speed, acceleration and road grade are required to obtain VSP or STP. Three scenarios are proposed to generate the activity input, noted as $P_{v,veh,grade}$, representing SAJD of vehicle type *veh* operating in average speed of *v* from road segment with grade level *g*:

Scenario 1 (S1): Includes the combined impact of grade and observed operating conditions. Employs the joint distribution of second-by-second GPS data (speed and acceleration) and paired second-by-second grade data. This is essentially the same as decomposing the Watson plot into Watson plots for each each grade level.

Scenario 2 (S2): Assumes Grade = 0, but employ observed operating conditions. Assumes flat terrain (ignores all grades), but employs observed onroad operating conditions for each link.

Scenario 3 (S3): Includes grade, but assumes independence between grade and on-road operating conditions. Under this assumption, we differentiate SAJD by vehicle type and average speed (Dai, et al., 2008; Lin and Niemeier, 2002), but not by road grade levels. The SAJD for each grade are treated the same within each vehicle type and average speed, equaling to $P_{v,veh}$, symbollically, it is:

$$P_{v,veh} = \sum_g P(grade) P_{v,veh,grade} \text{, and } P_{v,veh,g} = P_{v,veh} \quad (49)$$

Where, $P_{v,\,veh}$ is SAJD of *veh* in average speed *v* aggregated across all grade levels, and $P(grade)$ is proportion of vehicle operating at grade level

$grade$. That is, the overall "population" speed-acceleration joint distribution is employed for all roadways, rather than being decomposed by grade, to represent onroad vehicle operations across all grade level.

The term $P_{v,\,veh}$ is used to calculate VSP or STP and estimate energy consumption and emissions at grade level from -5% to +5% in 1%-interval, with each grade level g representing data collected from grade range of (g-0.5%, g+0.5%). For example, operations at grade level -2.0% essentially means operations collected from segment with grade greater than -2.5% and equal or smaller than -1.5%. The comparison of results between Scenario 1 and Scenario 2 indicates the impact of completely ignoring grade effect by setting grade as zero. The comparison of Scenario 1 and Scenario 3 indicates the impact of ignoring correlation between grade and vehicle operations.

Figure 58 shows the passenger car VSP distribution generated from three scenarios from freeway trips average speed of 65 mph, with each graph representing the distribution extracted from one grade level. Comparing blue curves (VSP from S1: true distribution) with green curves (VSP from S2: grade = 0%), it is obvious to see that ignoring grade leads to significant over-estimation of engine load on negative grades, and under-estimation on positive grades. Comparing blue curves (VSP from S1: true distribution) with red curves (VSP from S3: grade and SAJD as independent), it is observed that ignoring the grade-SAJD correlation causes under-estimation of VSP distribution at negative (downhill) grades, and over-estimation at positive (uphill) grades. Recall from the previous section, under uncongested conditions, the SAJD were moving from higher acceleration areas into lower acceleration areas with an increase in grade. Treating grade and SAJD as independent ends up with mixing of all SAJDs across

grades, and we are essentially adding more “low acceleration” points to downhill grades, leading to under-estimation of engine power, and more “high acceleration” points to uphill grades, leading to over-estimation of engine power. These trends hold for both light-duty vehicles and heavy-duty buses from traces with average speed levels at 40-80 mph.

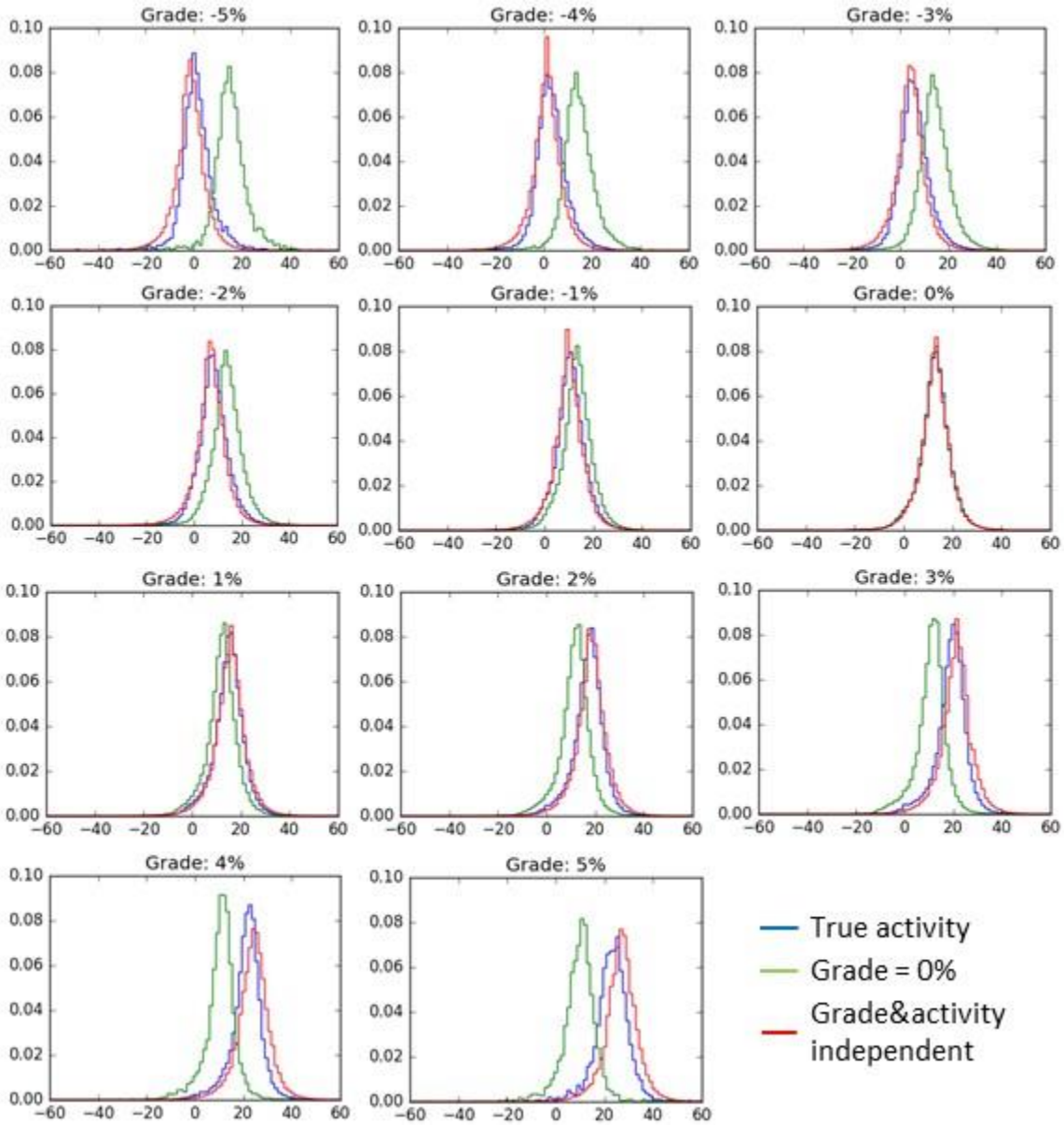

Figure 58 – Passenger Car VSP Distribution from 3 Scenarios at Avg Speed 65 mph

To conduct emission modeling efficiently, MOVES-Matrix is built upon a huge number of MOVES runs. The following formula is used to calculate energy consumption and emissions ($ER_{v,veh}$) of vehicle *veh* under a certain traffic conditions with average speed *v*:

$$ER_{v,veh} = \sum_{g_k}\sum_{a_j}\sum_{v_i} P(SAJD, g_k) \times ER_{veh,v_i,a_j,g_k} \quad (50)$$

$$P(SAJD, g_k) = \begin{cases} P\left(SAJD_{veh,v,g_k}\right) & if\ \ S1\ or\ S2 \\ P\left(SAJD_{veh,v}\right)P(g_k) & if\ \ S3 \end{cases} \quad (51)$$

$$ER_{veh,v_i,a_j,g_k} = \begin{cases} f_{veh}(v_i, VSP_{v_i,a_j,g_k}) & if\ \ S1\ or\ S3 \\ f_{veh}(v_i, VSP_{v_i,a_j,g_k=0}) & if\ \ S2 \end{cases} \quad (52)$$

Where:

$P(SAJD, g_k)$: the SAJD used for segment with grade g_k activity input

$P\left(SAJD_{veh,v,g_k}\right)$: the decomposed SAJD of vehicle *veh* in average speed *v* collected from segment with grade level g_k

$P\left(SAJD_{veh,v}\right)$: the SAJD of *veh* in average speed *v* at segment aggregated across all grade levels, i.e., $P\left(SAJD_{veh,v}\right) = \sum_{g_k} P\left(SAJD_{veh,v,g_k}, g_k\right)P(g_k)$

$P(g_k)$: proportion of road grade g_k

ER_{veh,v_i,a_j,g_k}: emission rate of *veh* with operation of speed v_i, acceleration a_j, at grade g_k

$f_{veh}(v_i, VSP_{v_i,a_j,g_k})$: emission rate as function of VSP_{v_i,a_j,g_k} and v_i defined by MOVES

Energy consumption and $PM_{2.5}$ emissions results of passenger car and express buses from trajectories with average speed of 20 mph (extremely congested), 40 mph (congested), and 65 mph (uncongested) are shown in Figure 59, Figure 60 and Figure 61, respectively, with SAJD and grade input from three scenarios. The results indicate a significant impact on energy consumption and emissions results if grade is ignored. For example, at an average speed of 20 mph, ignoring grade at -2% grade level yields a 13.5% and 10% over-estimation of energy rate and $PM_{2.5}$ emission rate for passenger cars, and 60% and 37% over-estimation for express buses. Ignoring grade at +2% grade level yields a 12% under-estimation of energy rate and $PM_{2.5}$ emission rate for light-duty vehicles, yet 30% under-estimation for express buses. These biases increase on segments with more extreme grades. Furthermore, the bias of ignoring road grade becomes significantly larger for operations under uncongested conditions. For example, in average speed of 65 mph, at -2% grade, ignoring road grade causes over-estimation of energy rates by as much as 30% for light-duty vehicles, and 100% for express buses. For $PM_{2.5}$, these numbers are 29% and 50%. At +2% grade, energy rates can be under-estimated by as much as 22% for light-duty vehicles, and 40% for express buses. For $PM_{2.5}$, these numbers are around 30%.

Treating grade and SAJD as independent also leads to bias in energy consumption and emissions estimates at an average speed of 65 mph, and the bias becomes larger at more extreme uphill and downhill grades. In general, ignoring this correlation yields an under-estimation of energy and emissions results on downhill grades, and over-estimation on uphill grades. For example, at -3% grade, energy rates are under-estimated by 8% for light-duty vehicles, and 13% for express buses. For $PM_{2.5}$, these numbers are around 7%.

At +3% grade, energy rates can be over-estimated by around 10% for light-duty vehicles, and 8% for express buses. For $PM_{2.5}$, these numbers are around 20% and 8%. This phenomenon can be explained by the impact of road grade on engine load as previously shown in Figure 58. While the impact of grade-SAJD correlation (Scenario 3) is significant under uncongested condition, just like the operations impacts observed in previous section, there is no clear trend of energy consumption and emissions result observed in response to grade changes observed under congested conditions. More congested operations data paired with grade data will be needed to reach more robust conclusions about grade impacts under congestion.

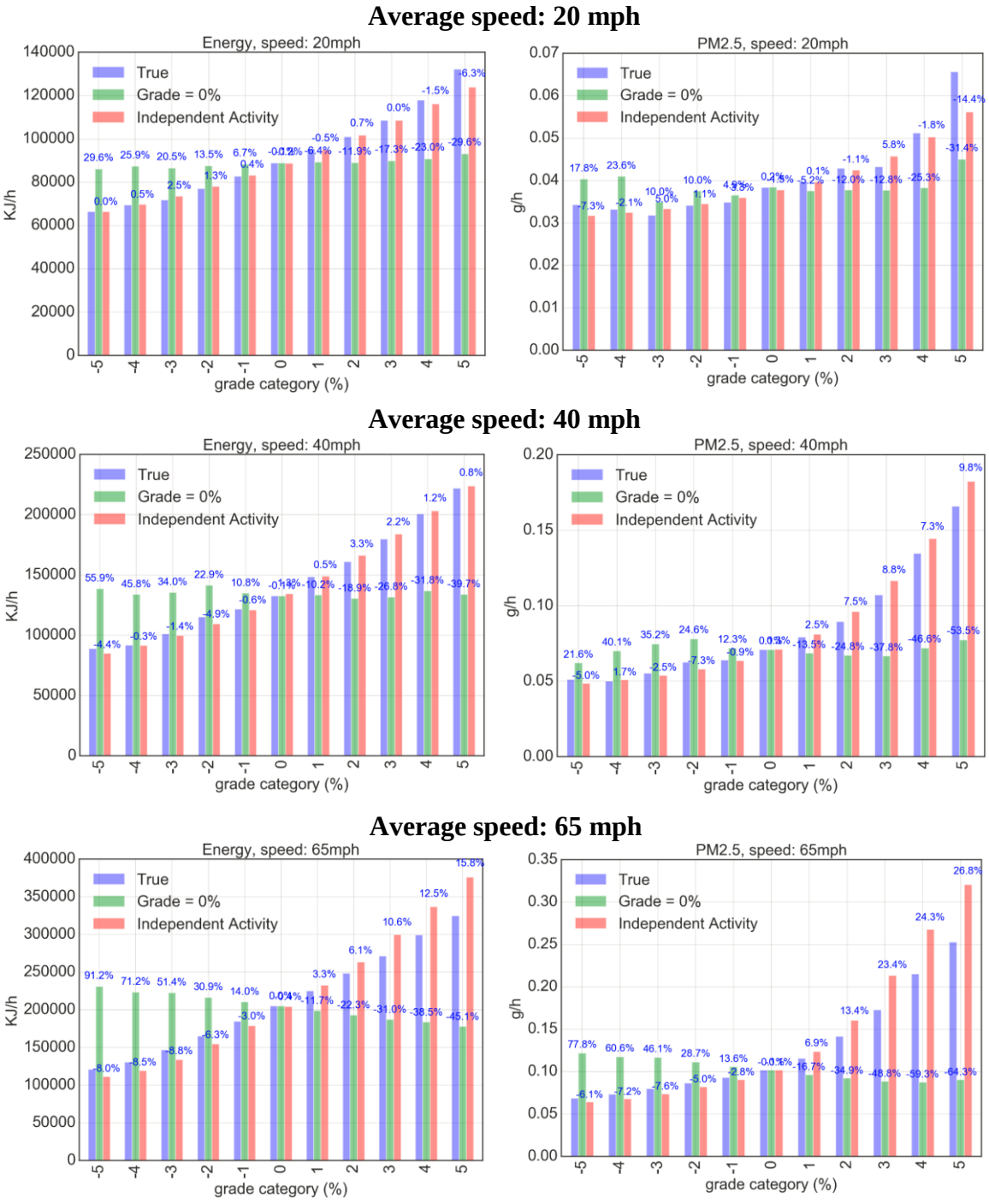

Figure 59 – Passenger Car Energy Rate (KJ/hr) and PM2.5 Rate (grams/hr)

Average speed: 20 mph

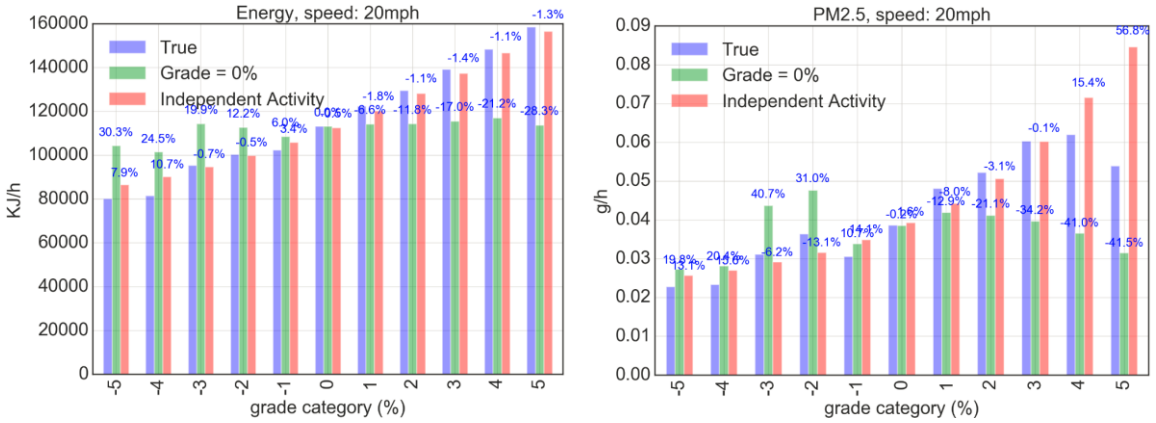

Average speed: 40 mph

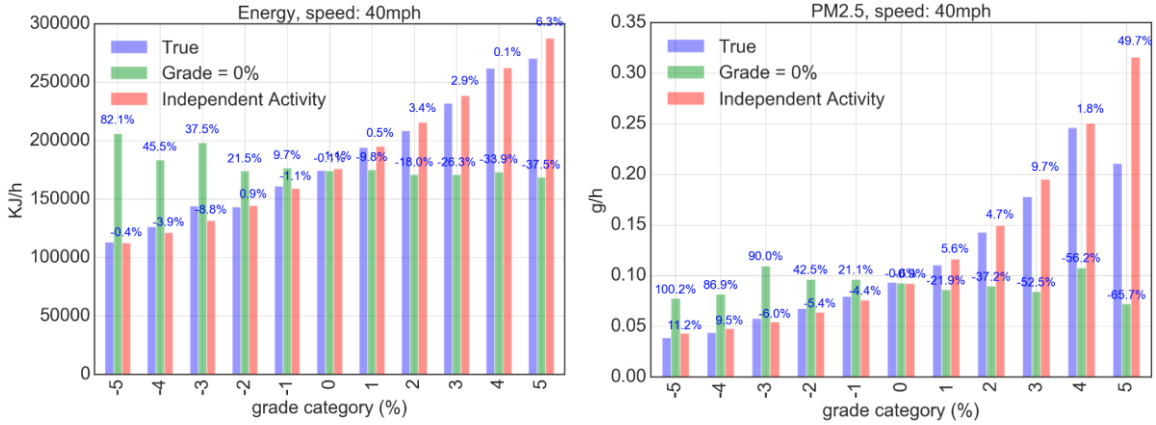

Average speed: 65 mph

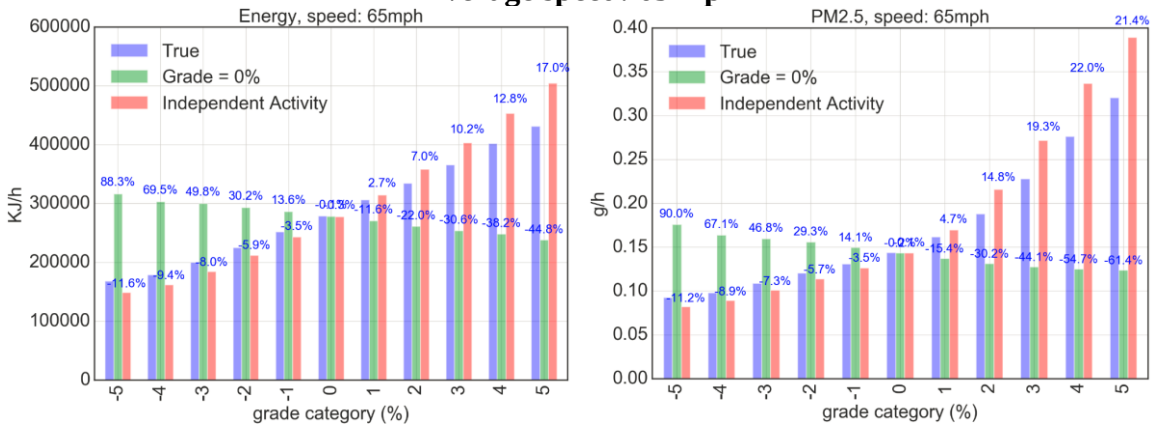

Figure 60 – Passenger Truck Energy Rate (KJ/hr) and PM2.5 Rate (grams/hr)

Average speed: 20 mph

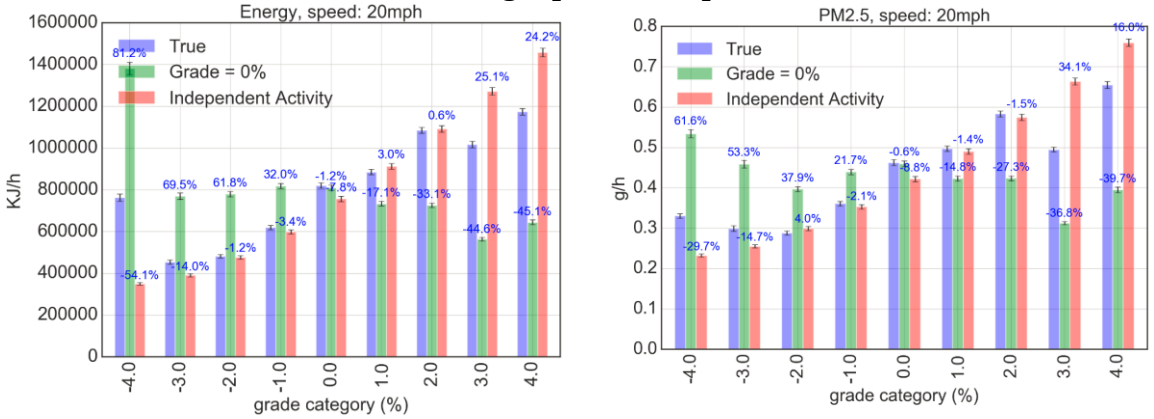

Average speed: 40 mph

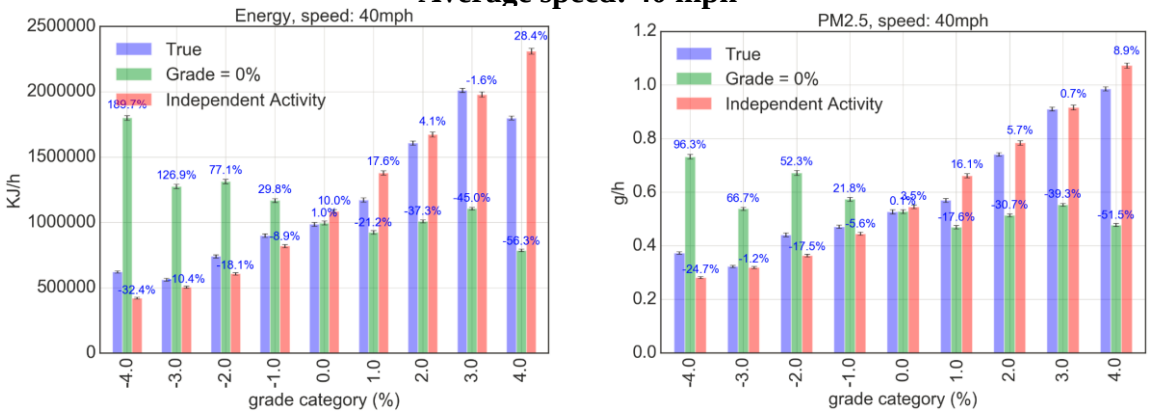

Average speed: 65 mph

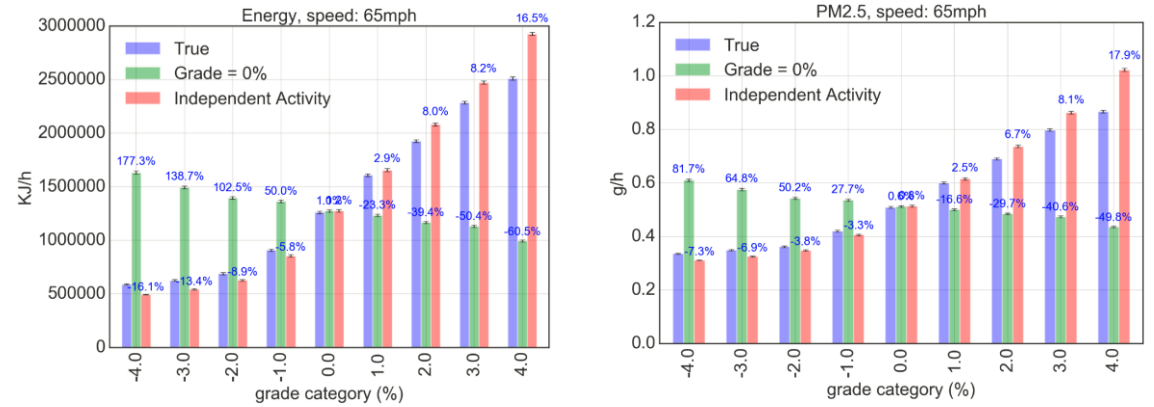

Figure 61 – Express Bus Energy Rate (KJ/hr) and PM2.5 Rate (grams/hr)

For air pollutant emissions, both the amount of emissions and the spatial distribution of emissions matter. Hence, a near-road project-level PM2.5 hotspot analysis is performed explore the impact of ignoring grade and grade-SAJD correlation on predicted pollutant concentrations, as well as potentially policy impacts of potential prediction bias when comparing predictions with National Ambient Air Quality Standards (NAAQS). A freeway case study is introduced in the next section.

6.2 Near-Road PM2.5 Dispersion Impact - A Case Study

Hot spot analysis is defined in 40 CFR 93.101 as an estimation and comparison of likely future localized pollutant concentration with current pollutant concentration and National Ambient Air Quality Standards (NAAQS) (USEPA, 2016a). Hotspot analysis requires detailed modeling of the impacts of transportation project emission sources on the surrounding environment using microscale dispersion analysis (Vallamsundar and Lin, 2012). The USEPA has published transportation conformity guidance for hotspot analysis in particulate matter (PM) nonattainment and maintenance area, as well as project-level carbon monoxide (CO) hotspot analysis guidance (USEPA, 2016a). According to the conformity guidance, MOVES (MOtor Vehicle Emission Simulator) is the official mobile emission model (USEPA, 2015) for air quality analysis. AERMOD and CAL3QHCR are the recommended air dispersion models (USEPA, 2016a). In this study, MOVES and AERMOD are used to model the 2016 $PM_{2.5}$ annual concentrations for the corridor.

Considering the significant impact of grade on emissions estimates, ignoring grade effects, or ignoring the correlation between grade and SAJD, are expected to lead

to biased results in dispersion modeling. This section will explore such impact by showing a 9.5-mile corridor (two-way, 6 lanes in each direction, 70 mph speed limit) in I-85 freeway case study in Atlanta, GA. AERMOD is used in this study for dispersion modeling in 9-mile × 1.86-mile area near the corridor. The AERMET 2016 hourly meteorology data required by AERMOD were obtained from Georgia Environmental Protection Division (Georgia EPD, 2018).

For emissions modeling, local subfleet and on-road vehicle operating data were prepared. On-road license plate data were transcribed from video, and matched to the motor vehicle registration database to obtain vehicle model year distributions. Traffic volumes for light-duty vehicles were set as 8000 vehicle/hour (i.e., 192,000 vehicles/day, including passenger cars and passenger trucks, with an observed ratio of 10:7) in each direction for light-duty vehicles, and 500 vehicles/hour (i.e., 12,000 vehicles/day) heavy-duty vehicles was based on the daily volume from Georgia NaviGAtor System operated by Georgia Department of Transportation (GDOT). For this analysis, the grade response of express buses is assumed to represent the responses of the heavy-duty fleet (this limitation is acknowledged and discussed later). Figure 62 shows distribution of speeds from light-duty vehicles and express buses collected by GPS devices in the corridor.

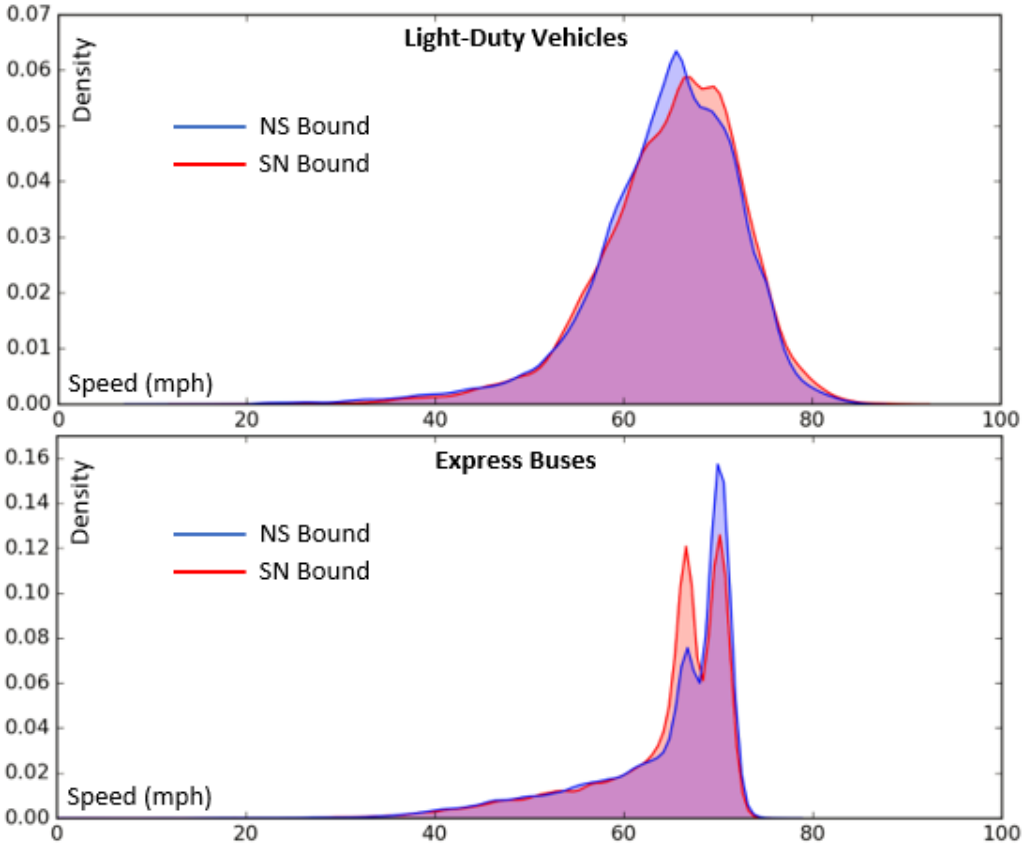

Figure 62 – Speed Distribution of I-85 Case

Results from previous research have suggested that insufficient resolution of receptors may yield inaccurate concentration contours (Wu and Niemeier, 2016). From the USEPA project-level hotspot analysis guidance (USEPA, 2016b), receptors should be sited as close as five meters from the road source. The guidance also recommends that receptors be placed with a finer spacing (e.g., at least 25 meters) closer to the source, and with wider spacing (e.g., at least 100 meters) farther away from the source. In this study, high-resolution receptors were placed in interval of 15 meters from 5 to 100 meters from I-85, every 50 meters from 100 to 200 meters from I-85, and every 100 meters farther away. The wind distribution, roadway and layout, grade distribution, and receptor locations for the case study is shown in Figure 63.

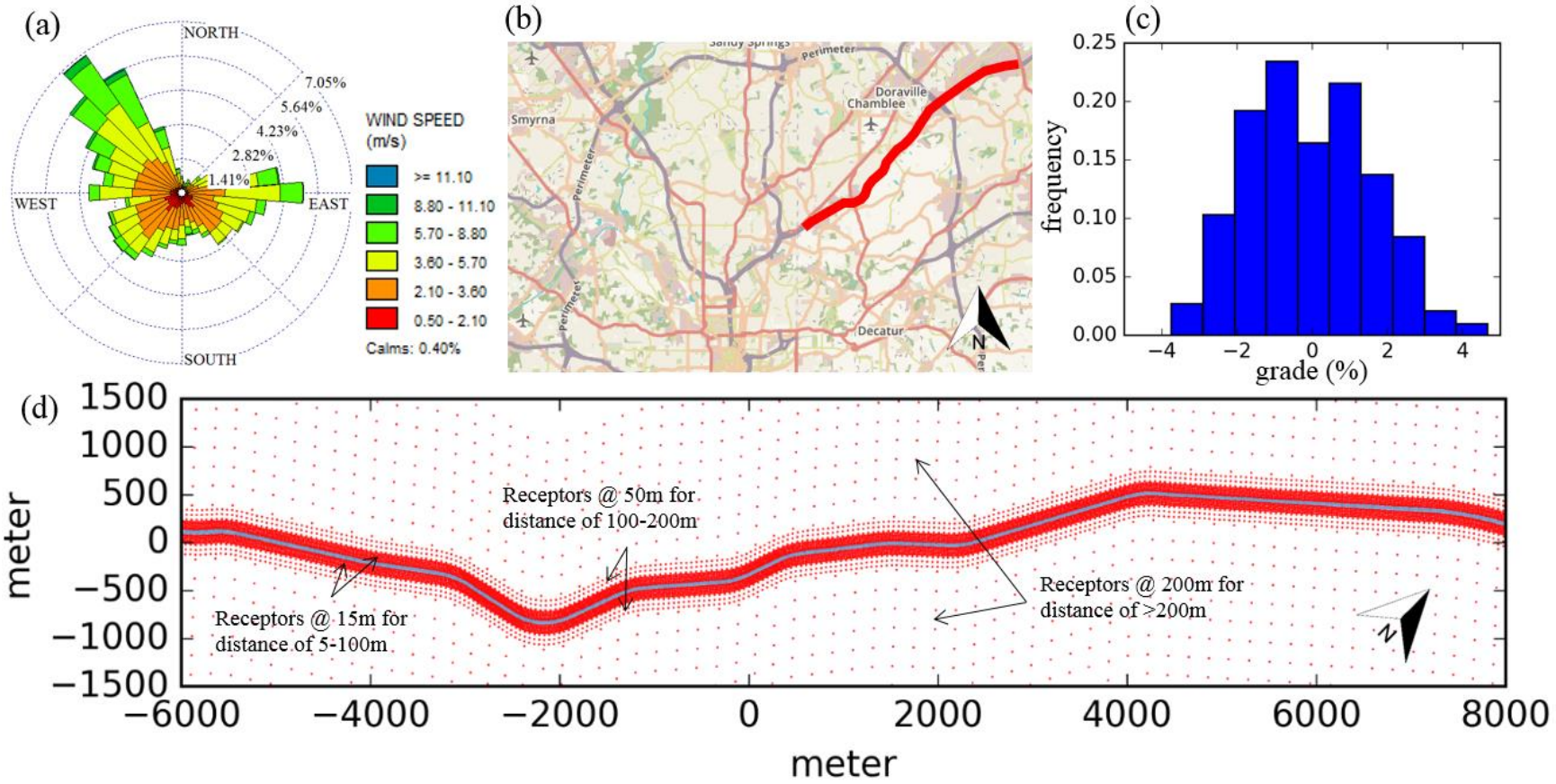

Figure 63 – I-85 Line Source Dispersion Modeling Case Study. (a) Wind Rose Diagram for Atlanta in 2016. (b) Case Study Map. (c) Grade Distribution. (d) Line Source and Receptors Setup

In AERMOD, the two-way I-85 corridor is decomposed into 206 links based on grade level, with each link assigned a grade level from -5% to +5% in 1%-interval. This decomposition process can simplify modeling work, since the grade input within each segment can be treated as constant. The "AREA" method in AERMOD was utilized to simulate each link (Wu and Niemeier, 2016), with the coordinates of multiple nodes to create the polygon that approximates the link shape. MOVES-Matrix emission rates were obtained in units of grams per vehicle per operating hour, and converted to emission rate of "AREA" source in grams per unit square meter per second through Equation (53):

$$E_i = \frac{\sum_{veh}\sum_{v}[(\frac{L_i}{v}) \times E_{veh,v,g_i} \times Vol_i \times P_{veh,v,i})]}{area_i \times 3600} \quad (53)$$

Where:

E_i: $PM_{2.5}$ emission rate of road segment i in unit of g/m^2/s.

$Erate_{veh,v,g_i}$: emission rate of vehicle type *veh* in average speed level *v* at grade g_i, which represent the grade level of link *i*, in unit of g/vehicle/hour.

$Vol_{veh,i}$: throughput traffic volume in segment i in unit of number of vehicles/hour.

$P_{veh,v,i}$: volume percentage of vehicle type *veh* that are in average speed bin *v* in link *i*. $area_i$: area of link i in unit of m^2.

Road grade affects dispersion result through E_{veh,v,g_i}. to calculate E_{veh,v,g_i} from observed real-world traces, GPS points are assigned to the link according to longitude and latitude. Next, for each link, the SAJD is aggregated from the assigned GPS

information, as shown in Figure 64. The emissions E_{veh,v,g_i} for each link can be calculated through equation (50)-(52) using MOVES-Matrix by vehicle type *veh* and average speed level *v* at segment *i*.

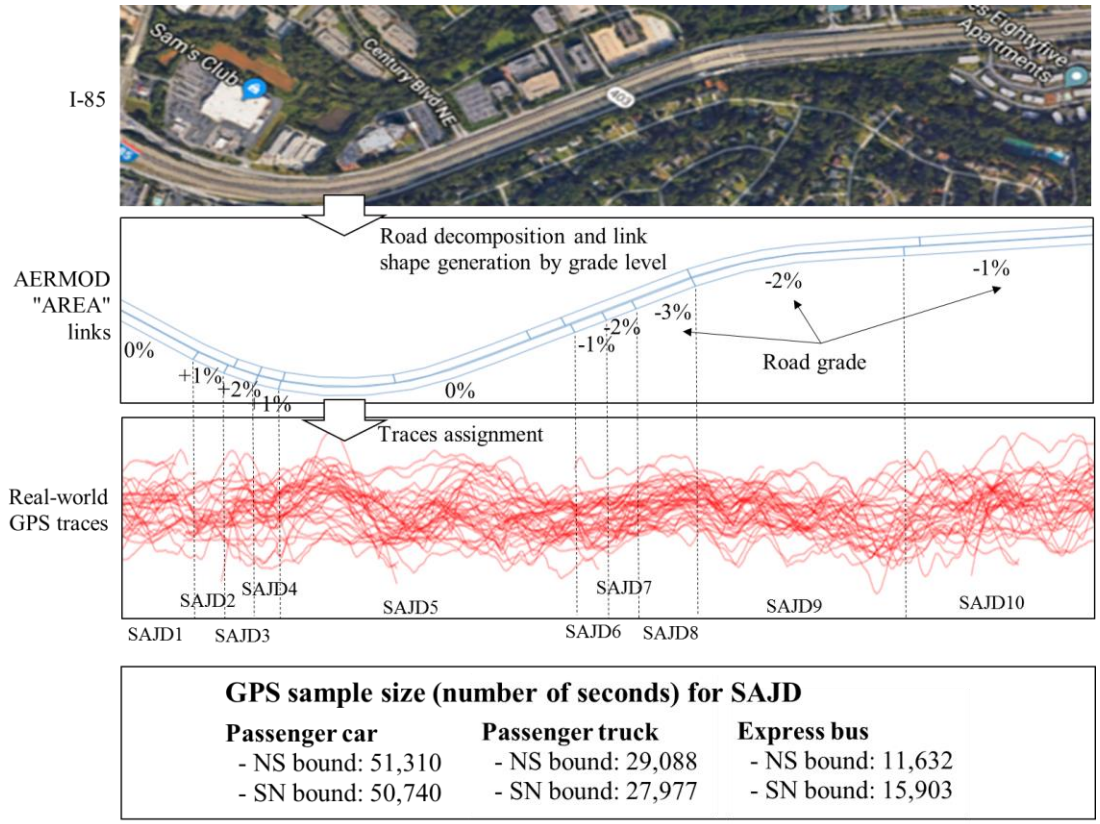

Figure 64 - Road Segmentation by Grade for Real-world Trace Assignment

The estimated annual average $PM_{2.5}$ concentration contributed from I-85 case study is shown in Figure 65 with assumed traffic volume. In general, the near-road average concentration contributed from I-85 can reach 6 μg/m^3 or higher, while the impact shrinks to less than 0.5 μg/m^3 in 500 meters or farther away from the corridor.

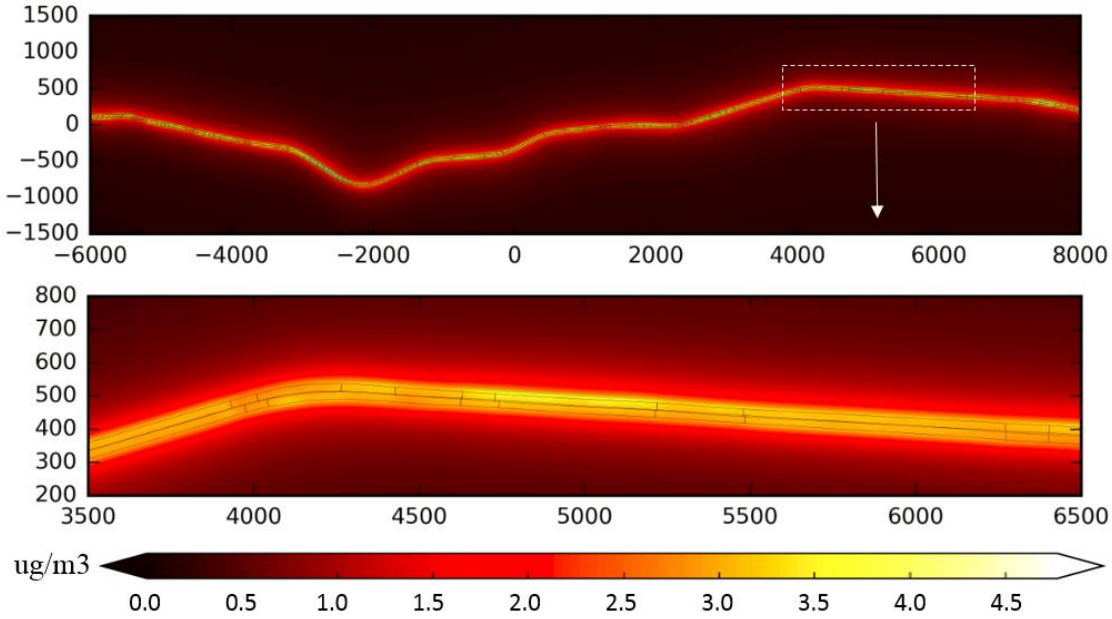

Figure 65 – Annual Average $PM_{2.5}$ Concentration from AERMOD

The estimated concentration profile from observed real-world operation is treated as baseline scenario (S1: true distribution, result shown in Figure 65), and compared with concentration profiles that are modeled using emission rate E_{veh,v,g_i} based on Scenario 2 (S2: grade = 0%) and Scenario 3 (S3: grade and SAJD independent). In that case, E_{veh,v,g_i} from S2 is obtained by setting grades of all segments in S1 as 0%. For S3, SAJD is aggregated by vehicle type and average speed, but aggregated through all grade levels, i.e., $SAJD_{veh,v}$. vehicle types of the segment i in average speed v were assigned $SAJD_{veh,v}$, and then appended with grade g_i.

A survey of state departments of transportation and metropolitan planning organizations revealed that of the agencies that often used MOVES default activity input for project-level analysis, with fewer than 15% used local counts collected for the specific project. About 47% of the survey respondents indicated that the source type

inputs for links were based on state or regional analysis MOVES defaults (Kall, 2013). It is important to show the impact of using MOVES driving cycles. In that case, E_{veh,v,g_i} is also calculated with MOVES default driving cycles based on average speed of each segment, with actual grade and zero grade applied respectively.

The profiles of absolute concentration difference between baseline and other scenarios are shown in Figure 66, with the root mean squared error (RMSE) used to estimate average errors. The calculation of RMSE is:

$$RMSE_i = \frac{\sqrt{\sum_{j=1}^{N}\left(e_{sce_{i\,j}} - e_{base_j}\right)^2}}{N} \tag{54}$$

Where:

$RMSE_i$: RMSE between baseline and scenario i.

e_{base_j}: modeled concentration of receptor j from S1 (baseline).

$e_{sce_{i\,j}}$: modeled concentration of receptor j from scenario i.

N: number of receptors in the study area.

The absolute difference of estimated concentration between baseline (estimation based on observed operations with actual grade applied in each segment) and candidate scenarios listed above (calculated as $|e_{sce_{i\,j}} - e_{base_j}|$) are shown in Figure 66, with corresponding RMSEs in Figure 67. We can find that:

1. From Figure 66 (1), Figure 66 (2), and Figure 66 (3), using MOVES default driving cycle or ignoring grade (grade = 0% scenario) causes the largest biased results from baseline, especially, the difference can be as large as 2 ug/m^3 in near-road area, with RMSE equals to 0.079 - 0.090 ug/m^3. This indicate the importance of applying localized operation and integrating grade on localized hot-spot analysis at project level.
2. Figure 66 (4): when we include road grade, but treating grade and operation as independent by using mixed SAJD rather than decomposed ones in this corridor, the concentration differences shrinks a bit with largest difference 0.72 ug/m^3, and RMSE decreases to 0.024 ug/m^3. The results also demonstrate the importance of considering grade in concentration estimation. Even by incorrectly ignoring the grade-operation correlation, integrating grade can significantly improve modeling of engine load distribution compared with a zero grade scenario.
3. Figure 66 (5): by applying classified SAJD with grade level, although we do not apply observed traces in this corridor, the largest concentration differences further shrink to 0.560 ug/m^3, and RMSE reduced to 0.014 ug/m^3. The results show the importance of including grade-operation correlation in dispersion modeling.

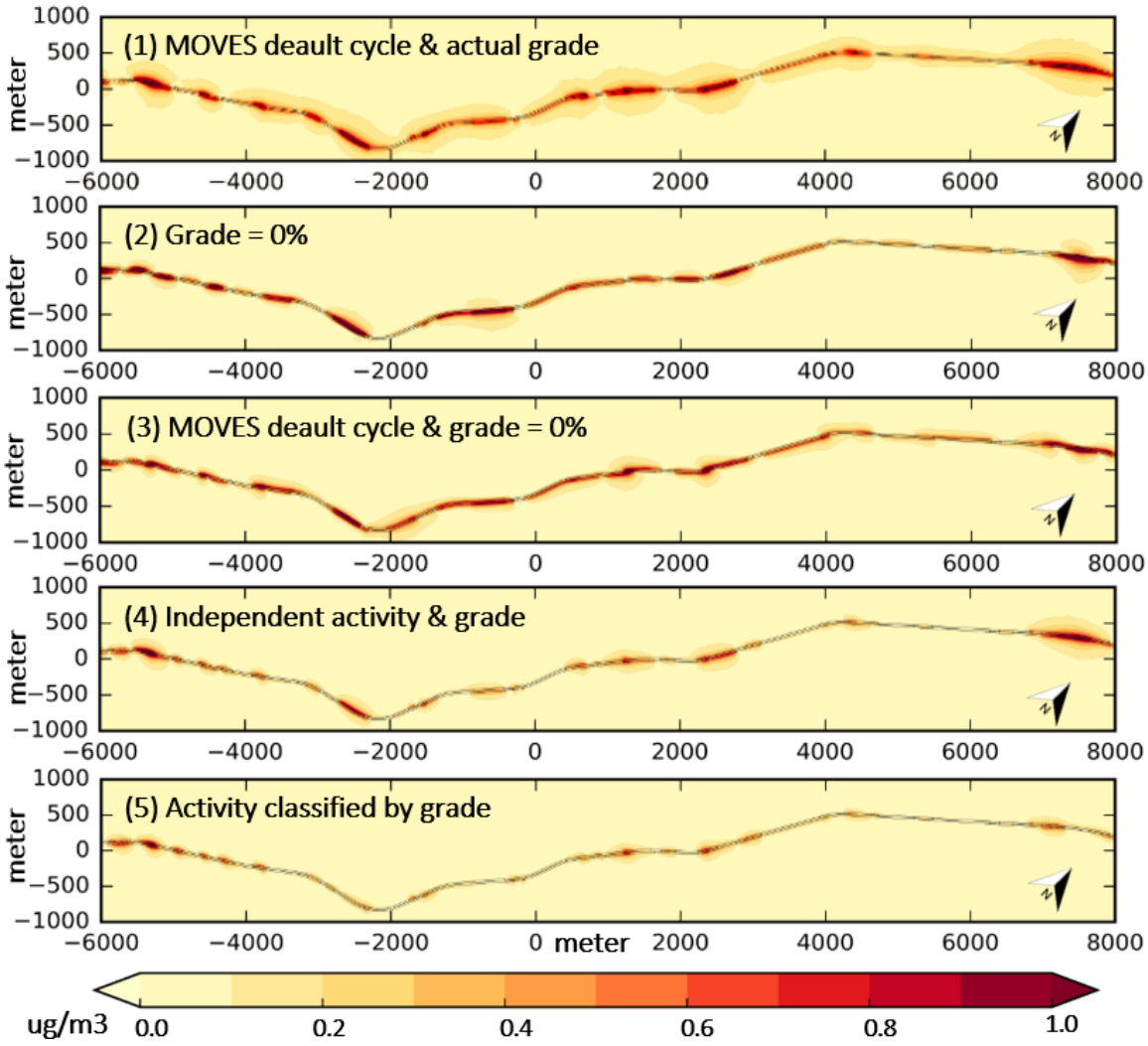

Figure 66 – Absolute Difference of Concentration between Baseline (Observed Real-World Operations with Actual Grade Applied in Each Segment) and Candidate Scenarios

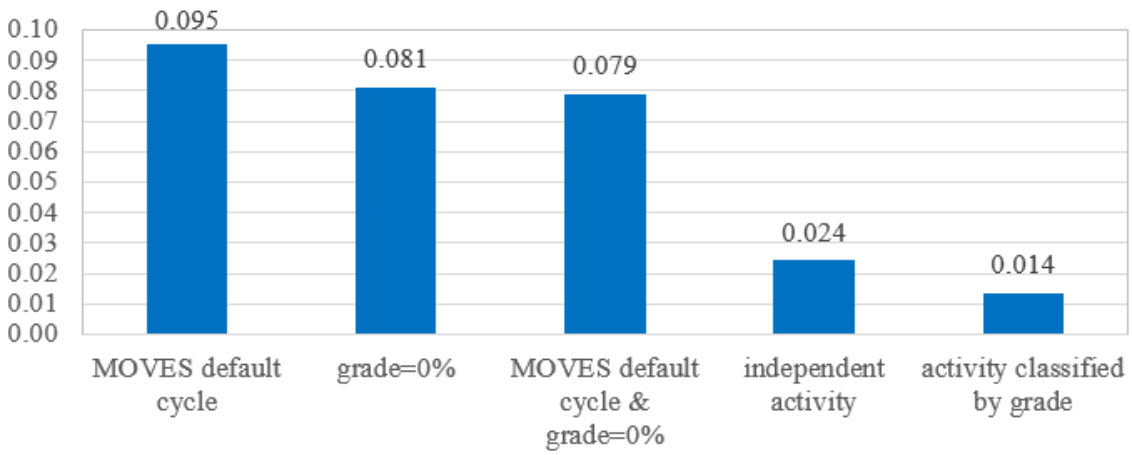

Figure 67 – RMSEs of Candidate Scenarios

More detailed profiles of concentration difference are shown in Figure 68 in a subset segment of the corridor, where the upgrade and downgrade shift frequently. It is interesting to find that:

1. In Figure 68 (1) and (4), shows that ignoring grade ends up with significant over-estimation of concentration within 50 meters of downhill segment, and under-estimation of concentration within 50 meters of uphill segment. Over-estimation and under-estimation are shifted at two sides of segment along the road, following the fluctuation of grade profile along the corridor.
2. In Figure 68 (2) shows that ignoring grade and operation correlations ends up with under-estimation of concentration within 50 meters of downhill segment, and over-estimation of concentration within 50 meters of uphill segment.
3. In Figure 68 (5), clearly shows that considering grade, as well as grade and operation correlation, can improve the accuracy of dispersion modeling.

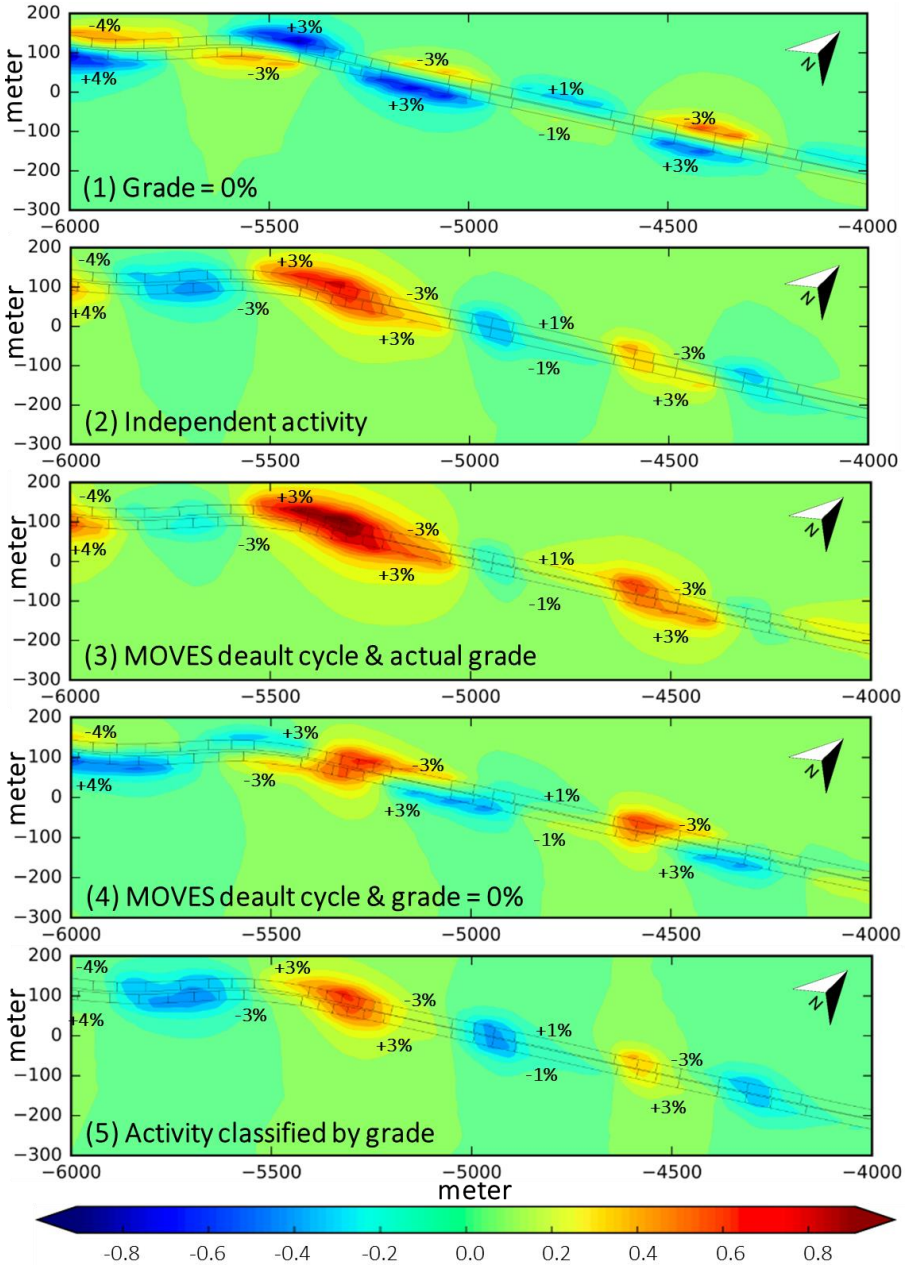

Figure 68 – Actual Difference of Concentrations between Baseline and Candidate Scenarios (Candidate Scenario – Baseline Scenario)

The result from Figure 69 (a) shows that ignoring grade (grade = 0% scenario) causes a large bias in results compared to baseline. The difference can be as large as 2.7 μg/m^3 in near-road area with large grades, which is meaningful compared with the absolute concentration values from S1 (5-9 μg/m^3 near corridor), and the NAAQS limit

(12 µg/m^3). The RMSE between S2 and S1 is 0.08 µg/m^3. This indicates the importance of integrating grade on localized hotspot analysis at the project level. The result from Figure 69 (b) shows that when we include road grade, but treat grade and SAJD as independent, the concentration differences shrinks to a maximum difference of 1.2 µg/m^3, which is about 10% of NAAQS limit value, and RMSE reduced to 0.02 µg/m^3.

None of the scenarios in this case study exceed the NAAQS limit for annual PM2.5 concentrations (12 µg/m^3), but background concentrations have been ignored. The magnitude of the bias introduced by applying grade but treating grade-SAJD independent appears to be manageable. If the addition of background concentration pushes the total value to 10 µg/m^3 or higher, the bias of estimation caused of ignoring grade-SAJD correlation (S3) may become influential in determining a NAAQS violation, and might mean that more detailed analysis should be required.

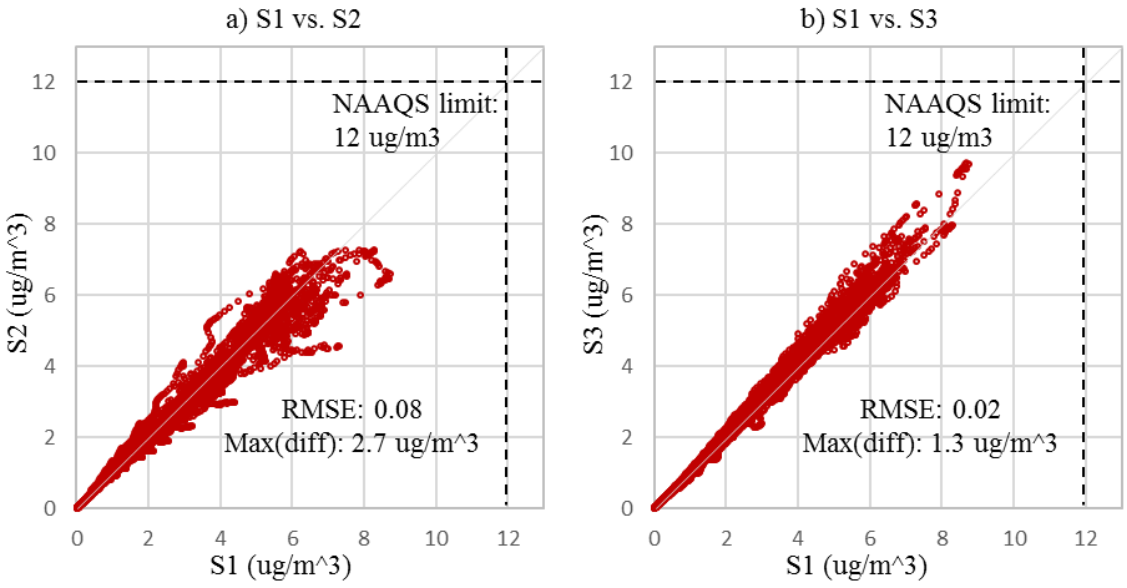

Figure 69 – Concentration Differences between S1 (Baseline) and (a) S2: grade = 0%, and (b) S3: Grade and SAJD Independent

6.3 Summary

Chapter 6 evaluated the impact of ignoring grade, and ignoring the negative correlation between grade and operation on energy consumption and emissions modeling, as well as on near-road air quality modeling on freeways. The following conclusions can be drawn from this chapter:

1. Among all the scenarios tested, the largest bias is from ignoring grade in energy consumption and emissions modeling, with these bias becomes larger in segments with more extreme upgrade and downgrade.
2. Treating grade and operations as independent can also lead to bias in emissions estimate, and the bias becomes larger at more extreme grades. In general, under uncongested condition, ignoring correlation between grade and vehicle operations will end up with under-estimation of energy and emissions results at downhill segments, and over-estimation at uphill segments of freeways.
3. Grade also significantly impacts near-road air quality modeling. Ignoring grade yields a significant over-estimation of concentrations near downhill segments, and under-estimation of concentration near uphill segments. When we include road grade, but treating grade and operation as independent, the concentration differences shrinks.
4. The large difference of concentrations between baseline and scenarios of MOVES default driving cycle indicates the importance of using localized operation and integrating grade impact on localized hot-spot analysis in project level.

CHAPTER 7. ACCELERATION BEHAVIOR ON ARTERIALS

Arterials elevations fluctuate much more significantly than freeways, and variability in vehicle operations also increases, due to the interference of traffic signals, intersections, and high vehicle saturation levels compared with freeways. Understanding how vehicles operate on grades of arterials will lead to a better strategy of operation classification and modeling for engine load distribution, and improve energy consumption and emissions analysis.

7.1 Trace Segmentation in Arterials

Because vehicle operations are much more complicated on arterials, with more acceleration and deceleration operations, than on freeways, traces were partitioned into smaller mode segments, with each representing one of the four modal behaviors types: acceleration, cruising, deceleration, and idling. This process helps decompose the arterial operation problem into sub-problems for analysis: we can analyze grade impact on each modal types.

A methodology has been developed to identify modal types given second-by-second traces. Idling is determined as speed ≤ 1 mph based on the idling definition from MOVES model. For acceleration, we firstly using cubic smoothing spline to smooth time-speed traces, and wipe off short-term (usually shorter than 3 seconds) effects arising from gear-shifts or short duration traffic disturbances (see the area highlighted with black circle in Figure 70). Next, with smoothed time-speed traces, a bracket is used to include 5-consecutive seconds of operation and speed/acceleration values in these five seconds are scrutinized. If all speed values are larger than 1 mph, and the average acceleration is

larger than 0.2 mph/second, then these points are regarded as acceleration behavior, and the bracket is moved forward by 5 second. The process is continued until the points in the bracket violate the criteria, within which the first point with acceleration smaller than 0.1 mph/second is then set as the boundary of the acceleration segment. Note that smoothed trace is only for the criterial judgment, yet the raw speed trace is used for the following analysis. Deceleration is determined in the same manner as acceleration, but just moving the bracket in the inverted time order, and identifying negative acceleration criteria. The remaining parts of the traces are defined as cruising. Table 11 summarizes the criteria for segmenting traces.

Table 11 – Criteria for segmenting traces

Modal Type	Criterial
Idling	Speed ≤ 1 mph
Acceleration	(1): In the bracket, average acceleration > 0.2 mph/s (2): Move the bracket in time order, once (1) does not meet, identify the first point in the bracket that acceleration < 0.1 mph/s as the end of acceleration mode
Deceleration	(1): In the bracket, the average deceleration < -0.2 mph/s (2): Move the bracket in reversed time order, once (1) does not meet, identify the first point in the bracket that acceleration > -0.1 mph/s
Cruising	Others

An example of decomposed time-speed traces is shown in Figure 70 with modal types labeled in different colors. Note that the decelerations highlighted with black circles are short, and regarded as slight perturbations within acceleration segments, rather than deceleration segments. This is because it is normal acceleration feature of manual transmission vehicles (especially heavy-duty vehicles), or when there is small temporary disturbance in traffic flow. Smoothing splined cuves for mode segmentation ensure that

these spots do not break the acceleration traces into smaller pieces that is not convenient for analysis.

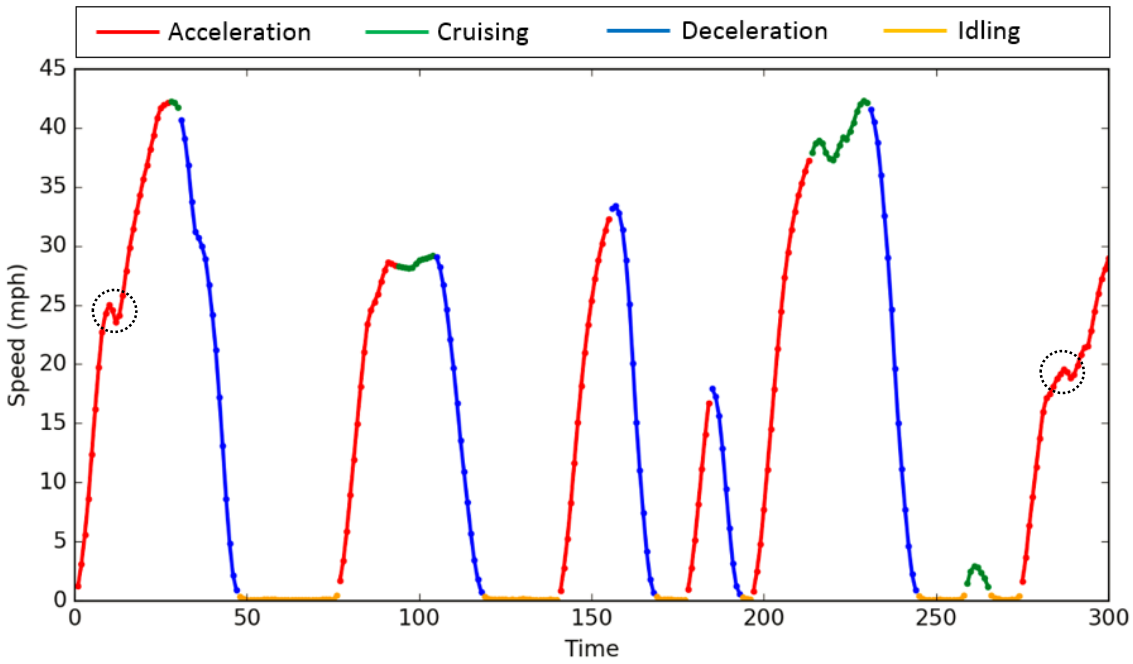

Figure 70 – Decomposed time-speed traces by modal types

7.2 Acceleration Data

For energy consumption and emissions modeling purpose, it is critical to understand the grade impact on acceleration, as high engine load is often associated with acceleration activity. Also, vehicles are more likely to approach the engine working limit in acceleration mode compared to other modes, and the incremental load or surplus power from grade is more likely to affect vehicle performance, or driver behavior.

Similar to freeway operations, the time-speed acceleration traces can be displayed as speed-acceleration paths that better represent vehicle engine power. Figure 71 and Figure 72 shows time-speed traces accelerating from 0 mph to around 40 mph, and the

corresponding speed-acceleration paths collected from passenger car and transit buses. For passenger cars, the accelerations at the beginning of traces are high, and then gradually decay with the increase of speed. For transit buses, initial acceleration is low in take-off stages but reached peak at around 10-15 mph, followed by the decay as speed continues to increase.

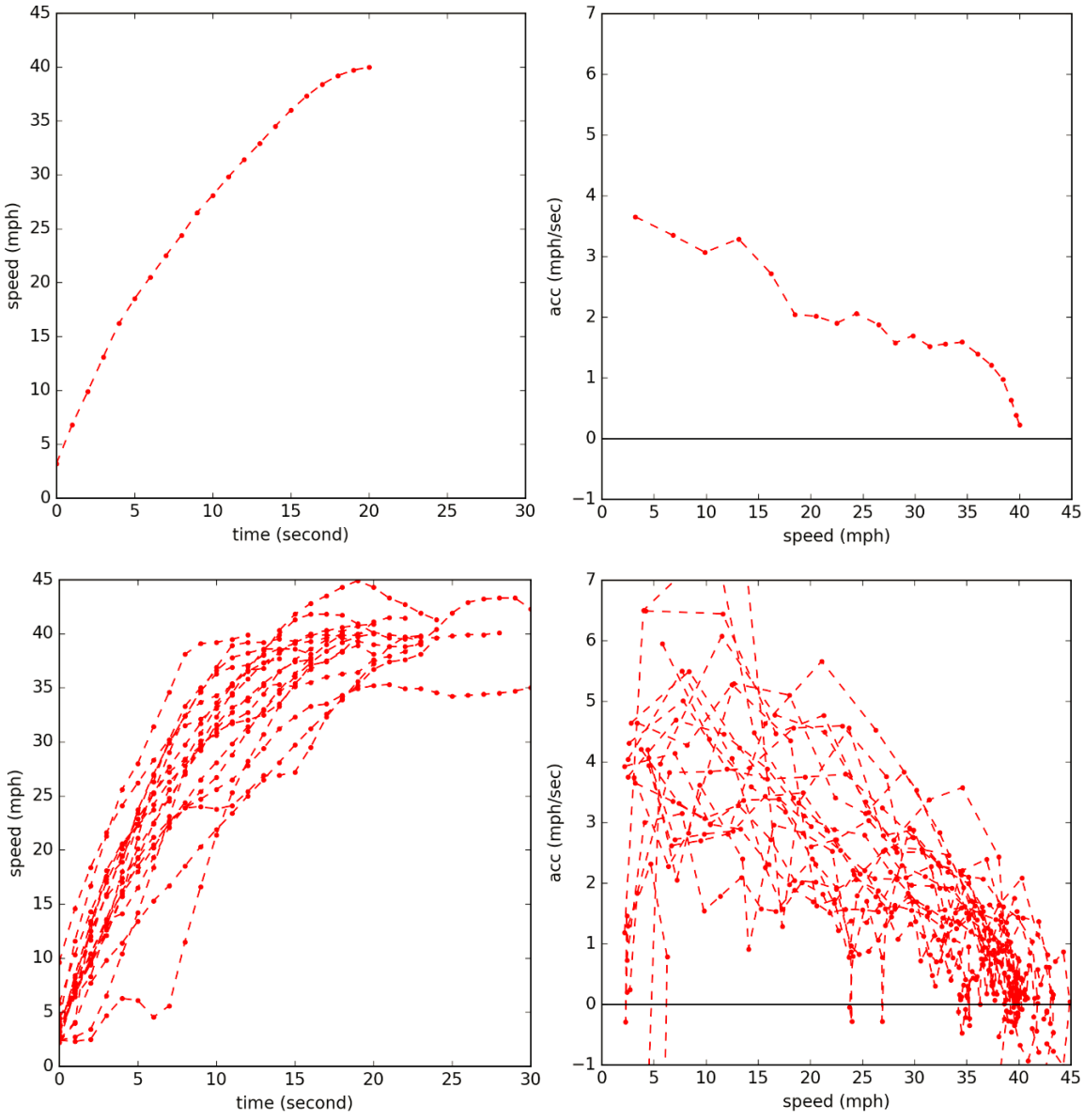

Figure 71 – Passenger car time-speed and speed-acceleration (1 trace and 20 traces)

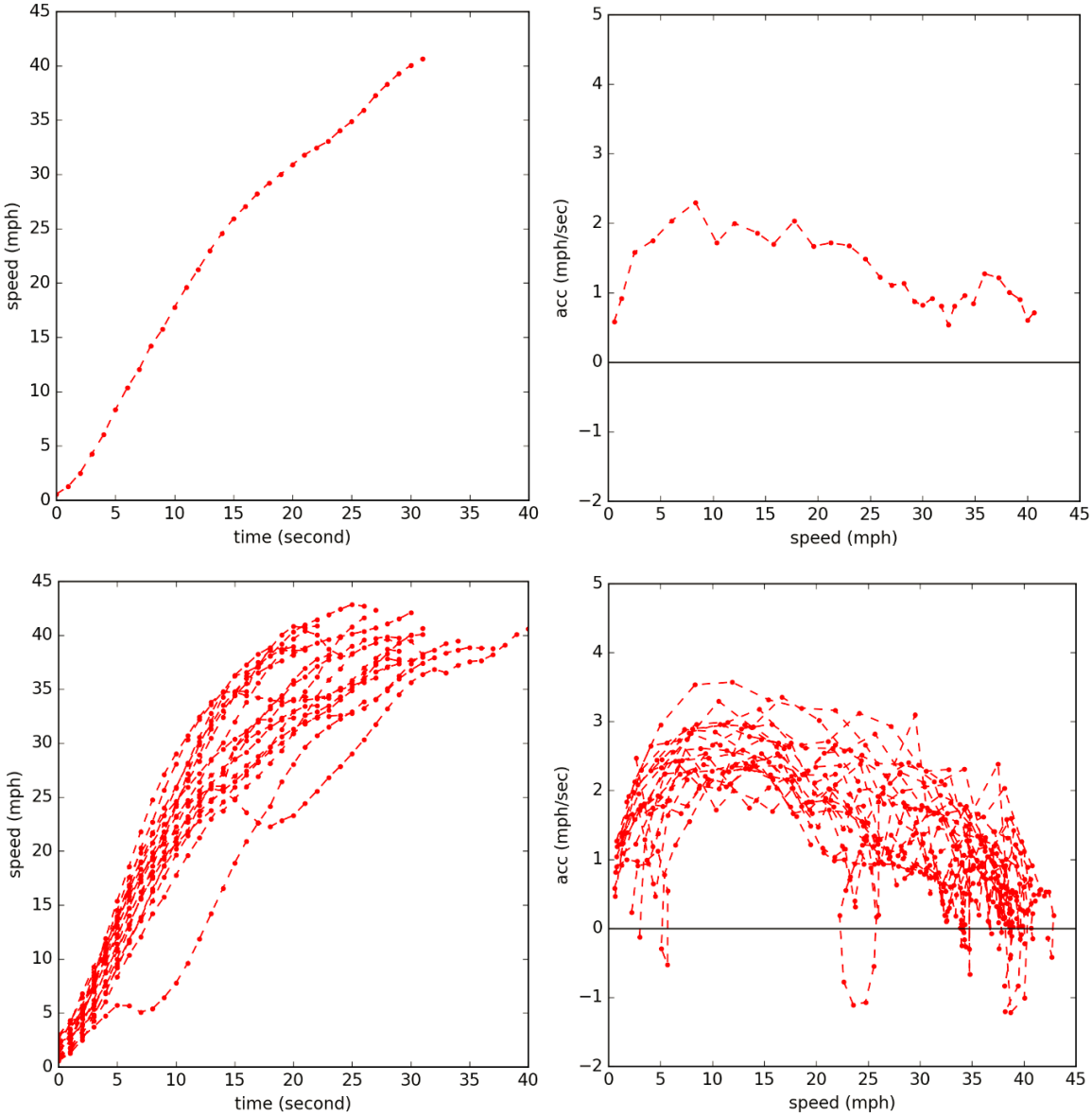

Figure 72 – Transit bus time-speed and speed-acceleration (1 trace and 20 traces)

The study only focuses on grade impact on acceleration activity starting from idle. Assessing the impacts on the other three modes is suggested as a future research need. Two factors are explored to describe grade impact on acceleration:.

1. Assessing whether grade impacts target speed (the final speed reached in the acceleration trace) and whether the effect varies across vehicles.

2. For a given target speed, assessing how acceleration traces (or speed-acceleration paths) are impacted by grade.

Statistical models are built in the following sections to explore the grade impact on target speed selection and the characteristics of speed-acceleration paths to reach target speeds. In modeling speed-acceleration characteristics of acceleration traces, accelerations traces are grouped by target speed ranging from 20 mph to 60 mph in 5 mph interval. The sample size (number of traces) by vehicle type and target speed group are shown in Table 12. Models are built for each acceleration group (by target speeds and by vehicle types) respectively.

Table 12 – Number of Acceleration Traces by Vehicle Type and Target Speed Group

Target speed (mph)	Passenger car	Passenger truck	Transit bus
20 (17.5-22.5)	3,014	2,121	5,717
25 (22.5-27.5)	3,937	2,562	8,723
30 (27.5-32.5)	5,000	3,394	9,119
35 (32.5-37.5)	6,256	4,382	6,852
40 (37.5-42.5)	6,436	4,746	3,624
45 (42.5-47.5)	5,190	4,318	1,402
50 (47.5-52.5)	3,405	2,992	398
55 (52.5-57.5)	1,704	1,522	94
60 (57.5-62.5)	678	552	23

7.3 Target Speed Model

7.3.1 Regression Model

Target speed is defined as final speed or end speed reached by a given acceleration trace. By using a simplified version of Bayesian Hierarchical Linear method applied in Chapter 5, we express target speed as:

$$y_{i,j} = \boldsymbol{u_{i,j}\xi} + \boldsymbol{x_{i,j}\beta_i} + \varepsilon_{i,j}$$
$$\varepsilon_{i,j} \sim N(0, \sigma^2) \quad (55)$$

Where $y_{i,j}$ is observed target speed at the trace j from vehicle i. i = 1, 2, …, m, and j = 5, 10, …, n_i. $\boldsymbol{\xi}$ is array of parameter for population variable matrix $\boldsymbol{u_{i,j}}$ that have consistent impact on target speed regardless of vehicles. Control variables, such as "Day(1-Day, 0-Night)", "#Lanes", "Horizontal curves", and vehicle information (e.g., weight, engine displacement, etc.) are included as population variables. $\boldsymbol{\beta_i}$ represents the array of parameters for the variable matrix $\boldsymbol{x_{i,j}}$ for which the impact on target speed varies across vehicles. Grade variables, including "AvgGrade (<0%)": average grade of traces if it is negative (downhill), and "AvgGrade (≥0%)": average grade of traces if it is positive (uphill), are treated as vehicle-level variables. The vehicle-specific variables can be aggregated to population-level, reflecting the overall impact on the population. The error term $\varepsilon_{i,j}$ is normally distributed with mean 0 and variance σ^2. MCMC simulation with Gibbs sampler method can be easily applied to obtain numerical distribution of parameters. Vehicle-related variables and horizontal curve variables are omitted from the model since they are not significant across all three vehicles types.

7.3.2 Model Results

Results of population-level parameters are shown in Table 13. In this model, intercept represent average target speed at zero grade. Average target speeds for light-duty vehicles are around 40 mph, while average target speed of transit buses is 32 mph. The stop-and-go operations and acceleration performances should be the two main factors that cause lower target speed of transit buses.

Grade causes different impacts on target speed between downhill and uphill segments. For all three vehicle types, target speed is not significantly impacted by change of average grade at downhill operations. While for uphill operations, target speed dropped by average of 1.5 mph for 1% of average grade increase (changing from flat to more extreme upgrade), with credible interval of >99.9% for all vehicle types. The similarity of grade coefficients implies that grade has in overall similar impacts of target speed of light-duty vehicles and transit buses. This further validates the necessity of decomposing grade as downhill and uphill part in target speed modeling.

Table 13 – Speed (mph) Model Result: Population-Level Effect

Speed Model	**Passenger Car**	**Passenger Truck**	**Express Bus**
Variables	**Coef.**	**Coef.**	**Coef.**
Intercept	40.69***	42.19***	32.015***
AvgGrade (<0%)	0.134**	-0.071	0.145***
AvgGrade (≥0%)	-1.508***	-1.545***	-1.512***
Day(1-Day, 0-Night)	-1.336***	-2.439***	0.211*
#Lanes	-0.311*	-0.179	-0.396***
Sigma (**σ**)	8.98	9.18	7.08

***99.9%, **99%, *95%, ^90%

Figure 73 shows the posterior distribution of population-level and vehicle-level grade coefficients from target speed model of passenger car and light-duty truck. For downhill grade, the fact that coefficients of "AvgGrade (<0%)" is concentrated around zero only indicates that the population average of vehicle-level is around zero. It does not indicate that any given vehicle-specific impact is in-significant. Notice that this posterior predictive distribution is much more spread out than the posterior distribution of population-level parameter, reflecting the heterogeneity in slopes across vehicles. For uphill grade "AvgGrade (≥0%)", although the coefficients in population-level is around -

1.5, vehicle-level coefficients spread from nearly 0 to -3. This indicates that drivers' sensitivity of target speeds choices in response to grades are different. Also, it supports the assertion that hierarchical models should be applied to estimate these impacts.

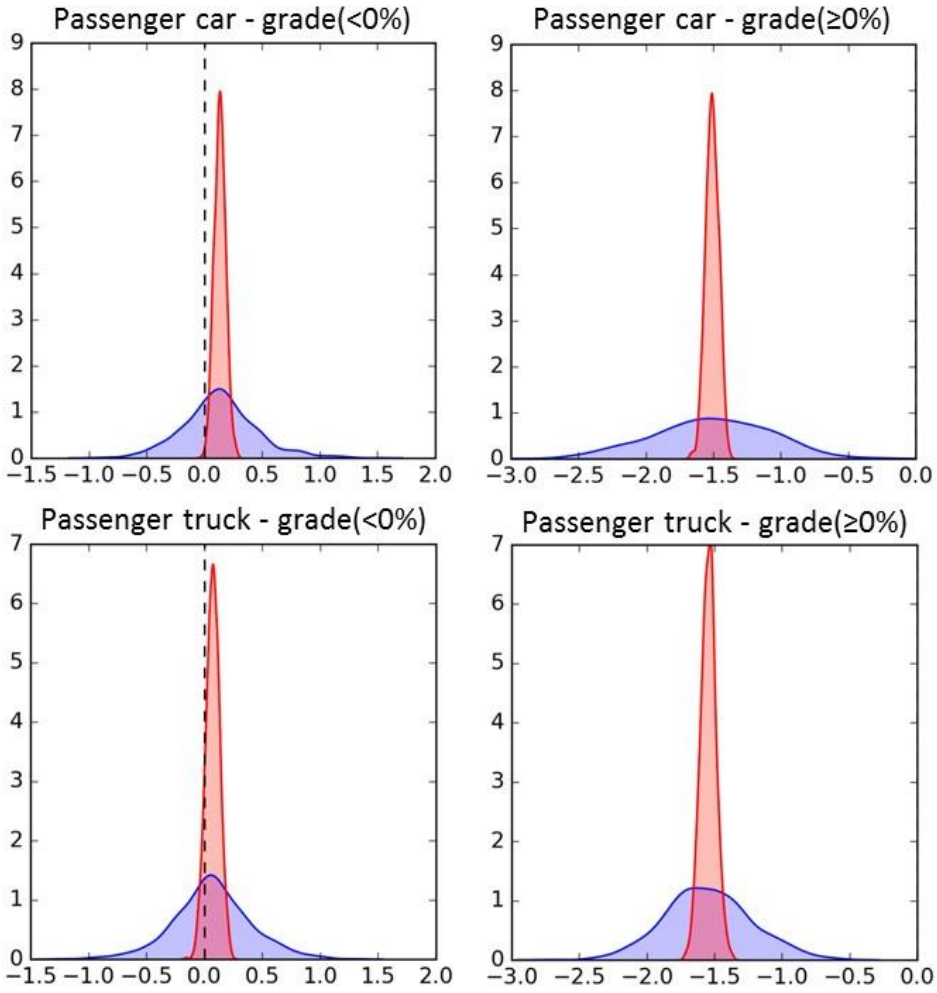

Figure 73 – Grade Impact in Population-Level and Vehicle-Level

7.3.3 Impact on Extreme Target Speeds and Distributions

Using regression analysis, the distributions of target speed in response to average grades are further explored. Distribution and 97.5-percentile of target speed (or extreme large target speed) by grade levels are shown in Figure 74, with curves labelled with cold

colors representing distribution from downhill grades, and warn colors representing uphill grades. At downgrade cases, distributions of target speeds do not change significantly as average grade of traces increases from -5% to -1%, and so do the extreme large target speed (97.5-percentile target speed). The 97.5-percentile target speeds of light-duty vehicles are concentrated in 55-60 mph, and 45-50 mph for transit buses. In contrast, at upgrade cases, distribution of target speed of all three vehicle types significantly shifts to lower ranges with grade increases from 0% to +5%. This is consistent with average changes shown in regression model.

Uphill grades have more significant impact on extreme target speed of transit buses than passenger cars and passenger trucks, likely because it is more challenging for heavy-duty vehicles than light-duty vehicles to reach higher speeds on extreme uphill segments. In Figure 74, extreme target speed of light-duty vehicles decreases by 7 mph from 57 mph to 50 mph as grade increases from 0% to +5%, while extreme target speed of transit buses decreases by 13 mph from 48 mph to 35 mph. One explanation on impact differences between downhill and uphill is on downhill segments, for safety issue, drivers can adjust acceleration rate to avoid vehicle from running too fast. While on uphill segments, accelerations are objectively restricted by engine capability.

While the target model is potentially useful in predicting vehicles' target speed choices on segments with different grade levels, it is suggested the model could be greatly improved by including observed traffic conditions (e.g., travel speed) and car following information, if available, in the future research.

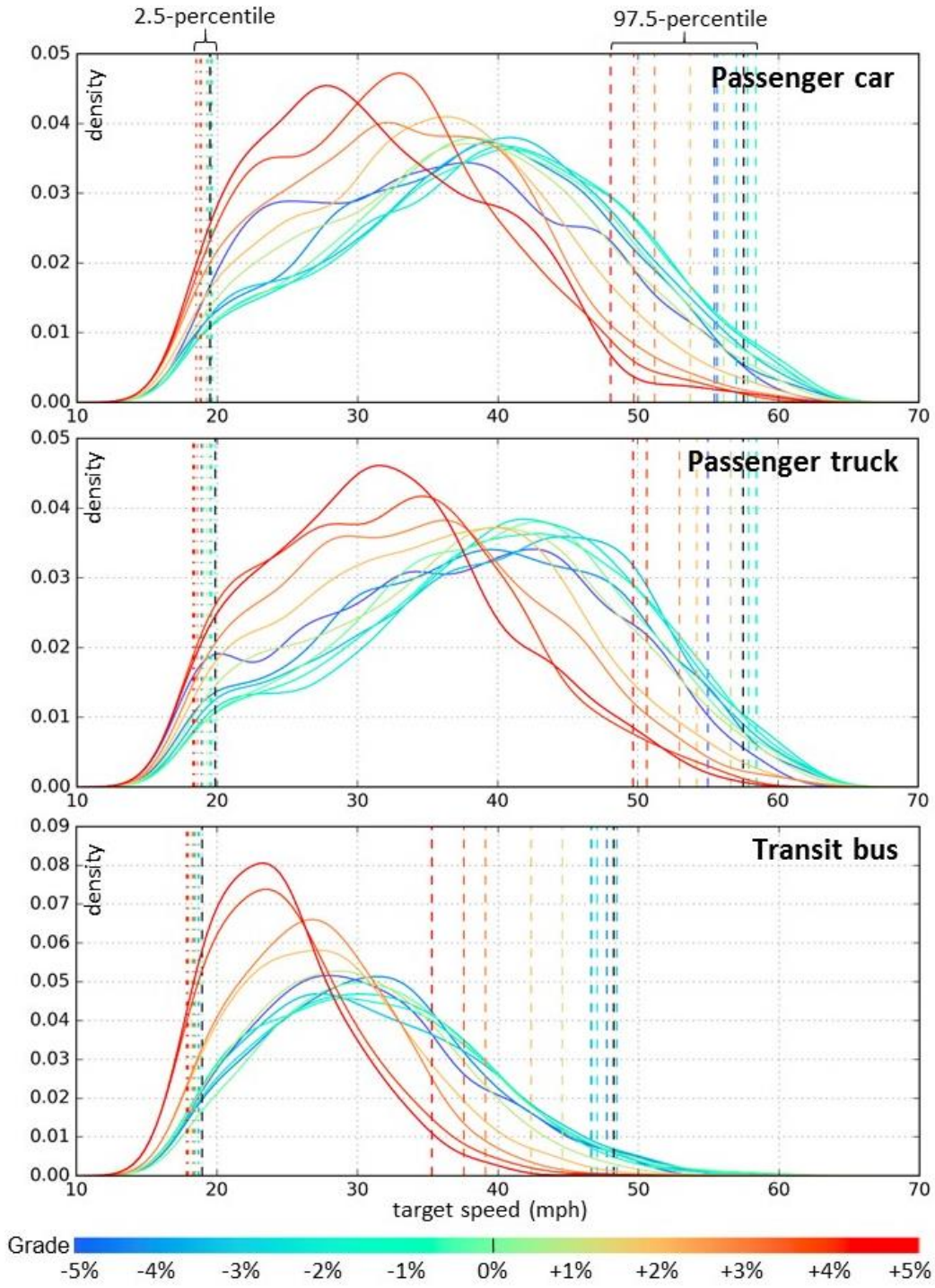

Figure 74 – Grade Impact on Distribution and 97.5-percentile of Target Speed

7.4 Speed-Acceleration Path Model

7.4.1 Preliminary Analysis

Given target speeds that vehicle traces can reach, this section explores how acceleration traces (or essentially SAJDs) are impacted by grade. For each target speed group, the traces are further decomposed into smaller speed pieces, with each speed piece representing speed-acceleration relationship in 5 mph interval starting from 2.5 mph until reaching the target speed. For example, an acceleration trace with target speed 40 mph can be decomposed to 8 pieces: 2.5-7.5 mph (bin 5), 7.5-12.5 mph (bin 10), …, 32.5-37.5 mph (bin 35), and 37.5-42.5 mph (bin 40). After acceleration values from each speed range aggregated, the average accelerations by speed piece and grade level from -4% to +4% are shown in Figure 75, ranging from acceleration traces of 0-25 mph to 0-45 mph. Speed-acceleration paths from passenger cars, passenger trucks, transit buses are shown in the first, second and third column of graph set in Figure 75, respectively.

The figure provides an intuitive visualization showing speed-acceleration paths of passenger car and passenger truck, including the impact in response to grade changes, are very similar: vehicles tend to accelerate a little more "gently" in more upgrade grade levels, with lower acceleration observed as grade increases. This impact, however, becomes much more significant for transit buses acceleration traces, with acceleration dropped by nearly 50% from grade of -4% to +4% at the same speed piece. A statistical model will be constructed to further describe the grade impacts, including average impact, and how impact varies across vehicle types and target speed.

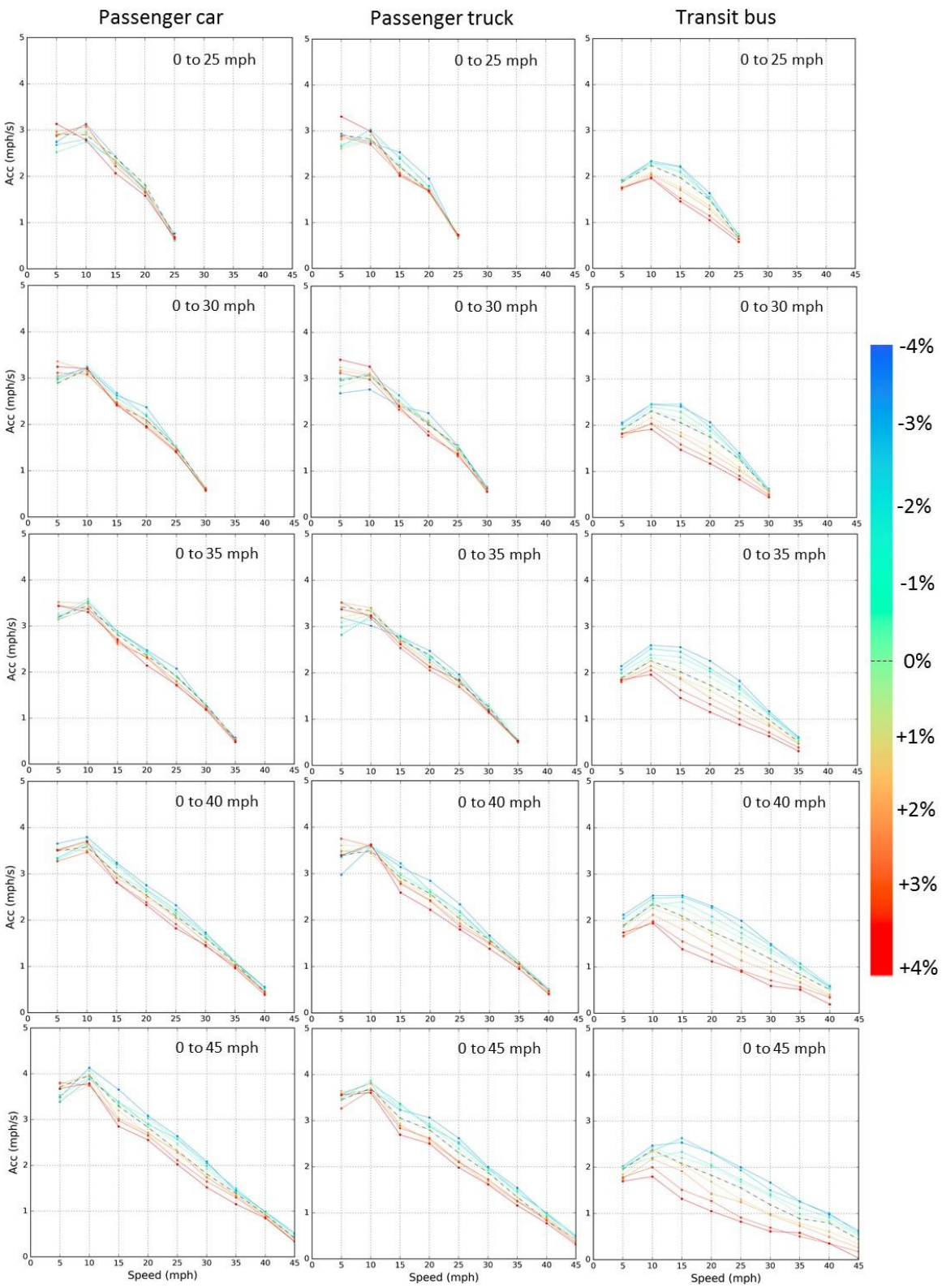

Figure 75 – Mean of Accelerations by Grade

7.4.2 Model Setup

The speed-acceleration paths of acceleration traces can be expressed as piecewise linear function, with each function estimating characteristics of one speed piece as defined in the beginning of section 7.4.1. Expressed symbolically, the model is:

$$y_{i,j,k} = \boldsymbol{u_{i,j,k}\xi_j} + \boldsymbol{x_{i,j,k}\beta_{i,j}} + \varepsilon_{i,j,k}$$
$$\varepsilon_{i,j,k} \sim N(0, {\sigma_j}^2) \quad (56)$$

Where $y_{i,j,k}$ is observed acceleration at the point k of speed piece j from vehicle i. i = 1, 2, …, m, and j = 5, 10, …, V_{target} (target speed or end speed). $\boldsymbol{\xi_j}$ is array of parameter for variable matrix $\boldsymbol{u_{i,j,k}}$ that have consistent impact on accelerations regardless of vehicles. $\boldsymbol{\beta_{i,j}}$ is array of parameter for variable matrix $\boldsymbol{x_{i,j,k}}$ from which impact on accelerations varies across speed pieces and vehicles. For example, vehicles at speeds of 20 mph may behave differently than at speeds of 40 mph in response to the same grade changes, and the impact may also be different across vehicles. The differences are then be reflected in the difference of $\boldsymbol{\beta_{i,j}}$ across speed pieces. The error term $\varepsilon_{i,j,k}$ is normally distributed with mean 0 and variance ${\sigma_j}^2$, indicating the heteroscedasticity of accelerations are assumed across speed pieces. This assumption will be verified in the error term of model result. The model can be graphically presented as a piecewise flat function imitating the speed-acceleration paths as shown in Figure 76, with each flat function determined by a linear function $\boldsymbol{u_{i,j,k}\xi_j} + \boldsymbol{x_{i,j,k}\beta_{i,j}}$. The benefit of using a model with such pairwise structure is that the simple structure can model speed-acceleration paths of any shape (and the shapes of passenger car and heavy-duty bus paths are different, as shown in Figure 71 and Figure 72). Plus, the differences of grade impact on accelerations across

speed pieces can be easily captured from differences of parameters across piecewise functions.

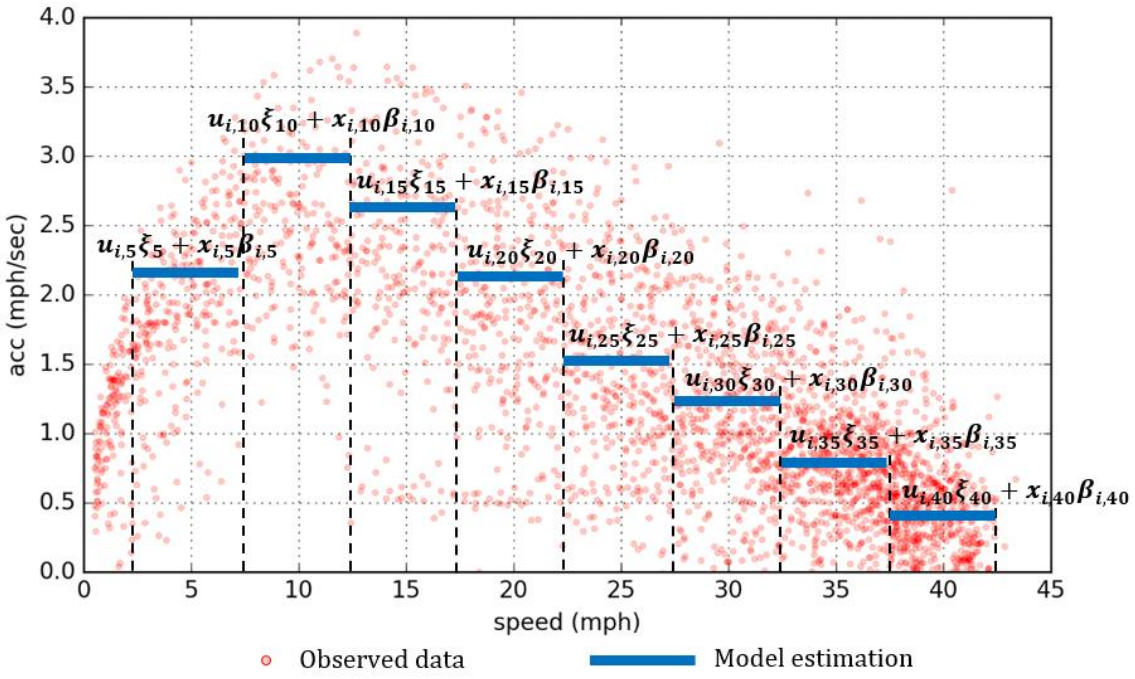

Figure 76 – Graphic expression of speed-acceleration model for vehicle i with Target Speed V_{target} = 40 mph (Acceleration Traces from 0 to 40 mph)

As mentioned in previous chapters, the vehicle operation data is hierarchically structured. Hierarchical models are used for describing the overall grade impact on acceleration behavior, as well as heterogeneity of grade impact across speed pieces and vehicles. A graphical representation of the hierarchical model for speed-acceleration traces with target speed V_{target} is shown in in Figure 77. For example, $\boldsymbol{\beta_{2,10}}$ is vehicle-specific effect, referring to array of parameter to estimate vehicle #2's acceleration value at speed piece 10 mph (7.5-12.5 mph) from acceleration behavior with target speed V_{target}. The vehicle-level parameters $\boldsymbol{\beta_{i,j}}$ are assumed to correlate within the speed piece and within the vehicle, but are expected to be independent for different vehicles

considering each vehicle has its own performance characteristics with relatively fixed driver(s) driving it. Also, $\boldsymbol{\beta_{i,j}}$ parameters are assumed to be independent across speed pieces. This is to say, the impact of variables on acceleration at speed piece i, is independent from the impact of variables at any other speed piece j. This assumption greatly simplifies the model solution through significantly reducing parameters in variance-covariance matrix of $\boldsymbol{\beta_{i,j}}$. The parameter $\boldsymbol{\theta_j}$ and $\boldsymbol{\Sigma_j}$ are the overall coefficients and its variance-covariance matrix of variables $\boldsymbol{x_{i,j}}$ after summarizing the heterogeneity $\boldsymbol{\beta_{i,j}}$, indicating the population level effect of $\boldsymbol{x_{i,j}}$. Alternatively speaking, $\boldsymbol{\beta_{i,j}} \sim \boldsymbol{MVN}(\boldsymbol{\theta_j}, \boldsymbol{\Sigma_j})$.

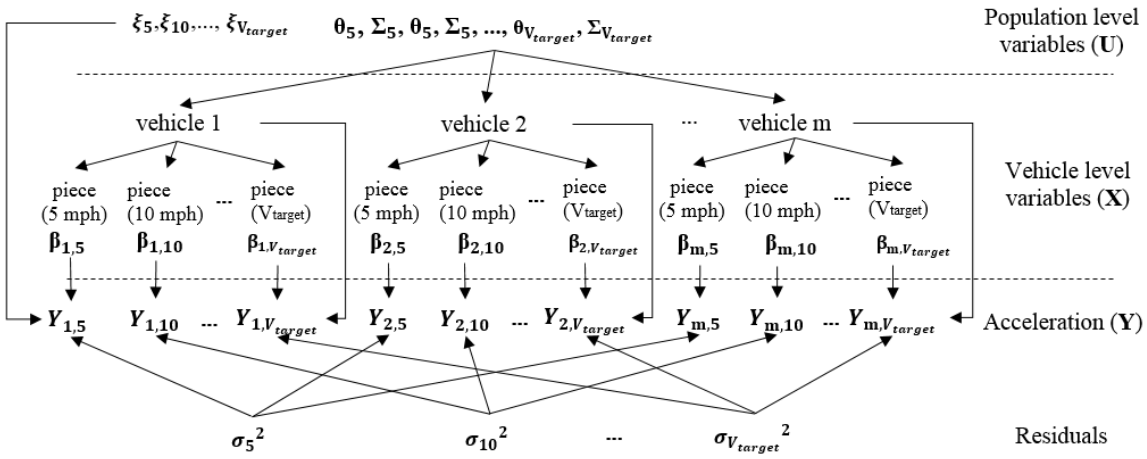

Figure 77 – Structure of Hierarchical Regression Acceleration Model

Bayesian method is applied to estimate posterior distribution of parameters. As mentioned in Chapter 5. The idea of estimating posterior joint distribution of parameters based on Bayesian method is expressed as:

$$\boldsymbol{P(\psi|u,x,y)} = \frac{\boldsymbol{P(y,\psi|u,x)}}{\boldsymbol{P(y|u,x)}} = \frac{\boldsymbol{P(y|\psi,u,x)P(\psi)}}{\boldsymbol{P(y|u,x)}} \propto \boldsymbol{P(y|\psi,u,x)P(\psi)} \quad (57)$$

Where $\boldsymbol{\psi}$ is a vector of parameters need to be estimated. For this model, the parameters refer to:

$$[\boldsymbol{\xi_5}, \boldsymbol{\xi_{10}}, \dots, \boldsymbol{\xi_{V_{target}}}, \quad \boldsymbol{\theta_5}, \boldsymbol{\Sigma_5}, \boldsymbol{\theta_{10}}, \boldsymbol{\Sigma_{10}}, \dots, \boldsymbol{\theta_{V_{target}-5}}, \boldsymbol{\Sigma_{V_{target}-5}}, \boldsymbol{\theta_{V_{target}}}, \boldsymbol{\Sigma_{V_{target}}}, \boldsymbol{\beta_{1,1}}, \dots, \boldsymbol{\beta_{1,V_{target}}}, \dots, \boldsymbol{\beta_{m,1}}, \dots, \boldsymbol{\beta_{m,V_{target}}}, \quad {\sigma_5}^2, {\sigma_{10}}^2, \dots, {\sigma_{V_{target}}}^2]$$

$\boldsymbol{P}(\boldsymbol{\psi})$ is prior distribution of $\boldsymbol{\psi}$, and $\boldsymbol{P}(\boldsymbol{\psi}|\boldsymbol{u}, \boldsymbol{x}, \boldsymbol{y})$ is posterior distribution given observations. Markov Chain Monte Carlo (MCMC) techniques are used to sample the distribution of parameters, and the posterior approximation can be made with Gibbs sampler.

7.4.2.1 Vehicle-Level Parameters $\boldsymbol{\beta_{1,5}, \beta_{1,10}, \dots, \beta_{m,V_{target}}}$

The joint probability density of observed data $y_{i,j,1}, y_{i,j,2}, \dots, y_{i,j,n_{ij}}$conditional upon $\boldsymbol{u_{i,j}}$, $\boldsymbol{x_{i,j}}$, $\boldsymbol{\xi_j}$, $\boldsymbol{\beta_{i,j}}$, and ${\sigma_j}^2$:

$$\begin{aligned} P\left(y_{i,j,1}, y_{i,j,2}, \dots, y_{i,j,n_{ij}} \middle| \boldsymbol{u_{i,j,k}}, \boldsymbol{x_{i,j,k}}, {\sigma_j}^2, \boldsymbol{\beta_{i,j}}, \boldsymbol{\xi_j}\right) \\ = (2\pi)^{-\frac{\boldsymbol{n_{ij}}}{\boldsymbol{2}}} |\sigma^2 \boldsymbol{I}|^{-\frac{\boldsymbol{1}}{\boldsymbol{2}}} \exp\{-\frac{1}{2}\big(\boldsymbol{y_{i,j}} - \boldsymbol{u_{i,j}}\boldsymbol{\xi_j} \\ - \boldsymbol{x_{i,j}}\boldsymbol{\beta_{i,j}}\big)^T \big({\sigma_j}^2 \boldsymbol{I}\big)^{-1} \big(\boldsymbol{y_{i,j}} - \boldsymbol{u_{i,j}}\boldsymbol{\xi_j} - \boldsymbol{x_{i,j}}\boldsymbol{\beta_{i,j}}\big)\} \end{aligned} \tag{58}$$

The prior distribution of $\boldsymbol{\beta_{i,j}} \sim \boldsymbol{MVN}\big(\boldsymbol{\theta_j}, \boldsymbol{\Sigma_j}\big)$ suggests that a multivariate normal prior distribution for $\boldsymbol{\beta_{i,j}}$ is conjugate. Based on the same idea shown in Appendix A, the full conditional distribution $\{\boldsymbol{\beta_{i,j}}|\boldsymbol{y_{i,j}}, \boldsymbol{u_{i,j}}, \boldsymbol{x_{i,j}}, {\sigma_j}^2, \boldsymbol{\theta_j}, \boldsymbol{\Sigma_j}, \boldsymbol{\xi_j}\}$ has a multivariate normal distribution with:

$$Var(\boldsymbol{\beta_{i,j}}|\boldsymbol{y_{i,j}}, \boldsymbol{u_{i,j}}, \boldsymbol{x_{i,j}}, {\sigma_j}^2, \boldsymbol{\theta_j}, \boldsymbol{\Sigma_j}, \boldsymbol{\xi_j}) = \big(\boldsymbol{\Sigma_j}^{-\boldsymbol{1}} + \boldsymbol{x_{i,j}}^{\boldsymbol{T}}\boldsymbol{x_{i,j}}/{\sigma_j}^2\big)^{-1} \tag{59}$$

$$E(\boldsymbol{\beta_{i,j}}|\boldsymbol{y_{i,j}}, \boldsymbol{u_{i,j}}, \boldsymbol{x_{i,j}}, {\sigma_j}^2, \boldsymbol{\theta_j}, \boldsymbol{\Sigma_j}, \boldsymbol{\xi_j}) = \left(\boldsymbol{\Sigma_j}^{-1} + \boldsymbol{x_{i,j}}^T \boldsymbol{x_{i,j}}/{\sigma_j}^2\right)^{-1}\left(\boldsymbol{\Sigma_j}^{-1}\boldsymbol{\theta_j} - \boldsymbol{x_{i,j}}^T \boldsymbol{u_{i,j}}\boldsymbol{\xi_j}/{\sigma_j}^2 + \boldsymbol{x_{i,j}}^T \boldsymbol{y_{i,j}}/{\sigma_j}^2\right) \quad (60)$$

7.4.2.2 Conditional Distribution of $\boldsymbol{\theta_j}, \boldsymbol{\Sigma_j}$

The sampling model for the $\boldsymbol{\beta_{i,j}}$'s is that the vehicle level effects in vehicle i are i.i.d. samples from a vehicle i-specific multivariate normal population with mean $\boldsymbol{\theta_j}$ and variance $\boldsymbol{\Sigma_j}$. Therefore, the full distribution of population mean $\boldsymbol{\theta_j}$ is multivariate normal with expectation equal to a combination of prior expectation and the sample mean $\boldsymbol{\beta_{i,j}}$, and precision equal to the sum of the prior and data precisions. In the context of hierarchical regression model, given $\boldsymbol{\Sigma_j}$ and samples of regression coefficients $\boldsymbol{\beta_{1,j}}, \boldsymbol{\beta_{2,j}}, \dots, \boldsymbol{\beta_{m,j}}$, a convenient prior distribution for the multivariate mean $\boldsymbol{\theta_j}$ is a multivariate normal distribution, which we parameterize as:

$$\boldsymbol{\theta_j} \sim MVN(\boldsymbol{\theta_{j,0}}, \boldsymbol{\Sigma_{j,0}})$$

Following the similar procedures in deriving $[\boldsymbol{\varphi_i}|\boldsymbol{\gamma_{i,1}}, \boldsymbol{\gamma_{i,2}}, \dots, \boldsymbol{\gamma_{i,n_i}}, \boldsymbol{\Sigma_i}]$ in chapter 5, the full conditional distribution of $\boldsymbol{\theta_j}$ is the multivariate normal distribution:

$$Var(\boldsymbol{\theta_j}|\boldsymbol{\beta_{1,j}}, \boldsymbol{\beta_{2,j}}, \dots, \boldsymbol{\beta_{m,j}}, \Sigma_j) = (\boldsymbol{\Sigma_{j,0}}^{-1} + m\Sigma_j^{-1})^{-1} \quad (61)$$

$$E(\boldsymbol{\theta_j}|\boldsymbol{\beta_{1,j}}, \boldsymbol{\beta_{2,j}}, \dots, \boldsymbol{\beta_{m,j}}, \Sigma_j) = (\boldsymbol{\Sigma_{j,0}}^{-1} + m\Sigma_j^{-1})^{-1}(\boldsymbol{\Sigma_{j,0}}^{-1}\theta_{j,0} + m\Sigma_j^{-1}\overline{\boldsymbol{\beta_j}}) \quad (62)$$

Where m is number of vehicles that operation data is collected, $\overline{\boldsymbol{\beta_j}}$ is the vector average $\frac{1}{\boldsymbol{m}}\sum_i \boldsymbol{\beta_{i,j}}$. $\theta_{j,0}$ and $\boldsymbol{\Sigma_{j,0}}$ are prior mean and variance-covariance matrix of θ_j, respectively.

As mentioned, a convenient prior distribution for the variance-covariance matrix $\Sigma_{\boldsymbol{\beta}}$ is an inverse-Wishart distribution.

Following the similar procedures in deriving $[\boldsymbol{\Sigma_i}|\boldsymbol{\gamma_{i,1}}, \boldsymbol{\gamma_{i,2}}, \dots, \boldsymbol{\gamma_{i,n_i}}, \boldsymbol{\varphi_i}]$ in chapter 5, the full conditional distribution of $\Sigma_{\boldsymbol{j}}$ is:

$$[\Sigma_{\boldsymbol{j}}|\boldsymbol{\beta_{1,j}}, \boldsymbol{\beta_{2,j}}, \dots, \boldsymbol{\beta_{m,j}}, \boldsymbol{\theta_j}] \sim \text{inverse} - \text{Wishart}(\eta_0 + m, [S_0 + \sum_{i=1}^{m}(\boldsymbol{\beta_{i,j}} - \theta_{\boldsymbol{j}})(\boldsymbol{\beta_{i,j}} - \theta_{\boldsymbol{j}})^T]^{-1}$$

Where η_0 and S_0 are parameters of prior distribution $\Sigma_{\boldsymbol{j}}$.

7.4.2.3 Population Fixed-Effects $\boldsymbol{\xi_j}$

If there are effects that do not vary across vehicles, or only the population effects are of interest, we can classify them to population effects $\boldsymbol{\xi_j}$, assuming homogeneity impact across all vehicles. Following the similar procedure presented in deriving $[\boldsymbol{\beta_{i,j}}|\boldsymbol{y_{i,j}}, \boldsymbol{u_{i,j}}, \boldsymbol{x_{i,j}}, {\sigma_j}^2, \boldsymbol{\theta_j}, \boldsymbol{\Sigma_j}, \boldsymbol{\xi_j}]$, $[\boldsymbol{\xi_j}|\boldsymbol{y_j}, \boldsymbol{u_j}, \boldsymbol{x_j}, \boldsymbol{\beta_j}, {\sigma_j}^2, \boldsymbol{\theta_{\xi_{j,0}}}, \boldsymbol{\Sigma_{\xi_{j,0}}}]$ exhibits a multivariate normal distribution with:

$$Var(\boldsymbol{\xi_j}|\boldsymbol{y_j}, \boldsymbol{u_j}, \boldsymbol{x_j}, \boldsymbol{\beta_j}, {\sigma_j}^2, \boldsymbol{\theta_{\xi_{j,0}}}, \boldsymbol{\Sigma_{\xi_{j,0}}}) = \left(\boldsymbol{\Sigma_{\xi_{j,0}}}^{-1} + \boldsymbol{u_j}^T\boldsymbol{u_j}/{\sigma_j}^2\right)^{-1} \tag{63}$$

$$\begin{aligned} E(\boldsymbol{\xi_j}|\boldsymbol{y_j}, \boldsymbol{u_j}, \boldsymbol{x_j}, \boldsymbol{\beta_j}, {\sigma_j}^2, \boldsymbol{\theta_{\xi_{j,0}}}, \boldsymbol{\Sigma_{\xi_{j,0}}}) \\ = \left(\boldsymbol{\Sigma_{\xi_{j,0}}}^{-1} + \boldsymbol{u_j}^T\boldsymbol{u_j}/{\sigma_j}^2\right)^{-1}\left(\boldsymbol{\Sigma_{\xi_{j,0}}}^{-1}\boldsymbol{\theta_{\xi_{j,0}}}\right. \\ \left. - \boldsymbol{u_j}^T\boldsymbol{x_j}\boldsymbol{\beta_j}/{\sigma_j}^2 + \boldsymbol{u_j}^T\boldsymbol{y_j}/{\sigma_j}^2\right) \end{aligned} \tag{64}$$

Where $\boldsymbol{\theta_{\xi_{j,0}}}$ and $\boldsymbol{\Sigma_{\xi_{j,0}}}$ refers to the mean and variance-covariance matrix of prior distribution $\boldsymbol{\xi_j}$. $\boldsymbol{y_j}$ refers to observations of all vehicles at speed piece j, $\boldsymbol{y_j} =$

$[\boldsymbol{y_{1,j}}, \boldsymbol{y_{2,j}}, \dots, \boldsymbol{y_{m,j}}]^T$. Similarly, $\boldsymbol{u_j}, \boldsymbol{x_j}$ and $\boldsymbol{\beta_j}$ are aggregated from vehicle-level to the population.

7.4.2.4 Conditional Distribution of σ_j^2

The parameter σ_j^2 represents the error variance, assumed to be different across speed pieces. Similar to chapter 5, the posterior distribution

$$[\sigma_j^2 | \boldsymbol{y_j}, \boldsymbol{u_j}, \boldsymbol{x_j}, \boldsymbol{\beta_j}, \boldsymbol{\xi_j}] \sim \text{inverse} - \text{gamma}([\nu_0 + \sum_i n_{i,j}]/2, [\nu_0 {\sigma^2}_0 + \sum_{i=1}^{m} \sum_{k=1}^{n_{i,j}} (\boldsymbol{y_{i,j,k}} - \boldsymbol{x_{i,j,k}}\boldsymbol{\beta_{i,j}} - \boldsymbol{u_{i,j,k}}\boldsymbol{\xi_j})^2] \Big/ 2)$$

Where ν_0 and ${\sigma^2}_0$ are prior parameters of σ_j^2. $\sum_i n_{i,j}$ refers to the total sample size from speed piece i.

7.4.2.5 MCMC Simulation Based on Gibbs Sampler

Similar to the MCMC process in Chapter 5, because we didn't acquire any prior information, all the prior information can be set as non-informative by setting large variance (10,000). MCMC simulation based on Gibbs sampler method are realized to generate the joint distribution of parameters in the model. The iteration strategy of MCMC random draws is presented in Figure 78. The loop runs 1,200 times and uses parameter values from the 201st to 1100th iterations. Values from first 200th iterations were removed as they are draw from "burn-in" period (Holf, 2009), in which the Markov chain moves from its initial value to a region of the parameter space that has high posterior probability.

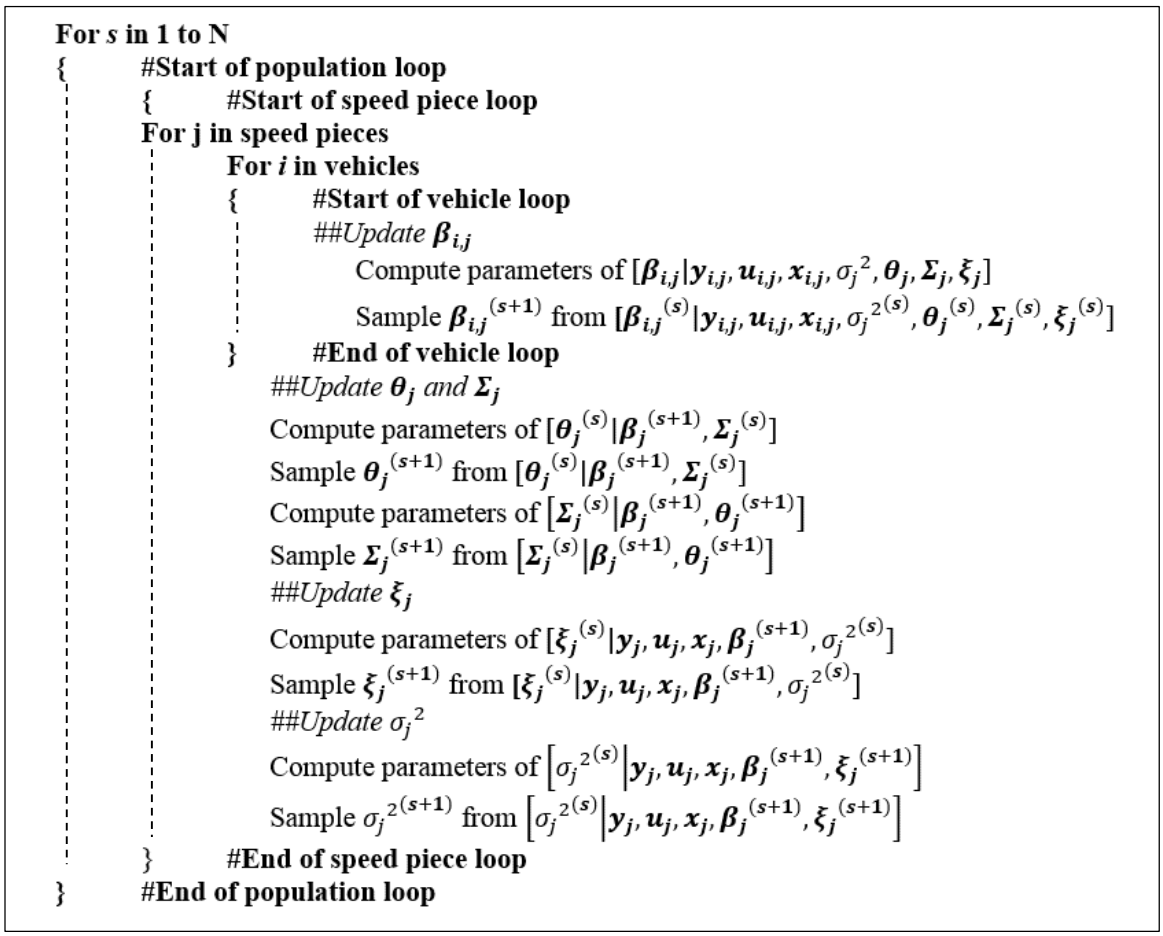

Figure 78 – MCMC Simulation Process

7.4.3 Model Result

In the first model development iteration, all variables were fed into the model. However, most of vehicle parameters were not significant and were therefore removed. The grade variable is decomposed to negative (<0%) and positive (≥0%) grade to capture the difference of impact between downgrade and upgrade. Eight factors are included in the final model: Intercept, Grade (<0%), Grade (≥0%), 100/Radius, Day (1-Day, 0-Night), GradeDiff (ToUphill), GradeDiff (ToDownhill), and Tier 2 (1) vs Tier 1 (0). The impact of each factor on each acceleration and speed piece is regarded one variable. That

is to say, for model representing acceleration of 0-40 mph, there are eight (8) speed pieces × eight (8) factors, or 64 parameters that need to be estimated. The full set of population-level parameters of models representing acceleration traces of 0-25 mph, 0-30 mph, 0-35 mph, 0-40 mph, and 0-45 mph are shown in Appendix D. Three factors are focused and discussed:

1. Intercept: representing average accelerations in each speed piece on flat segment (grade = 0%) as reference values
2. Grade (<0%): representing negative grade impact on accelerations
3. Grade (≥0%): representing positive grade impact on accelerations

The simulated σ_j distribution from model of acceleration trace 0-40 mph are shown in Figure 79 by speed piece and by vehicle types. The significant differences of σ_j's across speed pieces further validate the necessity of estimating error terms by speed piece separately in capturing such heteroscedasticity. It shows that error term shrinks in higher speed pieces.

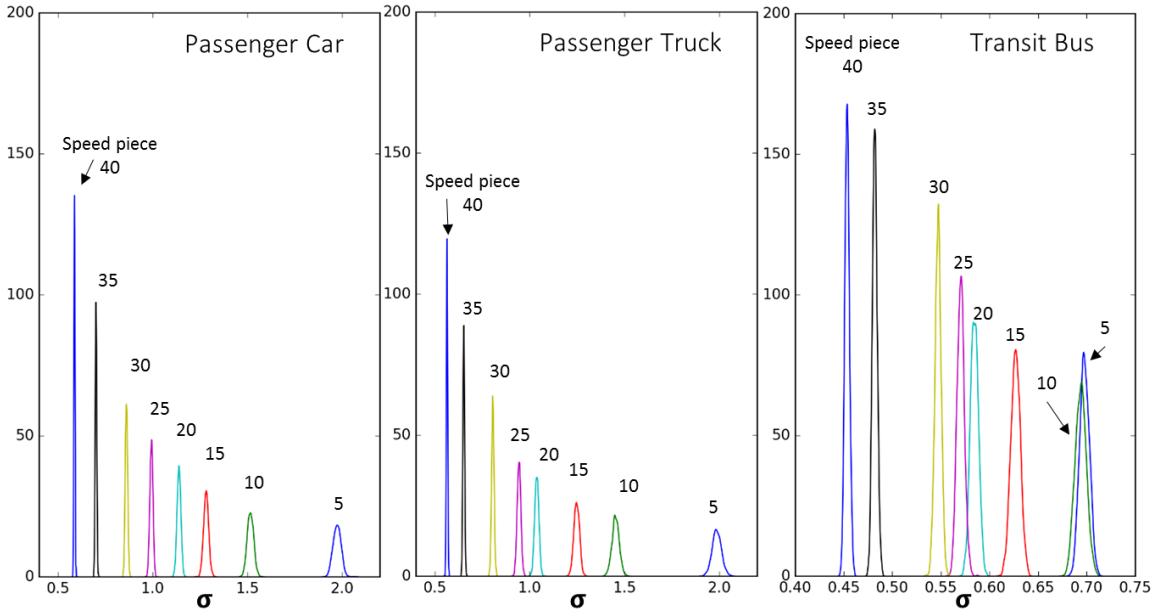

Figure 79 – Simulated σ_j of Acceleration Trace Model (0-40 mph) by Speed Piece

The estimated intercepts of three vehicle types are presented in Table 14 for comparison purpose, representing average accelerations in each speed piece on zero grade. It shows that average accelerations of passenger cars and passenger trucks are quite similar, and they are 30%-50% higher than accelerations of transit buses across all speed pieces and target speeds. Also, the average take-off acceleration of light-duty vehicles are almost twice as large as that of transit buses.

Table 14 – Intercept (Speed-Accelerations with Grade = 0%)

	Acceleration type (initial - end speed, mph)					
Speed piece (mph)	**0-20**	**0-25**	**0-30**	**0-35**	**0-40**	**0-45**
Speed piece (mph)	**Passenger car**					
5	3.225***	3.549***	3.415***	3.617***	3.609***	3.577***
10	2.644***	3.141***	3.404***	3.747***	3.676***	4.284***
15	1.975***	2.544***	2.837***	2.986***	3.026***	3.693***
20	0.542***	1.97***	2.181***	2.587***	2.748***	2.946***
25		0.606***	1.64***	1.98***	2.205***	2.671***
30			0.535***	1.332***	1.776***	2.067***

Speed piece (mph)	Acceleration type (initial - end speed, mph)					
	0-20	**0-25**	**0-30**	**0-35**	**0-40**	**0-45**
35				0.482***	1.158***	1.732***
40					0.462***	1.087***
45						0.41***
Speed piece (mph)	**Passenger truck**					
5	2.529***	2.467***	3.102***	3.464***	3.802***	3.765***
10	2.897***	2.952***	3.15***	3.3***	3.773***	3.951***
15	2.069***	1.984***	2.298***	2.783***	3.287***	3.394***
20	0.477^	2.087***	2.193***	2.538***	2.705***	2.785***
25		0.791***	1.332***	1.878***	2.283***	2.542***
30			0.481***	1.257***	1.606***	1.922***
35				0.557***	1.146***	1.505***
40					0.454***	0.99***
45						0.404***
Speed piece (mph)	**Transit bus**					
5	1.785***	1.846***	1.882***	1.876***	1.85***	1.934***
10	2.167***	2.266***	2.317***	2.374***	2.372***	2.417***
15	1.797***	2.03***	2.159***	2.187***	2.248***	2.295***
20	0.888***	1.565***	1.769***	1.857***	1.902***	1.982***
25		0.749***	1.268***	1.519***	1.594***	1.648***
30			0.615***	1.086***	1.296***	1.266***
35				0.55***	0.918***	0.985***
40					0.504***	0.817***
45						0.456***

***99.9%, **99%, *95%, ^90%

The estimated negative grade impacts on accelerations of three vehicle types are presented in Table 15, representing 1% grade changes on average acceleration impact at downhill segments at each speed piece. Results for light-duty vehicles indicate that for acceleration traces with low target speed (20 mph, 25 mph, and 30 mph), grade does not significantly impact most of the speed pieces. This is probably because the traces are very likely extracted from segments with heavy traffic conditions, where car following and queueing are the main constrain to vehicle acceleration behavior. For accelerations with

higher target speed, where traces are likely extracted from uncongested conditions and less interruptions from traffic are expected, and accelerations become lower in response to grade increase.

In contrast, parameters from transit bus models shows that the rise of grade lowers accelerations across all speed-pieces and all trace types, with parameters more negative than in the light-duty models, and almost of all parameters meet the 99.9% significance level. Hence, it is expected that operations of heavy-duty buses are much more likely to be impacted by grade changes.

Table 15 – Negative Grade Impact on Accelerations

	Acceleration type (initial - end speed, mph)					
Speed piece (mph)	**0-20**	**0-25**	**0-30**	**0-35**	**0-40**	**0-45**
Speed piece (mph)	**Passenger car**					
5	0.113^	0.032	-0.028	0.059*	-0.04	-0.043
10	-0.001	-0.029	-0.011	0.019	-0.075***	-0.026
15	-0.002	-0.037	-0.059*	-0.037*	-0.103***	-0.066**
20	-0.015	0.003	-0.096***	-0.041*	-0.081***	-0.102***
25		-0.012	-0.055**	-0.051***	-0.083***	-0.101***
30			-0.015^	-0.027**	-0.06***	-0.104***
35				-0.022***	-0.015^	-0.021
40					-0.033***	-0.007
45						-0.03***
Speed piece (mph)	**Passenger truck**					
5	-0.029	-0.083	-0.055	0.033	0.064^	0.033
10	-0.02	-0.054	-0.067*	-0.001	-0.031	-0.049^
15	-0.106**	-0.02	-0.089***	-0.029	-0.051*	-0.063*
20	-0.008	0.013	-0.026	-0.048*	-0.072***	-0.08***
25		-0.018	-0.035	-0.072***	-0.082***	-0.085***
30			-0.028*	-0.058***	-0.066***	-0.064***
35				-0.014^	-0.02*	-0.04**
40					-0.023***	-0.033***
45						-0.028***
Speed piece (mph)	**Transit bus**					
5	-0.022***	-0.038***	-0.044***	-0.054***	-0.063***	-0.038***

	Acceleration type (initial - end speed, mph)					
Speed piece (mph)	**0-20**	**0-25**	**0-30**	**0-35**	**0-40**	**0-45**
10	0.021***	-0.038***	-0.047***	-0.05***	-0.048***	-0.022*
15	-0.015***	-0.067***	-0.086***	-0.1***	-0.104***	-0.104***
20	0.04***	-0.022***	-0.069***	-0.1***	-0.131***	-0.092***
25		0.009***	-0.036***	-0.073***	-0.102***	-0.12***
30			-0.001	-0.019***	-0.061***	-0.118***
35				-0.015***	-0.045***	-0.087***
40					-0.018***	-0.045***
45						-0.036***

Estimated parameters showing positive grade impact of accelerations on three vehicle types are presented in Table 16, representing 1% grade changes on average acceleration impact at uphill segments in each speed piece. Similar to grade impacts on downhill segments, results of light-duty vehicles indicate that for acceleration traces with low target speed (20 mph, 25 mph, and 30 mph), grade does not have significant impact on most of speed pieces. For accelerations with higher target speeds, an increase in grade significantly lowers accelerations. Parameters from the bus models shows increase of grade lower accelerations across all speed-pieces and all trace types in uphill segments, with almost of all parameters in the 99.9% significance level. Results from Table 15 and Table 16 implies that for transit buses, even constraints of heavy traffic conditions and car following do not dominate the acceleration impact of grade.

Table 16 – Positive Grade Impact on Accelerations

	Acceleration type (initial - end speed, mph)					
Speed piece (mph)	**0-20**	**0-25**	**0-30**	**0-35**	**0-40**	**0-45**
Speed piece (mph)	**Passenger car**					
5	0.058	0.028	0.09*	0.085*	0.034	0.058
10	0.021	0.047	0.022	-0.033	0.026	-0.056*
15	-0.032	-0.031	-0.039^	-0.059***	-0.002	-0.083***

	Acceleration type (initial - end speed, mph)					
Speed piece (mph)	**0-20**	**0-25**	**0-30**	**0-35**	**0-40**	**0-45**
20	0.023	-0.03	-0.006	-0.059***	-0.035*	-0.047**
25		-0.004	0.001	-0.035**	-0.032*	-0.075***
30			0	-0.018*	-0.042**	-0.029^
35				-0.01^	-0.02*	-0.05***
40					-0.003	-0.036***
45						-0.012^
Speed piece (mph)	**Passenger truck**					
5	0.274**	0.148*	0.108*	0.061	0.029	-0.022
10	0.086	0.05	0.055^	0.006	-0.021	-0.018
15	-0.018	-0.013	0.026	-0.014	-0.056*	-0.084***
20	0.004	-0.017	-0.05*	-0.032^	-0.036^	-0.064**
25		0.008	-0.021	-0.009	-0.049**	-0.044*
30			0.011	0.001	-0.014	-0.043**
35				-0.004	0	-0.039**
40					-0.02***	-0.021*
45						-0.022**
Speed piece (mph)	**Transit bus**					
5	-0.018***	-0.019***	-0.02***	-0.019***	-0.028***	-0.046***
10	-0.087***	-0.084***	-0.097***	-0.103***	-0.113***	-0.111***
15	-0.142***	-0.154***	-0.174***	-0.188***	-0.208***	-0.201***
20	-0.056***	-0.128***	-0.161***	-0.18***	-0.198***	-0.222***
25		-0.048***	-0.113***	-0.159***	-0.189***	-0.197***
30			-0.041***	-0.112***	-0.178***	-0.157***
35				-0.053***	-0.109***	-0.118***
40					-0.072***	-0.155***
45						-0.1***

***99.9%, **99%, *95%, ^90%

In addition to the limitation of crawling capability, another possible reason for the significant grade impact on transit bus accelerations may be bus driver behavior. Bus drivers may intentionally slow down or step on gas pedal more gently in more uphill segments to ensure stability and keep passengers safe, especially, if there are disabled people on wheelchairs, or passengers standing on the corridor of the bus. Such information is unfortunately not available in this study. It should be noticed that this

unique characteristic may lead transit buses to accelerate differently not only compared to light-duty vehicles, but also to heavy-duty trucks. Additional research is needed to explore contribution of bus drivers' acceleration behaviour in response to combined effect of grade and passenger load, and how bus operate differently compared with trucks.

A comparison of observed and estimated speed-acceleration paths in response to grade level from acceleration traces 0-40 mph are shown in Figure 80, with the left column showing observed paths, and right column showing estimated paths. The figure shows the validity of the Bayesian Hierarchical piecewise model in describing acceleration behaviour of all three vehicle types. Also, acceleration characteristics of passenger cars and passenger trucks are quite similar, indicating that in cases where operation data size is limited, it may be feasible that acceleration data from these two vehicles can be shared to obtain more robust operation distributions.

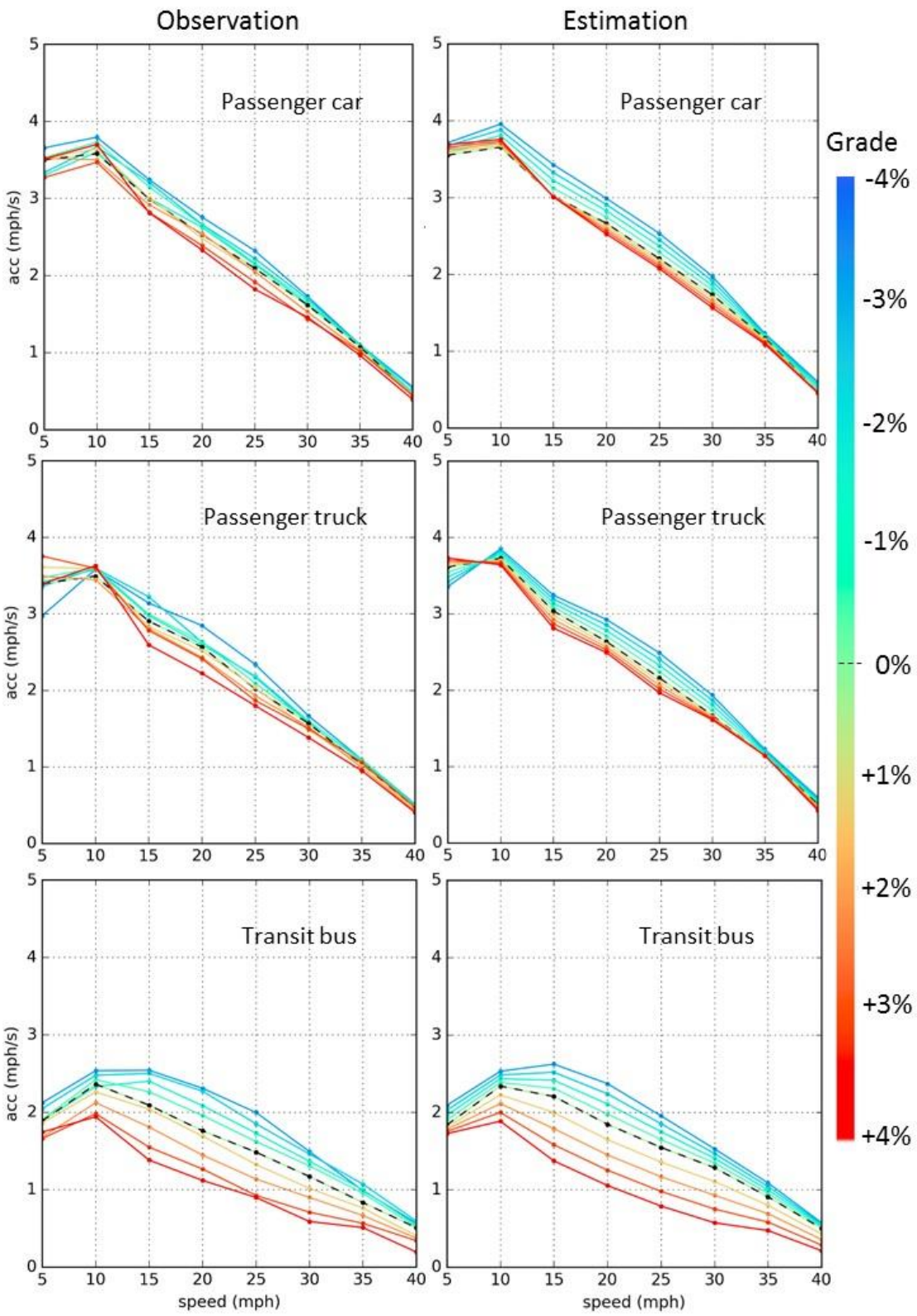

Figure 80 – Observed v.s. Estimated 0-40 mph Speed-Acceleration by Grade

7.5 Shape of SAJD Formed by Accelerations

The Bayesian Hierarchical model only shows grade impacts on average accelerations within speed bins. This section introduces how grade impacts the overall shape of SAJD formed by acceleration traces. We group all speed and acceleration points by speed piece and grade level. The 2.5 percentile acceleration (representing extreme small or lower boundary of acceleration), and 97.5 percentile acceleration (representing extreme large or upper boundary of acceleration), are extracted from each speed piece for accelerations traces with target speed from 25 to 45 mph, and across grade range of -4% to +4%, as shown in Figure 81, representing operations of passenger car, passenger truck and express bus in column 1, 2 and 3, respectively.

A clear trend in curve of 97.5-percentile accelerations moving from larger to smaller values can be observed for all vehicle types as grade increases from -4% to +4%, while the trend is not clear at 2.5-percentile acceleration. The extreme accelerations of transit buses drop much more significantly than light-duty vehicles. A clearer illustration can be seen in Figure 82, showing the acceleration distribution, 97.5-percentile and 2.5-percentile acceleration from acceleration traces 0-40 mph by speed piece and grade level. For passenger cars and passenger trucks, only the 97.5-percentile accelerations show a decreasing trend as grade increases, while the change of overall acceleration distributions is not obvious. This is not the case for transit buses, where acceleration distributions demonstrate a very obvious shift towards lower acceleration values across all speed pieces as grade increases. Such significant impact on accelerations of transit buses will be reflected in energy consumption and emissions modeling, which will be shown in Chapter 8.

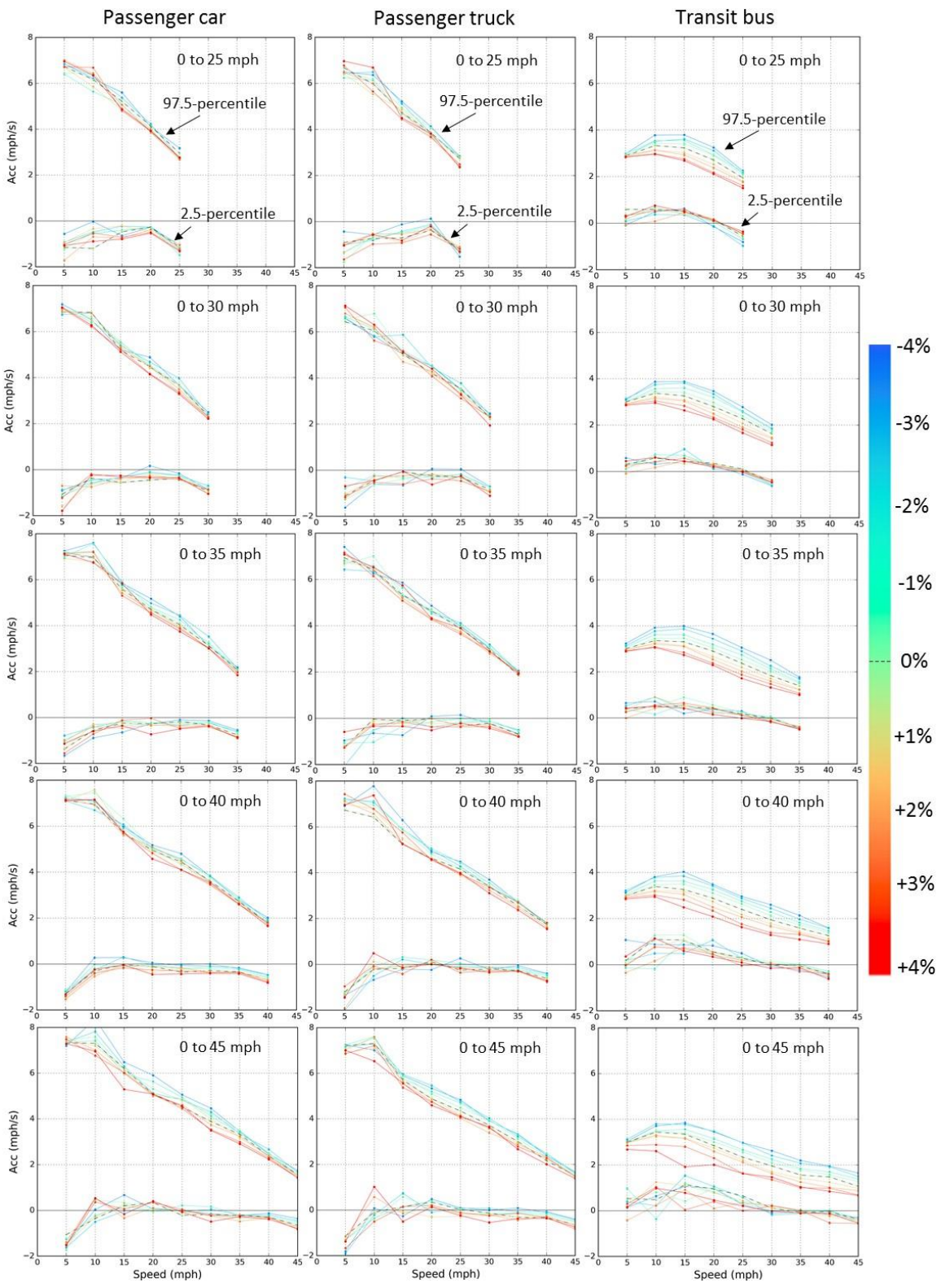

Figure 81 – 2.5-Percentile (Extreme Deceleration) and 97.5-Percentile (Extreme Acceleration) of SAJD by Grade

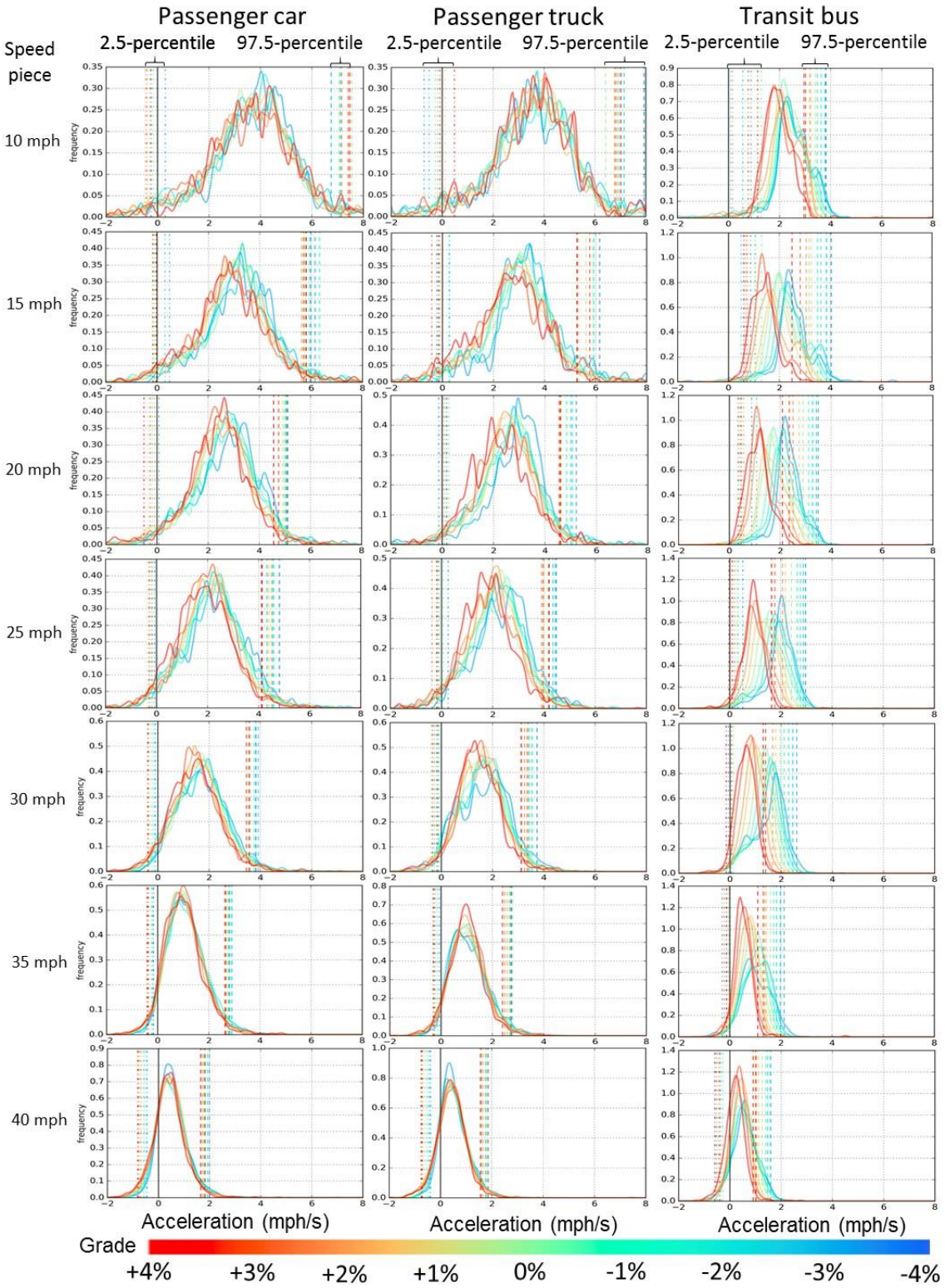

Figure 82 – Acceleration Distribution by Speed and Grade in 0-40 mph Traces

7.6 Acceleration Distance and Duration

This section shows acceleration distance and duration that vehicles need to reach to target speed on different average grade levels. Average acceleration distance (meter) and duration (second) are shown in Figure 83 and Figure 84, with 95%-CI range. There is no clear trend observed on acceleration distance and duration of light-duty vehicles. In contrast, transit buses need longer distance and duration to reach target speed.

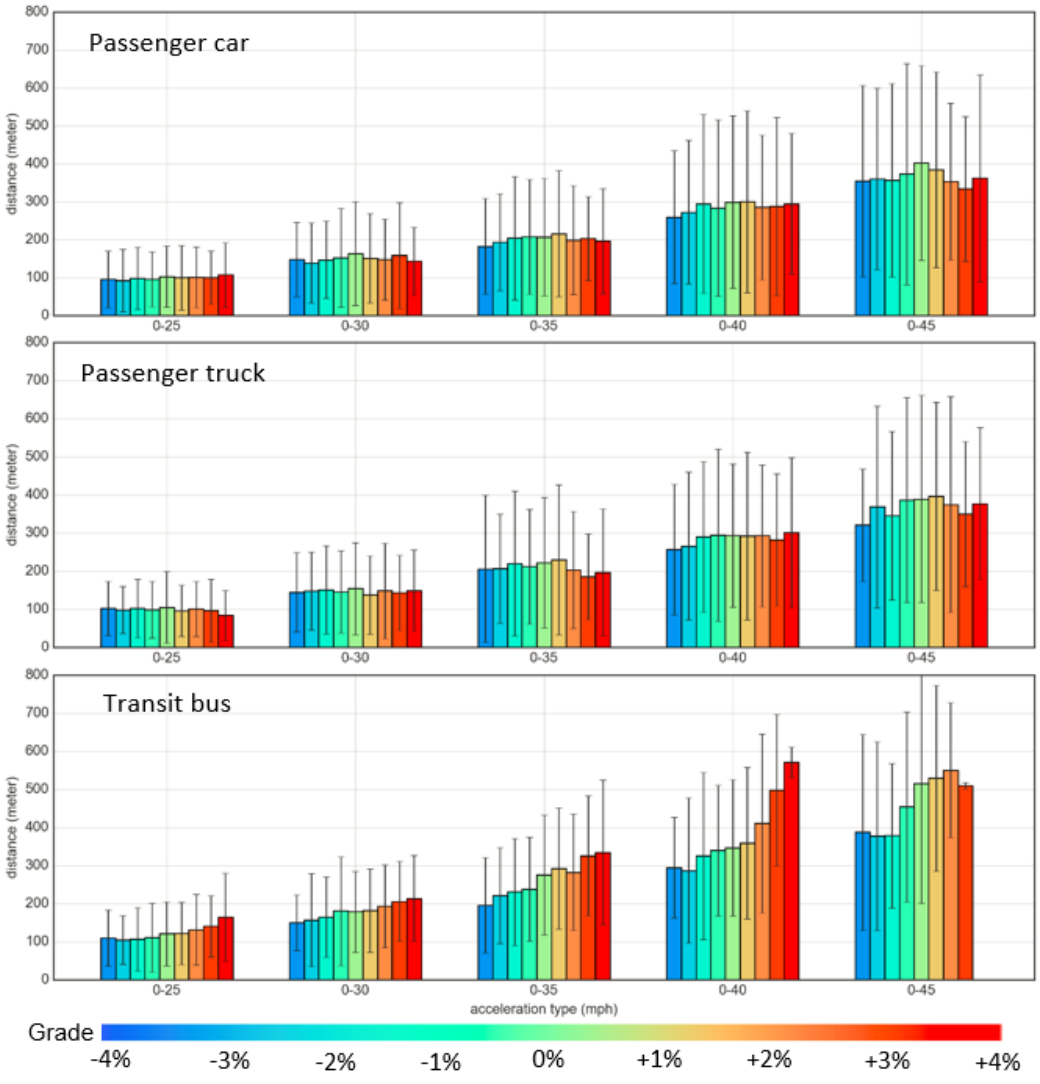

Figure 83 – Acceleration mean distance (meter) and 95%-CI range

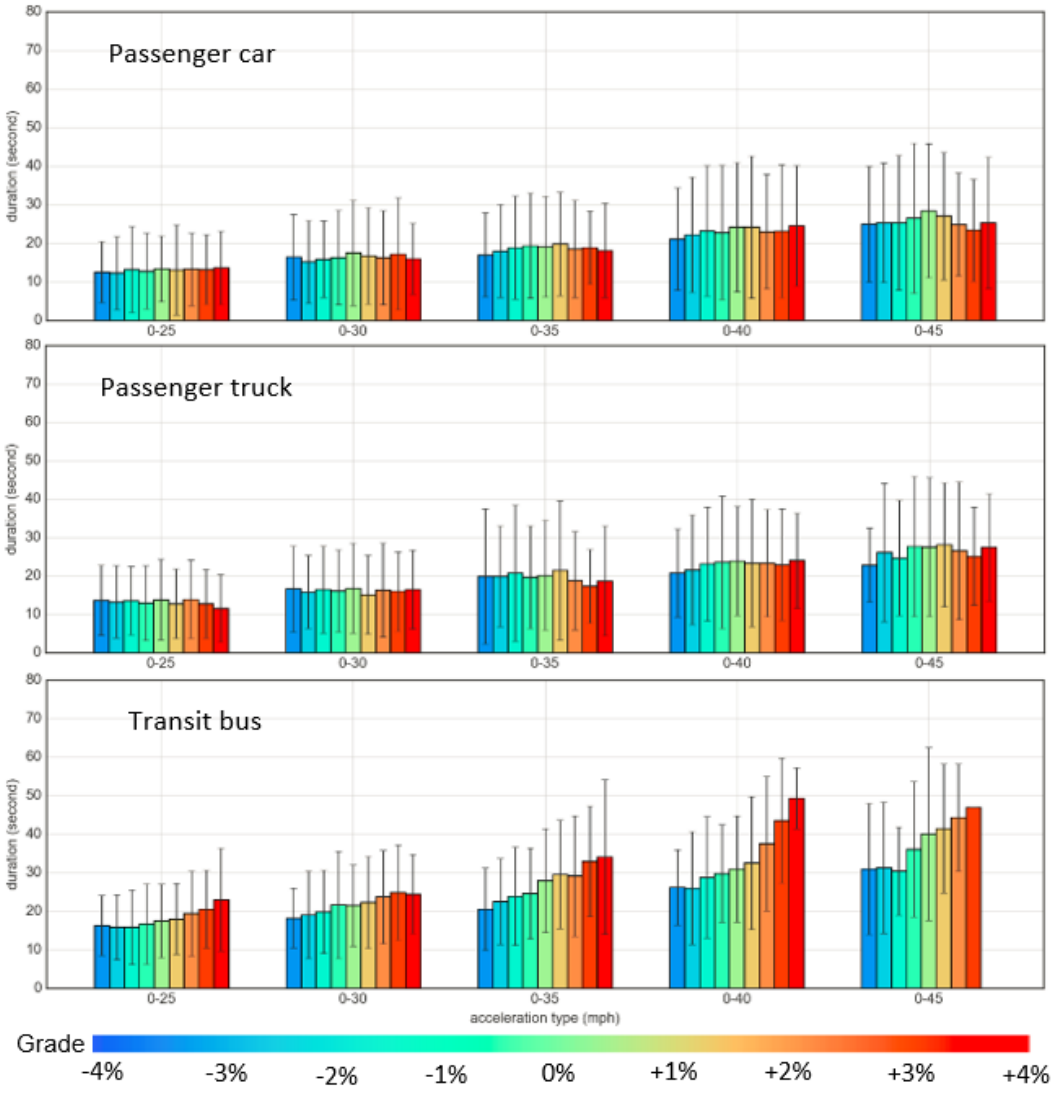

Figure 84 – Acceleration mean duration (second) and 95%-CI range

The relationship between grade and acceleration duration will be used in the next chapter, explaining the impact of road grade on emission ditributions and dispersion result along acceleration direction.

7.7 Summary

This chapter explored grade impact on acceleration behaviors in arterials. Several findings are provided below:

1. Grade causes different impacts on average target speed between downhill and uphill segments. For passenger cars, passenger trucks, and transit buses, target speed is not significantly impacted by grade on downhill operations. While for uphill operations, target speed dropped in average of 1.5 mph for each 1% of grade increase for all vehicle types. The similarity of grade coefficients implies that grade has in overall similar impacts of target speed of light-duty vehicles and transit buses. In additions, uphill grades have more significant impact on extreme target speed of transit buses than passenger cars and passenger trucks, as heavy-duty buses may be incapable of reaching high speeds on extreme uphill segments.
2. For a given target speed, the acceleration traces for low target speeds (20 mph, 25 mph, and 30 mph), are not significant impacted by grade for light-duty vehicles in most speed pieces. This is probably because the traces are extracted under heavy traffic conditions, where car following and queueing are the main constrain to vehicle acceleration behaviours. For accelerations with higher target speed, where traces are likely extracted from uncongested conditions and fewer expected traffic interruptions, accelerations of light-duty vehicles become lower in response to the rise of road grade.
3. Results show that acceleration of heavy-duty buses are more likely to be restricted (not only from average value, but also the distribution of accelerations) as grade increases, compared with operations of light-duty vehicles. Such significant grade impact on accelerations of transit buses

should be reflected in modeling of energy consumption and emissions on arterials, which will be introduced in Chapter 8.

CHAPTER 8. ENERGY AND EMISSIONS ON ARTERIALS

In Chapter 7, grade impact on acceleration behaviors of passenger cars, passenger trucks, and transit buses at arterials, were explored and traces of transit buses were found to be much more sensitive to grade changes than light-duty vehicles. Chapter 8 provides its application on vehicle energy consumption and emissions modeling.

Similar to the comparative analysis in Chapter 6, three scenarios are proposed to estimate the potential impact on energy and emission estimation when grade is ignored, or, when the correlation between grade and acceleration behavior is ignored. Scenario 1 refers to the acceleration traces and paired grades from direct collection of real-world data. Scenario 2 is assumes that grade is ignored by setting grade as zero. Scenario 3 is assuming grade does not affect acceleration behaviors and combines all speed-acceleration traces irrespective of the grades upon which they were collected. Under these three scenarios, energy consumption and emissions are assessed at the trace level, by estimating average energy consumption, spatial distribution of $PM_{2.5}$ emissions, and near-road concentrations of acceleration segments.

From the last section of Chapter 7, we learned that several traces from downhill segment reach target speed faster than from uphill, with less distance traveled. To make a fair comparison, acceleration traces with short distances are extended after reaching target speed using cruising speed of target speed and average grade until the trace reaches the same proposed distance. Based on the distance distribution shown in the last section of Chapter 7, the proposed distances for acceleration traces in target speed of 25 mph, 30 mph, 35 mph, 40 mph, and 45 mph are 150, 200, 300, 500, and 600 meters. Using similar

ideas in Chapter 6, three scenarios are proposed to generate the SAJD from acceleration traces, noted as $T_{v,veh,g}$, representing acceleration trace of vehicle type *veh* with target speed *v* in road segment of grade level *g*:

Scenario 1 (S1): True distribution: Uses actual second-by-second speed-acceleration traces and paired second-by-second grade data.

Scenario 2 (S2): Assume Grade = 0, but employ observed operating conditions: Assumes flat terrain and uses observed speed-acceleration traces (ignore all grade).

Scenario 3 (S3): Independent grade and operations, Ignores grade impact on acceleration operations. Under this assumption, the speed-acceleration traces for each average grade level are mixed within each vehicle type and target speed, equaling to $T_{v,veh}$. Expressed symbolically:

$$T_{v,veh} = T_{v,veh,g}, \quad T_{v,veh,g} \in T_{v,veh},\ T_{v,veh,g} = T_{v,veh}\ where\ g\ is\ average\ grade$$

The comparison of energy consumption and emissions results between Scenario 1 and Scenario 2 indicates the impact of completely ignoring grade. The comparison of Scenario 1 and Scenario 3 indicates the impact of ignoring correlation between grade and acceleration behaviors.

8.1 Impact on Energy Consumption

Under three scenarios, the average trace energy consumption by average grade level ranging from -4% to +4% are presented in Figure 85, with target speed 30 mph, 35 mph, and 40 mph as show case example. It is obvious to see significant impact from

ignoring grade in energy consumption (Scenario 1 vs. Scenario 2): over-estimating energy consumption of traces on downgrade, and under-estimating energy consumption of traces on upgrade. For example, in traces with target speed of 35 mph, ignoring grade at -2% grade level yields a 13% and 14% over-estimation of energy consumption for passenger cars and passenger trucks, and 28% over-estimation for express buses. Ignoring grade at +2% grade level yields a 12% and 13% under-estimation of energy consumption for passenger cars and passenger trucks, and 20.4% under-estimation for express buses.

Treating grade and accelerations as independent does not show a significant meaningful bias in the estimation of energy consumption for light-duty vehicles. Although the bias is more significant for transit buses (the largest bias is within 8%.), for light-duty vehicles, most of biases are within 2%. A potential bias of only associated with ignoring the grade operations correlation of only 2% may be reasonable. Nevertheless, grade itself still needs to be included.

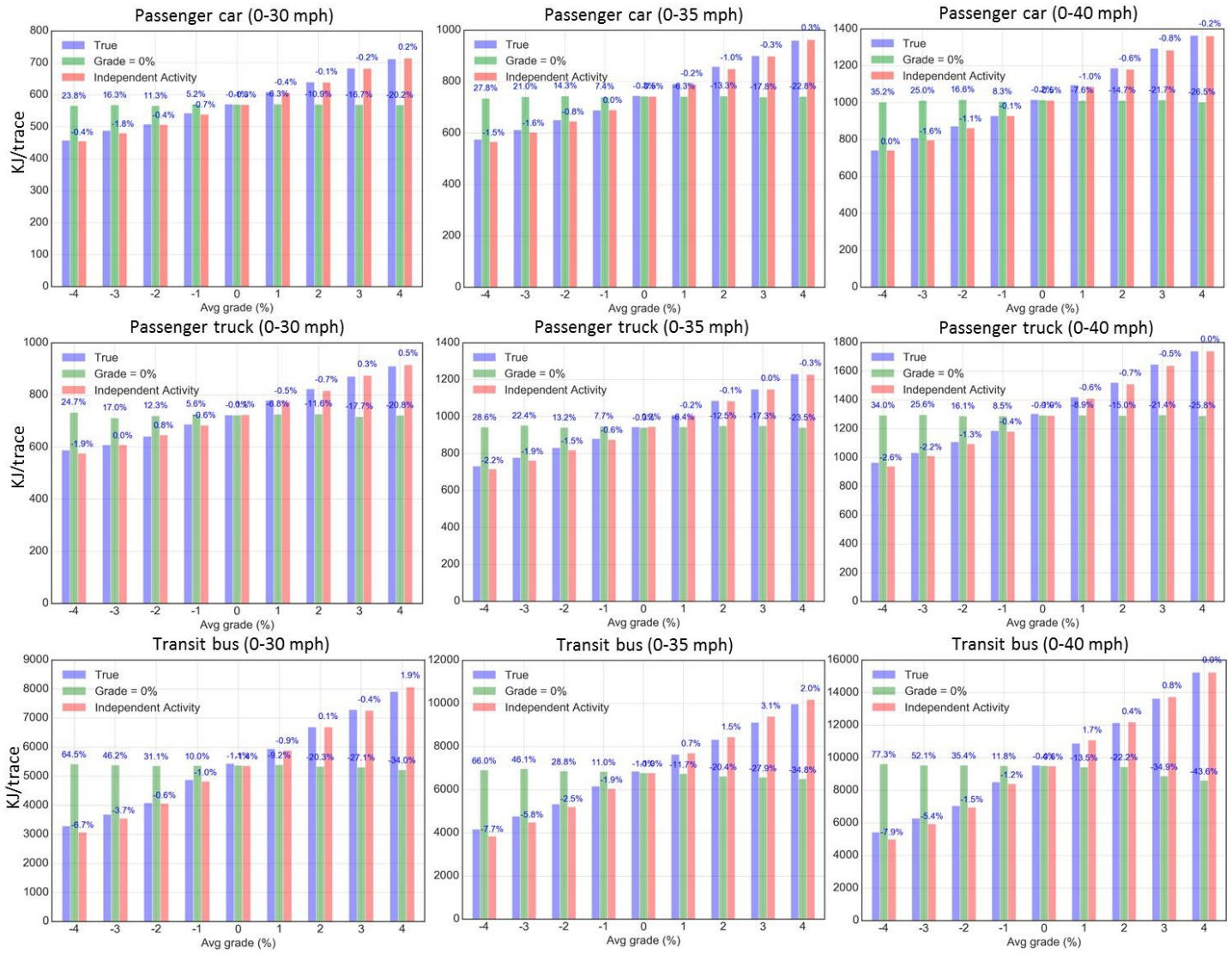

Figure 85 – Energy Consumption of Acceleration Traces

8.2 Spatial Distribution of $PM_{2.5}$ Emissions

For air pollutant emissions, not only are the mass emissions important, but the spatial distribution also matters. Spatial distributions of $PM_{2.5}$ emissions under the three scenarios are explored. The way we design the comparative analysis is to align all acceleration traces with the same starting point from zero meters, and plot emission rate in g/meter along travel distances towards the same direction. Next, emission rate in each distance bin (10 meters in this study) are averaged, and we obtain a smoothed relationship of emission rate versus accelerating distance from 0 mph. Again, emission rates from three scenarios are applied. Figure 86, Figure 87, and Figure 88 represent $PM_{2.5}$ emissions rate versus acceleration distances for passenger cars, passenger trucks and transit buses, respectively, with target speed ranging from 25 mph to 45 mph. The first column of these graphs represent emission distribution based on true activity and paired grade (Scenario 1). The second and third columns of these graphs represent emission distribution based on assumption of ignoring grade (Scenario 2) and assumption of independence between grade and acceleration behavior (Scenario 3). Several findings are listed below:

1. The comparison of graphs between Scenario 1 (first column) and Scenario 2 (second column) shows that ignoring grade will significantly overestimate $PM_{2.5}$ emissions on downhill segments, and underestimate $PM_{2.5}$ emissions on uphill segments.
2. For light-duty vehicles, including passenger cars and passenger trucks, graphs between Scenario 1 (first column) and Scenario 3 (third column) in Figure 86 and Figure 87 do not show significant differences, indicating that ignoring the

correlation between acceleration traces and grade does not introduce significant bias in emissions modelling. Models from Chapter 7 demonstrated that there is no obvious correlation between grade and SAJD of acceleration traces observed on light-duty vehicles models. In fact, graphs of the second column of Figure 86 and Figure 87 also supports this findings: when ignoring grade, emission distributions would reflect contributions "purely" from operations. For light-duty vehicles, emission curves of acceleration traces from different average grade levels are concentrated together. This implies that for light-duty vehicles, there may be no significant differences of emission contributions that comes from differences of operations in response to grade, since operations are not significantly different across grades.

3. For transit buses, graphs between Scenario 1 (first column) and Scenario 3 (third column) in Figure 88 show significant differences, indicating that ignoring correlation between acceleration traces and grade does introduce significant bias in emissions modelling. This bias is especially obvious in the beginning of acceleration traces (within 100 meters of start point). In the beginning stage of accelerations, ignoring grade-operation correlation yields an under-estimation of emission rates on downhill segments, and over-estimation of emission rate on uphill segments. This is because buses tend to accelerate more gently on more uphill grades, while ignoring the negative correlation ends up with putting more "aggressive" operations on uphill segments, and more "gentle" operations on downhill segments.

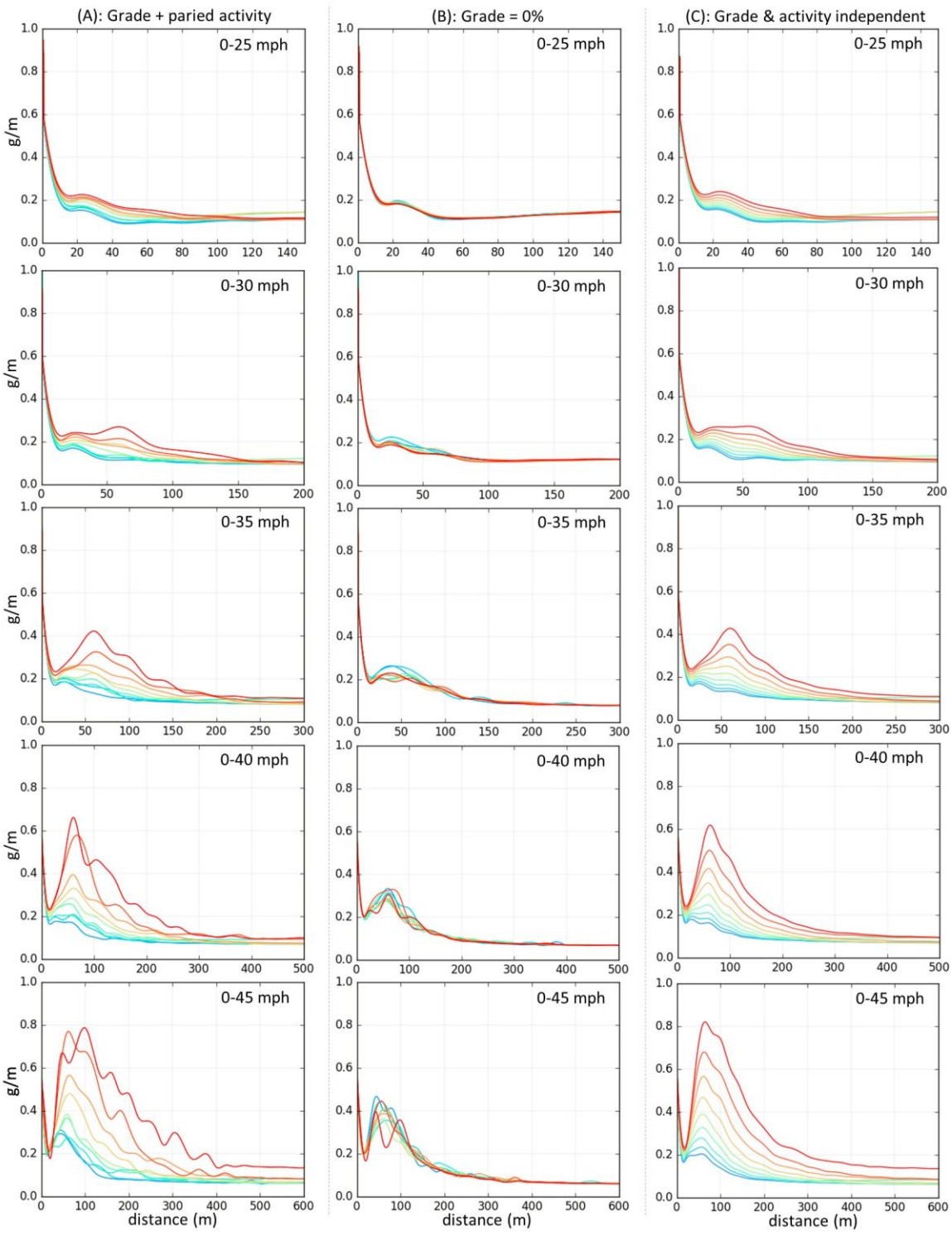

Figure 86 – $PM_{2.5}$ Emissions Rate in Acceleration Distances: Passenger Car

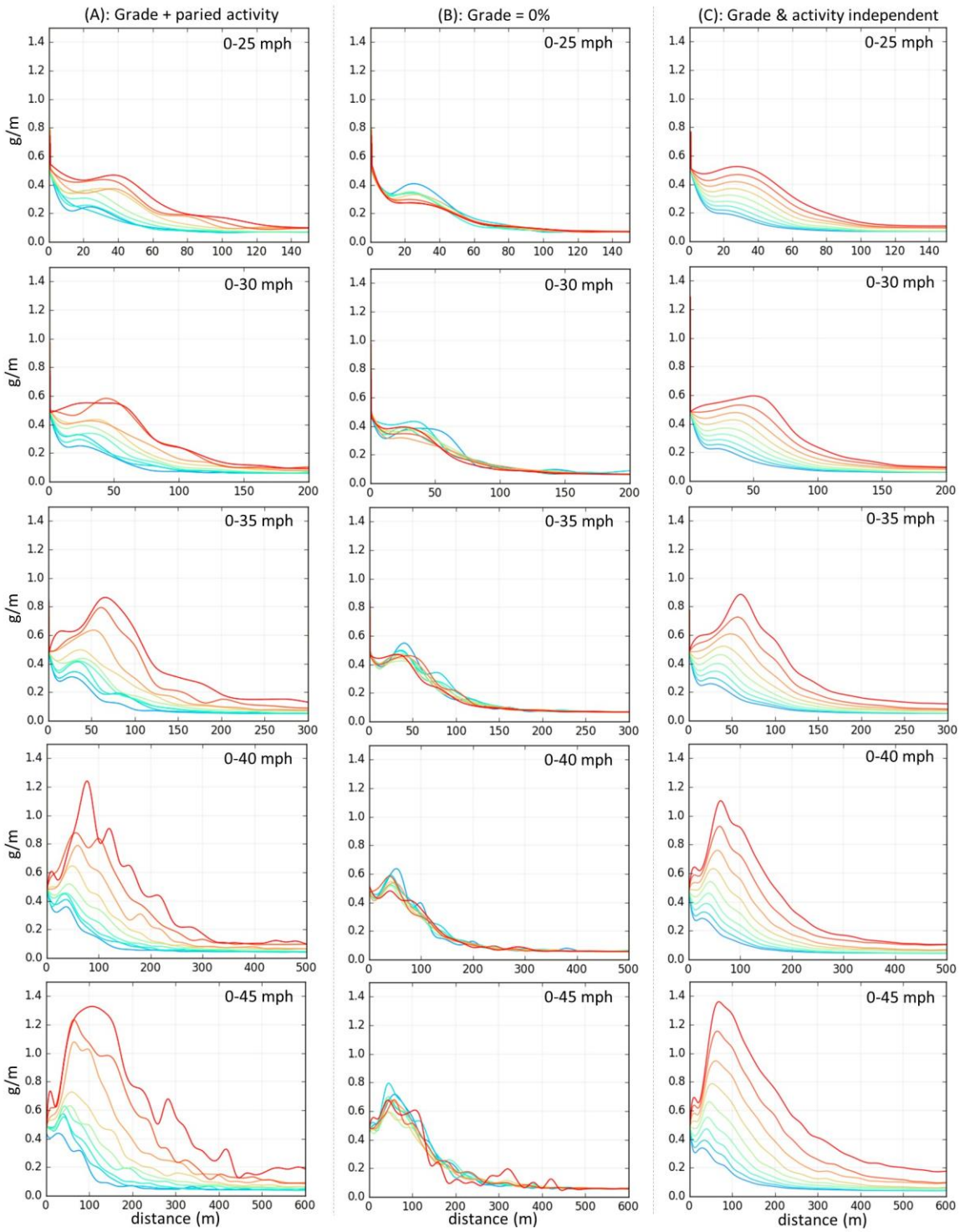

Figure 87 – $PM_{2.5}$ Emissions Rate in Acceleration Distances: Passenger Truck

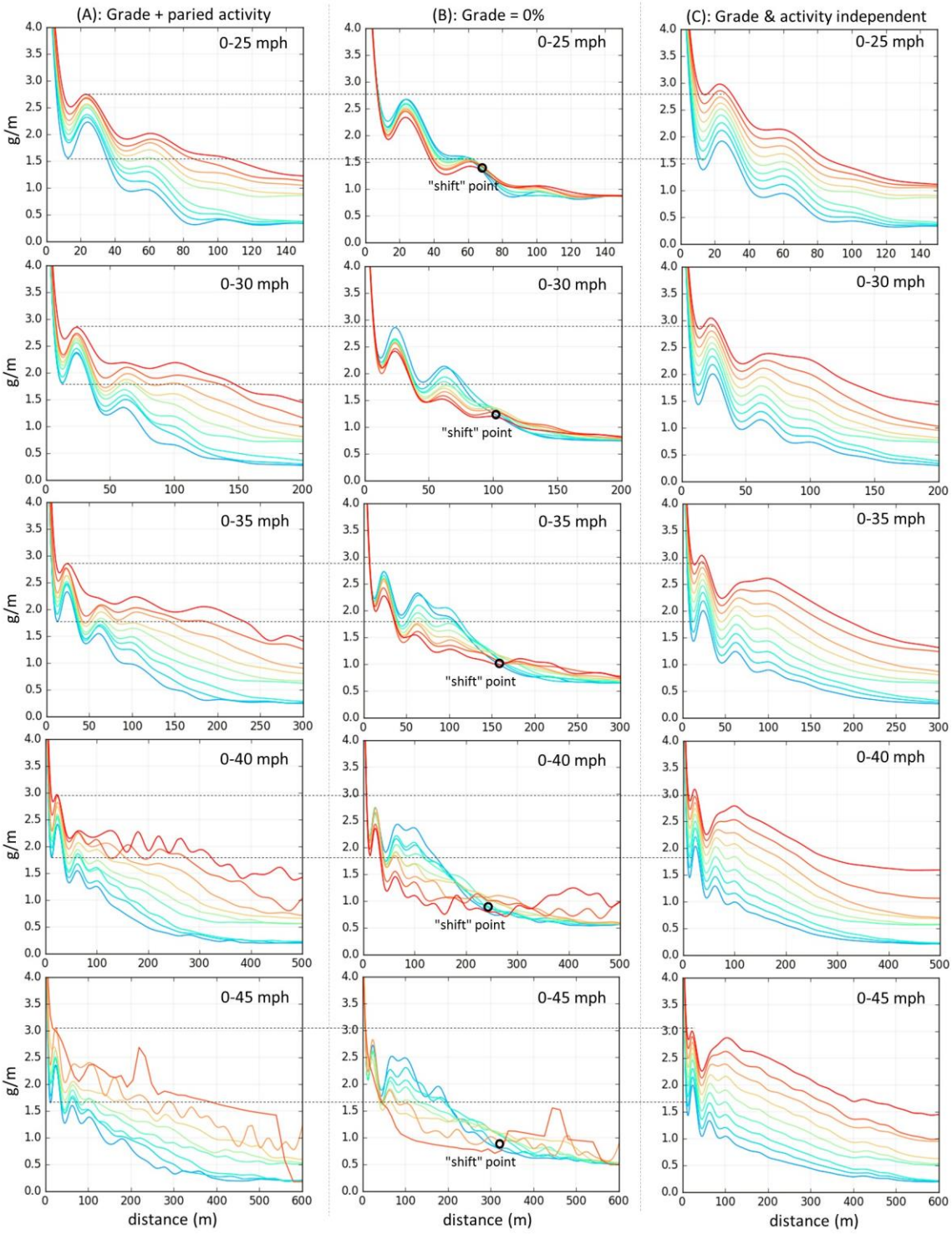

Figure 88 – $PM_{2.5}$ Emissions Rate in Acceleration Distances: Transit Bus

4. It is also interesting to notice that at the middle to ending stages of the acceleration period, ignoring grade-operation correlation causes bias in opposite direction: over-estimation of emission rate in downhill segments, and under-estimation of emission rate in uphill segments. This is because traces in more uphill segments are supposed to accelerate in longer distance to reach target speed. While Scenario 3 ignores this feature. In uphill segments, after certain stages, Scenario 3 assumes most of traces has reached target speed and has entered cruising mode that was arbitrarily extended, while in reality, vehicles operating on uphill segments may continue accelerating until they reached target speed over a longer distance. This ends up with under-estimation of emissions in Scenario 3 on the second half stage of uphill segments. For downhill segments, it is the other way around. In fact, graphs of the second column (Scenario 2) in Figure 88 shows emissions impact purely from operations of different grade level, and thus better shows the "shift" of impact: In the beginning, operations from uphill segments contributes less emissions than operations from downhill segments, and there is a "shift" position highlighted in the figure, after which, operations from uphill segments contributes more emissions than operations from downhill segments. A clearer description of this characteristics are shown in Figure 89, showing differences of $PM_{2.5}$ emission rates between results from Scenario 3 and Scenario 1 for transit buses. A "shift" point appears in the middle of acceleration processes after which signs of emission differences between uphill and downhill segments shifts.

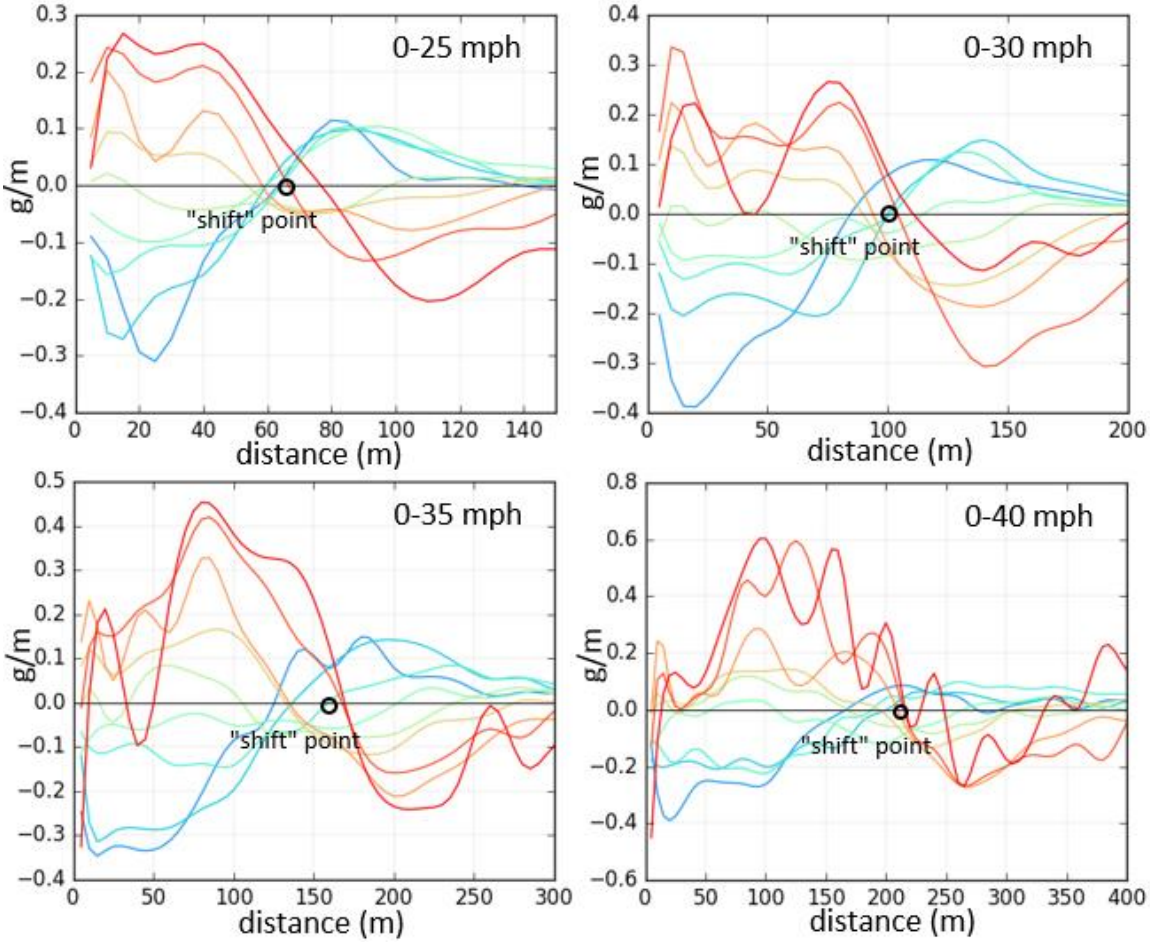

Figure 89 – Emission Rate Differences (Scenario 3 – Scenario 1) by Distance

These findings are useful in assessing the appropriate length of acceleration links in microscale dispersion modeling, and has the potential to improve accuracy of near-road air quality modeling especially for signalized intersections. More details will be introduced in the next section.

8.3 Near-Road Air Quality Modeling

Given the observed $PM_{2.5}$ distributions in response to various grade levels, this section explores the impact of grade on near-road air quality modeling from acceleration behavior. Based on the emission rates shown in Figure 86, Figure 87, and Figure 88, a

novel acceleration segment is built to simulate acceleration segments from a signalized intersection. The novel segment is assumed to be 10 meters in width, from west to east. Depending on the target speed, the length of this segment is extended length as shown in beginning of this chapter. The novel segment source is modeled using square-shaped "AREA" source in AERMOD, with each square representing emission source of the segment in 10 meters long and 10 meters wide. Emission rate of each square are aggregated from points into which the speed-acceleration traces fall. The volume of light-duty vehicles is assumed as 800 vehicles/hour with ratio of passenger cars to passenger trucks as 6/4. The volume of transit buses (representing heavy-duty cehicles) is set to 80 vehicles/hour. These are normal volume values at one intersection approach. Adding volume is just for rescaling purpose to avoid the estimated concentrations being too high or too low. The segment and receptor setup is shown in Figure 90. The unit of emission rate used for AERMOD "AREA" source is g/m^2/second, calculated in the same manner as the freeway case study in Chapter 6. Receptors are set as close as 5 meters from the novel segment, and in interval of 10 meters towards 200 meters from the segment. In this case study, only concentration profile of acceleration traces with target speed of 35 mph is shown. The AERMET 2016 hourly meteorology data required by AERMOD is obtained from Georgia Environmental Protection Division (Georgia EPD, 2018).

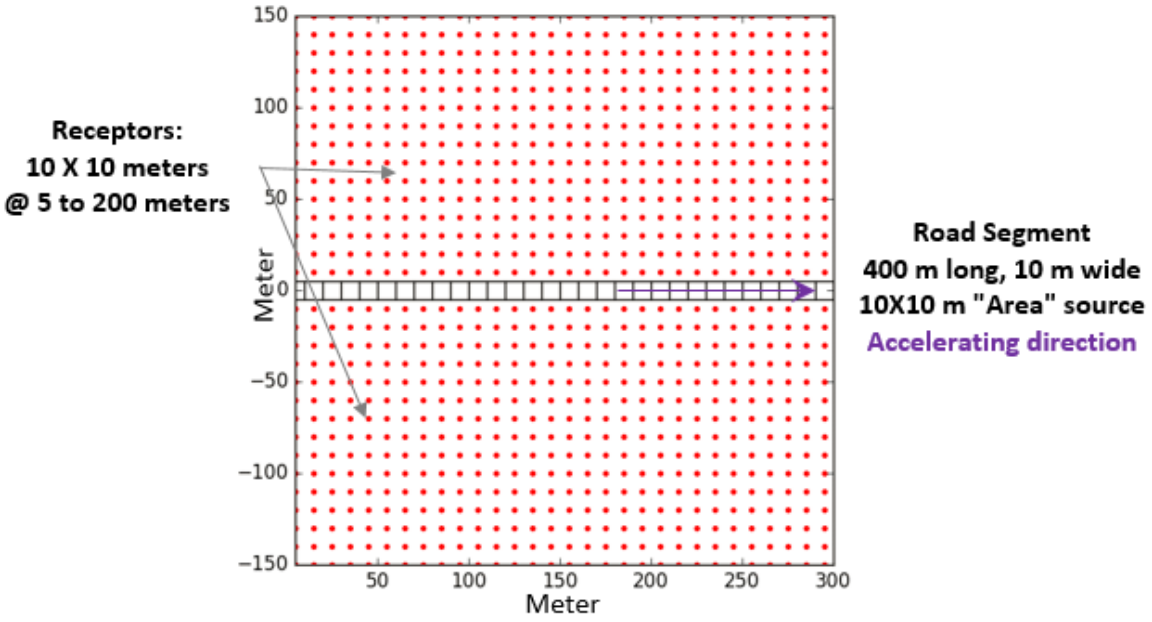

Figure 90 – Novel Acceleration Segment and Receptors Setup

The estimated baseline scenario annual average $PM_{2.5}$ concentration contributed from the novel acceleration segment is shown in Figure 91 with assumed traffic volume and grade ranging in -3%, 0% and +3%. Notice that in Figure 91, only traces with paired grade levels are used as baseline scenario. Segments with higher grade obviously contribute higher concentrations. In general, the near-road average concentration contributed from the segment can reach 3.5 ug/m^3 or higher, while the impact shrinks to less than 0.5 ug/m^3 in 150 meters or farther away from the segment.

The estimated concentration profiles from paired acceleration traces on these three grade levels are treated as baseline scenario (Figure 91), and compared with concentration profiles that are modeled based on emission rate from Scenario 2 and Scenario 3 as mentioned in previous section: treating grade as zero, or grade and accelerations as independent. Emission rates are derived from column 2 and column 3,

respectively, of Figure 86, Figure 87, and Figure 88. The difference in estimated concentration between candidate scenarios (scenario 2 and scenario 3) and baseline are calculated as $(e_{sce_{i_j}} - e_{base_j})$, with concentration difference profiles of acceleration traces from light-duty vehicles and transit buses shown separately in Figure 92 and Figure 93.

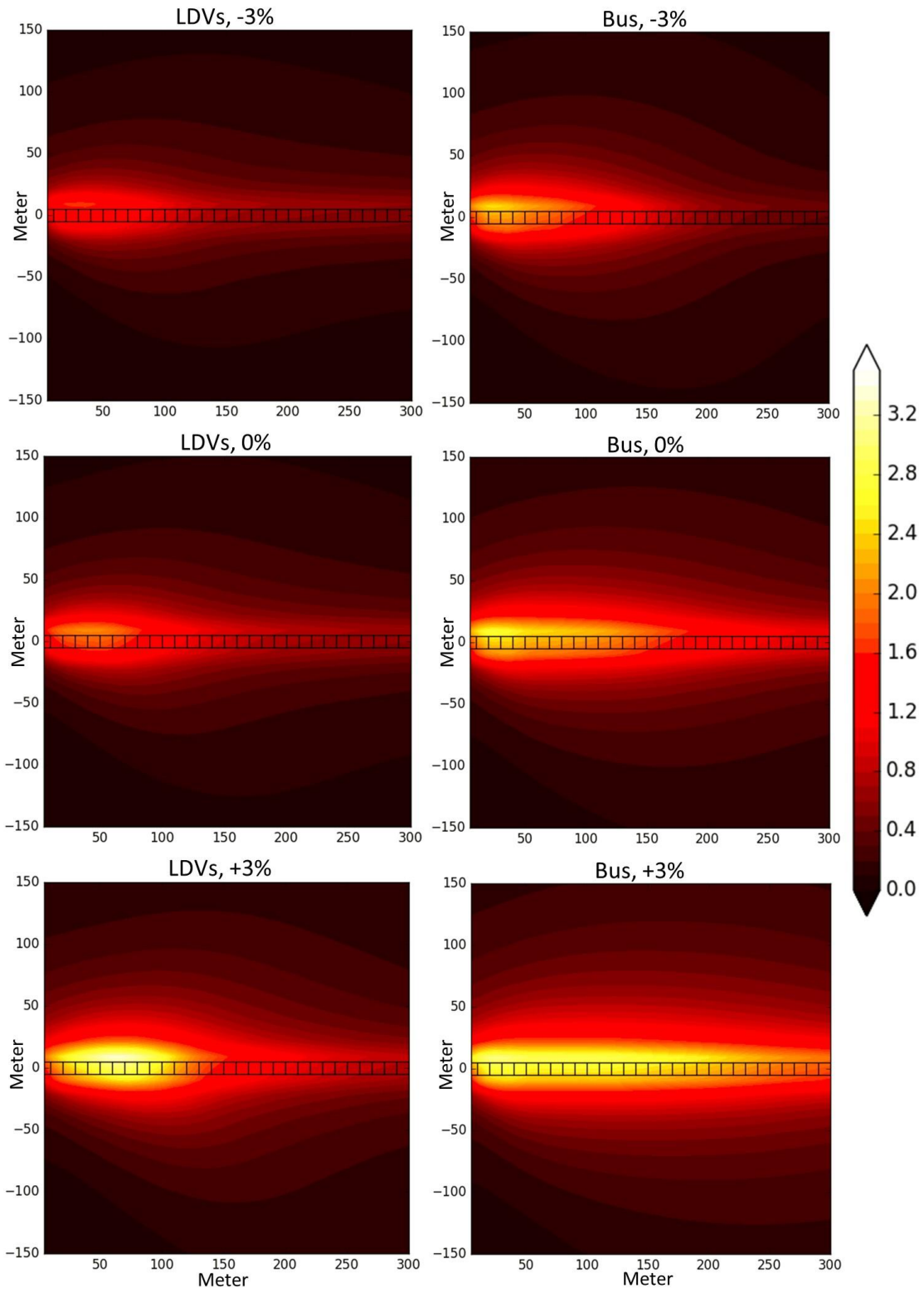

Figure 91 – Concentrations (0.4 ug/m^3) Based on Accelerations and Paired Grades

The differences of $PM_{2.5}$ concentrations from light-duty vehicles between Scenario 2 (grade = 0%) and Scenario 1 (base scenario) are shown in (a1), (a2) and (a3) of Figure 92, with average grade of -3%, 0%, and +3%, respectively. (a1), (a2) and (a3) of Figure 93 show the same information from transit buses. It is obvious to see that ignoring grade over-estimates concentration on average grade of -3% segment by 0.5 ug/m^3 or more within 25 meters of segment, and under-estimates concentration on average grade of +3% segment by 0.5 ug/m^3 or more within 25 meters of segment. This is especially obvious in the first half stage of acceleration period, where hard accelerations are taking places. The difference in average grade of 0% (shown in (a2) of the figures) reflects the variance of concentrations caused by variance of terrain while with average grade of 0% (zero elevation changes from start of the end of the acceleration) are within 0.05 ug/m^3

The differences of $PM_{2.5}$ concentrations from light-duty vehicles between scenario 3 (grade and acceleration activity are independent) and scenario 1 (base scenario) are shown in (b1), (b2) and (b3) of Figure 92, with average grade of -3%, 0%, and +3%, respectively. In general, for light-duty vehicles, the differences caused by ignoring grade-operations correlation are small. In contrast, (b1), (b2) and (b3) of Figure 93 shows the differences of $PM_{2.5}$ concentrations from transit buses between Scenario 3 (grade and acceleration activity are independent) and Scenario 1 (base scenario), with average grade of -3%, 0%, and +3%, respectively. It is interesting to observe that, for segment with average grade of -3%, ignoring grade-operation correlation would cause under-estimation of near-road concentration in the first half stage of acceleration period by as much as 0.3 ug/m^3, and over-estimation of concentration in the second half stage of

acceleration period, since the acceleration processes on downgrade reaches target speed with shorter distance than the population traces. For segment with average grade of +3%, ignoring grade-operation correlation causes the opposite impact: over-estimation of near-road concentration in the first half stage of acceleration period by as much as 0.3 ug/m^3, and under-estimation of concentration in the second half stage of acceleration period, since the acceleration processes on upgrade reaches target speed with longer distance than the population traces.

In the final guidance for quantitative PM_{10} and $PM_{2.5}$ hot-spot analysis released by EPA (USEPA, 2015), segments of the intersections, especially congested intersections are recommended to be decomposed into cruise, deceleration, idle, and acceleration sub-segments if second-by-second driving data are available, to differentiate emission differences caused by operation differences. However, integration of grade, although proved critical in air quality modeling, is not mentioned in the USEPA guideline. The finding from Figure 92 and Figure 93 shows the importance of not only including road grade in analysis, but also the necessity of research on the link segmentation strategy, with grade and grade-operation correlation involved.

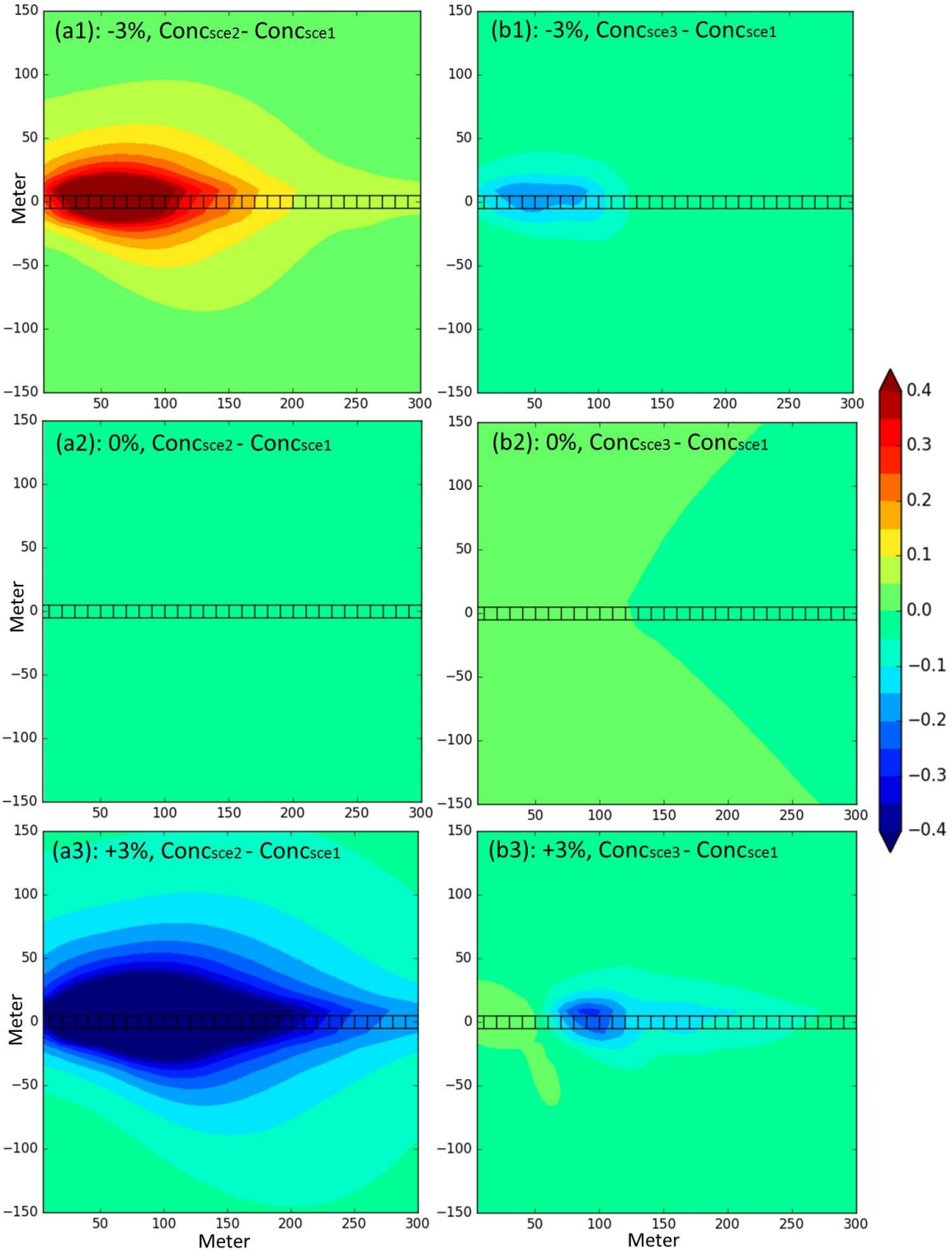

Figure 92 – LDVs: Concentration Differences (0.4 ug/m^3) Compared to Scenario 1

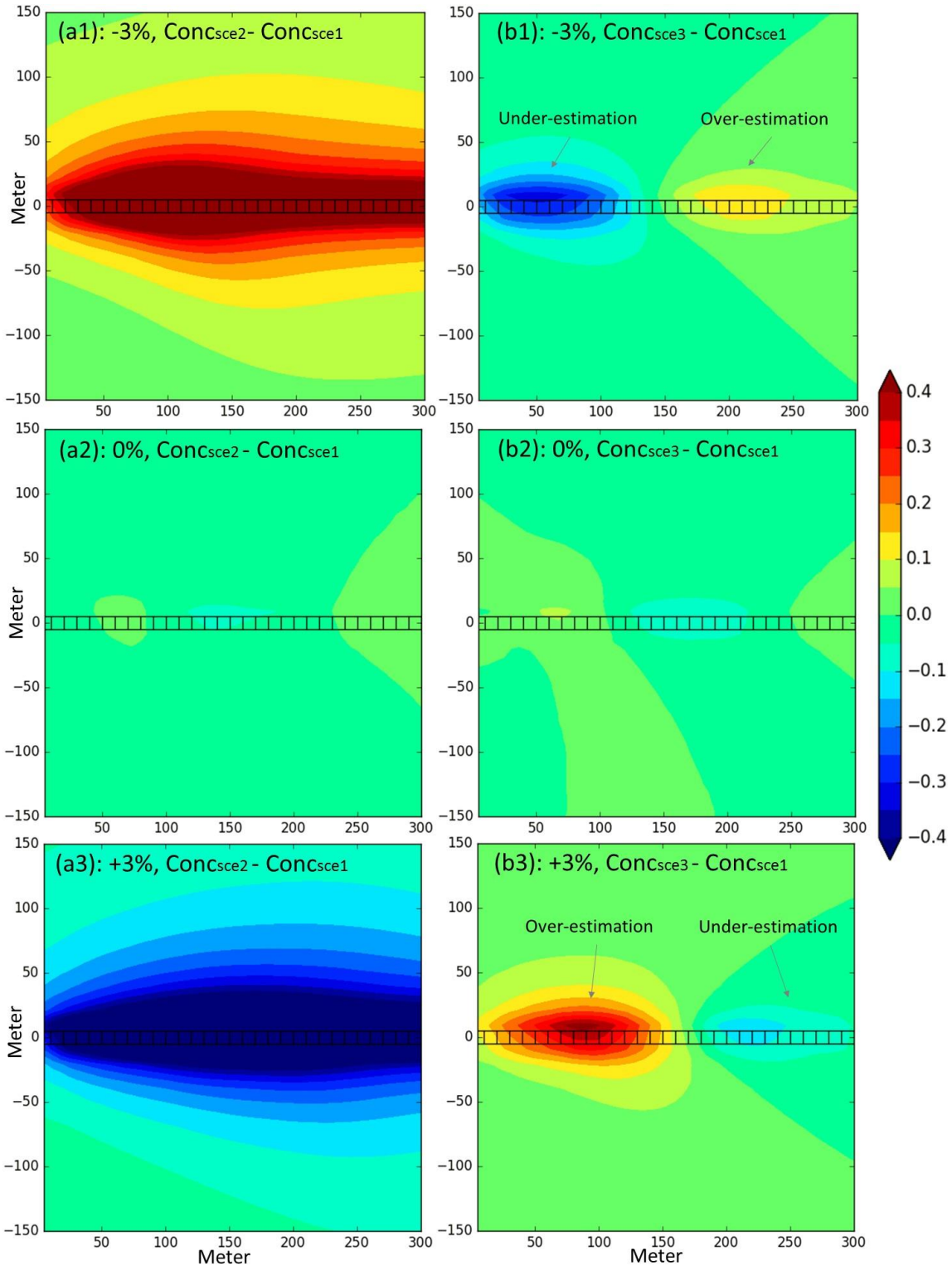

Figure 93 – Bus: Concentration Differences (0.4 ug/m^3) Compared to Scenario 1

8.4 Summary

This chapter explored the impact of road grade on energy consumption and emissions modeling of accelerations at arterials. Based on a near-road air quality modeling of a novel acceleration segment, the most interesting finding in this chapter is the grade impact, especially grade-operation correlation impact on the spatial distribution of $PM_{2.5}$ emission, and near-road concentration profile contributed from transit buses. Transit buses accelerate more gently and require more time and distance to reach target speeds on segments with more uphill grade. On downhill segments, the results show that ignoring grade-operation correlation would incorrectly add more "gentle" accelerations in modeling, and hence cause under-estimation of near-road concentration in the first half stage of acceleration period, and add more "aggressive" accelerations in the second half stage of acceleration period, hence cause over-estimation of concentration. It is the other way around for downhill segment.

The integration of grade was shown to be important for air quality modeling; however, grade is not currently considered in the EPA Transportation Conformity and PM hot-spot analysis guideline (USEPA, 2015). This work shows the importance of not only including road grade in analysis, but also the necessity of research on the link segmentation strategy, with grade and grade-operation correlation involved in project-level hot-spot analysis at intersections.

CHAPTER 9. CONCLUSION AND FUTURE RESEARCH

Chapter 9 summarizes conclusions and contributions of research presented in this dissertation, including road grade generation based on USGS DEM, implication of grade impact on vehicle operations, and impact of grade-operation interactions on energy consumption and emissions modeling. Some limitations of the dissertation research are listed and future research needs are suggested.

9.1 Conclusion of Road Grade Generation

A streamlined procedure was proposed to pair monitored second-by-second GPS data with second-by-second grade data (deriving road grade and appending these data to vehicle trajectories). The study developed a strategy for generating high-accuracy roadway grade based on USGS DEM database that is publicly available and covers most of the nation in the United States. The strategy included elevation extraction, erroneous elevation cleaning and infill, and applying a cubic smoothing spline. The data cleaning and infill strategy can effectively interpolate elevation, and predict road grade where erroneous elevation data were provided by the DEM (e.g., in river/bridge, and highway/overpass intersections). This is because roads are generally flat, and sharp elevation fluctuations associated with bridges are relatively easy to detect. The cubic smoothing spline was successfully applied in this study to minimize the impact of noisy data, and to improve grade estimation accuracy. One of the most important findings in applying cubic smoothing spline method, is that the key parameter λ needs to be selected carefully to tradeoff least squares error (goodness of fit) with smoothness. It is recommended that λ be selected by segment, based on the elevation fluctuation of the

road, which is represented by the absolute rate of grade change $\overline{|S''(x)|}$ in Chapter 3. The result demonstrated the USGS DEM is a valuable resource, and the elevation data from USGS DEM along the road are sufficiently accurate for generating road grade. While the higher resolution DEM data are recommended when available, the verification results indicate good accuracy at all three resolutions (1×1 meter, 3×3 meter, and 10×10 meters). Although the study focused on the application of USGS DEM, for grade generation purpose, it is reasonable to infer that the proposed strategy can be applied with other source of LiDAR data or survey data that include position and elevation information. The study also developed a procedure to append derived grade data on vehicle GPS trajectories. By extracting the trip route based on GPS coverage, it eliminated interfere from adjacent roads.

9.2 Implications of Modeling Grade Impact on Operations

The research shows a significant grade impact on vehicle speed and accelerations under uncongested conditions (average speed > 55 mph): vehicles tend to operate more gently as grade increases, with lower speed and lower acceleration identified in Bayesian Hierarchical Model. While the population level effect of the model shows such trends, it is important to note from the distribution of vehicle-level parameters that significant heterogeneity of road grade impact exists across vehicles. The "shape" of SAJD is also impacted by grade. By exploring impact of grade on extreme accelerations/deceleration, width of SAJD, and skewness of acceleration distribution by speed bins, the SAJD of light-duty vehicles shifts from higher accelerations to lower accelerations as grade increases, with the width between extremes remaining relatively fixed. For express buses, the extreme acceleration curve significantly decreases (twice as fast as for light-duty

vehicles), while the curve for extreme deceleration does not change significantly. Hence, the SAJD "envelope" for express buses narrows as grade increases. Such impacts were not observed under congested conditions, where traffic flow likely constrains and dominates vehicle operations.

From the analysis of grade impact on accelerations at arterials, grade significantly affects vehicle target speeds on uphill segments, but not for downgrades. On uphill grades, target speed dropped by average of 1.5 mph for 1% of grade increase for all vehicle types.

Also, for a target speed, grade does not significantly impact speed/acceleration characteristics of light-duty vehicles for most of the speed pieces of low target speeds (20 mph, 25 mph, and 30 mph). This is probably because the traces are extracted under heavy traffic conditions, where car following and queueing are the main constrain to vehicle acceleration activity. For accelerations of light-duty vehicles with target speed of 35 mph or higher speed, where traces are likely extracted from uncongested condition and fewer interruptions from traffic are expected, grade impact on accelerations become obvious, with vehicles accelerating more gently in upgrades. Results also show that accelerations of transit buses are significantly affected by grade, regardless of traffic condition. The average accelerations drop by 50% or more from -4% downgrade to +4% upgrade.

9.3 Implications for Energy Consumption and Emissions Modeling

Given the observed relationships between road grade and on-road vehicle operations, the study evaluated the impact of ignoring grade, accounting for grade but ignoring the correlation between grade and SAJD, and accounting for both grade and

observed SAJD interaction on energy consumption, emissions, and near-road air quality modeling on freeways. Significant bias in prediction of energy use and emissions estimation is observed if grade is ignored, with increasing bias for segments with more extreme uphill and downhill grades. Under uncongested conditions, applying road grade but ignoring the correlation between grade and on-road operating conditions under-estimates energy use and emissions on downhill freeway segments, and over-estimates energy use and emissions on uphill freeway segments of freeways (but the bias is much less than results from completely ignoring road grade).

The emissions impacts are also reflected in microscale pollutant dispersion model results, based on I-85 corridor case study on near-road $PM_{2.5}$ dispersion modeling. Results show that the bias caused by ignoring road grade is non-negligible. In contrast, the bias caused by applying actual grade, but ignoring grade-SAJD correlation is much less significant. Comparing the dispersion results with the NAAQS limit (12 $\mu g/m^3$), the study confirms transportation conformity and $PM_{2.5}$ hotspot analysis should probably include road grade. However, ignoring grade-SAJD correlation did not appear to result in significant bias in near-road air quality modeling that would require serious attention, unless the predicted concentrations are close to NAAQS limit, where 10% bias might matter in predicting area NAAQS violation. However, such "close to the limit" scenarios may not be rare in locations where heavy-duty truck operations are significant. As noted earlier, given that these conclusions were reached through the analysis of heavy-duty bus activity, additional research on grade and on-road operation interactions is needed for heavy-duty trucks.

For accelerations at arterials, it is interesting to find that at upgrades segments, since transit buses accelerate more gently and requires more time and distance to reach target speed, ignoring grade-operation correlation incorrectly adds more "aggressive" accelerations in modeling, and hence over-estimates near-road concentrations in the first half stage of acceleration period. While more "gentle" accelerations in the second stage of acceleration period, causes an under-estimation of concentration. The bias goes towards opposite direction on downgrades. This finding shows the importance of not only including road grade but also the necessity of the exploration of link segmentation strategy for project-level hot-spot analysis for intersections.

9.4 Limitations and Future Research

In road grade generation method, future research may continue to explore the strategy λ selection, by collecting more road grade data with different terrain characteristics, and seeking to identify other factors that may affect λ selection. It may also be feasible to classify road segment by the vertical curve, and provide recommended λ ranges by road class and fluctuation range. In addition, this study used a 1-dimensional smoothing spline method. Road pavement can be intuitively treated as a surface, so 2-dimensional spline method might be worth trying to see if there is a potential to further improve grade accuracy. In addition to the smoothing spline, other smoothing method like OLS regression, kernel smoothing, or Kalman filtering could also be explored to improve accuracy and calculation efficiency.

This study employed data for heavy-duty bus operations, but did analyze any data for heavy-duty trucks. Freeway speed-choice relationships for heavy-duty diesel trucks in

the Highway Capacity Manual (HCM) depend significantly on grade (TRB, 2010). Grade impacts on truck operations are also expected to vary with payload. Automatic emergency braking systems employed by many trucks may also affect downhill truck operations (on long downgrades, heavy-duty trucks often have to reduce their speeds to avoid brake overheating). The trucks fleet is a large contributor to NOx and $PM_{2.5}$ emissions, heavy-duty truck speed-acceleration activity on grade is likely to be interactive with grade (even more so than was noted for express buses), and the operations of trucks on grade likely affects the operations of the surrounding vehicle fleet. Hence, new studies to assess the impact of grade on truck operations, and new strategies to integrating grade and grade-operation correlations in truck emissions modeling, are critical.

With respect to the data support for freeway studies, GPS data used in this dissertation mainly describe operations under uncongested conditions (average speed >55 mph). While a clear grade impact was observed for uncongested conditions in Chapter 5, it was not observed under congested conditions. Under congested conditions, traffic flow and car following may become the dominant factors that determine vehicle operations, overwhelming any potential impacts of grade. However, considering the complex and non-stationary operations under congested conditions, a larger sample size describing operations is definitely required to reach a more robust conclusion.

In terms of arterial studies, the dissertation only focused on acceleration traces starting from idle. Future research is also suggested to explore grade impact on operations and emissions modeling in cruising and deceleration modes. Signalized intersections are often chosen as sites for project-level hot-spot analysis, because of frequent stop-and-go,

as well as long idling activities involved in. To explore impact of considering grade, and grade-operation correlation on hot-spot analysis at intersections, the spatial distribution of $PM_{2.5}$ emissions modeling are suggested at the intersection level. An example of collected trajectories from light-duty vehicle and transit buses for a signalized intersection is shown in Figure 94. The locations of adjacent signal, as well as transit bus stops are also labeled. From the trajectories, we learned that in this intersection, most of vehicles were stopped by traffic signal, while some vehicles passing through the intersection with slight deceleration (rather than completely stop).

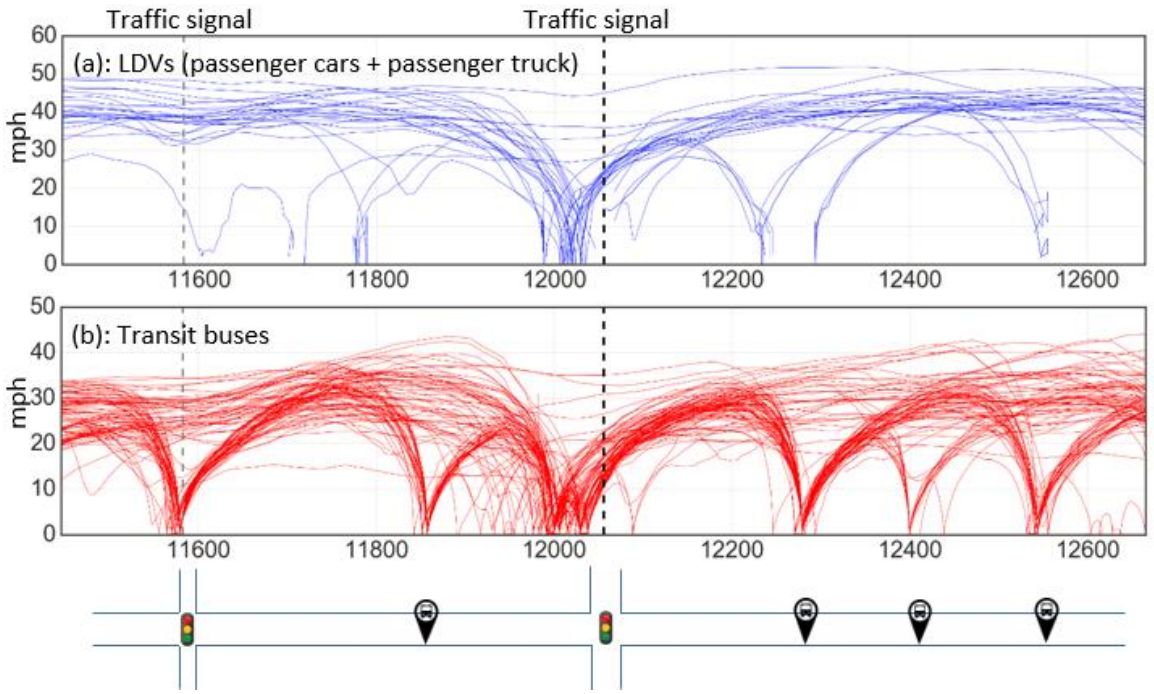

Figure 94 – Trajectories of LDVs and Buses Near Intersection

The time duration, and $PM_{2.5}$ emission contributions (with actual and zero grade) by operating mode along the segment are shown in Figure 95 (for light-duty vehicles) and Figure 96 (for transit buses), with grade profile also aligned. The large differences in emissions at the beginning of the segment with and without grade highlights the

importance of integrating grade not only at acceleration mode, but also in the cruising mode. Also, the figures show a large proportion of $PM_{2.5}$ emissions attributed by idling and acceleration modes near the intersection. In Chapter 7, we have explored that transit buses need more time and distance to accelerate at upgrades. This has potential to influence the emission distributions in the intersection, and can be assessed by examining the differences of emissions distributions with or without grade. A comprehensive research on the impact of grade integration on link source segmentation at intersection for hot-spot analysis appears to be important in further improving transportation conformity analysis.

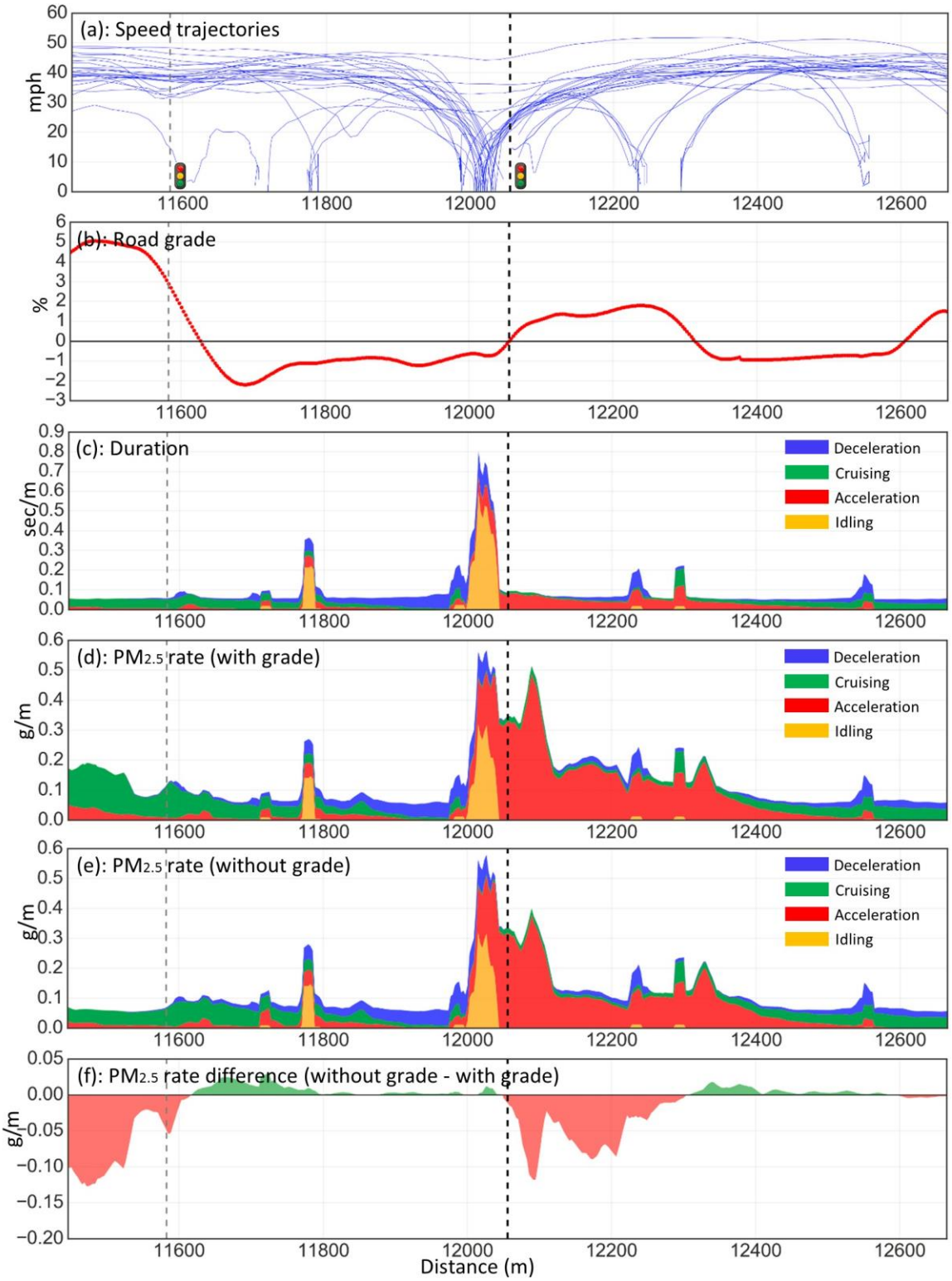

Figure 95 – LDV Trajectories, Grade, Duration, and PM2.5 Rates Near Intersection

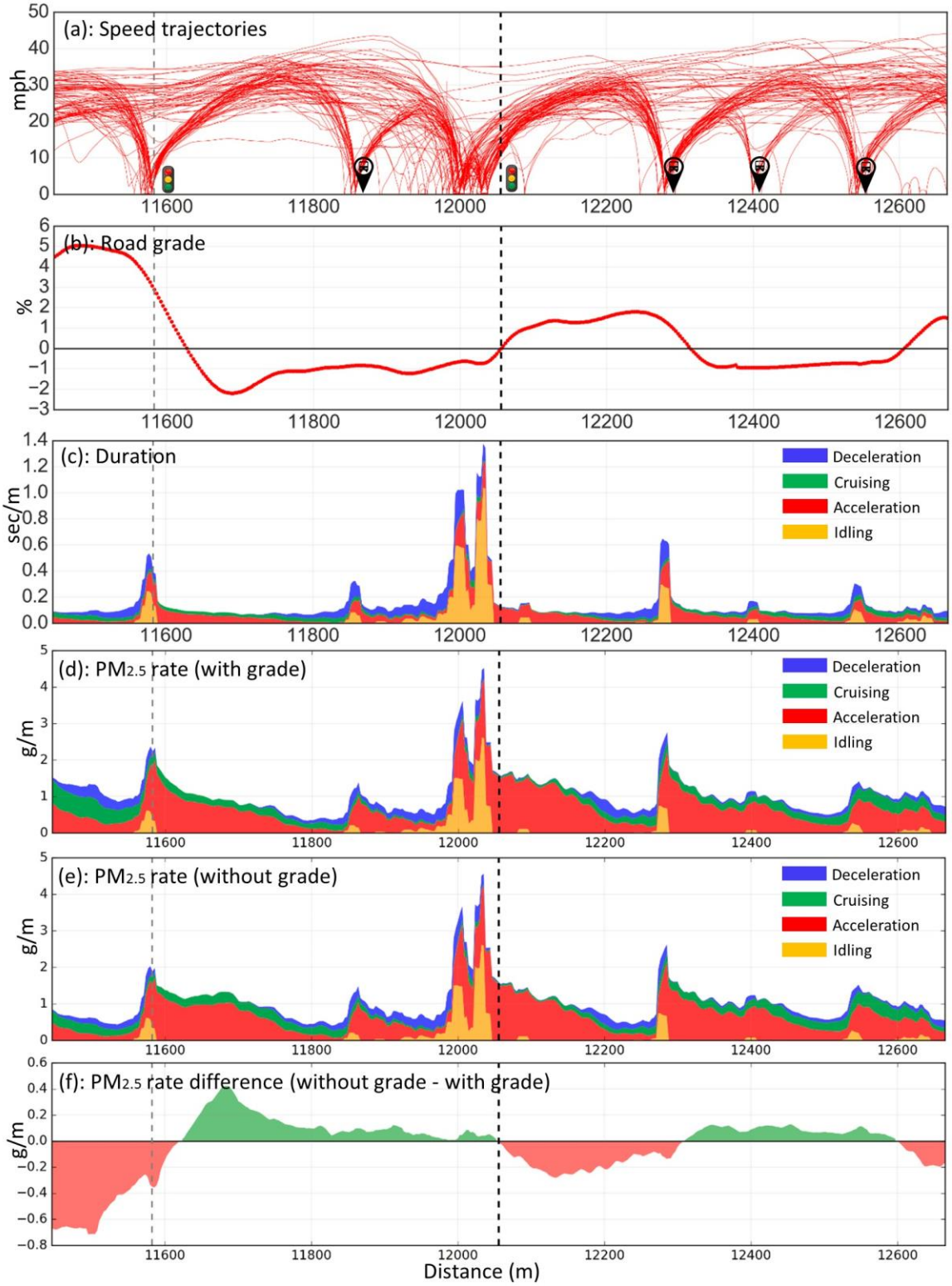

Figure 96 – Bus Trajectories, Grade, Duration, and PM2.5 Rates near Intersection

Car following and vehicle interaction data were not available for this research. Future research is also suggested to differentiate grade impact on operations of leading vehicles and queueing vehicles across different vehicle types for both freeway and non-freeway studies. Such research is especially useful for integrating grade in car following modeling methods to improve microscopic simulation models.

Data used in this study were collected in 2013 or earlier. With the alternative fuel and technology applied in vehicles in recent five years, the use hybrid and electric vehicles in private vehicle fleet is becoming more and more popular. Similarly, CNG, plug-in hybrid and pure electric buses are being put into transit service for environmental consideration. A number of national-level and state-level consumer incentives for purchasing or leasing alternative fuel vehicles have been implemented to address the market barriers, and to help consumers overcome the incremental initial purchase costs of low-carbon vehicles compared to conventional gasoline or diesel equivalents. The market share and population of alternative fuel fleet is expected to continuously grow, and the importance exploring grade impact on alternative fuel fleet will continue to increase.

Emission rates from MOVES were used for analysis in the dissertation. The reason that MOVES rates were used is because MOVES is the regulatory model required for transportation conformity analysis. However, for research purposes, it should be noted that MOVES employs a binning approach to emissions modeling, and classifies 23 bins with each assigned with energy rate and emission rate. For transient mode such as accelerations, MOVES may not appropriately represent engine load: it is possible that vehicle engines reache higher work load conditions that exceed the highest VSP bin category captured by MOVES. Also, engine combustion process, including the

corresponded energy consumption and emission production should be short-term auto-correlated process with respect to time, while MOVES does not count for the auto-correlation in emissions modeling. It may be reasonable to develop or use models that can better estimate vehicle power during hard acceleration processes, as applicable real-world measurements from Portable Emissions Measurement System (PEMS) become available.

9.5 Contributions

The dissertation has proposed a straightforward strategy for generating high-accuracy roadway grade based on USGS DEM, and appending grade data to vehicle operations data. Due to the wide coverage in the United States and convenient access of DEM data (and zero cost), the method can be easily implemented for researchers and engineers in most of other regions across the country. With real-world vehicle operation data available from GPS devices, OBD devices, and smartphones, the proposed grade generation and appending method makes it feasible to integrate large-scale grade information to support energy consumption and emissions modeling, driver behavior research, safety analysis, and other transportation analyses as needed.

The statistical modeling and empirical analysis of grade impact on freeway operations and arterial accelerations can enhance the accuracy of energy and emission modeling. Through comparative analysis of energy consumption and emissions modeling results with and without grade, or with or without considering grade-operation correlations, the study draws researchers' and agencies' attention to the importance of integrating grade and grade-operation correlation into energy consumption analysis,

emissions analysis, and near-road air quality modeling. Results of this study also demonstrates potential improvements that could be made driving behavior modules in microscopic simulation models, speed choices modules for freeways, target speed choice modules, and acceleration behavior module for arterials in response to road grades.

The findings of grade and grade-operation correlation impact on AERMOD-based near-road air quality modeling indicated policy implications as the study has potential to improve transportation conformity and hot-spot analysis, given that the current guideline of PM transportation conformity released by the USEPA does not include the consideration of grade in hot-spot analysis. This study could lead to enhanced agency guidance on improved emissions and near-road air quality modeling.

APPENDIX A.CONDITIONAL DISTRIBUTION OF $\boldsymbol{\gamma_{i,j}}$

The joint probability density of observed data $y_{i,j,1}, y_{i,j,2}, \dots, y_{i,j,n_{ij}}$conditional on $\boldsymbol{u_{i,j}}$, $\boldsymbol{x_{i,j}}$, $\boldsymbol{z_{i,j}}$, $\boldsymbol{\xi}$, $\boldsymbol{\beta_i}$, $\boldsymbol{\gamma_{i,j}}$ and σ^2:

$$
\begin{aligned}
P\left(y_{i,j,1}, y_{i,j,2}, \dots, y_{i,j,n_{ij}} \middle| \boldsymbol{u_{i,j,k}}, \boldsymbol{x_{i,j,k}}, \boldsymbol{z_{i,j,k}}, \boldsymbol{\psi}\right) & \\
= \prod_{\boldsymbol{k=1}}^{\boldsymbol{n_{ij}}} P\left(\boldsymbol{y_{i,j,k}} \middle| \boldsymbol{u_{i,j,k}}, \boldsymbol{x_{i,j,k}}, \boldsymbol{z_{i,j,k}}, \sigma^2, \boldsymbol{\gamma_{i,j}}, \boldsymbol{\beta_i}, \boldsymbol{\xi}\right) & \\
= (2\pi)^{-\frac{\boldsymbol{n_{ij}}}{\boldsymbol{2}}} \left|\sigma^{\boldsymbol{2}}_{\boldsymbol{v_{i,j}}} C_\rho\right|^{-\frac{\boldsymbol{1}}{\boldsymbol{2}}} \exp\{-\frac{1}{2}\left(\boldsymbol{y_{i,j}} - \boldsymbol{u_{i,j}}\boldsymbol{\xi} - \boldsymbol{x_{i,j}}\boldsymbol{\beta_i}\right. & \\
\left. - \boldsymbol{z_{i,j}}\boldsymbol{\gamma_{i,j}}\right)^T \left(\sigma^{\boldsymbol{2}}_{\boldsymbol{v_{i,j}}} C_\rho\right)^{-1}\left(\boldsymbol{y_{i,j}} - \boldsymbol{u_{i,j}}\boldsymbol{\xi} - \boldsymbol{x_{i,j}}\boldsymbol{\beta_i}\right. & \\
\left. - \boldsymbol{z_{i,j}}\boldsymbol{\gamma_{i,j}}\right)\Big\} &
\end{aligned}
\tag{65}
$$

If the prior distribution of $\boldsymbol{\gamma_{i,j}} \sim MVN(\boldsymbol{\varphi_i}, \boldsymbol{\Sigma_i})$, it suggests that a multivariate normal prior distribution for $\boldsymbol{\gamma_{i,j}}$ is conjugate:

$$
\begin{aligned}
&P\left(\boldsymbol{\gamma_{i,j}}\middle|\boldsymbol{y_{i,j}}, \boldsymbol{u_{i,j}}, \boldsymbol{x_{i,j}}, \boldsymbol{z_{i,j}}, \boldsymbol{\psi}\right) \\
&\qquad \propto P\left(\boldsymbol{y_{i,j}}\middle|\boldsymbol{u_{i,j,k}}, \boldsymbol{x_{i,j,k}}, \boldsymbol{z_{i,j,k}}, \sigma^2_{v_{i,j}}, \rho, \boldsymbol{\gamma_{i,j}}, \boldsymbol{\beta_i}, \boldsymbol{\xi}\right) \boldsymbol{P}(\boldsymbol{\gamma_{i,j}}|\boldsymbol{\varphi_i}, \boldsymbol{\Sigma_i}) \\
&\qquad \propto \exp\{-\frac{1}{2}\left(\boldsymbol{y_{i,j}} - \boldsymbol{u_{i,j}}\boldsymbol{\xi} - \boldsymbol{x_{i,j}}\boldsymbol{\beta_i} - \boldsymbol{z_{i,j}}\boldsymbol{\gamma_{i,j}}\right)^T (\sigma^2_{v_{i,j}} C_\rho)^{-1}\left(\boldsymbol{y_{i,j}}\right. \\
&\qquad \left. - \boldsymbol{u_{i,j}}\boldsymbol{\xi} - \boldsymbol{x_{i,j}}\boldsymbol{\beta_i}\right. \\
&\qquad \left. - \boldsymbol{z_{i,j}}\boldsymbol{\gamma_{i,j}}\right)\} \exp\left\{-\frac{1}{2}\left(\boldsymbol{\gamma_{i,j}} - \boldsymbol{\varphi_i}\right)^T \boldsymbol{\Sigma_i}^{-1}\left(\boldsymbol{\gamma_{i,j}} - \boldsymbol{\varphi_i}\right)\right\} \\
&\qquad \propto \exp\left\{-\frac{1}{2\sigma^2_{v_{i,j}}}\left(-2\boldsymbol{y_{i,j}}^T C_\rho^{-1} \boldsymbol{z_{i,j}}\boldsymbol{\gamma_{i,j}} + 2\boldsymbol{\beta_i}^T \boldsymbol{x_{i,j}}^T C_\rho^{-1} \boldsymbol{z_{i,j}}\boldsymbol{\gamma_{i,j}}\right.\right. \\
&\qquad + \boldsymbol{\gamma_{i,j}}^T \boldsymbol{z_{i,j}}^T C_\rho^{-1} \boldsymbol{z_{i,j}}\boldsymbol{\gamma_{i,j}} + 2\boldsymbol{\gamma_{i,j}}^T \boldsymbol{z_{i,j}}^T C_\rho^{-1} \boldsymbol{u_{i,j}}\boldsymbol{\xi}\Big) \\
&\qquad \left.\left. - \frac{1}{2}\left(\boldsymbol{\gamma_{i,j}}^T \boldsymbol{\Sigma_i}^{-1}\boldsymbol{\gamma_{i,j}} - 2\boldsymbol{\gamma_{i,j}}^T \boldsymbol{\Sigma_i}^{-1}\boldsymbol{\varphi_i}\right)\right\} \\
&\qquad = \exp\left\{\boldsymbol{\gamma_{i,j}}^T \left(\boldsymbol{\Sigma_i}^{-1}\boldsymbol{\varphi_i} - \boldsymbol{z_{i,j}}^T C_\rho^{-1} \boldsymbol{u_{i,j}}\boldsymbol{\xi}/\sigma^2_{v_{i,j}}\right.\right. \\
&\qquad - \boldsymbol{z_{i,j}}^T C_\rho^{-1} \boldsymbol{x_{i,j}}\boldsymbol{\beta_i}/\sigma^2_{v_{i,j}} + \boldsymbol{z_{i,j}}^T C_\rho^{-1} \boldsymbol{y_{i,j}}/\sigma^2_{v_{i,j}}\Big) \\
&\qquad \left.\left. - \frac{1}{2}\boldsymbol{\gamma_{i,j}}^T \left(\boldsymbol{\Sigma_i}^{-1} + \boldsymbol{z_{i,j}}^T C_\rho^{-1} \boldsymbol{z_{i,j}}/\sigma^2_{v_{i,j}}\right)^{-1} \boldsymbol{\gamma_{i,j}}\right\}
\end{aligned}
\tag{66}
$$

This is proportional to a multivariate normal density, so the full conditional distribution $\boldsymbol{[\gamma_{i,j}|y_{i,j}, u_{i,j}, x_{i,j}, z_{i,j}, \psi]}$ is a multivariate normal distribution with:

$$
Var(\boldsymbol{\gamma_{i,j}}|\boldsymbol{y_{i,j}}, \boldsymbol{u_{i,j}}, \boldsymbol{x_{i,j}}, \boldsymbol{z_{i,j}}, \boldsymbol{\psi}) = (\boldsymbol{\Sigma_i}^{-1} + \boldsymbol{z_{i,j}}^T C_\rho^{-1} \boldsymbol{z_{i,j}}/\sigma^2_{v_{i,j}})^{-1} \tag{67}
$$

$$
\begin{aligned}
&E\left(\boldsymbol{\gamma_{i,j}}\middle|\boldsymbol{y_{i,j}}, \boldsymbol{u_{i,j}}, \boldsymbol{x_{i,j}}, \boldsymbol{z_{i,j}}, \boldsymbol{\psi}\right) \\
&\qquad = \left(\boldsymbol{\Sigma_i}^{-1} + \boldsymbol{z_{i,j}}^T C_\rho^{-1} \boldsymbol{z_{i,j}}/\sigma^2_{v_{i,j}}\right)^{-1} \left(\boldsymbol{\Sigma_i}^{-1}\boldsymbol{\varphi_i}\right. \\
&\qquad - \boldsymbol{z_{i,j}}^T C_\rho^{-1} \boldsymbol{u_{i,j}}\boldsymbol{\xi}/\sigma^2_{v_{i,j}} - \boldsymbol{z_{i,j}}^T C_\rho^{-1} \boldsymbol{x_{i,j}}\boldsymbol{\beta_i}/\sigma^2_{v_{i,j}} \\
&\qquad \left. + \boldsymbol{z_{i,j}}^T C_\rho^{-1} \boldsymbol{y_{i,j}}/\sigma^2_{v_{i,j}}\right)
\end{aligned}
\tag{68}
$$

APPENDIX B. CONDITIONAL DISTRIBUTION OF $\boldsymbol{\varphi_i}$ AND $\boldsymbol{\Sigma_i}$

The joint probability density of trace level parameters $\boldsymbol{\gamma_{i,1}, \dots, \gamma_{i,n_i}}$ conditional upon $\boldsymbol{\varphi_i}$ and $\boldsymbol{\Sigma_i}$:

$$
\begin{aligned}
P\left(\boldsymbol{\gamma_{i,1}, \gamma_{i,2}, \dots, \gamma_{i,n_i}} \middle| \boldsymbol{\varphi_i, \Sigma_i}\right) &= \prod_{\boldsymbol{j=1}}^{\boldsymbol{n_i}} P\left(\boldsymbol{\gamma_{i,j}} \middle| \boldsymbol{\varphi_i, \Sigma_i}\right) \\
&= \prod_{\boldsymbol{j=1}}^{\boldsymbol{n_i}} (2\pi)^{-\frac{\boldsymbol{p}}{\boldsymbol{2}}} |\boldsymbol{\Sigma_i}|^{-\frac{\boldsymbol{1}}{\boldsymbol{2}}} \exp\left\{-\frac{1}{2}\left(\boldsymbol{\gamma_{i,j}} - \boldsymbol{\varphi_i}\right)^T \boldsymbol{\Sigma_i}^{-1}\left(\boldsymbol{\gamma_{i,j}} - \boldsymbol{\varphi_i}\right)\right\} \\
&= (2\pi)^{-\frac{\boldsymbol{n_i p}}{\boldsymbol{2}}} |\boldsymbol{\Sigma_i}|^{-\frac{\boldsymbol{n_i}}{\boldsymbol{2}}} \exp\left\{-\frac{1}{2}\sum_{j=1}^{\boldsymbol{n_i}}\left(\boldsymbol{\gamma_{i,j}} - \boldsymbol{\varphi_i}\right)^T \boldsymbol{\Sigma_i}^{-1}\left(\boldsymbol{\gamma_{i,j}} - \boldsymbol{\varphi_i}\right)\right\} \\
&\propto \exp\left\{-\frac{\boldsymbol{n_i}}{2}\boldsymbol{\varphi_i}^T \boldsymbol{\Sigma_i}^{-1}\boldsymbol{\varphi_i} + \boldsymbol{n_i}\boldsymbol{\varphi_i}^T \boldsymbol{\Sigma_i}^{-1}\boldsymbol{\bar{\gamma}_\iota}\right\}
\end{aligned}
\tag{69}
$$

The posterior distribution is:

$$
\begin{aligned}
\mathrm{P}\left(\boldsymbol{\varphi_i} \middle| \boldsymbol{\gamma_{i,1}, \gamma_{i,2}, \dots, \gamma_{i,n_i}, \Sigma_i}\right) &\propto \exp\left\{-\frac{\boldsymbol{n_i}}{2}\boldsymbol{\varphi_i}^T \boldsymbol{\Sigma_i}^{-1}\boldsymbol{\varphi_i} + \boldsymbol{n_i}\boldsymbol{\varphi_i}^T \boldsymbol{\Sigma_i}^{-1}\boldsymbol{\bar{\gamma}_\iota}\right\} \\
&\times \exp\left\{-\frac{1}{2}\boldsymbol{\varphi_i}^T \boldsymbol{\Sigma_{i,0}}^{-1}\boldsymbol{\varphi_i} + \boldsymbol{\varphi_i}^T \boldsymbol{\Sigma_{i,0}}^{-1}\boldsymbol{\varphi_{i,0}}\right\} \\
&= \exp\left\{-\frac{1}{2}\boldsymbol{\varphi_i}^T\left(\boldsymbol{\Sigma_{i,0}}^{-1} + \boldsymbol{n_i}\boldsymbol{\Sigma_i}^{-1}\right)\boldsymbol{\varphi_i}\right. \\
&\left. + \boldsymbol{\varphi_i}^T\left(\boldsymbol{\Sigma_{i,0}}^{-1}\boldsymbol{\varphi_{i,0}} + \boldsymbol{n_i}\boldsymbol{\Sigma_i}^{-1}\boldsymbol{\bar{\gamma}_\iota}\right)\right\}
\end{aligned}
\tag{70}
$$

This is proportional to a multivariate normal density, so the full conditional distribution $\boldsymbol{[\varphi_i | \gamma_{i,1}, \gamma_{i,2}, \dots, \gamma_{i,n_i}, \Sigma_i]}$ is a multivariate normal distribution with:

$$Var(\boldsymbol{\varphi_i}|\boldsymbol{\gamma_{i,1}}, \boldsymbol{\gamma_{i,2}}, \dots, \boldsymbol{\gamma_{i,n_i}}, \boldsymbol{\Sigma_i}) = (\boldsymbol{\Sigma_{i,0}}^{-1} + \boldsymbol{n_i}\boldsymbol{\Sigma_i}^{-1})^{-1} \tag{71}$$

$$\begin{aligned} E\big(\boldsymbol{\varphi_i}\big|\boldsymbol{\gamma_{i,1}}, \boldsymbol{\gamma_{i,2}}, \dots, \boldsymbol{\gamma_{i,n_i}}, \boldsymbol{\Sigma_i}\big) \\ = \big(\boldsymbol{\Sigma_{i,0}}^{-1} + \boldsymbol{n_i}\boldsymbol{\Sigma_i}^{-1}\big)^{-1}\big(\boldsymbol{\Sigma_{i,0}}^{-1}\boldsymbol{\varphi_{i,0}} \\ + \boldsymbol{n_i}\boldsymbol{\Sigma_i}^{-1}\bar{\boldsymbol{\gamma}}_{\boldsymbol{i}}\big) \end{aligned} \tag{72}$$

Where n_i is number of traces collected from vehicle i, $\bar{\boldsymbol{\gamma}}_{\boldsymbol{i}}$ is the vector average $\frac{1}{\boldsymbol{n_i}}\sum_j \boldsymbol{\gamma_{i,j}}$. $\boldsymbol{\varphi_{i,0}}$ and $\boldsymbol{\Sigma_{i,0}}$ are prior mean and variance-covariance matrix of $\boldsymbol{\varphi_i}$. It is important to notice that a convenient prior distribution for the variance-covariance matrix $\boldsymbol{\Sigma_i}$ is an inverse-Wishart distribution. A convenient prior distribution for the variance-covariance matrix $\boldsymbol{\Sigma_i}$ is an inverse-Wishart distribution, which were parameterized as:

$$\boldsymbol{\Sigma_i} \sim \text{inverse} - \text{Wishart}(\eta_{i,0}, \mathrm{S}_{i,0}{}^{-1})$$

The inverse-Wishart density $(\eta_{i,0}, \mathrm{S}_{i,0}{}^{-1})$ is given by:

$$\begin{aligned} P(\boldsymbol{\Sigma_i}) = \left[2^{\eta_{i,0}/2}\pi^{\binom{p}{2}/2}\left|\mathbf{S_{i,0}}\right|^{-\eta_{i,0}/2}\prod_{\boldsymbol{j=1}}^{\boldsymbol{p}}\Gamma([\eta_{i,0}+1-j]/2)\right]^{-\mathbf{1}} \\ \times |\boldsymbol{\Sigma_i}|^{(\eta_{i,0}+p+1)/2} \times \exp\{-tr(\mathbf{S_{i,0}}\boldsymbol{\Sigma_i}^{-\mathbf{1}})/2\} \end{aligned} \tag{73}$$

The joint probability density of trace level sampling distribution for $\boldsymbol{\gamma_{i,1}}, \boldsymbol{\gamma_{i,2}}, \dots, \boldsymbol{\gamma_{i,n_i}}$conditional upon $\boldsymbol{\varphi_i}$ and $\boldsymbol{\Sigma_i}$:

$$\begin{aligned} &P\big(\boldsymbol{\gamma_{i,1}}, \boldsymbol{\gamma_{i,2}}, \dots, \boldsymbol{\gamma_{i,n_i}}\big|\boldsymbol{\varphi_i}, \boldsymbol{\Sigma_i}\big) = \\ &(2\pi)^{-\frac{\boldsymbol{n_i p}}{2}}|\boldsymbol{\Sigma_i}|^{-\frac{\boldsymbol{n_i}}{2}}\exp\Big\{-\tfrac{1}{2}\textstyle\sum_{j=1}^{\boldsymbol{n_i}}\big(\boldsymbol{\gamma_{i,j}}-\boldsymbol{\varphi_i}\big)^T\boldsymbol{\Sigma_i}^{-1}\big(\boldsymbol{\gamma_{i,j}}- \\ &\boldsymbol{\varphi_i}\big)\Big\} \propto |\boldsymbol{\Sigma_i}|^{-\frac{\boldsymbol{n_i}}{2}}\exp\Big\{-\tfrac{1}{2}tr\Big[\textstyle\sum_{j=1}^{\boldsymbol{n_i}}\big(\boldsymbol{\gamma_{i,j}}-\boldsymbol{\varphi_i}\big)\big(\boldsymbol{\gamma_{i,j}}- \\ &\boldsymbol{\varphi_i}\big)^T\boldsymbol{\Sigma_i}^{-1}\Big]\Big\} \end{aligned} \tag{74}$$

By combining the prior distribution with the sampling distribution for $\boldsymbol{\gamma_{i,1}, \gamma_{i,2}, \dots, \gamma_{i,n_i}}$, the posterior distribution is:

$$\begin{aligned} \mathrm{P}\left(\boldsymbol{\Sigma_i} \middle| \boldsymbol{\gamma_{i,1}, \gamma_{i,2}, \dots, \gamma_{i,n_i}, \varphi_i}\right) &= P\left(\boldsymbol{\gamma_{i,1}, \gamma_{i,2}, \dots, \gamma_{i,n_i}} \middle| \boldsymbol{\varphi_i, \Sigma_i}\right) P(\boldsymbol{\Sigma_i}) \\ &\propto |\boldsymbol{\Sigma_i}|^{-\frac{\boldsymbol{n_i}}{2}} \exp\left\{-\frac{1}{2} tr\left[\sum_{j=1}^{\boldsymbol{n_i}} \left(\boldsymbol{\gamma_{i,j}}\right.\right.\right. \\ &\quad \left.\left.\left. - \boldsymbol{\varphi_i}\right)\left(\boldsymbol{\gamma_{i,j}} - \boldsymbol{\varphi_i}\right)^T \boldsymbol{\Sigma_i}^{-1}\right]\right\} \\ &\quad \times |\boldsymbol{\Sigma_i}|^{(\eta_{i,0}+p+1)/2} \exp\left\{-tr\left(\mathbf{S_{i,0}} \boldsymbol{\Sigma_i}^{-1}\right)/2\right\} \\ &= |\boldsymbol{\Sigma_i}|^{(\eta_{i,0}+n_i+p+1)/2} \\ \exp\left\{-tr\left(\left[\mathbf{S_{i,0}} + \sum_{j=1}^{\boldsymbol{n_i}} \left(\boldsymbol{\gamma_{i,j}} - \boldsymbol{\varphi_i}\right)\left(\boldsymbol{\gamma_{i,j}} - \boldsymbol{\varphi_i}\right)^T\right] \boldsymbol{\Sigma_i}^{-1}\right)\Big/ 2\right\} & \end{aligned} \tag{75}$$

Thus we get the posterior distribution:

$$\left[\boldsymbol{\Sigma_i} \middle| \boldsymbol{\gamma_{i,1}, \gamma_{i,2}, \dots, \gamma_{i,n_i}, \varphi_i}\right] \sim \text{inverse} - \text{Wishart}\left(\eta_{i,0} + n_i, \left[S_{i,0} + \sum_{j=1}^{n_i} \left(\boldsymbol{\gamma_{i,2}} - \boldsymbol{\varphi_i}\right)\left(\boldsymbol{\gamma_{i,2}} - \boldsymbol{\varphi_i}\right)^T\right]^{-1}\right)$$

Where $\eta_{i,0}$ and $S_{i,0}$ are parameters of prior distribution $\boldsymbol{\Sigma_i}$.

APPENDIX C.CONDITIONAL DISTRIBUTION OF $\boldsymbol{\sigma^2_{v_{i,j}}}$

The prior distribution $\sigma^2_{v_{i,j}}$ is:

$$\mathrm{P}(\lambda) = \frac{\lambda^{\frac{\nu_0}{2}-1}\exp(-\lambda\nu_0{\sigma^2}_0/2)}{\Gamma(\frac{\nu_0}{2})} \propto [\lambda^{\frac{\nu_0}{2}-1}\exp(-\lambda\nu_0{\sigma^2}_0/2)] \tag{76}$$

The joint probability density of sampling distribution for $\boldsymbol{y}$ conditional upon$\boldsymbol{\gamma}, \boldsymbol{\beta}, \lambda$ and $\boldsymbol{\xi}$:

$$\begin{aligned} P(\boldsymbol{y}|\boldsymbol{u},\boldsymbol{x},\boldsymbol{z},\boldsymbol{\psi}) &= \prod_{\boldsymbol{i=1}}^{\boldsymbol{m}}\prod_{\boldsymbol{j=1}}^{\boldsymbol{n_i}}\prod_{\boldsymbol{k=1}}^{\boldsymbol{n_{ij}}} P\left(\boldsymbol{y_{i,j,k}}\middle|\boldsymbol{u_{i,j,k}},\boldsymbol{x_{i,j,k}},\boldsymbol{z_{i,j,k}},\sigma^2_{v_{i,j}},\rho,\boldsymbol{\gamma_{i,j}},\boldsymbol{\beta_i},\boldsymbol{\xi}\right) \\ &= (2\pi\sigma^2)^{-\frac{\boldsymbol{n_{v_{ij}}}}{\boldsymbol{2}}}\exp\left\{-\frac{1}{2\sigma^2_{v_{i,j}}}\sum_{i=1}^{m}\sum_{j=1}^{n_i}\sum_{k=1}^{n_{i,j}}(\boldsymbol{y_{i,j,k}}-\boldsymbol{z_{i,j,k}}\boldsymbol{\gamma}_{i,j}\right. \\ &\quad -\boldsymbol{x_{i,j,k}}\boldsymbol{\beta_i}-\boldsymbol{u_{i,j,k}}\boldsymbol{\xi}){C_\rho}^{-1}(\boldsymbol{y_{i,j,k}}-\boldsymbol{z_{i,j,k}}\boldsymbol{\gamma}_{i,j}-\boldsymbol{x_{i,j,k}}\boldsymbol{\beta_i} \\ &\quad \left.-\boldsymbol{u_{i,j,k}}\boldsymbol{\xi})^{\mathrm{T}}\right\} \\ &= (2\pi)^{-\frac{\boldsymbol{n_{v_{i,j}}}}{\boldsymbol{2}}}\lambda^{\frac{\boldsymbol{n_{v_{i,j}}}}{\boldsymbol{2}}}\exp\left\{-\frac{\lambda}{2}\sum_{i=1}^{m}\sum_{j=1}^{n_i}\sum_{k=1}^{n_{i,j}}(\boldsymbol{y_{i,j,k}}-\boldsymbol{z_{i,j,k}}\boldsymbol{\gamma}_{i,j}\right. \\ &\quad -\boldsymbol{x_{i,j,k}}\boldsymbol{\beta_i}-\boldsymbol{u_{i,j,k}}\boldsymbol{\xi}){C_\rho}^{-1}(\boldsymbol{y_{i,j,k}}-\boldsymbol{z_{i,j,k}}\boldsymbol{\gamma}_{i,j}-\boldsymbol{x_{i,j,k}}\boldsymbol{\beta_i} \\ &\quad \left.-\boldsymbol{u_{i,j,k}}\boldsymbol{\xi})^{\mathrm{T}}\right\} \end{aligned} \tag{77}$$

Conditional on $\boldsymbol{\gamma}, \boldsymbol{\beta}$ and $\boldsymbol{\xi}$, the data provide information about $\sigma^2_{\mathbf{v_{i,j}}}$ via the sum of squared residuals from each group. The posterior distribution of λ becomes:

$$
\begin{aligned}
P\left(\lambda\middle|\boldsymbol{y},\boldsymbol{u},\boldsymbol{x},\boldsymbol{z},\sigma^2_{\boldsymbol{v}_{\mathrm{i,j}}},\boldsymbol{\rho},\boldsymbol{\gamma},\boldsymbol{\beta},\boldsymbol{\xi}\right) &\propto P\left(\boldsymbol{y}\middle|\boldsymbol{u},\boldsymbol{x},\boldsymbol{z},\sigma^2_{\boldsymbol{v}_{\mathrm{i,j}}},\boldsymbol{\rho},\boldsymbol{\gamma},\boldsymbol{\beta},\boldsymbol{\xi}\right)\mathrm{P}(\lambda)\\
&\propto \lambda^{\frac{\boldsymbol{n}_{\boldsymbol{v}_{i,j}}}{2}}\exp\left\{-\frac{\lambda}{2}\sum_{i=1}^{m}\sum_{j=1}^{n_i}\sum_{k=1}^{n_{i,j}}(\boldsymbol{y}_{\boldsymbol{i,j,k}}-\boldsymbol{z}_{\boldsymbol{i,j,k}}\boldsymbol{\gamma}_{i,j}-\boldsymbol{x}_{\boldsymbol{i,j,k}}\boldsymbol{\beta}_{\boldsymbol{i}}\right.\\
&\quad\left.-\boldsymbol{u}_{\boldsymbol{i,j,k}}\boldsymbol{\xi}){C_\rho}^{-1}(\boldsymbol{y}_{\boldsymbol{i,j,k}}-\boldsymbol{z}_{\boldsymbol{i,j,k}}\boldsymbol{\gamma}_{i,j}-\boldsymbol{x}_{\boldsymbol{i,j,k}}\boldsymbol{\beta}_{\boldsymbol{i}}-\boldsymbol{u}_{\boldsymbol{i,j,k}}\boldsymbol{\xi})^{\mathrm{T}}\right\}\\
&\quad\times\left[\lambda^{\frac{\nu_0}{2}-1}\exp\left(-\frac{\lambda\nu_0{\sigma^2}_0}{2}\right)\right]\\
&\quad=\lambda^{\frac{\nu_0+\boldsymbol{n}_{\boldsymbol{v}_{i,j}}}{2}-1}\exp\left\{-\frac{\lambda}{2}\left[\nu_0{\sigma^2}_0\right.\right.\\
&\quad\left.+\sum_{i=1}^{m}\sum_{j=1}^{n_i}\sum_{k=1}^{n_{i,j}}(\boldsymbol{y}_{\boldsymbol{i,j,k}}-\boldsymbol{z}_{\boldsymbol{i,j,k}}\boldsymbol{\gamma}_{i,j}-\boldsymbol{x}_{\boldsymbol{i,j,k}}\boldsymbol{\beta}_{\boldsymbol{i}}-\boldsymbol{u}_{\boldsymbol{i,j,k}}\boldsymbol{\xi}){C_\rho}^{-1}(\boldsymbol{y}_{\boldsymbol{i,j,k}}\right.\\
&\quad\left.\left.-\boldsymbol{z}_{\boldsymbol{i,j,k}}\boldsymbol{\gamma}_{i,j}-\boldsymbol{x}_{\boldsymbol{i,j,k}}\boldsymbol{\beta}_{\boldsymbol{i}}-\boldsymbol{u}_{\boldsymbol{i,j,k}}\boldsymbol{\xi})^{\mathrm{T}}\right]\right\}\sim\\
&\mathrm{gamma}\left(\begin{bmatrix}\left[\nu_0+\boldsymbol{n}_{\boldsymbol{v}_{i,j}}\right]/2\,,\\ \nu_0{\sigma^2}_0+\sum_{i=1}^{m}\sum_{j=1}^{n_i}\sum_{k=1}^{n_{i,j}}\begin{matrix}(\boldsymbol{y}_{\boldsymbol{i,j,k}}-\boldsymbol{z}_{\boldsymbol{i,j,k}}\boldsymbol{\gamma}_{i,j}-\boldsymbol{x}_{\boldsymbol{i,j,k}}\boldsymbol{\beta}_{\boldsymbol{i}}-\boldsymbol{u}_{\boldsymbol{i,j,k}}\boldsymbol{\xi}){C_\rho}^{-1^{\mathrm{T}}}\\ (\boldsymbol{y}_{\boldsymbol{i,j,k}}-\boldsymbol{z}_{\boldsymbol{i,j,k}}\boldsymbol{\gamma}_{i,j}-\boldsymbol{x}_{\boldsymbol{i,j,k}}\boldsymbol{\beta}_{\boldsymbol{i}}-\boldsymbol{u}_{\boldsymbol{i,j,k}}\boldsymbol{\xi})\end{matrix}\end{bmatrix}\Big/2\right)
\end{aligned}
\tag{78}
$$

So the posterior distribution of σ^2 is inverse-gamma distribution:

$$
\begin{aligned}
\left[\sigma^2_{\boldsymbol{v}_{\mathrm{i,j}}}\middle|\boldsymbol{y},\boldsymbol{u},\boldsymbol{x},\boldsymbol{z},\boldsymbol{\psi}\right]\sim\mathrm{inverse}-\mathrm{gamma}(&\left[\nu_0+\boldsymbol{n}_{\boldsymbol{v}_{i,j}}\right]/2,\\
[\nu_0{\sigma^2}_0+\sum_{i=1}^{m}\sum_{j=1}^{n_i}\sum_{k=1}^{n_{i,j}}&\begin{matrix}(\boldsymbol{y}_{\boldsymbol{i,j,k}}-\boldsymbol{z}_{\boldsymbol{i,j,k}}\boldsymbol{\gamma}_{i,j}-\boldsymbol{x}_{\boldsymbol{i,j,k}}\boldsymbol{\beta}_{\boldsymbol{i}}-\boldsymbol{u}_{\boldsymbol{i,j,k}}\boldsymbol{\xi}){C_\rho}^{-1^{\mathrm{T}}}\\ (\boldsymbol{y}_{\boldsymbol{i,j,k}}-\boldsymbol{z}_{\boldsymbol{i,j,k}}\boldsymbol{\gamma}_{i,j}-\boldsymbol{x}_{\boldsymbol{i,j,k}}\boldsymbol{\beta}_{\boldsymbol{i}}-\boldsymbol{u}_{\boldsymbol{i,j,k}}\boldsymbol{\xi})\end{matrix}\ ]\Big/2)
\end{aligned}
$$

Where ν_0 and ${\sigma^2}_0$ are prior parameters of $\sigma^2_{\boldsymbol{v}_{\mathrm{i,j}}}$. $n_{v_{i,j}}$ refers to the sample size (in seconds) from all traces with average speed $v_{\mathrm{i,j}}$.

APPENDIX D.COEFFICIENTS OF ACCELERATION MODEL

Table A - 1 Coefficients of passenger car model

	Acceleration type (initial - end speed, mph)					
Speed piece (mph)	**0-20**	**0-25**	**0-30**	**0-35**	**0-40**	**0-45**
Speed piece (mph)	**Intercept**					
5	3.225***	3.549***	3.415***	3.617***	3.609***	3.577***
10	2.644***	3.141***	3.404***	3.747***	3.676***	4.284***
15	1.975***	2.544***	2.837***	2.986***	3.026***	3.693***
20	0.542***	1.97***	2.181***	2.587***	2.748***	2.946***
25		0.606***	1.64***	1.98***	2.205***	2.671***
30			0.535***	1.332***	1.776***	2.067***
35				0.482***	1.158***	1.732***
40					0.462***	1.087***
45						0.41***
Speed piece (mph)	**Grade (<0%)**					
5	0.113^	0.032	-0.028	0.059*	-0.04	-0.043
10	-0.001	-0.029	-0.011	0.019	-0.075***	-0.026
15	-0.002	-0.037	-0.059*	-0.037*	-0.103***	-0.066**
20	-0.015	0.003	-0.096***	-0.041*	-0.081***	-0.102***
25		-0.012	-0.055**	-0.051***	-0.083***	-0.101***
30			-0.015^	-0.027**	-0.06***	-0.104***
35				-0.022***	-0.015^	-0.021
40					-0.033***	-0.007
45						-0.03***
Speed piece (mph)	**Grade (≥0%)**					
5	0.058	0.028	0.09*	0.085*	0.034	0.058
10	0.021	0.047	0.022	-0.033	0.026	-0.056*
15	-0.032	-0.031	-0.039^	-0.059***	-0.002	-0.083***
20	0.023	-0.03	-0.006	-0.059***	-0.035*	-0.047**
25		-0.004	0.001	-0.035**	-0.032*	-0.075***
30			0	-0.018*	-0.042**	-0.029^
35				-0.01^	-0.02*	-0.05***
40					-0.003	-0.036***
45						-0.012^
Speed piece (mph)	**100/Radius**					
5	0.519	0.402	0.724*	0.421*	0.546***	0.369
10	0.014	0.099	0.383^	0.325*	0.337*	0.32^
15	0.051	0.153	-0.181	0.04	0.292*	0.279*
20	0.003	0.343***	0.03	0.219*	0.011	-0.003
25		-0.021	0.161	0.085	0.104	0.009
30			0.16**	0.052	-0.09	0.012
35				-0.136**	-0.137*	-0.089
40					-0.074^	-0.214**
45						0.017
Speed piece (mph)	**Day (1-Day, 0-Night)**					

	Acceleration type (initial - end speed, mph)					
Speed piece (mph)	**0-20**	**0-25**	**0-30**	**0-35**	**0-40**	**0-45**
5	-0.153	-0.48**	-0.458*	-0.164	-0.185	0.028
10	0.093	-0.033	-0.215	-0.047	-0.101	-0.22^
15	-0.015	-0.076	-0.165^	-0.097	-0.066	-0.262**
20	0.256^	-0.051	-0.113	-0.201*	-0.239***	-0.103
25		0.133**	-0.161*	-0.138**	-0.149*	-0.276***
30			0.031	-0.036	-0.16***	-0.202***
35				0.059***	-0.05	-0.192***
40					0.021	-0.095*
45						-0.004
Speed piece (mph)	**GradeDiff (ToUphill)**					
5	0.009	0.131	0.256^	0.104	0.159^	0.063
10	0.149	-0.163	0.171^	0.149^	0.089	0.22^
15	0.148	0.035	0.085	0.094^	0.171*	0.286***
20	-0.066	0.073	0.185***	0.028	0.153*	0.169**
25		0.026	0.048	0.061^	0.112*	0.16*
30			0.046^	0.046	0.11*	0.172***
35				0.024	0.131***	0.124*
40					0.047***	0.087*
45						0.095***
Speed piece (mph)	**GradeDiff (ToDownhill)**					
5	-0.029	-0.189	-0.216^	0.026	-0.288**	-0.297**
10	-0.063	-0.031	-0.07	-0.047	-0.232***	-0.113
15	0.026	0.152^	-0.029	0.051	-0.074	-0.095
20	-0.077	-0.03	-0.109^	0.127**	-0.017	0.101^
25		-0.027	0.043	0.065	0.004	0.137*
30			0.024	0.098***	0.12***	0.11^
35				0.048*	0.124***	0.197***
40					0.086***	0.111***
45						0.06*
Speed piece (mph)	**Tier 2 (1) vs Tier 1 (0)**					
5	-0.296	-0.089	0.094	-0.063	0.127	0.049
10	-0.029	-0.041	0.095	-0.008	0.079	0.115
15	0.041	0.000	0.029	0.051	0.056	-0.01
20	-0.051	-0.137	0.063	0.107^	0.156*	0.128
25		-0.037	-0.005	0.093^	0.149*	0.147
30			0.033	0.043	0.12*	0.09
35				0.019	0.06	0.021
40					-0.015	0.09
45						0.021

***99.9%, **99%, *95%, ^90%

Table A - 2 – Coefficients of passenger truck model

	Acceleration type (initial - end speed, mph)					
Speed piece (mph)	**0-20**	**0-25**	**0-30**	**0-35**	**0-40**	**0-45**
Speed piece (mph)	**Intercept**					
5	2.529***	2.467***	3.102***	3.464***	3.802***	3.765***
10	2.897***	2.952***	3.15***	3.3***	3.773***	3.951***
15	2.069***	1.984***	2.298***	2.783***	3.287***	3.394***
20	0.477^	2.087***	2.193***	2.538***	2.705***	2.785***
25		0.791***	1.332***	1.878***	2.283***	2.542***
30			0.481***	1.257***	1.606***	1.922***
35				0.557***	1.146***	1.505***
40					0.454***	0.99***
45						0.404***
Speed piece (mph)	**Grade (<0%)**					
5	-0.029	-0.083	-0.055	0.033	0.064^	0.033
10	-0.02	-0.054	-0.067*	-0.001	-0.031	-0.049^
15	-0.106**	-0.02	-0.089***	-0.029	-0.051*	-0.063*
20	-0.008	0.013	-0.026	-0.048*	-0.072***	-0.08***
25		-0.018	-0.035	-0.072***	-0.082***	-0.085***
30			-0.028*	-0.058***	-0.066***	-0.064***
35				-0.014^	-0.02*	-0.04**
40					-0.023***	-0.033***
45						-0.028***
Speed piece (mph)	**Grade (≥0%)**					
5	0.274**	0.148*	0.108*	0.061	0.029	-0.022
10	0.086	0.05	0.055^	0.006	-0.021	-0.018
15	-0.018	-0.013	0.026	-0.014	-0.056*	-0.084***
20	0.004	-0.017	-0.05*	-0.032^	-0.036^	-0.064**
25		0.008	-0.021	-0.009	-0.049**	-0.044*
30			0.011	0.001	-0.014	-0.043**
35				-0.004	0.000	-0.039**
40					-0.02***	-0.021*
45						-0.022**
Speed piece (mph)	**100/Radius**					
5	0.174	-0.073	0.834*	0.576*	0.7**	0.521^
10	-0.492	0.104	0.41	0.241	0.3	0.002
15	-0.107	0.196	0.149	0.058	0.102	-0.136
20	0.148	-0.194	0.208	-0.037	0.003	0.098
25		0.008	0.061	-0.09	0.068	0.099
30			0.143	-0.064	-0.007	-0.118
35				-0.154***	-0.14	0.186
40					-0.08	-0.102
45						-0.152***
Speed piece (mph)	**Day (1-Day, 0-Night)**					
5	-0.394	0.287	-0.11	-0.095	-0.129	0.1
10	-0.254	-0.221	-0.171	0.077	-0.047	0.095
15	-0.181	0.141	-0.007	0.018	-0.188*	-0.159
20	0.273*	0.023	-0.146	-0.2*	-0.079	0.005
25		-0.178	0.065	-0.05	-0.08	-0.179*

	Acceleration type (initial - end speed, mph)					
Speed piece (mph)	**0-20**	**0-25**	**0-30**	**0-35**	**0-40**	**0-45**
30			0.114*	-0.046	0.054	-0.082
35				0.032	-0.023	-0.036
40					0.048*	-0.012
45						0.062***
Speed piece (mph)	**GradeDiff (ToUphill)**					
5	0.731**	0.106	0.118	0.333**	-0.036	-0.188
10	0.043	0.358*	0.212	0.391***	-0.02	-0.187
15	0.064	0.173	0.186^	0.137*	0.204**	-0.047
20	-0.004	0.145	0.087	0.126*	0.086	0.203*
25		0.208**	0.14*	0.12*	0.1^	0.169*
30			-0.007	0.117***	0.06	0.212***
35				0.001	0.056^	0.171***
40					0.063***	0.109***
45						0.065***
Speed piece (mph)	**GradeDiff (ToDownhill)**					
5	0.218	-0.045	0.038	0.073	-0.206^	0.118
10	0.519**	0.048	-0.035	0.024	-0.16*	0.023
15	0.242	-0.118	-0.061	0.009	-0.018	0.157*
20	0.05	0.008	-0.064	0.057	-0.018	0.077
25		0.016	0.013	0.078	0.098*	0.053
30			0.071^	0.011	0.15**	0.113*
35				0.06**	0.062*	0.096*
40					0.049*	0.145***
45						0.042*
Speed piece (mph)	**Tier 2 (1) vs Tier 1 (0)**					
5	0.246	0.13	-0.086	0.032	-0.062	0.022
10	-0.011	0.209	0.054	0.128	-0.002	-0.01
15	-0.018	0.264^	0.203	0.083	-0.065	0.125
20	0.01	-0.264	0.098	0.096	0.011	0.118
25		0.075	0.161*	0.085	-0.039	0.024
30			0.011	0.096^	0.011	0.157
35				-0.005	0.019	0.013
40					0.002	0.011
45						-0.004

***99.9%, **99%, *95%, ^90%

Table A - 3 – Coefficients of transit bus model

	Acceleration type (initial - end speed, mph)					
Speed piece (mph)	**0-20**	**0-25**	**0-30**	**0-35**	**0-40**	**0-45**
Speed piece (mph)	**Intercept**					
5	1.785***	1.846***	1.882***	1.876***	1.85***	1.934***
10	2.167***	2.266***	2.317***	2.374***	2.372***	2.417***
15	1.797***	2.03***	2.159***	2.187***	2.248***	2.295***
20	0.888***	1.565***	1.769***	1.857***	1.902***	1.982***
25		0.749***	1.268***	1.519***	1.594***	1.648***
30			0.615***	1.086***	1.296***	1.266***
35				0.55***	0.918***	0.985***
40					0.504***	0.817***
45						0.456***
Speed piece (mph)	**Grade (<0%)**					
5	-0.022***	-0.038***	-0.044***	-0.054***	-0.063***	-0.038***
10	0.021***	-0.038***	-0.047***	-0.05***	-0.048***	-0.022*
15	-0.015***	-0.067***	-0.086***	-0.1***	-0.104***	-0.104***
20	0.04***	-0.022***	-0.069***	-0.1***	-0.131***	-0.092***
25		0.009***	-0.036***	-0.073***	-0.102***	-0.12***
30			-0.001	-0.019***	-0.061***	-0.118***
35				-0.015***	-0.045***	-0.087***
40					-0.018***	-0.045***
45						-0.036***
Speed piece (mph)	**Grade (≥0%)**					
5	-0.018***	-0.019***	-0.02***	-0.019***	-0.028***	-0.046***
10	-0.087***	-0.084***	-0.097***	-0.103***	-0.113***	-0.111***
15	-0.142***	-0.154***	-0.174***	-0.188***	-0.208***	-0.201***
20	-0.056***	-0.128***	-0.161***	-0.18***	-0.198***	-0.222***
25		-0.048***	-0.113***	-0.159***	-0.189***	-0.197***
30			-0.041***	-0.112***	-0.178***	-0.157***
35				-0.053***	-0.109***	-0.118***
40					-0.072***	-0.155***
45						-0.1***
Speed piece (mph)	**100/Radius**					
5	0.015	-0.033	-0.033	-0.053*	-0.114***	-0.087^
10	-0.014	-0.022	-0.017	-0.026	-0.034	0.03
15	-0.019	-0.122***	-0.131***	-0.137***	-0.111***	-0.162***
20	-0.015	-0.046**	-0.162***	-0.045^	-0.083*	-0.044
25		0.006	-0.143***	-0.183***	-0.124***	-0.104*
30			-0.11***	-0.257***	-0.347***	-0.242***
35				-0.164***	-0.266***	-0.456***
40					-0.131***	-0.159***
45						-0.069
Speed piece (mph)	**Day(1-Day, 0-Night)**					
5	-0.027*	-0.045***	-0.033***	0.014	-0.013	-0.032
10	-0.035**	-0.078***	-0.051***	-0.055***	-0.034*	-0.081**
15	-0.042***	-0.056***	-0.065***	-0.049***	-0.043***	-0.129***
20	-0.015	-0.066***	-0.017*	-0.039***	-0.056***	-0.065**
25		-0.011	-0.021***	-0.04***	-0.048***	-0.087***

	Acceleration type (initial - end speed, mph)					
Speed piece (mph)	**0-20**	**0-25**	**0-30**	**0-35**	**0-40**	**0-45**
30			-0.006	-0.016**	-0.012	-0.034*
35				-0.006	-0.01	0.001
40					-0.003	0.009
45						-0.012
Speed piece (mph)	**GradeDiff (ToUphill)**					
5	0	0.032***	0.003	0.031**	0	0.072*
10	-0.013	0.023*	0.059***	0.044*	0.055*	0.081^
15	0.024*	0.062***	0.03**	0.073***	0.083***	0.072^
20	0.001	0.059***	0.08***	0.114***	0.105***	0.008
25		0.05***	0.126***	0.161***	0.172***	0.052
30			0.041***	0.12***	0.166***	0.237***
35				0.062***	0.12***	0.157***
40					0.105***	0.109***
45						0.13***
Speed piece (mph)	**GradeDiff (ToDownhill)**					
5	0.054***	0.001	0.013^	0.031***	-0.046***	-0.024
10	0.056***	0.037***	0.051***	0.072***	0.023	0.049^
15	0.095***	0.062***	0.112***	0.119***	0.133***	0.163***
20	0.035***	0.061***	0.125***	0.16***	0.17***	0.208***
25		0.074***	0.13***	0.172***	0.2***	0.161***
30			0.07***	0.145***	0.185***	0.12***
35				0.072***	0.167***	0.142***
40					0.11***	0.208***
45						0.192***

***99.9%, **99%, *95%, ^90%

REFERENCES

AASHTO. (2001). A policy on geometric design of highways and streets, Washington, D.C.

Awuah-Baffour, R., Sarasua, W., Dixon, K., Bachman, W. and Guensler, R. (1997). Global Positioning System with an Attitude: Method for Collecting Roadway Grade and Superelevation Data. *Journal of the Transportation Research Record*, 1592, pp. 144-150. doi: 10.3141/1592-17

Bae, H., Ryu J. and Gerdes, J. C. (2001). Road Grade and Vehicle Parameter Estimation for Longitudinal Control Using GPS. In: *2001 IEEE Intelligent Transportation Systems. Proceedings.* [online] Oakland: IEEE, pp. 25-29. Available at: http://www-cdr.stanford.edu/dynamic/PATH/Papers/bae_ieee_its2001.pdf [Accessed Jun. 2018].

Barth, M., and Boriboonsomsin, K. (2009). Energy and Emissions Impacts of a Freeway-based Dynamic Eco-Driving System. *Transportation Research Part D: Transport and Environment*, 14(6), 2009, pp. 400-410. doi: 10.1016/j.trd.2009.01.004

Bonnedahl, T. (2010). *Road Slope Estimation using a Longitudinal Accelerometer and Kalman Filtering*. Master. Lund University.

Boroujeni Y., Frey, H.C. and Sandhu, G.S. (2013). Road Grade Measurement Using In-Vehicle, Stand-Alone GPS with Barometric Altimeter. *Journal of Transportation Engineering*, 139, pp. 605-611. doi:10.1061/(ASCE)TE.1943-5436.0000545

Boroujeni, Y. and Frey, H.C. (2014). Road Grade Quantification Based on Global Positioning System Data Obtained from Real-World Vehicle Fuel Use and Emission Measurements. *Atmospheric Environment*, 85, pp. 179-186. doi: 10.1016/j.atmosenv.2013.12.025

CARB, California Air Resource Board. (2016). EMFAC2014. Available at: http://www.arb.ca.gov/msei/categories.htm [Accessed Jun. 2018]

Castro, M., Iglesias, L., Rodrı´guez-Solano, R. and Sa´nchez, J. A. (2006). Geometric Modelling of Highways Using Global Positioning System (GPS) Data and Spline Approximation. *Transportation Research Part C: Emerging Technologies*, 14(4), pp. 233-243. doi: 10.1016/j.trc.2006.06.004

Cheng, M., Wang, Z. and Tao, G. (2012). Vehicle Parameter and Road Grade Estimation Based on Kalman Filter: Theory and Experiments. *Applied Mechanics and Materials*, 157-158, pp. 1376-1379. doi: 10.4028/www.scientific.net/AMM.157-158.1376

Dai, Z., Niemeier, D., and Eisinger, D. (2008). *Driving Cycles: A New Cycle-Building Method that Better Represents Real-World Emissions*.UC Davis Report. Available at: http://www.dot.ca.gov/hq/env/air/research/ucd_aqp/Documents/2008-Dai-arterial-cycles-final.pdf [Accessed 1 Jun. 2018]

EMISIA. (2016). COPERT 4. Available at: http://emisia.com/products/copert-4 [Accessed Jun. 2018]

Franzese, O. and Davidson, D. (2011). *Effect of Weight and Roadway Grade on the Fuel Economy of Class-8 Freight Trucks*. [online] Oak Ridge: ORNL. Available at: https://info.ornl.gov/sites/publications/files/Pub33386.pdf [Accessed Jun. 2018].

GDOT, Georgia Department of Transportation. (2018). Project Search (GeoPI). Available at: http://www.dot.ga.gov/BS/Projects/ProjectSearch [Accessed Jun. 2018]

Georgia EPD, Georgia Environmental Protection Division, (2018). Georgia AERMET Meteorological Data, Available at: https://epd.georgia.gov/air/georgia-aermet-meteorological-data [Accessed Jun. 2018]

Gelman, A., Carlin, J.B., Stern, H.S., Dunson, D.B., Vehtari, A. and Rubin, D.B. (2014). *Bayesian Data Analysis*. CHAPMAN & HALL/CRC.

Gesch, D.B., Oimoen, M.J. and Evans, G.A. (2014). Accuracy assessment of the U.S. Geological Survey National Elevation Dataset, and comparison with other large-area elevation datasets - SRTM and ASTER. [online] Reston: U.S. Geological Survey. Available at: https://pubs.usgs.gov/of/2014/1008/pdf/ofr2014-1008.pdf [Accessed Jun. 2018]. doi: 10.3133/ofr20141008

Gipps, P.G. (1981). A Behavioural Car-Following Model for Computer Simulation. *Transportation Research Part B: Methodological*, 15(2), pp.105-111.

Glennon, J. C. (1987). Effect of Alignment on Highway Safety, Relationship between Safety and Key Highway Features. Washington D.C.: Transportation Research Board, pp. 48–63. Available at: http://onlinepubs.trb.org/Onlinepubs/state-of-the-art/6/6-004.pdf [Accessed Jun. 2018].

Green, P. J. and Silverman, B.W. (1993). Nonparametric Regression and Generalized Linear Models: A roughness penalty approach. Chapman and Hall.

Guensler, R., Liu, H, Xu, X, Xu, Y. and Rodgers, M. (2016) MOVES-Matrix: Setup, Implementation, and Application. In *95th Annual Meeting of the Transportation Research Board.* Washington, DC.

Hamdar, S.H., Qin, L. and A. Talebpour. (2016). Weather and Road Geometry Impact on Longitudinal Driving Behavior: Exploratory Analysis Using an Empirically Supported Acceleration Modeling Framework. *Transportation Research Part C: Emerging Technologies*, 67, pp. 193-213. doi: 10.1016/j.trc.2016.01.017

Heywood, I., Cornelius, S. and Carver, S. (2006). *An Introduction to Geographical Information Systems*. 3rd ed. Harlow: Pearson Prentice Hall.

Holden, N.M., Owende, P.M. and Ward, S.M. (2001). The Effect of Peripheral Canopy on DGPS Performance on Forest Roads. *Journal of Forest Engineering*, 12. pp. 71-79.

Holf, P. (2009). *A First Course in Bayesian Statistical Methods*. New York: Springer.

Hong, S., Heo, J. and Vonderohe, A.P. (2013). Simulation-based Approach for Uncertainty Assessment: Integrating GPS and GIS. *Transportation Research Part C: Emerging Technologies*, 36, pp. 125-137. doi: 10.1016/j.trc.2013.08.008

Hummel, S., Hudak, A.T., Uebler, E.H., Falkowski, M.J. and Megown, K.A. (2011). A Comparison of Accuracy and Cost of LiDAR versus Stand Exam Data for Landscape Management on the Malheur National Forest. *Journal of Forestry*, 109(5), pp. 257-273. doi: 10.1093/jof/109.5.267

Ikwut-Ukwa, H. (2001). *Advances In Vehicle Emissions Modeling: Development of a Methodology for the Kinematic Acquisition of Roadway Grade Data*. Master. Georgia Institute of Technology.

Kall, D. (2013). Results of NCHRP 25-38: Survey on MOVES Data Sources. Cambridge Systematic, Inc. Presentation to MOVES User Group for MPOs.

Kamarianakis, Y., Gao, H.O. and Prastacos, P. (2010). Characterizing Regimes in Daily Cycles of Urban Traffic Using Smooth-Transition Regressions. *Transportation Research Part C: Emerging Technologies*, 18(5), pp. 821-840. doi: 10.1016/j.trc.2009.11.001

Laval, J.A., Toth, C.S. and Zhou, Y. (2014). A Parsimonious Model for The Formation of Oscillations in Car-Following Models. *Transportation Research Part B* 70 (2014) pp. 228-238. doi: https://doi.org/10.1016/j.trb.2014.09.004

Levin, M.W., Duell, M. and Waller, S.T. (2014). Effect of Road Grade on Networkwide Vehicle Energy Consumption and Ecorouting. *Transportation Research Record*, 2427, pp. 26-33. doi: 10.3141/2427-03

Li, H., Liu, H., Xu, X., Xu, Y. Rodgers, M. and Guensler, R. (2016). Emissions Benefits from Reducing Local Transit Service Deadheading: An Atlanta Case Study. In *95th Annual Meeting of the Transportation Research Board*. Washington, DC.

Li, J. and Smith, D. (2014). Modeling the Impact of Road Grade and Curvature on Truck Driving for Vehicle Simulation. *SAE Technical Paper*, 2014-01-0879. doi:10.4271/2014-01-0879

Lin, J. and Niemeier, D.A. (2002). An Exploratory Analysis Comparing a Stochastic Driving Cycle to California's Regulatory Cycle. *Atmospheric Environment*. 36 pp.5759-5770. doi: https://doi.org/10.1016/S1352-2310(02)00695-7

Liu, B., and Frey, H.C. (2015). Quantification and Application of Real-World Light Duty Vehicle Performance Envelope for Speed and Acceleration. *Transportation Research Record,* 2503. pp.128-136. doi: 10.3141/2503-14

Liu, H., Liu, H., Xu, Y., Rodgers, M.O., and Guensler, R. (2015b). Developing Vehicle Classification Inputs for Project-level MOVES Analysis. *Transportation Research Record*. 2503, pp.81-90, doi: https://doi.org/10.3141/2503-09

Liu, H., Xu, X., Rodgers, M., Xu, Y., and Guensler, R. (2016). MOVES-Matrix and Distributed Computing for Microscale Line Source Dispersion Analysis. *Journal of Air & Waste Management*. 67(7), pp.763-775 doi: https://doi.org/10.1080/10962247.2017.1287788

Luke, D.A. (2004). *Multilevel Modeling*. Sage Publications.

NCHRP, National Cooperative Highway Research Program. (2005). *Predicting Air Quality Effects of Traffic-Flow Improvements: Final Report and User's Guide*. NCHRP Report.

NHTSA, National Highway Traffic Safety Administration. (2012). *Corporate Average Fuel Economy*. Department of Transportation.

Ogaja, C.A. (2011). *Applied GPS for Engineers and Project Managers.* 1st Edition. Reston: ASCE Press.

Ogle, J., Guensler, R. and Elango, V. (2005). Georgia's Commute Atlanta Value Pricing Program: Recruitment Methods and Travel Diary Response Rates. *Transportation Research Record*, (1931), pp.28-37. doi: https://doi.org/10.3141/1931-04

Parviainen, J., Hautamaki, J., Collin, J. and Takala, J. (2009). Barometer-aided Road Grade Estimation. In *Proceedings of 13th IAIN World Congress*. IAIN.

Pinheiro, J.C. and Bates, D.M. (2000). *Mixed-Effects Models in S and S-Plus*. New York: Springer.

Rogers, K.J. and Trayford, R.S. (1984). Grade Measurement with and Instrumented Car. *Transportation Research Part B: Methodology,* 18, pp. 247-254. doi: 10.1016/0191-2615(84)90035-3

Sahlholm, P., Jansson, H., Kozica, E. and Johansson, K.H. (2007). A Sensor and Data Fusion Algorithm for Road Grade Estimation. In *Proceedings of 5th IFAC Symposium on Advances in Automotive Control,* 40(10), pp. 55-62. doi: 10.3182/20070820-3-US-2918.00010

Sahlholm, P. and Johansson, K.H. (2010). Road Grade Estimation for Look-ahead Vehicle Control using Multiple Measurement Runs. *Control Engineering Practice,* 18(11), pp: 1328-1341. doi: 10.1016/j.conengprac.2009.09.007

Sentoff, K.M., Aultman-Hall, L. and Holmen, B.A. (2015). Implications of Driving Style and Road Grade for Accurate Vehicle Activity Data and Emissions Estimates. *Transportation Research Part D: Transport and Environment*, 35, pp. 175-188. doi: 10.1016/j.trd.2014.11.021

Southwest Research Institute. (2014*). Mobile Autonomous Robotics Technology Initiative Program*. Available at: www.marti.swri.org [Accessed Jun. 2018]

Sugarbaker, L.J., Constance, E.W., Heidemann, H.K., Jason, A.L., Lukas, V., Saghy, D.L. and Stoker, J.M. (2014). *The 3D Elevation Program initiative - A call for action*. [online] Reston: U.S. Geological Survey. Available at: https://pubs.usgs.gov/circ/1399/ [Accessed Jun. 2018]. doi: 10.3133/cir1399

TomTom International. (2013). *MultiNet Advanced Driving Attributes 1.1: Data and Format Specifications*. Document Version 1.0.0.

TRB, Transportation Research Board. (2010). *Highway Capacity Manual*. 5th ed. Washington D.C.: TRB

TxDOT, Texas Department of Transportation. (2014). *Road Design Manual*. [online] Available at: http://onlinemanuals.txdot.gov/txdotmanuals/rdw/manual_notice.htm [Accessed Jun. 2018]

US Census Bureau. (2017). *TIGER Products: Line Shapefile*. Available at: https://www.census.gov/geo/maps-data/data/tiger-line.html [Accessed Jun. 2018]

USEPA, U.S. Environmental Protection Agency. (2009). Development of Generic Link-Level Driving Cycles. EPA-420-B-12-050.

USEPA, U.S. Environmental Protection Agency. (2012). Final Rule for Model Year 2017 and Later Light-Duty Vehicle Greenhouse Gas Emissions and Corporate Average Fuel Economy Standards.

USEPA, U.S. Environmental Protection Agency. (2015). MOVES2014a. Available at: https://www3.epa.gov/otaq/models/moves/ [Accessed Jun. 2018].

USEPA, U.S. Environmental Protection Agency. (2016a). Transportation Conformity. Available at: https://www3.epa.gov/otaq/stateresources/transconf/ [Accessed Jun. 2018].

USEPA, U.S. Environmental Protection Agency. (2016b). National Ambient Air Quality Standards (NAASQ). Available at: https://www.epa.gov/criteria-air-pollutants/naaqs-table [Accessed Jun. 2018].

USEPA, U.S. Environmental Protection Agency. (2018). Annual Certification Data for Vehicles, Engines, and Equipment. Available at: https://www.epa.gov/compliance-and-fuel-economy-data/annual-certification-data-vehicles-engines-and-equipment [Accessed Jun. 2018].

USGS, US Geological Survey. (2016). Digital Elevation Models. Available at: http://nationalmap.gov/elevation.html [Accessed Jun. 2018].

Wang, Q., Huo, H., He, K. Yao, Z. and Zhang, Q. (2008). Characterization of Vehicle Driving Patterns and Development of Driving Cycles in Chinese Cities. *Tranportation Research Part D: Transport and Environment*, 13(5), pp: 289-297, doi: 10.1016/j.trd.2008.03.003

Wasserman, L. (2006). *All of Nonparametric Statistics*. Springer Texts in Statistics.

Wing M.G., Eklund, A. and Kellogg, L.D. (2005). Consumer-grade Global Positioning System (GPS) Accuracy and Reliability. *Journal of Forestry*, 103(4), pp. 169-173. doi: 10.3923/rjf.2011.78.88

Wood, E., Burton, E., Duran, A. and Gonder, J. (2014a). Contribution of Road Grade to the Energy Use of Modern Automobiles Across Large Datasets of Real-World Drive Cycles Preprint. In: *SAE World Congress*. [online] Detroit: SAE International in United States. Available at: https://saemobilus.sae.org/content/2014-01-1789 [Accessed Jun. 2018].

Wood, E., Burton, E., Duran, A. and Gonder, J. (2014b). *Appending High-Resolution Elevation Data to GPS Speed Traces for Vehicle Energy Modeling and Simulation*. National Renewable Energy Laboratory. NREL/TP-5400-61109.

Wood, E., Duran, A., Burton, E., Gonder, J. and Kelly, K. (2015). *EPA GHG Certification of Medium- and Heavy-Duty Vehicles: Development of Road Grade Profiles Representative of US Controlled Access Highways.* National Renewable Energy Laboratory. NREL/TP-5400-63853.

Wyatt, D.W., Li, H. and Tale, J.E. (2014). The Impact of Road Grade on Carbon Dioxide (CO_2) Emission of a Passenger Vehicle in Real-World Driving. *Transportation Research Part D: Transport and Environment*, 32, pp. 160-170. doi: 10.1016/j.trd.2014.07.015

Xia, H., Wang, X., Qiao, Y., Jian, J. and Chang, Y. (2015). Using Multiple Barometers to Detect the Floor Location of Smart Phones with Built-in Barometric Sensors for Indoor Positioning. *Sensors*, 15(4), pp. 7857-7877. doi:10.3390/s150407857

Xu, X., H. Liu, H. Li, M.O. Rodgers, R. Guensler (2018). Integrating Engine Start, Soak, Evaporative, and Truck Hoteling Emissions into MOVES-Matrix. DOI: 10.1177/0361198118797208. Transportation Research Record. Washington, DC. 2018.

Xu, X., Liu, H. Xu, Y. Rodgers, M. and R. Guensler. (2016a). Regional Emission Analysis using Travel Demand Models and MOVES-Matrix. *Transportation Planning and Air Quality Conference.* Minneapolis, Minnesota.

Xu, X., Liu, H., Anderson, J. Xu, Y., Hunter, M., Rodgers, M. and Guensler, R. (2016b). Estimating Project-Level Vehicle Emissions with Vissim and MOVES-Matrix. In 95th Annual Meeting of the Transportation Research Board. Washington, DC. January

Xu, Y., Liu, H., and Guensler, R. (2014). Emission Impact of HOV to HOT Lane Conversion in I-85, Atlanta. In *107th Annual Conference and Exhibition of Air & Waste Management Association.* Long Beach, CA.

Xu, Y., Li, H., Liu, H., Rodgers,M., and Guensler, R. (2016c). *Eco-driving for Transit.* National Center for Sustainable Transportation.

Yu, R. and Abdel-Aty, M. (2014). Analyzing Crash Injury Severity for a Mountainous Freeway Incorporating Real-Time Traffic and Weather Data. *Safety Science*, 63, pp. 50–56. doi.org/10.1016/j.ssci.2013.10.012

Zhang, K. and Frey, H.C. (2006). Road Grade Estimation for On-road Vehicle Emissions Modeling Using Light Detection and Ranging Data. *Journal of Air Waste and Management Association*, 56(6), pp. 777-788. doi: 10.1080/10473289.2006.10464500

Zhang, W., Lu, J., Xu, P. and Zhang, Y. (2015). Moving towards Sustainability: Road Grades and On-Road Emissions of Heavy-Duty Vehicles-A Case Study. *Sustainability*, 7(9), pp.12644-12671. doi: 10.3390/su70912644

Zhu, W., Wright, B., Li, Z., Wang, Y. and Pu, Z. (2016). Analyzing the Impact of Grade on Fuel Consumption for the National Interstate Highway System. In *95th Annual Meeting of the Transportation Research Board.* Washington, DC.

VITA

HAOBING LIU

Haobing was born in Shaodong, Hunan Province in China. Before pursuing a doctorate in Civil Engineering from Georgia Institute of Technology, He has obtained a master's degree in Statistics from School of Industrial and System Engineering at Georgia Tech in 2017. Before joining Georgia Tech, He earned a Bachelor degree (2010) and a Master degree (2013) in Transportation Engineering from Tongji University in Shanghai, China.